ADELAIDE UNIVERSITY AUSTRALIA

SUB CRUCE LUMEN

# Predicting weld cooling rates and the onset of failure during in-service welding

Prakash N. Sabapathy

B.E. Hons. (Adelaide), 1995

The University of Adelaide

Department of Mechanical Engineering

South Australia 5005

*Submitted for the degree of Doctor of Philosophy, 1st February 2002.*

# Predicting weld cooling rates and the onset of failure during in-service welding

## ABSTRACT

A comprehensive numerical simulation of the in-service welding of high pressure gas pipelines has been developed. A system has been established for predicting the safe, suitable welding conditions at which in-service manual metal arc welding using low-hydrogen electrodes can be achieved on thin, high-strength pipes with flowing pressurised natural gas. The two main concerns of in-service welding are: the possibility of excessively hard heat affected zone microstructure due to fast cooling rates, and the possibility of failure of the pipe wall due to localised heating from the welding arc.

The finite element method was applied to calculate the cooling rates from circumferential fillet welds and branch on pipe welds. Initial development considered approximating the process in two dimensions, but was quickly rejected in favour of three-dimensional conduction only models which included temperature dependent material properties. The welding arc was approximated as a three-dimensional heat flux distribution function. Numerical simulations were validated using both laboratory and field trials. The experiments involved welding on a water cooled device which simulated in-service welding cooling conditions in a laboratory, while a second experiment involved welding onto a flow-loop attached to an actual operating pipeline. The results from the experiments were used to define the heat source distribution, to account for weld weaving, and shallow penetration welding. Weld pool flow was not calculated, but the effects of weld pool convection were included in the heat source.

An investigation was made to calculate the limits at which in-service welding can produce safe, mechanically sound welds under a combination of low wall thickness pipe and high pressure. Initial development consisted of calculating pipe wall deflection using three-dimensional thermal elastic-plastic models. Such models are very expensive computationally, which led to the development of a new model to calculate the limits of in-service

welding. This 'equivalent cavity' model primarily used a thermal field, as calculated from the thermal models, to calculate the maximum pressure at which a weld can be deposited. The accuracy and feasibility of the equivalent cavity model was determined by comparing its predictions with published data relating to pipe wall failure, and numerical simulations of pipe wall failure using thermal elastic-plastic finite element models.

In combination, the thermal and pipe wall failure models offer valuable savings during the design stage of in-service welding. While the models form an accurate system to predict weld cooling rate and the possibility of pipe wall failure, they avoid the cost of traditional trial and error experimentation, often chosen for the testing phase of in-service welding.

## STATEMENT OF ORIGINALITY

This thesis contains no material which has been accepted for the award of any other degree or diploma in any university or other tertiary institution, and to the best of my knowledge, contains no material previously published or written by another person, except where due reference has been made in the text.

I give consent to this copy of my thesis, when deposited in the University Library, being made available for loan and photocopying.

Prakash N. Sabapathy, 1st February 2002

**Acknowledgements**

The research contained within this thesis has been produced with the support and inspiration from many people.

I would like to thank Dr Wahab from the University of Adelaide for his initial suggestion on the area of research and never ending advice both professionally and academically.

Secondly, the University of Adelaide, both the cooperative research centres (CRC) for Materials Welding and Joining (MWJ) and later Welded Structures (WS) for their kind financial support and input into my work from industrial sponsors. In particular, Paul Grace (AGL), BHP, Hans Borek (Epic Energy), Duke Energy and finally Leigh Fletcher (CRC-MWJ).

The significant contribution provided by CSIRO-CMST based at Woodville North must especially be noted in particular for their generous provision for students in particular laboratory and computing equipment, and specialist advice on numerous aspects of this thesis. Moreover their contribution external to the thesis in the form of recreational sports namely soccer and table-tennis is acknowledged. Thanks to my colleagues Alex Dunstone and Alek Bachorski for providing an immensely enjoyable atmosphere.

The people outside of my research surrounding I cannot thank enough. First my mother Wije, and my brother Guhan for gently spurring me on. A very special mention to my wife Dora and father Saba for their open minds and hearts whenever and wherever I needed it.

Finally and most importantly I would like to express my gratitude to my principal supervisor Dr Mike Painter. His tireless contribution and guidance were the key influences for me to produce this thesis. He has been the ideal supervisor both in terms of professional support and encouragement.

# Contents

# Chapter 1

# Significance and objective

## 1.1 Overview

Metal welding processes are used for the fabrication of structures ranging from the large and complex to the small and simple. The significance of welding may not be directly noticeable, but it has an important role in the manufacture of many tools, consumer products and in almost all industrial structures. Fusion welding is a significant engineering process because of the unparallelled advantages it has over other joining methods and it is used extensively in the construction of a gas pipeline network.

Unfortunately, undesirable changes to material properties can occur during welding which in stressed structures, such as gas pipelines, can precipitate disastrous economic, environmental and possibly, fatal results. These adverse effects, have stimulated a large amount of research related to pipeline welding, in order to determine instigating factors, and to control and minimise such deleterious events.

A 'weld procedure' defines all the weld process parameters which must be calculated prior to depositing a weld with the required design properties; e.g. the type of welding process, Gas Metal Arc (GMA), Manual Metal Arc (MMA), electrode type, voltage and arc current range, welding speed etc. This thesis concerns the specialised requirements

of welding procedures used on operational gas pipelines. That is on pipelines containing flowing gas or other fluids often under considerable internal pressure. Clearly such welding is potentially unsafe since it may compromise the structural integrity of the pipeline. However, it has significant economic benefits to pipeline operation. Therefore, in particular, this work addresses the development of computerised process simulations to improve selection and development of safe in-service welding procedures. These special in-service welding procedures are applied to pipelines which are in continuous operational service. Due to these unique conditions, in-service welds and welding procedures have particularly demanding requirements.

## 1.2 Industrial significance of in-service welding

In-service welding is used as part of a pipeline construction technique referred to as 'Hot-Tapping', a procedure which enables the connection of a branch pipe to a pipeline without stopping or significantly disrupting the gas flow. The major advantage of hot-tapping is that it avoids the need to decommission the pipeline, which would be costly to the pipeline operator both in terms of wasted gas and in un-serviced customers. In a simplified hot-tap, a pipe sleeve is initially welded to the live pipe, and a slide valve is attached to the sleeve, see Figure 1.1(a). The hot-tap drill is then fitted to the valve, see Figure 1.1(b). Next, the drill is used to cut a hole in the wall of the pipe, see Figure 1.1(c). As the drill is extracted it carries with it the cut-out or coupon, see Figure 1.1(d). Finally the valve is closed allowing the drill assembly to be removed, see Figure 1.1(e). The success of the operation depends critically on the ability to weld the valve assembly or sleeve fitting onto the live pipeline.

The two major problems to in-service welding are:

- potential fracture in the heat affected zone (HAZ) encouraged by high hardness resulting from the high weld cooling rates generated by high gas flow

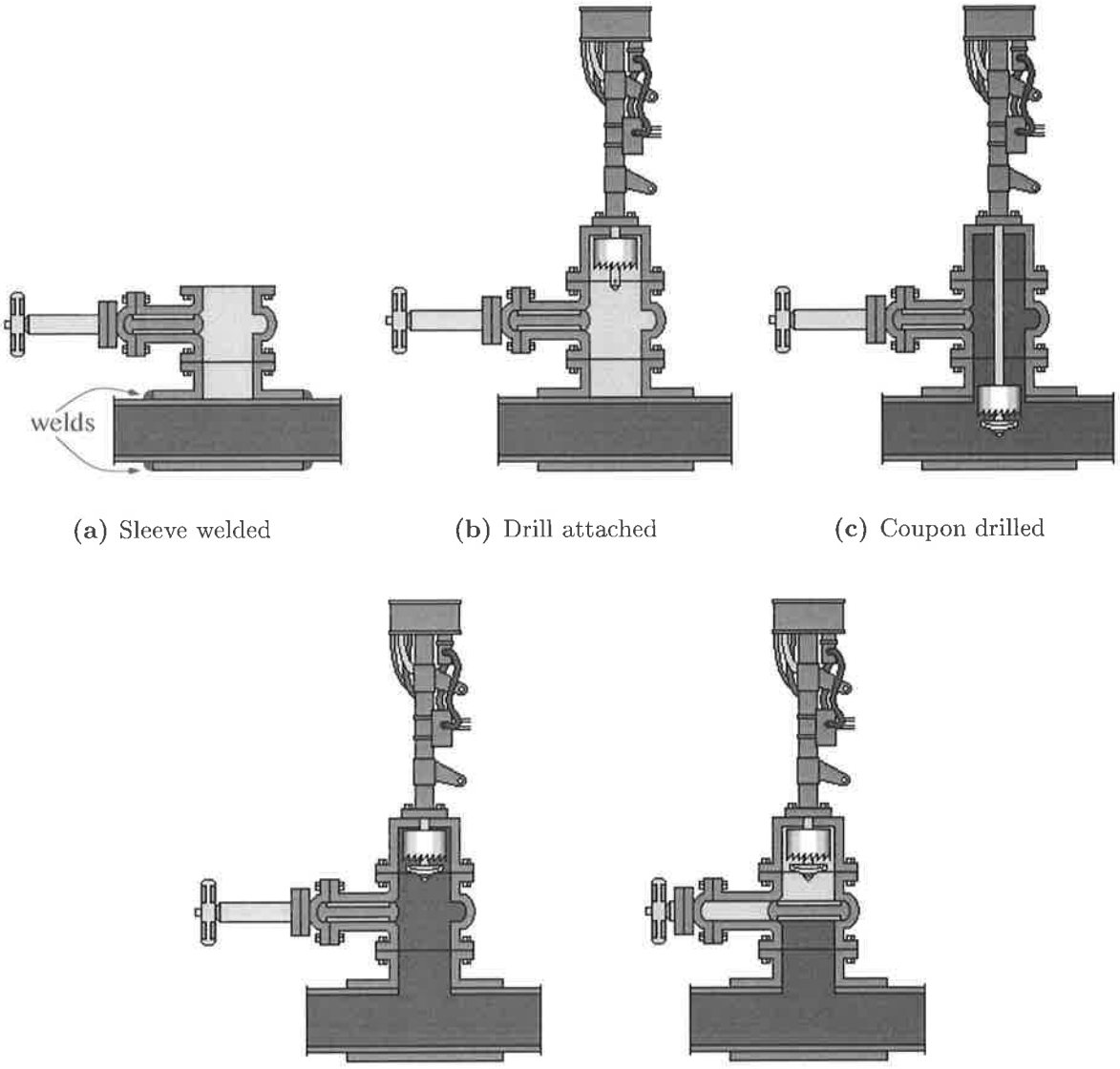


(a) Sleeve welded

(b) Drill attached

(c) Coupon drilled

(d) Coupon extracted, Valve closed

(e) Drill removed

**Figure 1.1:** A schematic illustration of the Hot-Tap process [44]

- the weakening of the pipe wall during welding which may lead to wall rupture or a phenomena termed 'burnthrough'.

Due to the difficulties associated with the welding operation, many in-service welds are currently deposited under conservative conditions. These conservative conditions are achieved by reducing the pipeline gas pressure and/or gas flow-rate, which has a significant impact on normal pipeline operation. Venton [81] (1996) estimates that lost gas and curtailment costs associated with such planned hot-taps in Australia from 1998-2002 to be approximately $4M. Further, as methane is a greenhouse gas, purging and venting pipelines of gas is potentially hazardous to the environment. TransCanada Pipelines Ltd [79] (1998), estimates that their use of hot-tapping will avoid an annual emission of 603 kTonne of carbon dioxide equivalent in 1999 and 2000. According to TransCanada's greenhouse gas management program, the avoidance of emissions through hot-tapping, represents a reduction of approximately 18% of the total emissions.

In-service welding is also used as a technique for pipeline maintenance: e.g. to weld circumferential sleeves at points of pipeline damage. Moreover, it has also been suggested, that weld deposits made directly on to a pipeline could be used to replenish pipe wall thickness that was lost by corrosion [16]. The success and safety of such operations critically depends on a comprehensive understanding of the controlling variables and on controlled and effective in-service welding procedures.

There are a number of different joint configurations used by the pipeline industry which require individual analysis. Broadly, Australian hot-tap fittings can be classified under three types:

- direct branch with reinforcement saddle (Figure 1.2(a))
- direct branch to pipe weld (Figure 1.2(b))
- circumferential sleeve fitting (Figure 1.2(c)).

**(a)** Reinforcing saddle

**(b)** Direct branch on pipe

**(c)** Full encirclement sleeve

**Figure 1.2:** Hot-tap joint types.

## 1.3 Technical challenges to in-service welding

The high gas flow within the pipe (up to $15m/s$) causes the weld to cool rapidly on account of the convective transfer of heat from the pipe wall to the flowing gas. The increased weld cooling rate results in greater hardness levels, within the weld, and in the surrounding HAZ. The increased hardness of the microstructure in the HAZ leads to increased possibility of hydrogen assisted cracking. The conditions needed for hydrogen assisted cracking include, hydrogen being present to a sufficient degree, tensile stresses acting on the weld, and a susceptible, hard, HAZ microstructure [14].

The second problem concerns the risk of pipe wall failure during welding. Pressurised natural gas (up to $10-15MPa$) causes a significant stress on the pipe wall. A possibility of pipe wall failure exists when the strength of the pipe is diminished by the localised heating during a welding procedure. The result can vary from the relatively innocuous to the highly deleterious, from a small localised 'bulging' (Figure 1.3(a)) of the pipe wall, to the bursting of the pipe. That extreme event is termed burnthrough (Figure 1.3(b)); it occurs when the region around the weld pool has insufficient strength to withstand the internal gas pressure.

The recent development in the manufacture of high yield strength controlled rolled micro-alloyed steels has allowed thinner steel pipes to have the same load capacity as the earlier low strength thicker pipes. The Australian Pipeline Standard AS 2885, designates that the maximum pressure allowed (maximum allowable operating pressure or MAOP) for pipeline design is one giving a hoop stress equal to 72% of the yield strength. That is:

$$\frac{PD}{2T_w} = 0.72\sigma_y \tag{1.1}$$

where P is the pipe pressure ($MPa$), D is the diameter of the pipe ($mm$), $T_w$ is the pipe wall thickness ($mm$) and $\sigma_y$ is the yield strength ($MPa$). Since the pipe wall thickness is inversely proportional to yield strength, for a given gas pressure and pipe diameter, the mass of pipe material required for the manufacture of a certain length of pipe is

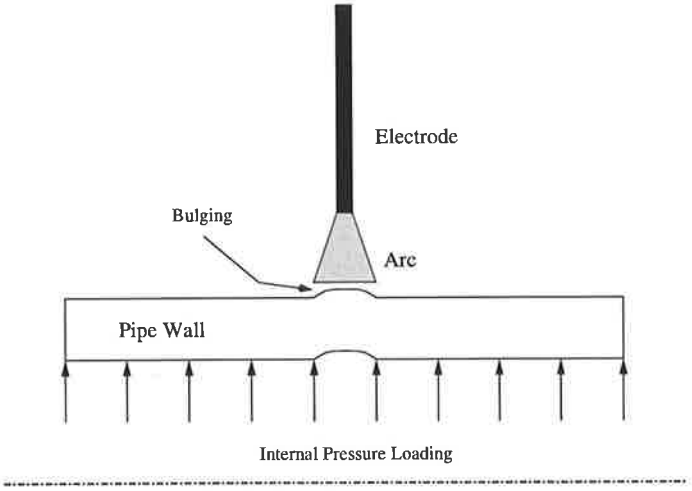


(a) Bulging

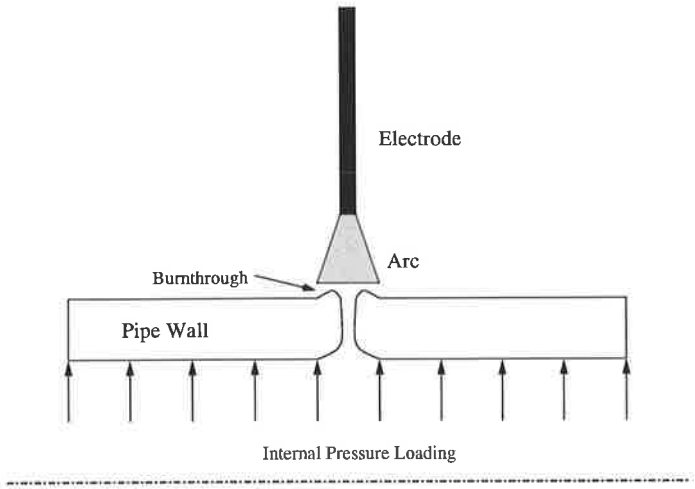


(b) Burnthrough

**Figure 1.3:** Types of pipe wall failure due to in-service welding.

significantly reduced, when material of high yield strength is used. Alternatively, using high yield strength pipe permits the transmission of natural gas at higher pressures and flow rates. The Australian Pipeline Industry clearly realises the economic advantages of using high strength steels. However, the drawback is that the use of thin-walled high strength steel pipelines exacerbates the above stated difficulties associated with in-service welding. With the combination of enhanced gas transmission and diminished pipe wall thickness, the weld cooling rate increases for a given weld procedure. High strength steels also have a greater sensitivity to strength reduction during welding. Consequently high

strength steels with the decreased wall thickness, are more prone to bulging or pipe wall failure.

## 1.4 Research strategy

Presently, the development of a weld procedure for in-service welding is essentially a trial and error process. For example, take the case of a hypothetical structure that requires a weld with predefined mechanical properties. Through experimental welding trials, involving welding on a replica or similar structure, many different weld procedures are tested and the one with the closest properties to those desired is chosen; and finally replicated in the field. Often weld procedures are set by standards based on past welding trials and as a result they lack a rigorous scientific footing.

The cost of establishing such a weld procedure can be large. In relation to hot-tap welding, the majority of research has involved welding trials either using a 'flow-loop' (a diversion adjacent to an operating pipeline which allows welding trials to be performed on a test section of pipe without disruption to the existing pipeline), or using a laboratory simulation. In the laboratory, test pipes cooled with water or oil have been used to simulate heat loss due to gas flow. The details of the past experimental approach and their significant limitations will be discussed later.

In brief, duplicating the convective heat transfer characteristics of natural gas under pipeline transmission flow conditions using water as the medium has proven to be difficult. When water is used in a laboratory welding simulation (with identical flow-rate as natural gas albeit different pressure) heat is removed at a faster rate than as with natural gas. An attempt to decrease the flow-rate of water causes it to boil; this is unwanted, as the effect of fluid phase transformation is not present in the in-service welding of natural gas pipelines.

Welding trials involving laboratory simulations address only part of the problem. Lab-

oratory trials examine the required penetration, bead shape and HAZ hardness but fail to consider pipe wall failure as such trials are usually unpressurised. In the laboratory it is difficult to safely replicate the magnitude of gas pressure found during in-service. To consider the risk of pipe wall failure associated with welding on pressurised pipe, additional trials are required. Some of the past tests have used pressurised non-flowing gas, which again is a compromise to the real pipeline conditions as the effect of accelerated cooling is not present in these tests. Due to the expense and time-consuming nature with such an experimental approach, there is a tendency to only examine a limited range of parameters. The result of such experiments is a lack of understanding of the sensitivity of the process to slight variation in welding parameters. Welding trials may not establish how close a particular weld is to the failure limit. Lack of knowledge about process sensitivity causes the welding trial to be both unreliable and unstable. The economic cost of performing in-service welding trials to an acceptable degree of accuracy is prohibitive.

The inherent difficulties with such an experimental approach, has shifted the focus of researchers to consider the development of a numerical approach, whereby temperatures and cooling rates are calculated using a thermal analysis. There are a number of significant advantages to be had by developing numerical simulations of in-service welding. Firstly, numerical modelling would avoid or minimise the use of time-consuming experimentation. Secondly, the wide range of fittings and pipe geometry that are used in in-service welding do not present a significant problem to numerical modelling, whereas in experimental methods they represent a significant additional variability. Similarly, the variation of gas flows and pressures could be economically dealt with. To date only two-dimensional models have been considered and these have only considered pipe wall failure in a simple fashion, suggesting that pipe wall failure is signified by an upper limit to the pipe wall temperature.

This thesis has focused on the development of 3D numerical models of in-service welding using the Finite Element Method. From the 3D numerical models of in-service welding, estimates of weld cooling rates are calculated from the predicted thermal histories. Link-

ing data from such thermal models to appropriate empirical equations relating hardness and cooling rate, the HAZ hardness can be calculated. The risk of pipe wall failure can also be assessed from the calculated thermal histories. Pipe wall failure analysis has been examined by performing an elastic-plastic stress analysis with the calculated temperature field. Such elastic-plastic stress analysis, while accurate, require considerable amounts of CPU time. New methods of predicting pipe wall failure from the calculated thermal histories alone are discussed within this thesis. The significant parameters which determine pipe wall failure according to the formulated model are: thermal field and its distribution, pipe wall thickness, internal gas pressure, and weld orientation.

Predominantly, the full encirclement sleeve is chosen for hot-tapping as it provides the best structural support to the pipe and attachments. This type of fitting is comprised of two sections: a lower and upper section which are then joined longitudinally when clamped onto the pipe. When joining the two halves together, usually by MMA welding, a backing bar or metal strip is placed between the fitting and the pipe to stop any penetration. Therefore, this longitudinal weld is not considered to be critical since it does not directly penetrate the pipe wall. The next step in joining the fitting to the pipe is to weld the ends of the fitting to the pipe. A circumferential fillet weld achieves this task. When hot-tapping thicker pipelines, the direct branch on pipe or reinforcing saddle fittings are more commonly used. This thesis focuses on in-service welding of circumferential sleeve fittings, however the analysis techniques developed are applicable to any type of joint.

The welding process commonly used for in-service welding in Australia is MMA welding, as seen in Figure 1.4, using hydrogen controlled electrodes. Unlike other welding processes, MMA welding requires relatively little equipment (power supply + stick electrode) and is the traditional process for in-field pipeline welding. The source of heat for MMA welding is provided by an electric arc between the electrode and the pipe. The electrode consists of a core of filler wire surrounded by a flux coating, comprising metal oxides and silicates. During welding the flux melts to form a slag which provides a protective layer between the molten metal and the atmosphere. The electrode melts and

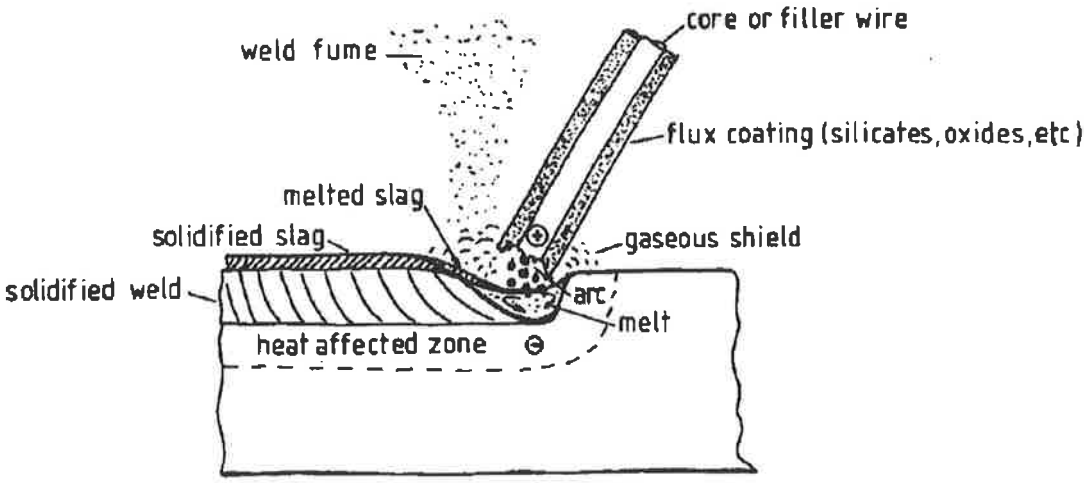


**Figure 1.4:** Schematic illustration of Manual Metal Arc Welding (MMAW).

droplets of molten metal are transferred across the arc into the weld pool.

Although there is a large body of work on numerical modelling of fusion welding, there is little specifically addressing MMA welding using low-hydrogen electrodes. This thesis addresses that deficiency, in particular it will consider appropriate modelling strategies to represent out of position, vertically-up or vertically-down MMA welding.

The developed models have been validated by comparing predicted values with:

- published weld cooling rate data for simulated and real in-service welds
- experiments involving welding on an un-cooled, unpressurised pipe
- experiments involving welding on a pressurised pipe with flowing gas.

The results of the thermal analysis have been compared with micrographs of test welds to ensure the correct calculation of HAZ and fusion zone geometry. Similarly, weld cooling rates predicted from the thermal models were compared with those recorded from experiments.

The validation of the proposed pipe wall failure model required a qualitative approach; simply because the amount of published information relating to pipe wall failure is small

and facilities to generate such data were not available. Moreover, research work undertaken by Bruce [13] (2001) involving welding onto a pressurised pipe until burnthrough is unavailable due to confidentiality. The proposed pipe wall failure models were compared with predictions using thermo-elastic-plastic finite element models, and some work reported earlier on remote longitudinal welding onto a statically pressurised pipe. In addition, the term pipe wall failure is also explored and as a result, a few different definitions are presented. The proposed pipe wall failure model calculates the maximum pressure at which safe welding can be deposited for a given weld procedure.

It is anticipated that through the development of improved numerical simulations of in-service welding and the establishment of their accuracy, scientific credibility will result in improved methods of weld procedure development. These numerical models will also allow an alternative method for determining safe pressures and appropriate gas flows for a given welding process; which will facilitate the efficient and effective management of hot-tapping and in-service welding procedures.

# Chapter 2

# Literature review

## 2.1 Introduction

The literature related to in-service welding can be considered in the following areas,

- experiment based research in in-service weld procedure qualification
- experiment based research into pipe-wall failure due to in-service welding and in-service weld repair
- research into numerical modelling of welding processes in general
- numerical modelling of in-service welding and its application.

A search of in-service welding related literature, indicated a short supply of published research and information. The majority of work related to in-service welding has been undertaken by 'Edison Welding Institute' (EWI) and and 'Battelle Memorial Institute' (BMI), largely under the sponsorship of the Pipeline Research Committee of the American Gas Association. The results of their work form the basis of the methodology commonly used to define appropriate in-service welding procedures. However, due to commercial sensitivity, restrictions have been placed on the availability of published data from EWI and BMI.

The literature review is split into two sections. The first section will examine literature from the experiment based work. The areas of post-weld hardness and the possibility of pipe wall failure during in-service welding will be the main areas of focus.

The second section will initially examine work related to the numerical simulation of in-service welding. Next, the Battelle software package developed to aid weld procedure development will be examined. Later, a broader insight into the numerical modelling of welding in general will be given. That critical examination will result in a strategy for the modelling of in-service welding. That strategy will aid in the weld procedure qualification of in-service welding, ensuring safe and effective in-service welds.

## 2.2 In-service welding

### 2.2.1 Post-weld hardness

In carbon steels, the deposition of welds with smaller fillet sizes increases the risk of cracking due to the reduction in heat input, and corresponding increase in cooling rate. Graville & Read [36] (1974) investigated the relationship between fillet weld size and cracking to determine the size of the smallest fillet weld that can be deposited without cracking. The authors cited work by Bailey [2], that for both low hydrogen and rutile electrodes identified, a critical HAZ hardness level of $350HV$ below which HAZ cracking did not occur. However, Graville & Read discovered that the electrodes which were used by Bailey had contained hydrogen levels which would normally be considered high. This finding suggests that the limit of $350HV$ is somewhat conservative. It is arguable that a greater hardness level criteria should be applied to in-service welding, which uses low hydrogen electrodes. However to date because of uncertainty and need for low risk in-service welding, this limit has become the accepted standard.

Cassie [17] (1974) undertook a study to examine the effects which influence hardness from in-service welding. Cassie argued that in a complete weld, not all of the HAZ

remains at the same hardness level. Commonly, the hot-tapping joint requires multipass welds to be deposited; the tempering effects of the subsequent weld passes on the HAZ is significant. The part of the HAZ which has had further welds deposited on top of it usually has a lower hardness value due to the extra heating and cooling by the subsequent runs. The 'toe' of the weld which is not tempered contains the highest hardness, as indicated in Figure 2.1.

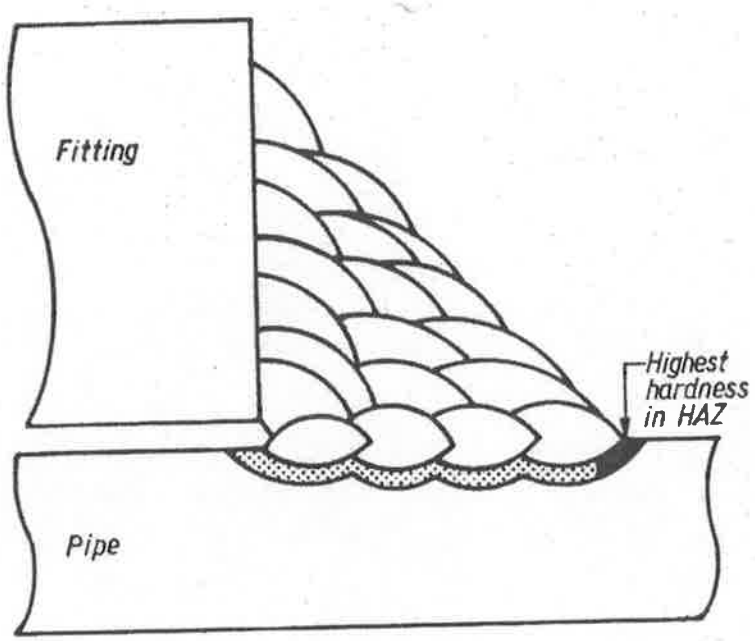


**Figure 2.1:** Highest region of hardness at the toe of the weld.

Preliminary experiments relating to post-weld hardness were conducted to study the effects of welding parameters on hardness. The experiments involved welding onto segments of pipe which were artificially cooled; solid carbon dioxide was added to methylated spirits and then allowed to flow around the inside of the pipe wall. The carbon equivalent of the pipe, calculated using Equation 2.1, was $CE = 0.47$ and was thought at the time to be a grade of pipe which was susceptible to cracking.

$$CE_{IIW} = \%C + \frac{\%Mn}{6} + \frac{\%Cr + \%Mo + \%V}{5} + \frac{\%Ni + \%Cu}{15} \tag{2.1}$$

In these experiments, welds were deposited using various combinations of preheat, postheat, bead deposition technique and welding directions (i.e. vertical up or vertical down weld-

ing). The preliminary experiments, revealed that using larger diameter electrodes created hardness which was marginally lower, than that achieved with smaller diameter electrodes. Cassie also found that preheating was effective in reducing the level of hardness. Furthermore, postheating was found to be effective at reducing hardness. Cassie recommended the use of heat from a Gas Tungsten Arc (GTA) torch applied to the toe of the weld once welding had been completed.

Experiments involving flowing gas were also conducted by Cassie using a flow-loop facility. Three pipes each of $220mm$ diameter were joined in series and then connected to the flow-loop facility. Natural gas at various pressures and flow-rates up to a maximum of $17,000m^3/hr$ and $5.5MPa$ were passed through the test loop while welding was simultaneously performed. A series of welds, with various values for heat input, preheat, and different weld procedures, were deposited to study the effects of these variables and welding parameters on weld hardness. The composition of the pipes varied from $CE = 0.25$ to $CE = 0.48$. Cassie concluded that weld composition and hardness were related. Moreover, when depositing identical welds on pipes of different compositions, hardness was noted to increase with increasing carbon equivalent. Cassie also concluded, as earlier experiments suggested, that preheating was an effective method of reducing post-weld hardness levels. An interesting observation by Cassie was that major variations in weld hardness were found when welding was carried out by individual welders; in some cases the variation went up to $50HV$. The authors suggested that the difference was principally due to travel speed, and that on pipes of wall thickness less than $5mm$, a minimum welding speed of $3.2mm/s$ was recommended. The order in which weld beads were deposited also affected hardness, and the results from the experiments are shown in Figure 2.2.

To study the effects of gas flow rates and preheat on hardness, De Hertogh & Illeghems [23] (1974) conducted experiments on a flow-loop facility. The electrodes were semi-volatile rutile type, AWS 7014 - NBN 63 R (100), of $2.5mm$ diameter. The welds were deposited in the vertical down manner with DC positive polarity and a welding speed of $2.5mm/s$. The authors studied the effects of varying levels of preheat, namely 50, 75,

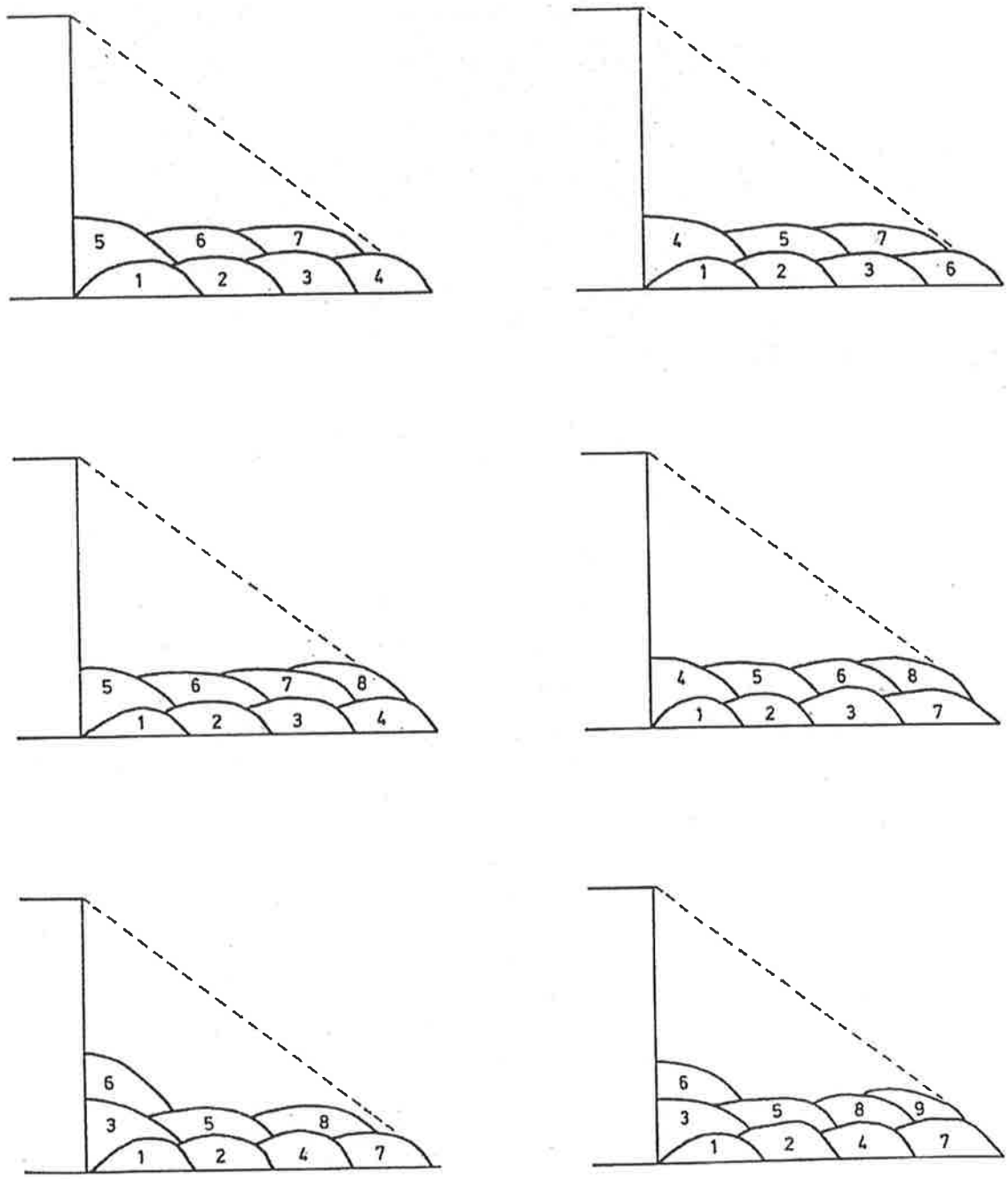


**Figure 2.2:** Different weld sequences attempted by Cassie [17].

$100°C$ and nil preheating. The authors found the size of the HAZ was related to the level of preheat, and as preheat temperatures decreased, the size of the HAZ decreased. The authors noted that in their tests, a preheat temperature of $80°C$ resulted in a drop of 50HV5 hardness.

Rietjens [70] (1986) suggests applying a 'temper bead' technique to minimise the

hardness in the HAZ. The temper bead technique, seen in Figure 2.2, utilises an additional weld pass to effectively apply heat treatment to an existing weld pass, and reduce the HAZ hardness. Knowing the position and heat input for the temper-bead technique is then a matter of experience.

A major problem with welding on operational pipelines is determining a welding procedure which achieves a satisfactory hardness under the accelerated cooling conditions generated by the pipe contents. Such cooling varies with pipe contents and operational conditions; e.g. pressure and flow rate. Cola & Threadgill [21] (1998) proposed a method to correlate the heat sink capacity, that is the ability of an operating pipeline to conduct heat away, to the cooling characteristics of the weld for a given heat input. This procedure is now known as the 'EWI Method'; the basis of it is to relate a given set of welding parameters including consumable type, the rate at which the pipe can extract heat and the susceptibility of the weld to cracking. The EWI method was devised to be a field usable, practical, empirical approach.

The cooling capacity of the pipe was measured by heating a $50mm$ diameter circle on the surface of the pipe with a gas torch to approximately $300°C$. The cooling rate was measured by the time taken for the centre of the circle to fall in temperature from 250 to $100°C$, and is denoted $t_{2.5/1}$ .

In developing the EWI method, extensive experiments were conducted in the laboratory. The laboratory tests were designed to simulate branch welds and sleeve welds. Branch on pipe welds were deposited manually while circumferential fillet welds were deposited automatically. All welds were deposited in the flat position and the parent plate was cooled artificially by either spraying water or compressed air onto the back of the weld. The heat sink capacity, or $t_{2.5/1}$ of the laboratory trials were measured, and the cooling rate was adjusted so that the laboratory and field cooling capacity were identical.

A total of 8 pipeline steels were tested with carbon equivalent ranging from 0.370 to 0.504. The consumables tested were E7018 basic electrodes of 3.2 and $4.0mm$ diameter, and E6010 and E8010 cellulosic electrodes at 3.2 and 4.0mm diameter.

The results of the laboratory experiments, revealed that when depositing welds with E6010 and E8010 electrodes with a heat input of $1kJ/mm$, cracking had occurred in all but the lowest carbon equivalent steel tested. Welding with $2kJ/mm$ heat input and E8010 electrodes had also induced cracking in all materials except for the steel with the lowest carbon equivalent. However, welds deposited with E7018 electrodes at both 1 and $2kJ/mm$ had only induced cracking in welds deposited on steels with the highest carbon equivalent. The results suggested that cracking is less prevalent in basic electrodes than in cellulosic electrodes. The authors concluded that when welding with basic electrodes, the risk of cracking is largely due to the HAZ hardness. The authors noted that very few instances of cracking had occurred in welds with HAZ hardness below 400HV. Comparing these findings with earlier work by Graville & Read [36] (1974), a critical hardness limit of 400HV is likely to be a safe, conservative upper limit, to avoid HAZ cracking, when depositing welds with MMA low hydrogen electrodes.

A set of field trials were conducted using a natural gas flow-loop. The test section comprised of three sections of line pipe, of unknown composition, welded end-to-end and placed in line in the test loop. The wall thickness of the test section were 4.8, 6.4 and 11mm. The flow-rate of natural gas was varied from 47.0 to $417.0mcf/d$, while the pressure was kept constant at $3.3MPa$. Fillet welds were deposited using both E6010 and E7018 electrodes, while the heat input was kept at $1kJ/mm$. The thermal cycle data was recorded by plunging thermocouples into the weld pool. The heat-sink capacity of each pipe was determined by measuring the $t_{2.5/1}$ cooling time.

A correlation between the measured weld cooling rate, $t_{8/5}$ , or time taken for the weld to cool from 800 to $500°C$, and $t_{2.5/1}$ , was then established for the field trials. The authors argued that although the data displayed a fair degree of scatter, it was not unexpected. The authors concluded that as the welds were deposited manually, variations in both the mean heat input over the length of the weld, and the instantaneous heat input at any point in time are probable.

Simulating the thermal conditions in the laboratory is a challenging task. The results

from an investigation by Bruce [12] (1994) found that care must be taken in the choice of fluid for a laboratory simulation. Bruce investigated the possibility of using flowing air, motor oil and water to simulate in-service welding. He concluded that the use of water as a cooling medium should be restricted to pipes of medium to heavy section, while motor oil should be used for thinner wall pipelines at low flow rates. In cases where even less cooling was required, the use of flowing air was recommended.

An interesting observation made by Bruce was that when either forced air or motor oil was used as the cooling fluid for laboratory tests, the weld cooling rate was found to increase as the wall thickness was increased for a given heat input. A possible explanation is that a greater proportion of heat was conducted away through the pipe wall rather than through the pipe wall by conduction and away due to the fluid by convection.

A similar observation was found when using water as the cooling fluid. For a given heat input, initially, decreasing the wall thickness from $12.7mm$ was accompanied by a reduction in weld cooling rate. After a certain critical thickness, further reduction in pipe wall thickness would result in an increasing weld cooling rate. A possible explanation is that when the pipe wall thickness is relatively heavy in section, the predominant method of heat transfer is through the cross-section of the pipe. Reducing the wall thickness results in lower cooling rate as the reduced wall thickness effectively forms an insulating layer. Once the proximity between the surface of the pipe and the cooling fluid is reached, at a certain low wall thickness, the predominant heat transfer mechanism is convection from the inside of the pipe wall.

#### 2.2.1.1 Summary & gaps in knowledge

Based on the available literature on empirical studies of in-service welding, the parameters which influence post-weld hardness are shown in Figure 2.3. The weld process parameters, especially heat input largely control the amount of heat which is applied when welding. To a lesser extent, electrode polarity as reported by Boran [7] was found to influence post-weld hardness. The polarity influenced the apportionment of heat between the electrode

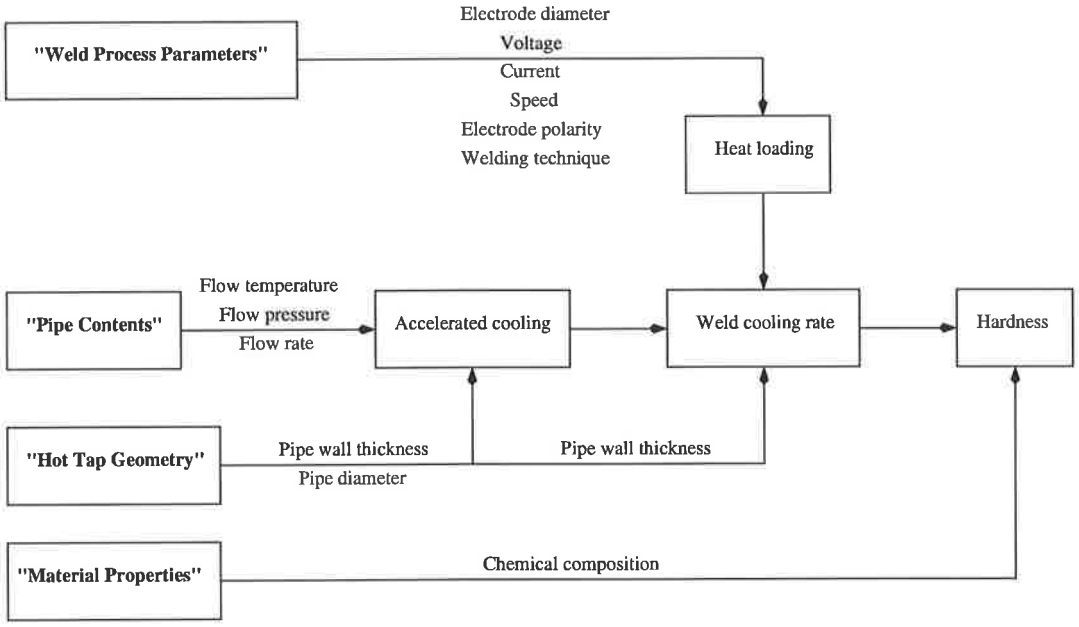


**Figure 2.3:** Parameters which influence post-weld hardness.

and the workpiece. DC electrode negative polarity (DCEN) gives the greater proportion of heat to the weld region, which reduces the weld cooling rate and gives the least post weld hardness for a given heat input.

Novel methods of avoiding excessively hard microstructures include the application of multi-pass weld sequencing, postheat and preheat. Weld sequencing was found to be advantageous as previously deposited welds were tempered by the heat from the newly deposited weld. Preheating was found to increase weld cooling times, although the application of preheat is seen to be difficult on account of the heat conducted through pipe wall thickness and away by convection due to the flowing pressurised natural gas. Moreover, the position and level of heat for temper beads needs to be reasonably accurate, if its heat is to be sufficient to temper the HAZ.

The effect of the fluid on weld cooling rates was only indirectly studied by Bruce, Cassie, and Cola & Threadgill; while to a lesser extent by De Hertogh & Illeghems. Moreover, empirical relationships of cooling rates and hardness developed to date do not include the effects of fluid temperature, pressure and flow rate. The effect of these parameters on convective heat transfer is significant [42]. Similarly, the intrinsic relationship

between pipe diameter and flow behaviour and ultimately convective heat transfer, has not been studied or included in the empirical models to date.

While the development of empirical cooling rate models include heat input, to date the effects of arc current and voltage on in-service welding, has not been incorporated into such models, although Cassie [17] (1974) highlighted the effect of electrode diameter, or current in a MMA weld, on post-weld hardness. Two welds deposited with identical heat input can have different fusion and HAZ shapes. Arc current and voltage significantly influence the heat transfer form the arc to the weldment [74], which in turn influences the fusion zone shape, and ultimately the HAZ.

To date, the development of cooling rate and hardness models has largely occurred in laboratory simulations or field experiments. A significant problem with laboratory simulations or weld procedure development of in-service welding using either oil or water is that the possibility of boiling is largely ignored. The EWI method dictates the flow rate of the laboratory tests so that the EWI cooling time, $t_{2.5/1}$ , for the laboratory trial is identical to that found in the field. When using oil or water for the laboratory trial, boiling of either fluid is rare for the wall temperatures attained during the EWI test. However, once weld procedure development is begun, the wall temperature at the inside surface of the laboratory test pipe is significantly higher and has the potential to boil the fluid. If boiling were to occur, the weld cooling rate would be higher due to the phase change occurring for the fluid [42]. In turn, further weld procedure development would involve increasing heat input to lower the weld cooling rate if a excessively hard microstructure were found. However, once the given weld procedure is implemented on the live natural gas pipeline, the added heat transfer of boiling does not occur and therefore higher wall temperature than expected may arise, therefore increasing the risk of burnthrough. Finally, the problem common to all field developed in-service welding models is a limited domain in which accurate results can be calculated. The models developed so far largely use interpolation of a field derived data set to calculate cooling rates and hardness. If a weld is outside this domain, accuracy is then compromised.

### 2.2.2 Burnthrough

Cassie [17] (1974) attempted preliminary tests to determine the level of weld penetration for various electrodes. The welds were deposited in a bead on plate manner, while the electrodes types tested were cellulosic, rutile, and basic. The welding positions were flat, vertical up, vertical down and overhead. The authors initial conclusion was that the least amount of penetration had occurred when welding in the vertical down position with either rutile or basic electrodes.

A second set of experiments was attempted to determine the effects of internal pressure on circumferential welds deposited on a pressurised pipe. The welding was performed using an automatic autogenous GTA welding torch located on top of a rotating pipe. The pipe was $150mm$ in diameter and $4.2mm$ in wall thickness. The pipe was internally pressurised to $14.5MPa$ to give a hoop stress of 72% of the yield strength of the pipe. The welding took place remotely inside a contained blast-proof test cell. Cassie increased the welding heat input on successive runs until failure had occurred. He observed that the failure occurred due to the internal pressure blowing the molten weld metal out of the pool. A small pinhole was observed at the deepest point of the remaining crater. From these preliminary experiments, Cassie concluded that the primary factor influencing burnthrough was heat input.

The next series of experiments involved welding onto a rotating pipe with the MMA welding process. Cassie decided for safety reasons that the welding was to be remotely controlled, and assembled a device to automatically feed the electrodes under gravity. Arc initiation was assisted by initially placing a ball of steel wool between the electrode and pipe. The aim of the experiments was to determine if the type of electrodes, diameter of the electrodes, the electrode polarity or the application of preheat, had any effect on the possibility of burnthrough. The test pipe was $450mm$ in diameter and $6.4mm$ in wall thickness. The pipe was internally pressurised to over $7MPa$, to give a hoop stress of 72% of the yield strength of the pipe. Cassie realised that the gravity fed, remotely controlled MMA process in this test was very different to the manually deposited welds experienced

in the field, and also included a set of welds deposited by an operator, but under reduced pressure, $0.35MPa$, for safety reasons.

Cassie briefly concluded, that for safe welding, basic coated electrodes using DCEN polarity, should be chosen over rutile or cellulosic electrodes. In addition, the basic coated electrodes should be used in the vertical downwards position along with the use of a buttering layer. Moreover, a buttering layer was recommended to be deposited in any instance. The authors also reported that the risk of burnthrough was highly dependent on welding current when welding on pipes with wall thicknesses below $5mm$.

De Hertogh & Illeghems [23] (1974) reported on tests involving welding onto pipe, API5L-X60 grade, $273mm$ diameter, $4.37mm$ in wall thickness, pressurised internally with nitrogen at pressures of 3.9, 4.9 and $6.1MPa$. The authors noted that considerable plastic distortion occurred in the fusion zone at pressures greater than $4.9MPa$. However, a further set of experiments under similar pressures and weld conditions, on thicker pipe did not result in any plastic distortion.

Phelps et al. [68] (1976) undertook experiments to investigate the sensitivity of burnthrough to welding parameters. An initial set of experiments involved autogenous GTA welding on a pressurised pipe in a reinforced concrete test cell; similar in concept to experiments by Cassie [17]. An API 5L X52 grade pipe of $168mm$ diameter and $4.2mm$ wall thickness was internally pressurised with nitrogen, which sat beneath a stationary GTA welding torch. The pipe was internally pressurised to $14.5MPa$ which gave a hoop stress in the pipe of 72% of the yield strength of the pipe ($390MN/m^2$). The welding speed was $2.97mm/s$ while the welding current was varied from 110 and 300A. The experiments revealed that pipe wall failure had occurred at welding currents of 250, 260 and $300A$. While the aforementioned welding currents were for the GTA process, the authors determined a corresponding set of welding parameters for the MMA process. The values for failure due to MMA electrodes were either 175A/32V or 200A/25V at identical welding speeds mentioned earlier. However, the values proposed for the MMA welding process should only be considered as an estimate. The relationship between GTA welding and

MMA welding heat input was established simply on the arc efficiencies of each welding process.

The authors also performed tests to determine the relationship between electrode diameter and weld penetration. They concluded that welding current played an important role in penetration, and that larger diameter electrodes in general gave greater levels of penetration. Similar tests on the effect of electrode polarity on penetration revealed that welding with negative polarity gave less penetration than positive polarity.

A final set of pipe wall failure experiments involved welding onto pressurised pipe with MMA electrodes; internal pressures were as high as $7MPa$. The authors found that there wasn't any obvious relationship between penetration and internal pressure. However, the authors noticed that there existed greater weld penetration at the 6 o'clock position than the 3 o'clock position.

Investigations undertaken by Wade [84] (1978) primarily focused on the relationship between welding heat input, internal gas pressure and wall thickness. The work was restricted to only one type of pipe material, API 5LX60 with a nominal wall thickness of $9mm$ and a diameter of $300mm$. Wall thicknesses of $3mm$, $5mm$, $6mm$ were investigated by machining the $9mm$ pipe. Welds were deposited in the longitudinal direction with target heat inputs of 1.0, 1.2, 1.4, 1.6 and $1.8kJ/mm$. The electrodes used in the test were $ASB130 - E6027$ with diameters 4.5, $3.25mm$, and a low hydrogen electrode complying with $ASB130 - E6027$ with a diameter of 3.25mm.

Wade defined a burnthrough failure if a bulge had formed in the weld zone which exceeded $1.0mm$ in height. A set of preliminary tests had revealed that burnthrough had occurred in material $3mm$ in wall thickness, but at an arc energy of $0.8kJ/mm$ when subjected to pressures of only $0.3MPa$; further testing at this thickness was discontinued. 'Blowout', the expulsion of the weld pool by the pressurised gas due to a perforation of the pipe wall, had only occurred in three instances, when penetration of the pipe wall was either complete or almost complete. Wade concluded that blowout was a failure mechanism which should not be seriously considered, as careful procedure development

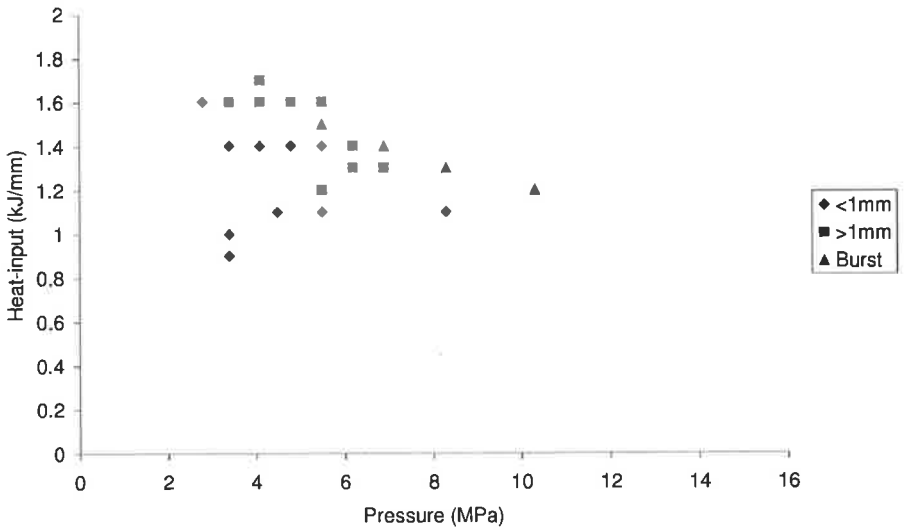


(a) $5mm$

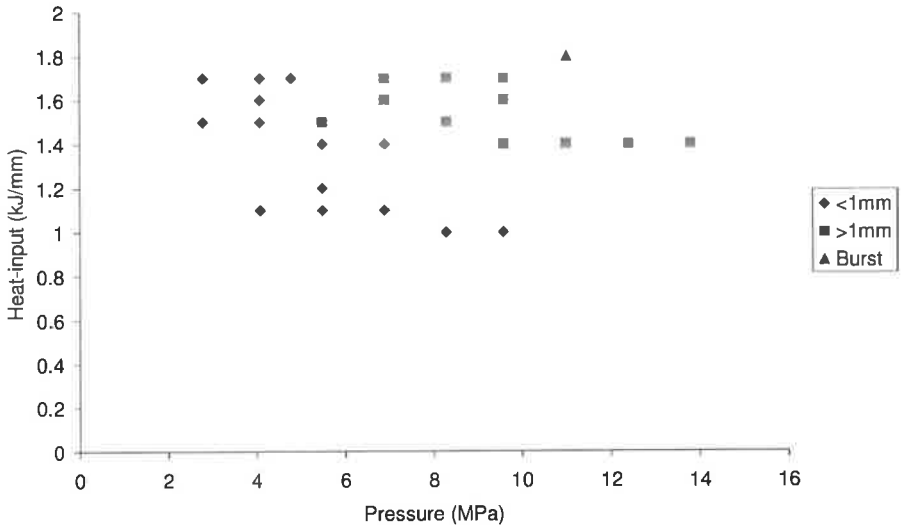


(b) $6mm$

**Figure 2.4:** Results of burnthrough tests on 5 and $6mm$ wall thickness pipe.

would lead to other modes of failure instead.

The results from work by Wade is shown in Figure 2.4. Wade concluded that welding up to an arc energy of $1.8kJ/mm$ was possible on material of $6mm$ wall thickness with normal line pressures, or assumed to be MAOP.Moreover, Wade also concluded that when welding onto material having thickness of $5mm$, considerable restriction should be placed on heat input (less than $1.4kJ/mm$) and pressure (below $3MPa$). Wade concluded that

burnthrough was probable for pipe with $3mm$ wall thickness even at low pressure. He also recommended that welding should be deposited using as high a welding speed as possible for any given heat input, so that the lateral spread of the temperature profile would also be reduced. Moreover, while restrictions are usually placed on the weld travel speed due to either electrode characteristics or welder capability, priority must be given to welding speed to reduce the risk of pipe wall failure. Weld weaving was also considered as a factor in pipe wall failure; minimising heat build up by minimising weld weave was also recommended. Similarly, depositing welds with short length was favoured to long weld runs.

The effect of preheat on pipe wall failure was the primary focus of additional research reported by Wade [83]. In a test setup similar to earlier experiments [84], longitudinal welds were deposited onto a pipe statically pressurised with nitrogen. Due to catastrophic failure experienced in initial investigations, the results were based on pipe with $9.5mm$ wall thickness. The welds were deposited with heat inputs of $1.5kJ/mm$ using $4.0mm$ diameter electrodes, and $1.0kJ/mm$ using $3.25mm$ diameter electrodes. Various internal pressures up to a maximum of $16MPa$ were applied while the preheating temperatures were ambient, 75 and $120^oC$.

The results showed that for any given weld heat input, the application of preheat had increased the bulge height; low heat input welds combined with low internal pressure being the exception. As expected, the rate at which the bulge height had increased, with increased preheating temperature, was greater with higher heat input welds. Wade concluded that a limit of $100^oC$ preheat was acceptable for material of $9.5mm$ wall thickness.

Hicks [41] (1983) suggested that to avoid pipe wall failure during welding, the pressure within the pipe should be limited. The author suggests applying the ASME Gas Piping Standards Committee's formula for welding on split repair sleeves on gas pipelines. The ASME formula is defined as:

$$P = \frac{2S(t-c)0.72}{D} \tag{2.2}$$

where $P$ is gas pressure, $S$ is the specified minimum yield strength of the pipe $(psi)$, $t$ is

the nominal wall thickness of the pipe ($inch$), $D$ is the nominal pipe diameter ($inch$), and $c$ is a correction factor; for which the ASME recommended a value of $3/32inch$. Hicks recommended the ASME formula as it was thought to be conservative.

The risk of pipe wall failure is of major concern when attempting to repair corrosion pits or mechanical damage in pipelines. Historically, two methods are often used to repair pipelines. The first method involves removing the section of pipe, and replacing the pipe with a new section. This method is the least attractive as it requires an active pipeline to be decommisioned, then finally purged of its contents before repair can take place; a similar situation to hot-tapping. The second option is to install a full encirclement sleeve; similar to the full encirclement sleeves used for hot-tapping. However, a new method used for the repair of corrosion in active pipelines involves the deposition of weld metal directly onto the pipe surface while the pipeline remains active. Weld metal deposition is attractive whenever the partial or full encirclement sleeve repair method is not able to be utilised.

The development of the direct deposition technique was reported by Bruce & Kiefner [16] (1993). The authors conducted experiments involving welding onto pipes which were pressurised with water and nitrogen. The pipe was $406mm$ in diameter and $6.35mm$ in wall thickness and the material grade was API 5LX-42 ERW. The experiments involving welding onto water pressurised pipes used E7018 electrodes with a diameter of $3.2mm$, and the experiments involving welding onto nitrogen pressurised pipe used E7018 electrodes with diameters of 2.0 and $2.4mm$. Sections of the pipe were machined to reduce the wall thickness; three nominal wall thickness of 3.2, 4 and $4.8mm$ were aimed for. The experiments involving water pressurisation deposited welds on three different wall thicknesses, while the nitrogen pressurisation experiment used only one wall thickness, $3.2mm$. Temperature was measured at the inside of the pipe wall using type K thermocouples. All test welds were deposited using a remotely operated mechanised welding system, with the weld deposited at the 12 o'clock location (flat position).

Test welds were deposited on water pressurised pipe under a variety of heat input

and internal pressure: target heat inputs were 0.5, 0.6, $0.9kJ/mm$ while internal pipe pressure was 1.4, 4.1 and $5.5MPa$. Burnthrough occurred when welding onto $3.2mm$ wall thickness at $0.9kJ/mm$ heat input when internally pressurised to $1.4MPa$. The remaining test welds did not give any indication of burnthrough. Each weld was then sectioned to measure HAZ width and fusion zone depth. The authors found that the weld penetration had remained the same for all levels of heat input on welds deposited on 4.0 and $4.8mm$ wall thicknesses. Moreover, for both wall thicknesses, there was very little difference in the measured penetration depth. However, for welds deposited on $3.2mm$ wall thickness, the penetration depth was found to increase with heat input.

Incipient burnthrough on $3.2mm$ wall thickness pipe was found to have occurred for a weld at a heat input of $0.6kJ/mm$ while at a internal pressure of $5.5MPa$; the fusion depth was half the wall thickness while the inside surface of the pipe had exhibited signs of melting. The authors suggested that a slightly higher heat input, or thinner wall would have resulted in burnthrough. The authors argued that the principal parameter controlling burnthrough was heat input and not internal pressure, since burnthrough had occurred for a weld deposited with 45% higher heat input but at 75% lower pressure. The authors concluded that when welding onto pressurised pipe with a wall thickness of $3.2mm$ with $3.2mm$ diameter E7018 electrodes, the maximum heat input should be $0.5kJ/mm$.

The second set of experiments involved welding onto a test cylinder pressurised with nitrogen to $2.8MPa$ using two E7018 electrodes of different diameters, 2.4 and $2.0mm$. Initially welds were deposited using $2mm$ diameter electrodes at a heat input of 0.3, 0.4 and $0.5kJ/mm$, while finally, a set of welds was deposited using $2.4mm$ diameter electrodes at a heat input of 0.5, 0.6 and $0.7kJ/mm$. Similar to the previous test, the authors sectioned the welds for metallographic examinations and measured HAZ width and weld penetration. The experiments revealed that incipient burnthrough had occurred for welds with heat inputs of 0.6 and $0.75kJ/mm$.

Based on the results of both experiments, the authors concluded that the main factor

influencing burnthrough was heat input. The authors concluded that welding was permissible on remaining wall thickness as low as $3.2mm$, in combination with internal pressures up to $5.5MPa$; so long as the given heat input was unlikely to cause total wall thickness penetration.

Interestingly, the authors also noted the importance of the electrode diameter on burnthrough. They argued that using smaller diameter electrodes permitted welding with higher heat inputs for a given remaining wall thickness, than comparatively with larger diameter electrodes. For example, a test weld deposited using a $2.4mm$ diameter electrode produced safe welds on $3.2mm$ thick pipe at heat inputs between $0.6-0.75kJ/mm$, while welding with a $3.2mm$ diameter electrode produced incipient burnthrough at $0.6kJ/mm$ heat input. The argument appears to be consistent with reports by Cassie [18]; as smaller diameter electrodes operate with less current than larger diameter electrodes.

A novel analysis of burnthrough was reported by Bout & Gretskii [8] (1995). The aim of their research was to determine the maximum pressure at which in-service welding could be applied on an active pressurised pipeline. The authors notedthat the strength of the pipeline steels at $800^oC$ is between $4-10\%$ of that at ambient temperature. Moreover, the strength of the steel pipe drops significantly at temperatures over $400^oC$. The authors noted that when burnthrough occurred due to longitudinal welding, the failure exhibited considerable deformation of the remaining wall thickness of the pipe, beneath the weld pool. The deformation was significant in both radial and circumferential directions. In further analysis of their earlier work, the authors noted that fracture was preceded by local wall buckling and that the inside surface of the pipe had a pronounced deflection towards the weld pool along the direction of welding. The region exhibiting fracture exhibited considerable plastic deformation.

An interesting observation made by the authors was that the type of failure exhibited during burnthrough was similar in character to the fracture caused by longitudinally oriented corrosion cavities in operating pipelines. They proposed applying existing procedures to determine the load carrying capacity of operating pipes due to corrosion cavities,

to determine the load carrying capacity of pipelines under longitudinal in-service welds.

The authors initially considered regions of pipe exhibiting temperatures in excess of the melting point as the size and shape of the defect. A series of experiments were initiated to determine the fracture pressure of various pipelines which had welds deposited on them. All welds provided incomplete penetration and the pressure was varied until failure had occurred. The $700^{o}C$ isotherm was then considered, as the strength of pipe steel was considered to be low at that temperature. Once the size and shape of the defect were determined, the authors proposed using the following equation to determine the maximum hoop stress that could be sustained during welding:

$$\sigma_{\theta} = \sigma_{0.2}\left(\frac{t}{r} - 0.85\right) / \left(\frac{t}{r} - \frac{0.85}{M}\right) \tag{2.3}$$

where $M = 1 + 0.4L/Rt$, where $R$ is the outside radius of the pipe, $t$, is the pipe wall thickness, $L$, is the axial length of the weld pool perpendicular to the hoop stress, and finally, $r$, is the maximum depth of the defect. Using the aforementioned formulae, the authors then derived an equation to calculate the critical length, $L_{cr}$, of the heated zone; the pipe would not be able to operate at its maximum load carrying capacity for $L \geq L_{cr}$.

$$L_{cr} = 1.12\sqrt{2Rr}\sqrt{[0.85/\left(0.1t/r - 0.935\right)] - 1} \tag{2.4}$$

The authors then calculated various values of $L_{cr}$ for different diameter pipes. The calculations revealed that the values of $L_{cr}$, were very limited. Moreover, in combination with the difficulty of safe longitudinal welding, the authors proposed an alternative to deposit in-service welds.

A novel practical method of depositing circumferential welds on thin pipes, at heat inputs which would have otherwise caused burnthrough, was proposed by the authors. From previous experiments, the authors suggested supporting the region either side of the intended weld, by reinforcing rings or bands, as seen in Figure 2.5. The gap between the rings could be adjusted to give varied support to pipes of different wall thickness or

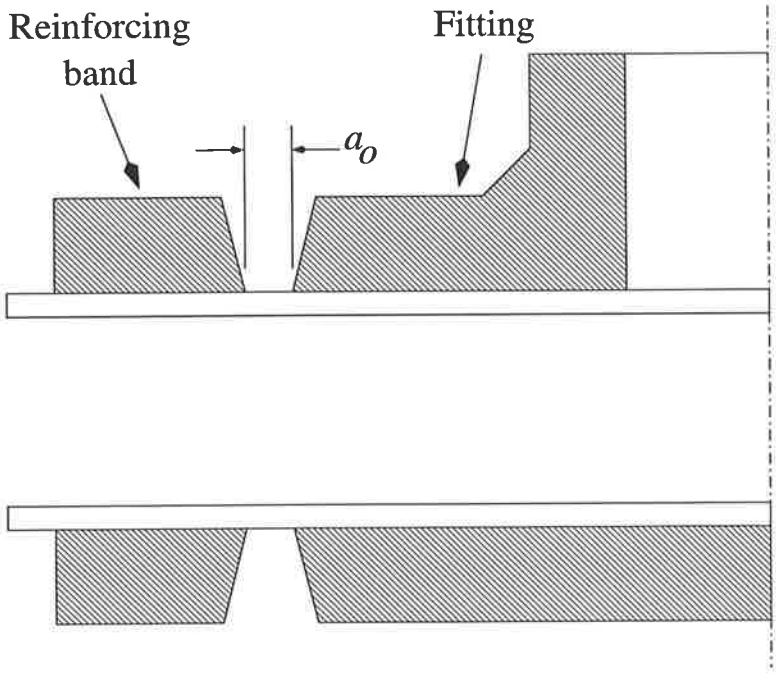


**Figure 2.5:** Joint configuration proposed by Bout & Gretskii [8].

pressure. The relationship between allowable pressure, effective thermal penetration and gap width $a_0$ between the reinforcing rings was given by the following equation:

$$p = 4\sigma_{0.2}^{T}\left(t - r\right)^2 / a_0^2 \tag{2.5}$$

From experiments, the authors stated that on a $3mm$ wall thickness, $320mm$ diameter pipe, pressurised to $4.0MPa$, burnthrough occurred for a heat input of $0.48kJ/mm$. With the application of the reinforcing rings, the heat input for burnthrough was $0.92kJ/mm$. The authors also suggested that when depositing circumferential welds, weaving movements should be included, as they decrease the level of penetration of the arc; which is in contrast with the suggestions made by Wade.

An extension of previous work [16] was attempted by Bruce et al. [15] (1996) to further investigate the effect of heat input and electrode size on the risk of burnthrough. In total, 12 welds were deposited under a variety of conditions: two wall thicknesses, 3.2 and $4.0mm$ and four target heat inputs, 0.4, 0.6, 0.8, 1.0 and $1.2kJ/mm$. In order to study the effect of electrode diameter on burnthrough, some welds were deposited under

identical conditions: i.e. heat input and wall thickness, only differing in current, voltage and electrode diameter. The electrode type chosen for the study was E7018, while 3 different diameters, 2.0, 2.4 and $3.2mm$ were used. The corresponding welding currents were 50, 80 and $110A$. All welds were deposited on a single pressure vessel fabricated from API 5LX-65 ERW, $508mm$ diameter, $8.0mm$ wall thickness line pipe. Sections of the pressure vessel were machined to achieve the necessary wall thickness for the study. All welds were deposited in the flat position using a remotely operated mechanised welding system, while the test vessel was pressurised to $6.2MPa$ with nitrogen.

Out of the 12 test welds, 2 welds produced burnthrough, while metallographic examination revealed that a further 4 welds had indicated incipient burnthrough. The authors noted that while some test welds were deposited with the same heat input, the weld with greater current had produced burnthrough or incipient burnthrough. For example, a weld deposited with the welding parameters: $50A$, $21V$, $1.2mm/s$ produced a safe weld when deposited on $3.2mm$ remaining wall thickness. Two further welds deposited on identical wall thickness with the following welding parameters: $80A$, $21V$, $1.9mm/s$, and $110A$, $21V$, $2.7mm/s$, both produced burnthrough while having the same heat input ($0.8kJ/mm$) as the first example. Interestingly, yet another weld, $80A$, $21V$, $2.7mm/s$, also deposited on identical wall thickness pipe, had produced incipient burnthrough while having a lower heat input, $0.6kJ/mm$, than the first example.

The authors concluded that it was important to consider the current level or electrode diameter in addition to heat input, when determining safe operating conditions for in-service repair welds. Suggested welding limits for a remaining wall thickness of $3.2mm$, were, welding with $2.0mm$ diameter electrodes restricted to $0.87kJ/mm$, while $2.4mm$ diameter electrodes should be limited to $0.51kJ/mm$ heat input. From an extrapolation of the results, the authors recommended against welding with $3.2mm$ diameter electrodes. Similarly, when welding on remaining wall thickness of $4.0mm$, the authors suggested welding with $2.4mm$ diameter electrodes with a maximum heat input of $0.95kJ/mm$, and $0.85kJ/mm$ for the $3.2mm$ diameter electrodes. Again, after extrapolating the data,

the authors recommended welding with 2.0$mm$ diameter electrodes with a maximum of 0.98$kJ/mm$. All recommendations were based on nominal current levels of 50, 80, and 110 amps for 2.0$mm$, 2.4$mm$ and 3.2$mm$ diameter electrodes. The aforementioned results can be seen in Figure 2.6.

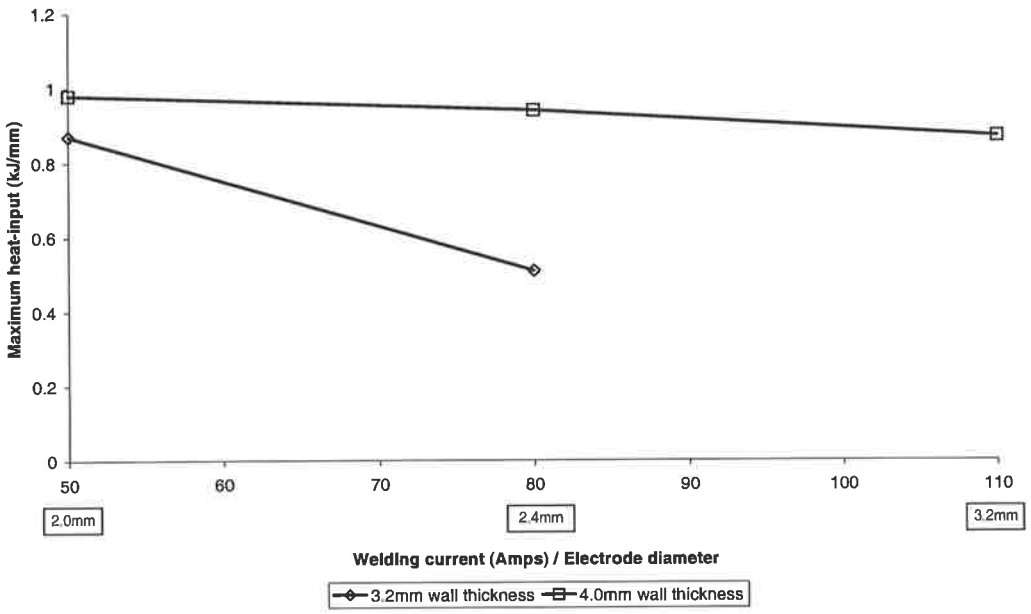


**Figure 2.6:** Recommended limits for repair welding proposed by Bruce et al. [15]

A study involving the prediction of material rupture and burnthrough was reported by Oddy & McDill [63] (1999). The authors suggested that creep rupture was the principal mechanism behind burnthrough, while complete penetration of the pipe wall would obviously also cause failure. The authors suggested that an analysis of burnthrough would require thermal, elastic, plastic, creep and rupture material properties of the pipe for temperatures ranging from ambient to molten. A numerical simulation was solved using software previously developed by the authors for the study of residual stress and distortion. The constitutive model incorporated in the FEA software included elastic, plastic, thermal, creep, transformational volume change, and transformation plasticity

strain rates; mathematically the model can be seen in Equation 2.6.

$$\dot{\epsilon}_{tot} = \dot{\epsilon}_{el} + \dot{\epsilon}_{pl} + \dot{\epsilon}_{th} + \dot{\epsilon}_{cr} + \dot{\epsilon}_{trv} + \dot{\epsilon}_{trp} \tag{2.6}$$

The model was compared with experiments reported by Bruce; as high temperature material property data is difficult to obtain for pipeline steels, the authors had used material properties which were conservative and were likely to cause burnthrough. The calculated predictions were conservative; by comparison to experiments, a number of welds were incorrectly predicted as exhibiting burnthrough. Clearly, the major sources of error were the material property definitions and to a lesser extent the calculation of the thermal field. The authors noted that some material properties, for example creep rate, were potentially inaccurate by $\pm 1$ order of magnitude.

#### 2.2.2.1 Summary & gaps in knowledge

Considering the safety implications, there have been few attempts to determine the conditions necessary to avoid pipe wall failure during in-service welding. Experimental work has generally used a small number of test welds under widely varied experimental conditions, so conclusions tend to be general directions rather than quantified limits.

Based on the limited literature available, a number of parameters influence burnthrough; as can be seen in Figure 2.7. Heat input is considered an important parameter when determining the risk of burnthrough. More importantly, work by Cassie [17] and Phelps et al. [68] found that welding current was strongly influential on the depth of penetration.

Work by Bruce & Kiefner [16], and Bruce [15] revealed an intrinsic relationship between electrode diameter and current, and the resulting depth of penetration. The authors suggested welding current was more influential than heat input when considering burnthrough. Experimental evidence displayed varying penetration depths for welds with identical heat input. Increasing welding current generally resulted in greater penetra-

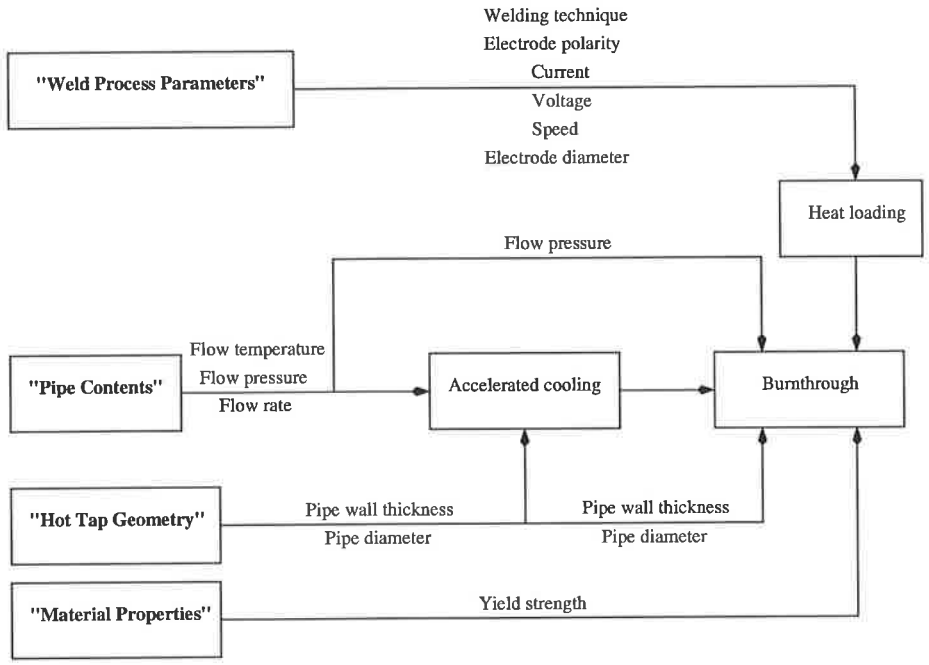


**Figure 2.7:** Parameters which influence burnthrough.

tion. Moreover, the authors investigations revealed that penetration had increased with electrode diameter for a given heat input.

The effect of wall thickness on the risk of burnthrough was examined through investigations reported by Bruce & Kiefner [16]. The authors found that penetration did not vary noticeably for thick-walled pipe for a given heat input. However, on wall thickness of $3.2mm$ and lower, for a given heat input, the penetration had increased with decreasing wall thickness.

A number of suggestions were proposed to reduce the risk of burnthrough. Wade [84] suggested to weld with as high welding speed as possible, to reduce the length of the weld and reduce the spread of heat. For the same reason, Wade also suggested limiting the degree of weaving when welding.

The results from work by Cassie [17] and Phelps et al. [68] had revealed that welding with DCEN polarity would give less penetration than DCEP polarity. Hicks [41] suggested limiting the pressure when welding. Cassie [17] suggested initially depositing a buttering layer; to effectively increase the wall thickness of the pipe.

Clearly, the risk of burnthrough is related to the loss of pipe wall strength in the weld zone, and its inability to resist local stress. The reduction in wall strength depends on the elevated temperature around the weld, and on the depth of weld penetration relative to the original wall thickness. Observations of burnthrough generally show significant local plastic distortion of the pipe wall, and a fracture along the weld pool axis.

A number of burnthrough mitigation strategies have been developed; the following paragraphs will discuss those, their benefits and shortcomings, ultimately to reveal that a new method is required.

Kiefner & Fischer [49] proposed that burnthrough was likely to occur if the inside wall temperature was to exceed $982°C$. However, this model does not consider the strength of the localised region adjacent to the weld pool. The size of the region where the temperature exceeds $982°C$ influences the behaviour of the pipe under a given pressure. Consider two in-service welds which are identical in, pipe geometry, gas flow, however, only differing in welding heat input. For example, the temperature field created by the weld with the

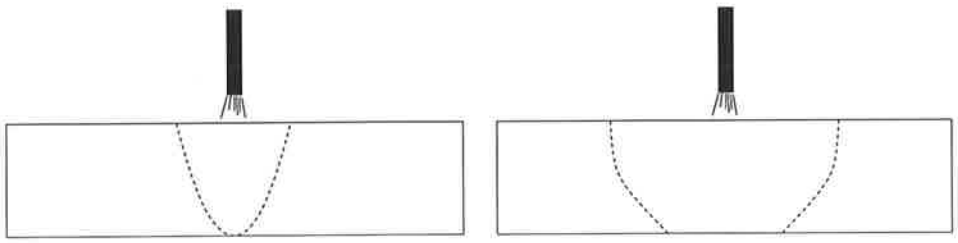

(a) Low heat input (b) High heat input

**Figure 2.8:** Varying support of pipe wall material adjacent to weld pool - dashed line represents an isotherm of $982°C$.

lower heat input can be represented as Figure 2.8(a), and the weld which was deposited with a higher heat input can be seen in Figure 2.8(b). While the model proposed by Kiefner & Fischer would imply that both welds would cause burnthrough, clearly, the support rendered by the cooler pipe wall surrounding the weld in Figure 2.8(a) is considerably greater than that in Figure 2.8(b). The support from the pipe wall adjacent to the weld clearly influences burnthrough. The second important aspect not considered

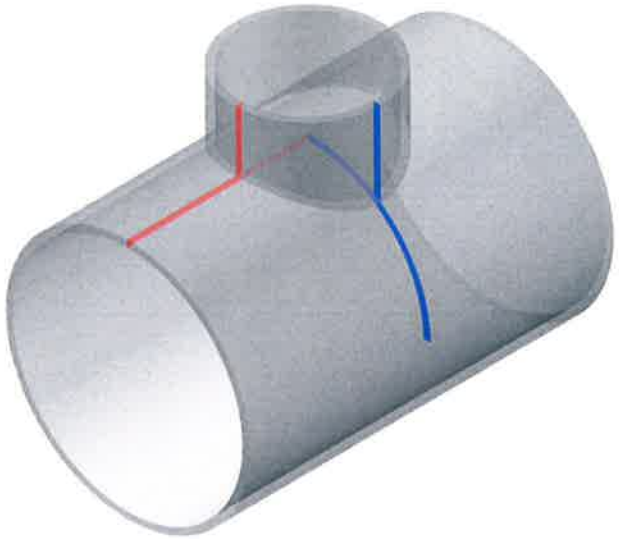

**Figure 2.9:** Two-dimensional approximations used by Kiefner & Fischer to calculate thermal fields due to branch on pipe welds.

from the burnthrough model proposed by Kiefner & Fischer, is the direction of welding. The burnthrough criteria of $982°C$ inside wall temperature applies to circumferential and branch on pipe welds. The thermal model proposed by Kiefner & Fischer considers the temperature field associated with branch on pipe welding as two cases: as seen in Figure 2.9: (a) at the bottom position of the joint, as illustrated in blue, and (b), at the top position of the pipe, as illustrated in red. In both cases, the effect of the applied stress field is considerably different. Calculating the 2D cross-sectional temperature field at the bottom position of the branch on pipe, weld is similar to that of a longitudinal in-service weld. It is known that welding onto a pressurised pipe in a longitudinal manner is more likely to burnthrough than circumferential welding for a given heat input and pressure. This is primarily due to the combination of both hoop and longitudinal stresses. Clearly, the effect of the direction of welding plays a significant role in the behaviour of a given in-service weld. Applying identical limits, as proposed by Kiefner & Fischer for both circumferential welding and longitudinal welding suggests a degree of conservatism.

While a method to limit the heat input of welding, for a given pressure, as proposed by Wade [84] is easy to calculate and implement, it does have a few shortcomings. The proposed method does not consider the direction of welding, the pipe wall thickness, or

the diameter of the electrode. The experimental work undertaken by Wade was for welds deposited in a longitudinal manner. The limits determined by Wade are conservative, when attempting to determine the heat input limit for circumferential fillet welding; the reasons for which are discussed earlier. The pressure limits proposed by Wade are derived empirically. Consequently, the limits were not designed for pipe of wall thickness of $5mm$ or less. Finally, the work undertaken by Wade was for static pressure tests; the effect of gas flow was not studied or incorporated into the model. The effect of gas flow is considerable when defining the limits of welding in order to avoid burnthrough and create a weld of sound mechanical properties.

The ASME Gas Piping Standards Committee's recommended formula for welding split repair sleeves on gas pipelines, as found in Equation 2.2, was proposed by Hicks [41] as a pressure limit to avoid burnthrough. While the proposed model incorporates wall thickness, material yield strength and pipe diameter, weld process variables and the resultant temperature fields are not taken into consideration. Moreover, the proposed model does not consider the heat input of the welding process, nor the gas flow within the pipe. The ASME formula was suggested due to its overly conservative estimates. The pressure limit was proposed for welds deposited in the circumferential direction.

The model proposed by Oddy & McDill [62] is arguably the most complete, in comparison with the those previously mentioned. However, the model has a number of shortcomings. As the model involves finite element analysis (FEA) involving constitutive equations, considerable information is required to describe the various mechanical and physical aspects of the pipe material. The models requires thermal, temperature dependent elastic, plastic and creep and rupture material properties of the pipe material. In addition, the constitutive modelling approach is highly computationally expensive. Finally, while the model is a scientifically intriguing method to understand the mechanism of burnthrough, ultimately, for the design of in-service welds, the failure limits is far lower.

The concepts proposed by Bout & Gretskii [8] are unique and offer a novel approach to calculating the limit at which in-service welding can be achieved without burnthrough

of pipe wall failure. The concept of approximating the welds as a corrosion cavity or defect raises considerable interest due to the speed of the calculation; only a thermal field calculation is required to calculate the remaining strength of the pipe using this approach.

The proposed models to date lie at either extremes; from the overly simple to the very complex and highly computing intensive. While traditional thermal elastic-plastic FEA is also capable of predicting the behaviour of in-service welds, the method is also reasonably involved and requires substantial computing resources. Clearly, there does exists some scope for developing a model which offers reasonable accuracy and speed of solution. The model proposed by Bout & Gretskii will be examined to determine its accuracy and usefulness in predicting the remaining strength of a pipe due to in-service welding.

## 2.3 Thermal modelling

### 2.3.1 Introduction

The partial differential heat transfer equation commonly used for the modelling of welding processes can be represented as:

$$\rho C_p \frac{\partial T}{\partial t} = k\frac{\partial^2 T}{\partial x^2} + k\frac{\partial^2 T}{\partial y^2} + k\frac{\partial^2 T}{\partial z^2} + q_g \tag{2.7}$$

where $\rho$ = density, $C_p$ = specific heat, $k$ = thermal conductivity, $q_g$ = heat generated per unit volume.

The assumptions made are that the heat conduction coefficient of the material is isotropic and that the fluid motion within the weld pool is not considered; conventionally, some correction factors applied to $k$, $\rho$ or $C_p$ may approximate the convective thermal effects of weld pool flow.

### 2.3.2 Analytical solutions

The earliest known attempt at deriving analytical solutions to heat flow during welding appears to have been made by Wilson [86] (1904); although Rosenthal [71] (1941) is commonly referred to as the pioneer of the analytical solution to heat flow in welding.

The solutions Rosenthal offered were for welds deposited in a straight line at a constant speed with the following assumptions:

- the physical coefficients of the material are constant
- the heat source can be considered as a *point* source with $Q = \eta VI$, where $Q$ is the net heat amount due to the welding source, $\eta$ is the efficiency of the welding process, $V$ is voltage and $I$ is current
- heat exchanges (losses) from the surface to surrounding atmosphere were neglected.

The significant solutions offered by Rosenthal were for welds deposited under 'thick-plate' and 'thin-plate' conditions. In both cases, the resultant thermal field from the welds was considered to be in a 'quasi-steady-state', i.e., if an observer stationed at the heat source could notice no change in the surrounding temperature distribution over time, then a quasi-steady-state exists.

Rather than approximating the arc welding process as a point heat source, Wells [85] (1952) proposed the idea of approximating the welding heat source as a line heat source. The heat flux was distributed uniformly through the thickness of the plate. Using this line source solution, Wells showed fair agreement between theoretical predictions and experiments. Wells also derived an implicit relationship to calculate maximum puddle weld width.

The effect of the variation in thermal properties with temperature on the temperature distribution in welding was reported by Grosh & Trabant [37] (1956). While the authors developed a theory of moving sources for solids with variable thermal properties,

fundamental assumptions such as neglecting heat losses from the surfaces of the plate remained.

Using the equations describing heat flow due to a moving heat source in either a semi-infinite or infinite plate, Adams [1] (1958) successfully derived equations to calculate peak temperatures and cooling rates. These equations were functions of plate geometry, thermal material properties and welding parameters.

Jhaveri et al. [46] 1962 went further by graphically describing generalised relationships of centreline weld cooling rates for a heat source moving on the surface of a plate having arbitrary thickness.

The analytical equations describing temperature for a moving heat source in a solid plate developed until then had difficulty in describing the temperature changes which take place in relatively thick plate. Rosenthal's thick-plate solution is rarely applicable and many welds fall in a category which is in between thick and thin. Historically, the only information pertinent to such welds until then had been gained experimentally. Barry et al. [5] (1963) attempted to refine existing theoretical methods to calculate the thermal cycles associated in the arc welding of moderately thick plate. They attempted to calculate peak temperatures at points close to the arc welds under thick plate conditions. Paley et al. [65] went further by deriving equations to calculate peak temperature distributions for welds deposited near the edges of the plate; which was achieved by using an array of fictitious heat sources to represent the actual welding heat source.

An extensive report by Christensen et al. [19] (1965) compared experimental results with those obtained by predictions using analytical equations based upon work by Rosenthal. Reasonable correlation was found between weld puddle shape, length and width but weld penetration was not accurate. The authors suggested that accuracy was better at locations further away from the weld centre line. The authors also suggested that better correlation was found at the surface of the plate than at mid-planar locations.

The difference between the theoretical and experimentally measured molten isotherm,

was found to be due to the fact that the latent heat of fusion, and molten pool convection, was largely ignored by the theory of a single point source in a continuous thermally conductive plate. Rykalin & Beketov [72] (1967) argued that much of the heat in the molten pool is transferred by convection and by the latent heat of fusion which is either evolving or being absorbed in regions of the molten isotherm. In their work, they proposed a method of calculating the temperature distribution near the molten pool.

Myers et al. [59] (1967) describes many of the analytical methods derived for calculating the temperature fields due to welding. The authors found that the point source theory without modification could not be used to predict cooling rates, but can be used to indicate trends as welding variables were changed. The authors concluded that the theory devised thus far only gave good approximate answers at locations far removed from the arc and also only at low welding speeds.

Rykalin & Nikolaev [73] (1971) considered deriving analytical equations for calculating the temperature fields along the centreline due to welding, by representing the arc welding heat source as a Gaussian surface heat source rather than a point or line heat source. They had successfully derived analytical equations for 2D planar welds, thin plate, and semi-infinite models.

Latent heat due to solid liquid phase change was largely unaccounted for by analytical derivations. At the front of the molten weld pool, latent heat is absorbed, while at the rear of the molten weld pool, latent heat is dissipated. The effects of thermal phase changes were included in the derivation of analytical equations for predicting temperature fields by Malmuth et al. [57] (1974) and Nunes [61] (1983). In deriving analytical equations to calculate temperature fields due to GTA welding, Malmuth et al. [57] (1974) had studied the effect of the latent heat of fusion with a point source simulation. Nunes [61] (1983) also argued that the effects of weld pool flow was important and approximated it in his derivation of an analytical solution. Nunes had included the effects of phase change by using thermal dipoles while he also included the effects of weld pool flow by thermal quadropoles.

Analytical equations to calculate the entire temperature field on semi-infinite plate using a 2D Gaussian distributed travelling heat source were derived by Eager & Tsai [24] (1983); while Tsai [80] (1983) had developed an analytical solution for a model incorporating a Gaussian distributed heat source and finite plate thickness. Eager & Tsai [24] (1983) also derived equations to calculate the shape and size of the weld pool for a travelling distributed heat source. The authors had found a considerable improvement in temperature prediction in near weld regions, however, many simplifying assumptions still remained.

As part of a large study of the equations used to calculate thermal histories, cooling times and HAZ shapes, Kasuya & Yurioka [48] (1993) derived equations to calculate weld cooling rates in welds which were locally preheated. The derived equations were for a two-dimensional heat flow model.

An analytical solution was developed to allow the calculation of transient temperature fields in fillet welds by Jeong & Cho [45] (1997). The authors found deriving an analytical solution for calculating thermal fields due to fillet welding complex and difficult. Consequently, the authors developed an innovative approach involving conformal mapping. First, the equations for calculating the transient temperature distribution for an arc weld

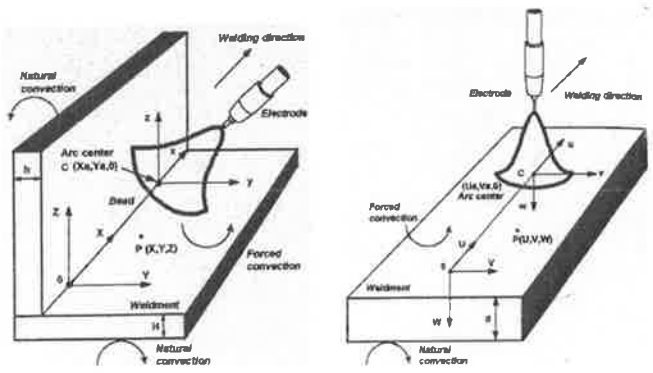


**(a)** Coordinates of the weldment for analysis

**(b)** The transformed coordinates

**Figure 2.10:** Conformal mapping used by Jeong & Cho [45].

on an infinite plate (Figure 2.10(b)) were derived. The heat from the arc was assumed to

be a two-dimensional bivariate normal distribution. Next, using conformal mapping, the temperature distribution was transformed onto a right-angle bend fillet weld geometry (Figure 2.10(a)).

When comparing the predictions of the analytical model with experiments, Jeong & Cho found that the calculated results had a larger throat penetration than those from experiments. In reality, the heat from the arc was applied only to the surface of the weld pool, while some heat was transferred through the weld pool due to molten droplets from the electrode. Moreover, less heat is transfered to the corner of the fillet than the surface of the weld pool. In the analytical model, the heat due to molten droplets was not considered, and a greater amount of heat was therefore incorrectly applied to the corner of the fillet. Another cause of error was due to the existence of a gap in the fillet weld. The thermal conductivity is effectively reduced and produces asymmetry in the shape of the HAZ and fusion zone. While natural convection was included, latent heat of fusion and weld pool convection were ignored.

While the two-dimensional Gaussian surface and other two-dimensional heat sources provided improved accuracy to calculate temperature fields compared to point or line heat sources, new and improved three-dimensional heat sources had not yet till then been included in a analytical derivation. The analytical solution for a moving three-dimensional travelling heat source was derived by Nguyen et al. [60] (1999). The double ellipsoidal power density distribution function initially proposed by Goldak [32] was used by the authors in the derivation. The equations related to a conduction only model but did produce encouraging results for weld pool depth and width.

#### 2.3.2.1 Summary

There are several advantages to be gained for using an analytical based solution for calculating temperature fields due to in-service welding. The principal advantage is the speed at which simulations can be calculated. However, fundamental aspects of analytical methods do not allow for the accurate prediction of thermal fields due to in-service welding.

Often, analytical solutions make the assumption that the geometry is considered infinite; expect in directions specifically noted. Fitting an analytical solution to a circumferential sleeve weld may be possible, albeit challenging; however, fitting an analytical solution to a saddle weld is very difficult. A circumferential weld can be viewed as essentially a prismatic problem, revolving around a central axis; but a saddle weld does not contain such symmetry. Further geometric problems arise due to the deposition of weld metal; the addition of metal has not yet been included in an analytical thermal solution.

A very important hurdle in using analytical solutions is the manner in which the thermal properties are approximated. So far an analytical solution has not been developed for a transient problem, including full temperature dependent thermal properties. Often, a mean value for thermal properties such as thermal conductivity, density and specific heat are calculated for each time step; which is a significant unrealistic assumption.

Another challenging problem is to include the convective properties of the flowing natural gas on the inside of the pipe wall. To date, analytical solutions only have regarded the problem of ambient natural convection and have not tackled the problem of varying convective boundary conditions.

While analytical solutions can be accurate for regions far from the weld pool, the analysis of in-service welding relies heavily on behaviour within the HAZ, and on the depth of penetration of the weld pool. Due to these limitations, many researchers have considered using numerical methods to solve problems related to welding.

The next sections will cover initially many significant achievements in the numerical thermal modelling of welding, with finally a summary on what aspects are usable in the thermal modelling of in-service welding.

### 2.3.3 Numerical solutions

The calculation of temperature histories for GTA welding by numerical methods was reported by Pavelic et al. [67] (1969). The governing differential equation of conduction was solved by a finite difference method. The temperature field calculation of GTA welds of thin plates was of principal interest. The temperature field due to GTA welding was considered to be essentially two-dimensional, as it was assumed that there was very little variation of temperature through the thickness. The analysis was calculated under quasi-steady-state conditions.

A significant innovation reported by the authors was the introduction of a new heat source to represent the heat transferred from the arc to the surface of the plate. The authors proposed that the heat source should have a Gaussian distribution and be circular in shape, as can be seen in Figure 2.11.

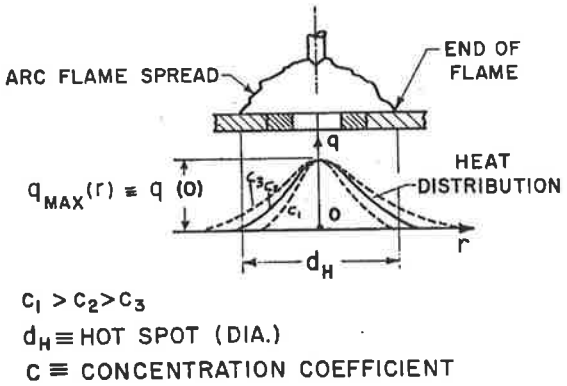


**Figure 2.11:** Normal circular source proposed by Pavelic et al. [67]

The distribution of heat flux is calculated by:

$$q(r) = q(0)e^{-Cr^2} \tag{2.8}$$

In Figure 2.11 it can be observed that when $C$ is large, $q(r)$ decreases rapidly with $r$ and the effective diameter, $d_H$, of the heat region is smaller.

If the total effective arc power absorbed at the anode is known (obtained experimen-

tally or correlated), the distribution function, Equation 2.8, may be integrated:

$$q_{TOT} = \int_0^\infty q(r)2\pi r dr = \int_0^\infty q(0)e^{-Cr^2}2\pi r dr = \eta V I \tag{2.9}$$

to obtain the value of the constant, $q(0)$. Since $q(0)$ is also the maximum value of the distribution function at the origin:

$$q(0) = \frac{C q_{TOT}}{\pi} \tag{2.10}$$

While Equation 2.10 should be integrated to $\infty$, if one is willing to integrate Equation 2.10 to something less than $\infty$, say a flux of $q(r)$ equal to 5% of the maximum value of the thermal flux, then:

$$q(r_H) = q(0)e^{-Cr_H^2} = 0.05q(0) \text{ or } r_H = \frac{1.732}{\sqrt{C}} \tag{2.11}$$

If $r_H$ is known, then the concentration coefficient C can be calculated by:

$$C = \frac{3.0}{\sqrt{r_H}} \tag{2.12}$$

Using the circular heat source, the authors compared the numerical calculations with experiments and found that the peak temperature in the HAZ was within 10%.

The application of the finite element method (FEM) to model the welding and loading of a structure was reported in a monumental report by Hibbit & Marcal [40] (1973). The authors had uncoupled the general problem into a thermal model followed by a mechanical model.

The work by Hibbitt & Marcal [40] (1975) was the basis of work undertaken by Friedman [27] (1975), which was to model the GTA welding process. The finite element method was used to model both the thermal and mechanical aspects of GTA welds. Friedman proposed a novel method for calculating the transient temperature field of a GTA weld. Firstly, the modelling of a weld under quasi-steady-state conditions was performed, and

then the transient temperature distribution was determined by translating a reference plane along the line of welding.

The temperature distribution in a quasi-steady-state solution is stationary with respect to the heat source's moving coordinate system. For a weld, illustrated in Figure 2.12, the

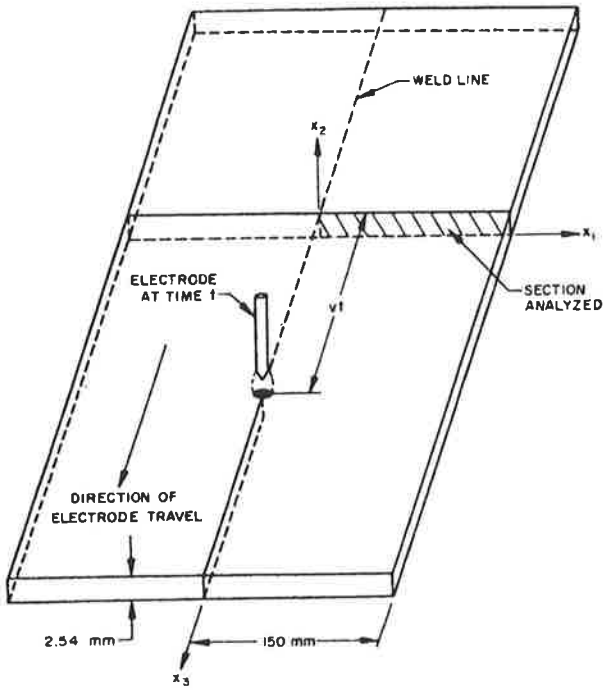


**Figure 2.12:** Quasi-steady-state model, proposed by Friedman [27].

temperature at any location of the weldment can be expressed as:

$$T(x_1, x_2, x_3, t) = T(x_1, x_2, x_3 - vt) \tag{2.13}$$

where $v$ is the welding speed. The transient temperature distribution for the weldment cross-section can now be determined by simply displacing the analysed section along the direction of welding. Mathematically the transient temperature distribution may be calculated as follows:

$$T(x_1, x_2, x_3, t) = T(x_1, x_2, 0, t - x_3/v). \tag{2.14}$$

Friedman stated that if the welding speed, relative to a characteristic diffusion rate of the

material is sufficiently high, then the amount of heat conducted in front of the weld pool is insignificant by comparison to the amount of heat received by the weld pool from the arc. Moreover, when examining an infinitesimally thin slice of the weldment, very little heat flow occurred through the slice, compared to the heat received from the arc and the heat flow diffused within the slice. Mathematically the assumption can be expressed as:

$$\frac{\partial}{\partial x_s}\left[k(T)\frac{\partial T}{\partial x_s}\right] = 0 \tag{2.15}$$

To calculate the heat flux due to welding, a modified version of the Gaussian surface heat source, originally proposed by Pavelic, was used in the analysis. Mathematically, the heat source distribution was expressed as:

$$q(x_1, t) = \frac{3Q}{\pi \bar{r}^2} e^{-3(\frac{x_1}{\bar{r}})^2} e^{-3(\frac{vt}{\bar{r}})^2} \tag{2.16}$$

where $\bar{r}$ defines the region in which 95% of the heat flux is deposited. Friedman therefore had reduced the complex three-dimensional heat flow problem to a two-dimensional unsteady-state temperature field at a section normal to the weld line.

The ability to calculate temperature fields for welds made under non-rectangular prismatic geometries was demonstrated by Paley & Hibbert [65] (1975). The authors had successfully calculated thermal histories for welds made under single and double V and U groove configurations using finite difference methods. The non-rectangular cross-section analysed led to the authors using a mesh which was not uniform; most significantly, fine mesh density was used at regions where large thermal gradients were expected. The authors had solved the problem under quasi-steady-state conditions, but with the advantage of applying temperature dependent material properties to their analysis. A different approach to represent the heat from the welding arc was taken; the authors had applied the heat source by designating one or more elements in the mesh as heated elements. Interestingly, the authors decided to apply an equal amount of heat to each element in the fusion zone. This assumption appears to be unrealistic as the heat transfered from the arc is at a maximum at the surface of the arc/weld pool interface while asymptotically

nearing zero at regions further away from the arc.

Friedman & Glickstein [28] (1976) applied the finite element method to calculate temperature fields due to stationary GTA welds in moderately thick plates. A sensitivity analysis examining the effects of changes in welding parameters and material properties was also performed. The heat source used in the analysis was identical to that proposed earlier by Friedman [27]. The parameters investigated were arc radius, thermal conductivity, latent heat effects and plate thickness. The study found that as arc radius increased, the calculated weld puddle width and depth decreased.

In an effort to correlate weld pool width/depth ratios between experiment and calculations, the authors investigated using anisotropic thermal conductivity. Initial investigations found that the weld pool width/depth ratio calculated was greater than that measured through experiment. Reducing the thermal conductivity in the thickness direction of the plate, resulted in an increase in weld pool width and a decrease in weld pool depth, therefore giving better correlation between experiments and predictions.

The effect of including latent heat effects was concluded to be significant only for full penetration, or thin plates, and less important for thick plate conditions.

Friedman & Glickstein found that there existed a critical weld pool penetration depth at which the under-surface of the weldment begins to exert an insulating effect on the heat flow through the thickness. It was found that predicted penetration depth increased for only a marginal increase in heat input. The authors concluded that at about 60% penetration, the weld puddle depth increased in greater amounts until full penetration was achieved, through only a slight increase in heat input.

Work undertaken by Krutz & Segerlind [52] (1978) involved a finite element calculation of the GTA process using a cross-sectional model with the assumption that the speed of the arc is high when compared to the diffusion rate of the material. Their model had included temperature dependent thermal material properties and included the effect of latent heat. A study of the effect of arc welding parameters and model properties displayed results

which are contrary to results published by Friedman. Interestingly, Krutz & Segelind had found that as the arc radius had increased, so did the peak temperatures. They had also found that when using larger values of liquid metal thermal conductivity, the peak temperatures increased correspondingly.

Kou & Le [50] (1983) were interested in the heat flow and solidification that occurred during autogenous GTA welding of aluminium plates. Previous thermal models were essentially two-dimensional and largely did not include the effects of heat flow in the direction of welding. The authors argued that the heat flow in the direction of welding was significant for their studies and developed a three-dimensional heat flow model which was solved using finite difference methods. The effect of weld pool convection was included indirectly by applying an effective thermal conductivity; i.e. an artificial enhancement was applied to the thermal conductivity to account for weld pool convective heat transfer on the heat flow during welding. Significant advantages were gained by approximating the weld pool convection in such manner. In addition, as the numerical solution was still based solely on the heat conduction equation, the need to solve complex fluid dynamics equations due to the weld pool flow was avoided

While the predictions based on the heat sources suggested by Pavelic, Paley & Hibbert provide reasonable correlation with experimental measurements, some effects due to welding, e.g. digging action of the arc due to deep penetration welds, can not be accurately reflected using such heat source definitions. Goldak et al. [32] (1984) proposed a non-axis-symmetric three-dimensional heat source model in order to overcome the shortcomings of previous derived heat sources. The authors considered using a hemispherical power density distribution to model high power density welding processes; however, the idea was rejected as molten pool shapes in many welds were far from spherical and in some cases were not symmetric. This led to the idea of an ellipsoidal volume source. While predictions using the ellipsoidal volume source improved, it was found that the temperature gradient in front of the heat source was not as steep as expected, while the temperature gradient at the trailing edge was steeper than expected. Goldak proposed a

double ellipsoidal power density distribution which mathematically is described as:

$$q_f(x,y,z,t) = \frac{6\sqrt{3}f_f Q}{abc\pi\sqrt{\pi}} e^{-3x^2/a^2} e^{-3y^2/b^2} e^{-3[z+v(\tau-t)]^2/c_f^2} \tag{2.17}$$

$$q_r(x,y,z,t) = \frac{6\sqrt{3}f_r Q}{abc\pi\sqrt{\pi}} e^{-3x^2/a^2} e^{-3y^2/b^2} e^{-3[z+v(\tau-t)]^2/c_r^2} \tag{2.18}$$

The front section of the heat source is calculated by $q_f$ while $q_r$ is used to calculate for the rear. The apportionment of heat between the front and rear is controlled by the relationship $f_f + f_r = 2$. For example, to apply greater heat to the rear section of the heat source, the values $f_r = 1.4$ and $f_f = 0.6$ may be chosen. Equations 2.17, 2.18 were derived so that the power density falls to $0.05q(0)$ at the surface of the ellipsoid. The coefficients $a$, $b$, $c_f$, $c_b$ are termed characteristic length parameters and the authors proposed that these parameters should equal the radial dimensions of the molten zone in front of, behind, to the side and underneath the arc. In Figure 2.13 the heat source configuration can be seen.

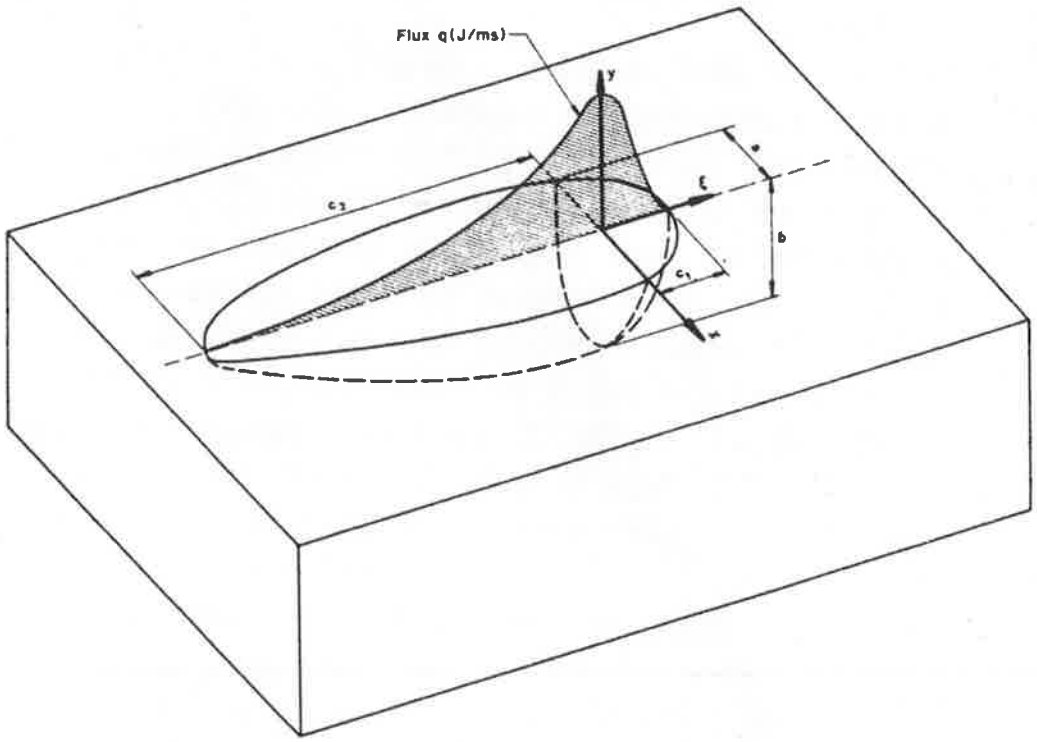


**Figure 2.13:** Double ellipsoid heat source (DEHS) configuration together with the power distribution function along the $\xi$ axis.

The study of heat flow during the autogenous GTA welding of pipes was reported by Kou & Le [51] (1984). The authors developed two finite difference computer models: one for calculating the steady-state three-dimensional thermal distribution due to seam welding, and the other for calculating the unsteady-state three-dimensional thermal distribution due to girth welding. While the correlation between experiment and theoretical prediction for the seam welding model was good, there were some discrepancies found in relation to the girth welding models. The authors found that when welding on small diameter pipe, a degree of preheat contributed to the weld pool, growing in size with time. Whereas, the computer models had not accounted for the possibility of preheat, or heat flow around the pipe.

The finite element method was applied to calculate the three-dimensional thermal history of a V-groove joint welded by the GMA welding process by Tekriwal & Mazumder [77] (1986). The authors acknowledged that when calculating the thermal field due to GMA welding, the mechanism of weld metal deposition will play a significant role and would have to be included in the model. Mathematically, the solution domain will grow continuously due the weld metal being deposited. Ideally, the deposition of weld metal would require solving the model in infinitesimally small time steps. At each time step, elements of infinitesimally small size corresponding to the filler metal, would need to be added. The addition of elements is halted when the deposition of weld metal has ended, when finally, larger time steps may then be used to calculate temperatures during cooling. The authors, realising the impracticality of using such small time steps and adding small elements opted to approximate the welding process by using larger time steps and a coarser mesh. The deposition of weld metal, by periodically adding new elements to the mesh can be seen in Figure 2.14.

Mahin et al. [56] (1986) had applied finite element methods to calculate the temperature fields due to stationary and travelling GTA welds. The authors had considered representing the heat source in two methods: first, to consider the heat source as a Gaussian distribution and next, more innovatively, to consider the heat source as a temperature

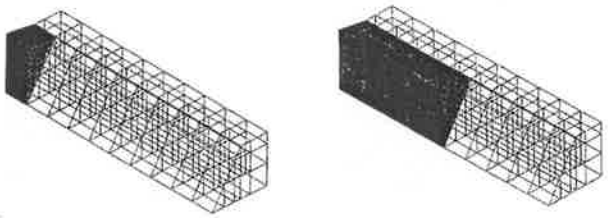

(a) First step (b) Second step

**Figure 2.14:** Addition of mesh due to weld metal deposition.

boundary condition. The strategy was to fix the upper temperature of the surface at the boiling point of the base metal. The authors had noted that using the temperature boundary condition approach, had reduced the computation times significantly, by a factor of 5. The reduction was primarily due to the reduced number of nodes and elements required. The authors had acknowledged the effect of convection due to the molten weld pool, and had approximated the phenomena by enhancing the thermal conductivity of the molten weld pool. The authors had linearly increased the thermal conductivity in the molten weld pool such that at 3000K, the thermal conductivity was 10 times greater, than at melting point. The authors had also introduced the idea of using anisotropic thermal conductivities in an attempt to correlate calculated weld pool width/depth ratios with those measured from experiment.

A study involving the effect of weld process variables and bead shape and penetration of GMA welds was performed by Pardo & Weckman [66] (1989). A three-dimensional steaty-state thermal model of the process was solved using the finite element method to predict plate temperature distribution, weld pool shape and weld reinforcement geometry. A Gaussian distribution of heat flux was used to represent the heat due to the arc. To simulate the effect of convection in the weld pool, the thermal conductivity was artificially enhanced. The latent heat of fusion was included in the model with the assumption that the effect occurred at one temperature. The weld bead geometry was calculated by the following equations:

$$Area = \frac{v_{wire}\pi d_{wire}^2}{4v} \tag{2.19}$$

where $v_{wire}$ is the wire feed rate, $d_{wire}$ the wire diameter, and $v$ the welding speed. With a parabolic profile, the reinforcement height, $H_r$, and reinforcement half width $W_r$ are related through the equation:

$$W_r H_r = \frac{3Area}{4} \tag{2.20}$$

To simulate the digging action of the arc due to spray transfer mode GMA welding, the thermal conductivity was modified anisotropically to correlate with measured weld pool width/depth ratios.

The application of the finite element code ABAQUS to calculate the two-dimensional cross-sectional thermal field and residual stresses of bead on plate submerged arc welding (SAW) was reported by Leung et al. [55] (1990). Heat losses due to radiation was simulated by decreasing the efficiency of the welding process. The effect due to latent heat was approximated by an artificial increase in the value of specific heat over the melting temperature range. The DEHS was chosen to represent the heat transfer from the arc while the effect of weld pool convection was approximated by increasing the thermal conductivity sixfold so that accurate predictions of weld pools can be made. Variable time steps and tolerances were chosen for the transient model; smaller tolerances and larger time steps were chosen during the initial heating period, while smaller tolerances and larger time steps were chosen when cooling was occurring.

The calculation of a cross-sectional model for temperature distribution due to multi-pass GMA welds was reported by Leung & Pick [54] (1990) which was based on earlier work by Leung et al. [55] (1990). The filler material of each weld pass was modelled as being deposited, immediately after the previous pass.

In the effort to apply numerical methods to calculate thermal fields due to welding, often, the heat from the arc has been approximated, largely as a distributed two or three-dimensional heat source. While such heat sources proved to be accurate, convenient and efficient to apply, there still existed weld pool phenomena which can not be predicted using numerical methods. For example, Barlow [4] (1982), had observed that under certain circumstances of submerged arc welding, two weld pools can exist. That observation had

confounded Gu et al. [38] (1991); the authors found that it was not possible to find a power density distribution to recreate the weld pools Barlow had reported. The authors began to develop a new method, while not entirely original [56], in which the heat from the welding arc was to be applied in a numerical model.

The authors argued that a prescribed temperature field was all that was required to model complex weld pools. For example, a model would have the temperature field of the physical weld pool as a distributed boundary condition; the fusion zone of the model, i.e. the outer edge of the weld pool, would be designated as the melting isotherm while at some location in the weld pool, a maximum temperature is assigned. Such a weld pool temperature distribution can be readily measured using metallography, with the liquid-solid interface being set to the melting point of the base metal. The prescribed temperature heat source model, while ideal for steady-state thermal analysis, has considerable limitations. If the temperature field prior to reaching steady-state conditions was desired, e.g. during the initial startup of welding, the changing weld pool temperature field would be difficult to implement with a prescribed temperature field heat source. The prescribed temperature field heat source is a candidate for calculating temperature fields from welding processes which exhibit steady-state behaviour. However, in-service welding is not steady-state, with varying dimensions of weld pool at any given instant. The prescribed temperature field heat source approach is therefore difficult to implement for the prediction of temperature fields due to in-service welding.

The three-dimensional steady-state thermal field due to moving GMA bead on plate welds was calculated using finite element analysis by Hong et al. [43] (1992). The authors found that in GMA welding, the input energy had two distinct components: the input energy due to the arc, $f_{arc}$, and the input energy carried into the weld pool due to the molten droplets from the electrode, $f_{droplet}$. The authors investigations had found that the metal droplets could in some instances carry as much as 62% of the input energy for bead on plate GMA welds. Consequently, the authors devised a new heat source which

was calculated by the following expression:

$$q(x,y) = \eta V I \left[ \frac{2 f_{arc}}{\pi \sigma_{arc}^2} e^{\left(\frac{-2r^2}{\sigma_{arc}^2}\right)} + \frac{2 f_{droplet}}{\pi \sigma_{droplet}^2} e^{\left(\frac{-2r^2}{\sigma_{droplet}^2}\right)} \right] \tag{2.21}$$

where $r$ is the radial distance from the centre of the arc, and $\sigma_{arc}$ and $\sigma_{droplet}$ are the distribution coefficients of the arc and droplet heat input distributions. The authors assumed that both the arc and the droplet distributions were to vary in a Gaussian manner. The effect of weld pool convection was simulated by an artificial enhancement of the thermal conductivity.

A combination of analytical and numerical methods was employed for the transient heat flow analysis problem by Kumar et al. [53] (1992). Numerical methods were used to calculate the heat flow near the heat source; i.e. the weld pool and the HAZ, while an analytical solution was used to calculate the temperature field at all other locations. The authors included temperature dependent material properties and also had simulated weld pool convection by modifying the thermal properties of the weld pool. The efforts were restricted to planar models which only allows for the calculation of heat flow in thin plates.

In work undertaken to calculate the distortions and residual stresses of structures, Brown & Song [10] (1992) examined the structure/weld interactions using two and three-dimensional numerical analysis. In particular, after negotiating the simulation of welding of ring stiffened cylinder, the authors concluded, verbatim:

> "Geometrically complicated weld paths also complicate thermal analyses, since asymmetric or geometrically varying weld joints make it difficult to select appropriate weld energy flux distributions and magnitudes."

The authors had used a Gaussian surface distribution as the welding heat source and they also minimised the mesh density of the welded region. The authors found that calculating residual stress and distortions in large structures does not require precise definition in the

weld region.

Further work, by Brown & Song [9] (1992) used an 'element birth' procedure to simulate the deposition of weld material. Elements prior to being deposited are inactive. When deposition occurs, these are made active, and the properties of the element are set identical to the metal at melting point. The created elements now remain active for the remaining cooling period. While the concept of element birth is not new, e.g. Tekriwal & Mazumder [77, 78], the fundamental improvement is that the elements are activated at each time step, rather than at the beginning of the analysis. The thermal modelling also included the effects of convection and radiation. Latent heat effects due to liquid-solid phase change, and solid-solid phase change were included by modifying the specific heat value of the material. Barberis & Rebora [3] (1996) applied the concept of element birth to the thermal simulation of GMA welding; the unborn elements are attributed a reduced thermal conductivity of six orders of magnitude, rendering them almost inactive.

While a three-dimensional heat transfer analysis offers the least level of compromise, often a two-dimensional heat transfer analysis, derived with acceptable assumptions, can provide accuracy within acceptable margins of error. A frequently used two-dimensional analysis; i.e. the two-dimensional cross-sectional analysis assuming negligible heat flow in the welding direction, is used to calculate thermal fields under transient conditions. Kamala & Goldak [47] (1992) had examined the error attained by approximating the three-dimensional heat transfer analysis as a two-dimensional cross-sectional analysis. In their investigations, a three-dimensional transient analysis and two-dimensional cross-sectional analysis were calculated. The results of the two-dimensional cross-sectional analysis were projected onto the three-dimensional mesh and the error was the difference in the temperature between the three-dimensional model predictions and the projected two-dimensional predictions. The authors found that the maximum temperature calculated at different nodes at any time was always higher in the three-dimensional analysis than with the two-dimensional cross-sectional analysis. They concluded that the temperature gradient in the longitudinal direction is significant and should not be assumed negligible.

Calculating a steady-state thermal field using numerical analysis, can also be obtained by running a transient analysis until the solution reached steady-state conditions. While the transient Lagrangian thermal analysis in welding is well documented and reasonably straightforward to implement, there does exist some significant disadvantages when attempting to calculate thermal fields due to steady-state welds. Firstly, the weld pool region and the HAZ contain large thermal gradients, and a very fine mesh is required in the region for accurate calculations. For a transient analysis, the requirements are for a very fine mesh along the entire weld path. Quite often, restrictions are inherently placed on the size of the models due to the computer resources available. The second limitation, essentially an extension of the first limitation, is that very small time steps are required to allow for a smooth calculation, rather than a series of discrete welds. Once again, the computing resources available quickly place a restriction on the number of time steps available for the solution. Finally, the modelling of weld metal deposition in a transient analysis is challenging to implement. Changing the mesh and geometry at each time step requires further computing power and time.

The idea of attempting to solve for a transient thermal field under Eulerian conditions using finite element method was attempted by Gu et al. [39] and Goldak & Gu [33]. The Eulerian reference frame used in the analysis required different boundary conditions to the Lagrangian reference frame. The schematic of the model is shown in Figure 2.15. The

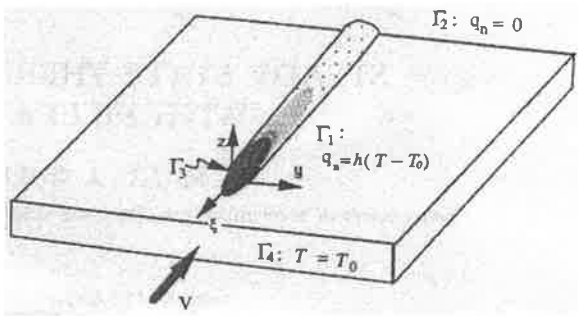


**Figure 2.15:** The Eulerian model and boundary conditions, proposed by Gu et al. [39]

boundary condition $\Gamma_1$ is a natural convection boundary condition, and was assigned to the top surface of the plate. $\Gamma_2$ is located at the surface downstream from the weld and was designated as an adiabatic boundary condition. The prescribed temperature heat source

was applied as boundary condition $\Gamma_3$, and consisted of prescribing the temperature at the liquid-solid interface of the weld pool. $\Gamma_4$, the upstream boundary condition, was assumed to be a Dirichlet boundary condition, having been assigned an ambient temperature. An advantage of the Eulerian model is that the mesh density can be distributed efficiently; high density at the weld pool while lower density at regions further away with lower temperature gradients. The problem of filler metal addition is natural when solving an Eulerian model, e.g. a mesh used in an Eulerian model by Gu et al. is shown in Figure 2.16, with an appropriate boundary condition, such as $\Gamma_4$ in Figure 2.15 effectively accounts for weld metal deposition.

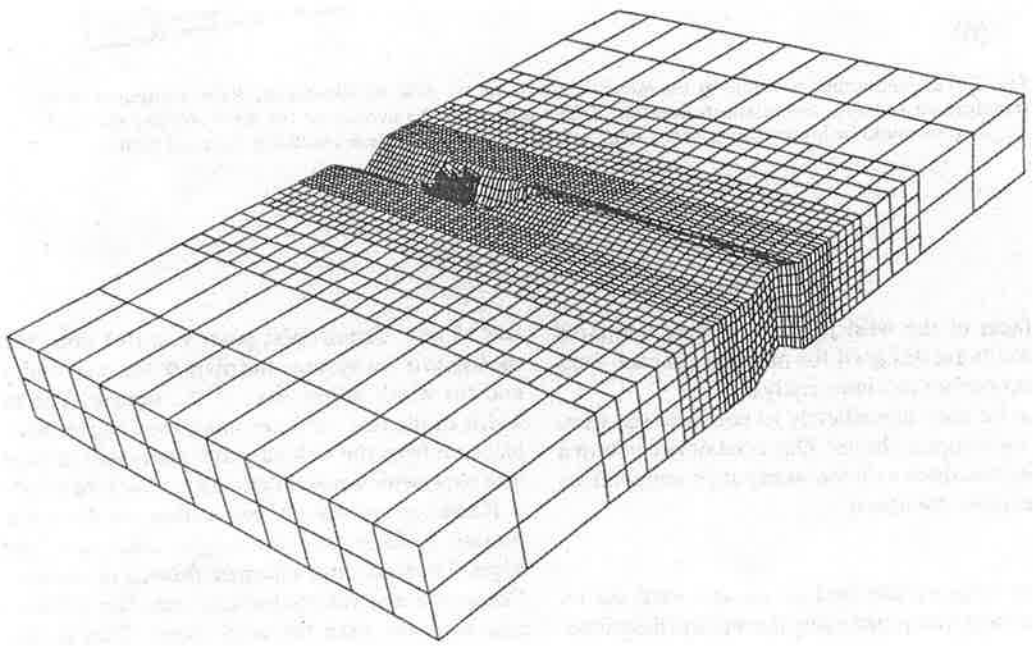

**Figure 2.16:** The FEM mesh built on a Eulerian model; Gu et al. [39]

While the Eulerian model offers significant advantages over the Lagrangian formulation, a few assumptions must be made. The downstream boundary condition, $\Gamma_2$ in Figure 2.15, must be at a sufficient length away from the weld pool. If the length is too short, the temperature gradient at the regions of interest may be affected and the model will display an overall rise in temperature. Secondly, while the Eulerian model provides accurate, fast solutions for prismatic models, a model such as the branch on pipe weld is impossible to analyse, unless attempted using a Lagrangian model.

An innovative method of calculating the solution to the Lagrangian model was proposed by Brown & Song [11] (1993). The authors propose the idea of applying rezoning and dynamic substructuring techniques to the Lagrangian FEM model in an effort to reduce lengthy computation times. The principal idea, is one of a travelling mesh. The Lagrangian model is remeshed at each time step, so that dense mesh is applied at regions of large thermal gradients, while coarse mesh exists for all other regions. Unlike earlier Lagrangian models, dense mesh only exists in a local zone, i.e. the HAZ and the molten weld pool. The reduction in mesh size due to dynamic remeshing offers a significant increase in the speed of the solution.

The model proposed by the authors had three distinct steps. First, for the initial time step, a mesh is generated, boundary conditions applied and the thermal field is solved for. The second step involves the dynamic meshing process; a new mesh is generated for each time step. For the third step, the results from the previous time step is interpolated onto the new mesh, while the boundary conditions for the new time step is applied. Finally, the thermal field is solved for and the steps are applied again until the final time step is reached.

The idea of using a transient adaptive mesh was also reported by Prasad & Narayan [75] (1996). The model was comprised of two-dimensional triangular elements, and the remeshing was controlled by the individual error of each element based on the previous time step. The size of an element was determined by the estimated error calculated for the element at the previous time step.

### 2.3.4 Summary & gaps in knowledge

The calculation of temperature fields due to welding has been successfully achieved by many researchers without explicitly calculating weld pool flow; instead, the calculation is primarily based on the solution of the heat conduction equation, as found in Equation 2.7. These conduction only finite element thermal models, are in general less computationally

expensive, and therefore have significantly lower solution time. Previous researchers have demonstrated that accurate thermal modelling can be achieved without the calculation of the weld pool velocity field. Instead, these researchers approximated the effect of weld pool convection, by subtle modifications to the heat source. In addition, using anisotropic material properties, for example thermal conductivity, has also been another method to simulate the thermal effects of weld pool convection.

The thermal effects associated with the impact of molten droplets in the weld pool for in-service MMA welding is considered to be comparatively less than for GMA welding. Compared with GMA welding, in general, MMA welding is deposited with lower heat input; both voltage and current being lower. In addition, in general, in-service MMA welding has lower deposition rates than GMA welding. Low deposition rates further suggest low momentum droplet transfer compared with GMA welding for a given heat input. Therefore, the greater considerable proportion of heat for low to moderate ($0.5 - 1.5kJ/mm$) heat input MMA welding is due to the arc. Previous research into GMA welding has suggested that penetration depth is related to droplet momentum and current. The variation of penetration depth with current is potentially significant for in-service welding. However, with the weaving present in the MMA welding technique, the variation of penetration depth with current is less significant. The effect of weaving effectively reduces the level of penetration, to an extent, where the variation of penetration depth with current is minor. It is considered that as heat input is increased, the resulting corresponding increase in penetration depth is not proportional. The combination of weaving and low momentum droplet transfer further suggests that the significantly greater proportion of heat applied to the weldment is from the arc; the proportion due to droplet transfer can be considered insignificant. Moreover, as the operating range of current and voltage is limited for MMA welding electrodes, the variation of penetration depth with current is considered to be insignificant for in-service welding.

Very little information has been published relating to the variation of weld pool flow with position, for MMA welding. Work by Phelps, has suggested that heat input, and

resultantly penetration, depending on welding technique and the extent of weaving, is dependent on the position of the weld for in-service welding. However, the study of such is considered to be out of the scope of the present study. As most work which has focused on burnthrough has used mechanised welding, the effect of position on heat input and penetration depth has not been studied.

As summarised earlier in Section 2.3.2.1, predicting thermal fields due to in-service welding requires many important simplifications if attempting to use an analytical thermal model. However, with considerable effort and difficulty, it is possible to develop an analytical model to an extent where reasonable predictions can be made. However, some fundamental assumptions still remain. A comparison between analytical models and finite element thermal models, undertaken by Moore et al. [58], found that the inability to consider temperature dependent material properties, alone as a significant reason for the poor correlation between experiments and predictions.

Predicting thermal fields due to in-service welding can be attempted using two-dimensional approximations. However, a number of significant disadvantages arising due to approximations made to allow the thermal analysis using a two-dimensional model can only be resolved using a full three-dimensional thermal model. Goldak et al. [34] (1986) suggests that important problems of welding, e.g. run-on (weld start) and run-off (weld stop) are ignored entirely by two-dimensional cross-sectional models. However, weld start and weld stop can be simulated with an in-plane two-dimensional analysis. However, in-plane two-dimensional analysis is only applicable to relatively thin plates or high heat input welds, where the through thickness heat flow is considered insignificant.

For in-service welding, the heat flow through thickness and in-plane is significant. Heat flow through thickness is very significant to the study and prediction of pipe wall failure. At a minimum, to calculate the maximum depth of penetration and HAZ depth, a two-dimensional cross-sectional model is required. However, forced convection due to the flowing pressurised natural gas is also very important, in the thermal simulation of in-service welding. The convective transfer of heat is highly dependent on the inside surface

temperature of the pipe wall. As the two-dimensional cross-sectional model ignores the flow of heat in the direction normal to the cross-section, it suggests that the temperature field calculated is identical to a three-dimensional model where the temperature field remains constant for any given cross-section. As the effect of forced convection is based on the difference in temperature between the inside pipe wall surface and the bulk temperature of the fluid, the two-dimensional cross-sectional model exaggerates the flow of heat from the pipe by forced convection. In reality, the temperature field found in-service welding is localised and does vary considerably with cross-section. As a result, the calculation of inside pipe wall surface temperatures is required to accurately reflect the effect of forced convection. At a minimum, to calculate the thermal field at the inside surface of the pipe, a two-dimensional in-plane model is required. However, the only manner in which the convective heat transfer due to the flowing pressurised natural gas, and the variation of temperature through thickness, can be accounted for in one model, is by using a three-dimensional thermal model. As past research [47] has found, considerable differences can be found when attempting to calculate thermal fields using a two-dimensional approximation. Moreover, for the successful numerical analysis of burnthrough, a three-dimensional temperature field is necessary.

The shape of the weld bead can significantly influence the predicted temperature fields from the numerical thermal analysis of in-service welding. Work by Goldak et al. [35] suggests that the weld reinforcing profile and shape alone can strongly influence the predicted weld cooling rate from a finite element thermal analysis of in-service welding. Work by Oddy & McDill [63] suggests that the height of the deposition is a critical variable in the thermal analysis. The authors found that changing the deposit height by as little as $0.3mm$ had changed the peak temperature on the inner surface by $100°C$. However, the sensitivity of the calculations performed by both authors is suggested to be due to the relationship of the datum plane of the chosen heat source, to the geometry of the weld bead. Any change in the geometry of the weld bead had changed the datum plane of the heat source therefore accounting for the significant variation. The influence of a small change in bead shape alone on numerical predictions is unknown. However, it is

considered that minor change in bead shape or volume independently of the heat source definition would not result in a significant change in the overall predicted temperature field.

Earlier work by Graville & Read [36] had yielded a weld bead geometry model where the dimensions of the deposited fillet were a function of heat input. Work by Battelle, to develop software to predict, amongst others, weld cooling rate and inside surface temperature due to in-service welding, had also developed a weld bead geometry model. Similarly, the weld bead geometry was a function of heat input and electrode type. For given arc voltage, and welding speed, the deposition rate from MMA welding electrodes is considered proportional to current; previous researchers have developed equations which imply that the deposition rate of MMA welding electrodes is a linear function of heat input.

The reinforcement profile of the in-service MMA welding weld bead has little published information available in the open literature. While Goldak et al. [35] argue that weld bead reinforcement and area has an effect on predicted cooling rates for FEM thermal calculations, it is unknown as to how much the effect of reinforcement alone, has on predicted cooling rates. The work by Graville & Read [36] and Battele [49] was undertaken by approximating the shape of the weld bead as a triangle; i.e. without any reinforcement. Experimental work is clearly required to resolve this area; a parabolic weld bead geometry model, similar to that proposed by Pardo & Weckman [66] may possibly be required.

There presently is no specific heat source definition for MMA welding using low-hydrogen electrodes or MMA welding in general. An excellent review of the history and development of heat sources for the thermal modelling of welding can be found in the work by Smailes [76]. The following is a brief summary of the heat source development, which is considered relevant for the thermal modelling on in-service MMA welding.

Central to the accuracy of the thermal modelling of welding is the definition of the heat source. Moreover, thermal models which do not explicitly calculate the fluid flow within the weld pool require the heat source to account for the thermal effects of weld pool convection. The simplest of all heat sources to apply to a thermal simulation is the point

heat source initially proposed by Rosenthal [71] (1941). However, calculations involving a point heat source predict unrealistic temperatures near the heat source. Work by Pavelic et al. [67] (1975) resulted in the formulation of a surface two-dimensional circular area heat source. The distribution, as defined in Equation 2.8, was radial, with the centre of the heat source having the maximum value and the circumference having the lowest; the distribution in between was Gaussian. The low penetration characteristics generated, in addition a wide and shallow weld pool, due to the surface heat source is advantageous to the thermal analysis of in-service welding. The dimensions of the weld pool and fusion zone is likely to be similar to those found during in-service welding.

Paley & Hibbert [65] (1975) attempted to apply heat to one or more elements in the finite element mesh. The method proposed by the authors would increase the level of penetration as compared to the heat source proposed by Pavelic et al. However, the penetration depth from a heat source similar to that proposed by Paley & Hibbert [65] (1975) is likely to over predict the penetration found in in-service welding. However, the width and length of the resulting weld pool is likely to be similar to that found in in-service welding.

A significant improvement in the definition of welding heat sources was reported by Goldak et al. [32] (1984). By appropriate choice in the heat source definition, the dimensions of the predicted weld pool are likely to be similar to that found in-service welding. It is considered, that the heat source proposed by the authors is applicable for the thermal modelling of in-service welding.

The novel idea proposed by Gu et al. [38] (1991) where defining the melting isotherm as a boundary condition is likely to create accurate predictions. However, as in-service welding is a manual process, no two welds are likely to have the same weld pool shape regardless of having been deposited under identical heat input.

A number of researchers have attempted to form a split heat source; where the heat from the arc is represented independently from the heat applied to the workpiece from the molten droplets. The work by Hong et al. [43] (1992), proposed the formation of a two-

dimensional circular surface heat source, which included the apportionment of heat due to the arc and droplet. A three-dimensional heat source, which includes the apportionment of heat from the arc and droplet does have considerable advantages. The advantage of a heat source that independently considers the heat from the arc, and the heat from the droplet, is that the relative proportions can be tuned for the MMA welding process. The concept of introducing a term to differentiate the heat from the arc and the droplet; or heat from the arc and arc current does have the potential for improved prediction of HAZ and penetration depth for in-service welding. However, as summarised earlier, the proportion of heat due to droplet transfer in in-service MMA welding, is considered to be low, and almost insignificant when the weld is deposited using a weaving technique.

In summary, the development of a heat source suitable for in-service welding is critical. The heat source definition proposed by Pavelic [67] and Goldak et al. [32] appear to represent either extremes; a heat source which provides weld pool width/depth ratios between the two is likely to be sufficient for the accurate thermal modelling of in-service welding. Moreover, due to the similarities of the three-dimensional DEHS to the circular Gaussian surface heat source, the heat source eventually to be included for the numerical thermal modelling of in-service welding is considered to be similar to a flattened shallow DEHS. In addition, it is also suggested that due to the periodic nature of weaving within the manual welding technique, it can be included as a modification to the Gaussian distribution found in the DEHS.

In addition, the development of a model to provide data to define the weld bead geometry due to in-service welding is necessary. Previous researches have approximated the shape of the weld bead from a triangular to a parabola. The shape suitable for in-service MMA welding is likely to be sufficiently approximated by a parabolic profile. However, a model to predict the size and shape of a weld bead is required; the data for such a model for predicting the shape of weld beads due to low-hydrogen electrodes is not present.

The combination of a heat source suitable for the thermal modelling of in-service

welding with an appropriate weld bead geometry model is likely to provide a model with accurate predictions. The conduction only approach favoured amongst past researches appears to be highly applicable for the thermal modelling of in-service welding. In addition, the finite element method, also commonly used by earlier researchers, is also likely to provide a reasonably accurate approximation. The development of both a quasi-steady-state and transient models is required for in-service circumferential fillet welding; for modelling welds which vary their heat distribution with time requires a transient approach, whereas, a weld which is considered to be essentially steady-state is accurately approximated with a quasi-steady-state approach. The thermal simulation of branch-on-pipe welds, is only possible using a transient analysis due to the non-symmetrical geometry of the joint.

# Chapter 3

# Thermal modelling

## 3.1 Introduction

The finite element method was established in the early 1960's [6]. During the last four decades, the potential of using finite element methods has been realised in many disciplines of engineering. The advantages and applications of finite element methods, are well established in many fields of engineering, for example in linear structural analysis enabling engineers to apply the techniques with confidence. However, applying the finite element method to the science of welding, is entirely a different matter, since welding is a highly dynamic process and is a product of non-linear behaviour. In such cases, the formulation of the finite element method is challenging and understanding the limitations of the finite element method is essential.

The calculation of thermal fields due to in-service welding is essential to the general simulation of in-service welding. Instantaneous temperature fields give an indication of penetration depth and an indication of the strength of the pipe during welding. Moreover, the calculation of weld cooling rates, can provide information on the risk of hydrogen assisted cracking, when combined, with a microstructure model, or with an empirically derived hardness-cooling rate model.

The thermal models used in this research make the assumption that heat flows in the body due to conduction only; mathematically the thermal model is expressed by Equation 2.7. As summarised in the literature review (Section 2.3.4), by choosing an appropriate heat source distribution, conduction models can be produced which allow the calculation of reasonably accurate thermal fields near the weld pool. Such heat sources must be related to the characteristics of the welding process and must often be controlled by empirical factors. This is a pragmatic approach which approximates the physical processes in the weld pool but results in stable numerical solutions within a reasonable time-frame. The special factors which require undivided attention in the thermal simulation of in-service welding are:

- generating a suitable finite element mesh
- calculating the appropriate heat flux distribution due to the manual arc welding
- applying a convective boundary condition due to the flowing pressurised natural gas.

The following sections, will provide detailed explanations of the thermal models proposed to calculate temperature fields due to in-service welding. Initially, the study of thermal fields due to circumferential fillet welding is described and later, the study of thermal fields due to branch on pipe in-service welding is presented.

The approximation of the convective heat transfer due to the flowing pressurised natural gas is presented in Section 3.4, while the modification of the DEHS to suit low-hydrogen electrodes is presented in Section 3.5.

### 3.1.1 Mesh generation

Modern day commercial software, allows the application of the finite element method to many disciplines in engineering. For example, *NISA*, the finite element software package

developed by *EMRC* [25], contains the ability to perform the following analysis: thermal, structural (linear/non-linear) and computational fluid dynamics (compressible and incompressible). They also provide many types of solvers, along with other additional features.

A 'pre-processor', a program which aids a user in generating a mesh, applying boundary conditions and designating other FEM related parameters, is generally incorporated with most commercial FEM software. Similarly, a 'post-processor', a tool which allows the user to extract specific data, e.g. cooling rate, is also included with commercial FEM software. Such tools, while useful and often indispensable, do contain subtle limitations. Modern FEM software, are designed with the concept of broad applicability; quite contrary to the specific needs often encountered in research. In this thesis, while the possibility of authoring a dedicated FEM solver was investigated; due to the considerable effort and resources such an action would have warranted, it was decided to use a sufficiently accurate simulation based on commercial software.

Therefore the general purpose finite element software *NISA* [25] was applied. The limitations of NISA's pre-processor and post-processor were quickly identified, and purpose-specific programs were written. These purpose-specific programs, enabled a user to quickly generate a finite element mesh, suitable for the thermal analysis of circumferential fillet welds and branch on pipe welds. The geometry of the mesh generated from the programs was found to be very accurate. In addition, the total wavefront of the resulting FEM model, was considerably lower than the counterpart produced by the commercial pre-processor.

It appears that the geometry of the circumferential fillet weld is essentially symmetrical and planar; and therefore, a straightforward and easy mesh to create. However, considerable difficultly was found when attempting to include non-rectangular features, such as a parabolic weld bead alongside regular rectangular surfaces, as found adjacent to the main pipe and sleeve. For the circumferential fillet weld, considerable geometrical inaccuracies, were found in the mesh generated by the commercial pre-processor; the

curvature of the pipe was never radially consistent, while the parabolic weld bead was difficult to create.

In the case of the direct branch on pipe model, the advantages of authoring a purpose-specific program to generate a mesh is immediately obvious. The intersection of two pipes proved difficult to generate using the commercial pre-processor. Even when such a mesh was generated by the commercial pre-processor, the geometry was found to be quite inaccurate. Further, including a parabolic weld bead, for the branch on pipe model, was extremely difficult using the commercial pre-processor. Moreover, the geometry of the weld bead changes with angular location further complicating accurate mesh generation. However, the mesh produced by the purpose-specific program was found to have very accurate geometry. In addition, the wavefront of the model was very low, supporting fast solution times.

The time taken to generate a mesh using the purpose-specific software was several orders of magnitude smaller, when compared with creating an identical finite element mesh using the commercial pre-processor. Moreover, if a subtle change in geometry, e.g. weld bead area, was required, considerable amount of time was saved by using the developed purpose-specific software. The mesh generated by the commercial pre-processor is essentially a once-off item; once created it cannot be easily or quickly modified for differing situations. In the case of the purpose-specific software, a change in, for example, an input variable such as weld bead area, was all that was required to create an entirely new and different mesh.

### 3.1.2 Boundary conditions

The thermal models include three unique boundary conditions:

- heat flux due to the welding process
- convection on the inside of the pipe wall due to the flowing pressurised natural gas

- boundary conditions due to ambient conditions.

Commercial finite element software are rarely designed for simulating welding process [76]; NISA not being an exception. As a result, further routines were included in the developed purpose-specific software to simulate the arc welding process, by applying heat flux at either the nodes or the elements. The specifics of calculating the heat flux for both geometries will be discussed in further detail, at later sections: Sections 3.2.3.3 & 3.2.4.3 for in-service circumferential fillet welding and Section 3.3.3.3 for branch on pipe welds.

Applying the convective boundary condition due to the flowing pressurised natural gas was also troublesome, when using the commercial pre-processor. Hence another set of routines were developed for the purpose-specific software; the convective boundary condition was applied to the face of each element at the inside of the pipe wall. Choosing the best method of approximating the flowing pressurised natural gas is described in detail later in Section 3.4.

The remaining boundary condition, relating to ambient natural convection, was applied in a manner similar to that, proposed for the internal forced convective boundary condition. Applying the natural boundary condition using the commercial pre-processor was tedious and difficult. A routine was therefore developed and included in the purpose-specific software, further reducing the time required for the pre-processing stage of the modelling process. The locations of where natural convection was applied, is discussed in a later sections; Sections 3.2.3.4 & 3.2.4.5 for circumferential fillet welding, and, Section 3.3.3.4 for direct branch-on-pipe welding.

In total, three different programs were written to create a specialised finite element mesh for in-service welds:

- the transient analysis of circumferential fillet welding
- the quasi-steady-state thermal analysis of in-service welding
- the transient analysis of branch on pipe welding.

These programs develop an optimised, graded finite element mesh based on pipe geometry, weld bead size and shape. In addition, the programs determined convective boundary conditions dependent on gas pressure and flow and applied these to appropriate elements. Finally, as stated earlier, these programs applied heat flux to those elements or nodes which lie within the path of the moving heat source.

### 3.1.3 Material properties

The thermal material properties, for the types of steel encountered in in-service welding are seldom measured, and very little published documentation exists. Previous investigations in heat transfer analysis and fluid flow due to welding have suggested that, for example, thermal conductivity alone, can change the shape and size, of both the HAZ and fusion zone, for a given weld. The variation of thermal material properties, density, specific heat, and thermal conductivity to chemical composition was found to be minor [42]. Previous research by Smailes [76] (1999), and Davies [22] (1995) were attempted using materials similar to the types of steel, typically encountered during in-service welding. Both these authors had used the thermal material property data originally published in work by Goldak et al. [31] (1986). The thermal material properties, used in both the transient and quasi-steady-state analysis of in-service welding, was therefore, based on the work reported by Goldak et al. [31] (1986).

The values of thermal conductivity, $k$, and specific heat, $c_p$ for different temperature are shown in Figures 3.1. The value of thermal conductivity at temperatures greater than melting point, was artificially increased to simulate weld pool convection; this is a technique which is commonly used in the heat transfer analysis of welding processes. The initial development of in-service welding thermal models, used a constant value of thermal conductivity, at temperatures exceeding melting point. As stated earlier in Section 2.3.3, the value of thermal conductivity, at temperatures exceeding melting point, were often arbitrarily chosen to reflect convection within the weld pool due to weld pool flow. This value of thermal conductivity is usually in the order of between 2-10 times its value at

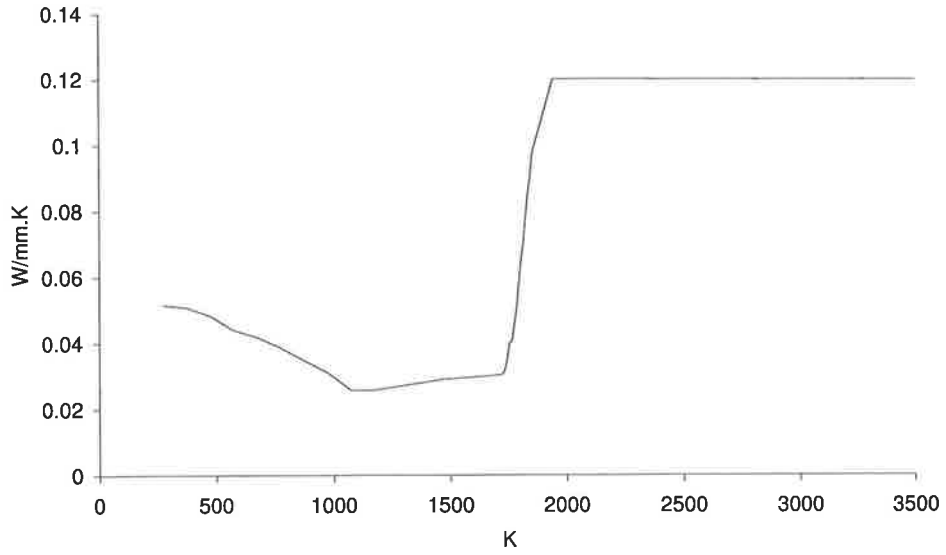


(a) Thermal conductivity

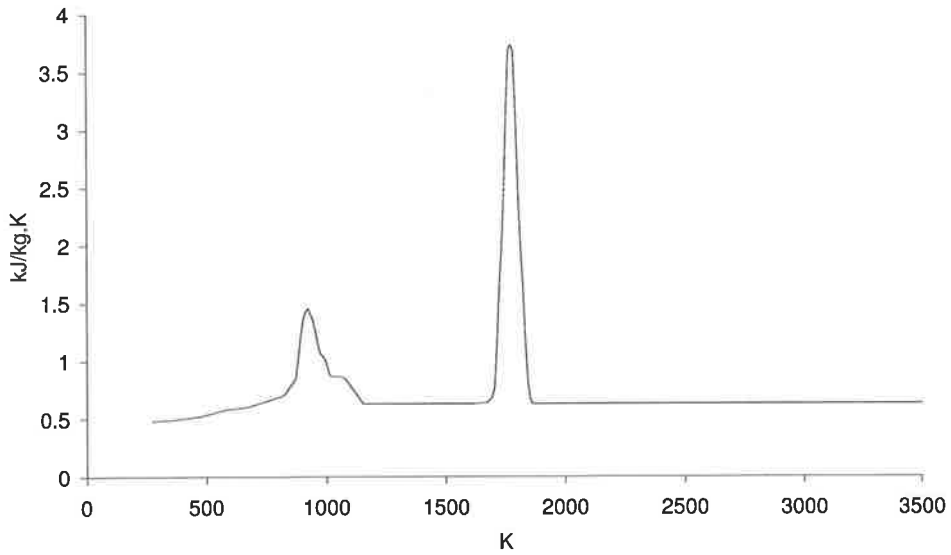


(b) Specific heat

**Figure 3.1:** Thermal material properties used for the thermal analysis of in-service welding on common pipe steels.

the molten temperature. As a result, a sudden step change is found for the thermal conductivity at the melting temperature. The resulting sudden step change, evident in the thermal conductivity curve, posed problems with convergence, for the finite element method. The rapid change, initially over $20K$, was then broadened until convergence, or 1% error, was achieved; a series of calculations, performed in succession for a given welding condition, led to a broader range of $200K$. The change in the shape, and size of

the fusion zone and HAZ, was found to be insignificant.

The weld bead, sleeve, and main pipe, are assumed to have the same thermal material properties; the thermal properties of the gap between the sleeve and pipe are taken to be for air at ambient conditions. Published literature suggests that a small gap exists between the sleeve and the pipe, at regions near the weld. The air gap is due to either surface irregularities or if the fitting of the pipe are out-of-round.

The effect of an air gap on the temperature fields, at regions far away from the weld pool is unknown. In practice, it is difficult to quantitatively measure the gap at all locations between the pipe fitting and the surface of the pipe. It may be argued, that such an unknown region of surface contact, between the pipe and the gap, should be approximated; for example, by applying an effective thermal contact resistance. However, the effect of the gap on temperature fields, near the weld pool region, is considered to be far more significant, than the similar effect of thermal contact resistance at locations far away from the weld pool. Hence, the effective thermal contact resistance approximation was abandoned in favour of a known gap thickness.

In practice, the overall size of the gap is difficult to determine; however, from macrographs of in-service welds, the gap near the weld bead could be easily measured. In conclusion, the effect of the size of the air gap on temperature fields is considered to be minor. Using the results of experiments relating to in-service welding, both in laboratory trials and flow-loop field trials, as discussed later in Section 4.2 & 4.3, a mean air gap thickness was found. The thermal properties assigned to the gap are given in Table 3.1

| | |
|---|---|
| $\rho$ | $1.1774 kg/m^3$ |
| $C_p$ | $1.0057 kJ/kg.K$ |
| $k$ | $0.02624 W/mK$ |
| $T_{gap}$ | $0.25 mm$ |

**Table 3.1:** Properties of air gap [42].

### 3.1.4 Solution parameters

The thermal diffusivity of steel, in combination with the speed of the moving heat source, plays a significant role, in determining how a transient heat conduction problem must be discretized, with respect to time. The time steps must be sufficiently small to allow for the smooth flow of heat from one time step to the next; however, the time steps must also not be too small, since the solution will require significant computing resources to complete.

The conditions at the start of the in-service welding process were not investigated. It can be argued that the commencement of in-service welding often begins with a small dwell time, which can significantly alter cooling rates and increase the risk of pipe wall failure. However, in-service welding is a process where multiple 'runs' are deposited; often, many MMA electrodes are required to complete a length of a circumferential weld. Usually, in between runs, a length of the previous run is ground away. The subsequent run then commences on the newly ground region of the previous run, while eventually depositing weld metal on un-welded pipe. The additional thickness encountered at the start of the run, obviates any concerns of pipe wall failure. Moreover, welding on top of a previous run, tempers the last section of a run while removing any concerns about excessive hardness.

A time step of $0.1s$ was chosen for all transient analysis; such a time step was considered to be a compromise between accuracy and speed of solution using present day computers.

### 3.1.5 Data extraction

The results from the thermal models can be directly compared with metallographic sections of real welds. A transient analysis calculates the temperature for all nodes for a number of time steps. Calculating the weld pool size using a transient analysis is a trivial task. The calculation of cooling rates and maximum temperatures from a transient analysis is also a trivial task, as the temperature history of a given node is available.

The calculation of weld pool size is also a trivial task with the results attained from a quasi-steady-state analysis. For a quasi-steady-state analysis, the data consists of the steady-state temperature at each node. However, the calculation of maximum temperature, and cooling rates for a quasi-steady-state analysis is not straightforward. A method to calculate such quantities was proposed by Friedman [27] (1975), and can be seen earlier in Section 2.3.3. Recapping, the variation of the temperature for a cross-section perpendicular to the travel of the arc, with time, is able to be calculated by applying an equation similar to that proposed by Friedman [27] (1975), or Equation 2.13. The results from a quasi-steady-state analysis is essentially the temperature variation for a cross-section normal to the direction of welding, with time; which is directly comparable with metallographic sections. Similarly, the processed data from the transient analysis is also comparable with metallographic sections.

An alternative post-processor was programmed, which enabled the calculation of cooling rates, HAZ shape, fusion zone shape, and maximum temperature. The commercial post-processor allowed external data to be read in and plotted. Consequently, the written post-processor and the commercial post-processor were combined together, for viewing and plotting the results of the thermal analysis. A summary of the programs written for the thermal modelling of in-service welding can be seen in Figure 3.2.

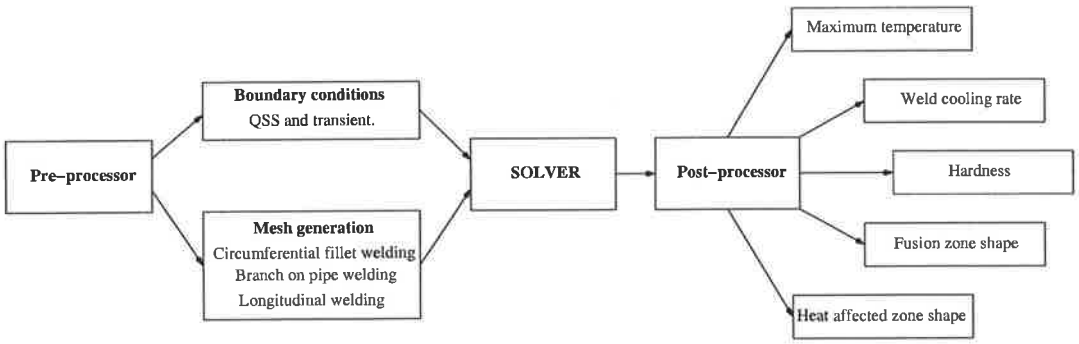


**Figure 3.2:** Software developed for the thermal modelling of in-service welding.

## 3.2 Circumferential fillet welding

### 3.2.1 Introduction

Previous work on the numerical thermal simulation of welding processes suggests that the calculation of thermal fields, due to in-service circumferential fillet welding, can be achieved by either a quasi-steady-state analysis, or by a transient analysis. A quasi-steady-state analysis is useful if the temperature fields of in-service welds are deposited under steady-state conditions; e.g. constant heat-input and welding speed, are required. However, a transient analysis is required if in-service welding is time dependent; i.e. heat-input, welding speed, and other welding parameters vary with time. Moreover, if temperature fields at the start and stop conditions of in-service welding were desired, a quasi-steady-state analysis is unable to calculate them; a transient heat transfer analysis is therefore required.

The following sections provide, a detailed description of the quasi-steady-state, and transient heat transfer analysis models, proposed for in-service welding. Initially, the design of a mesh suitable for a finite element heat transfer analysis will be discussed. From the literature review, a heat source, or distributed power density function was concluded to be the best solution, for simulating the flow of heat from the welding process, to the surface of the weldment. The second section, will discuss the methods developed to incorporate a given power density distributed function or heat source, to the proposed circumferential in-service welding thermal model. Finally, the selection and application of suitable boundary conditions, for both quasi-steady-state and transient heat transfer analysis will be discussed.

### 3.2.2 Mesh generation

The mesh developed for the thermal modelling of circumferential in-service welding has a constant cross-section; an example of the cross-section can be seen in Figure 3.3. where

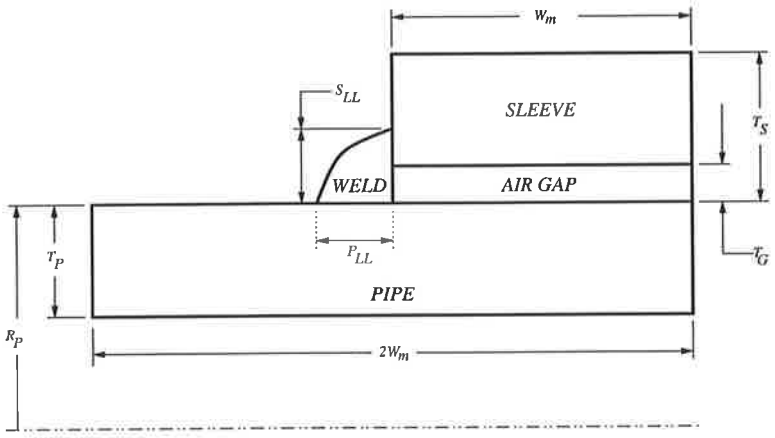


**Figure 3.3:** Schematic: Circumferential fillet weld.

$R_P$, is the radius of the pipe, $T_P$, the thickness of the pipe, $S_{LL}$, the sleeve leg-length or the height of the weld bead, $P_{LL}$, the pipe leg-length or the width of the weld bead, $T_S$, the thickness of the sleeve, $2W_m$, the total width of the model, and $T_G$, the thickness of the gap between the sleeve and the pipe. The width of the model, $2W_m$, is either chosen to reflect the dimensions encountered in the literature, experiments or in the field.

All the geometric terms discussed in the previous paragraph can be directly ascertained from either experiments or literature. The width of the model, $2W_m$ is difficult to quantify for a model of a real pipeline weld; numerical simulations of laboratory experiments, obviously, are much easier. In the modelling of in-service welding, an adiabatic boundary condition is applied at the edges of the model. The width of the model must therefore ensure that it does not significantly influence the region of the model where predictions are to be extracted from. To determine the minimum width, a number of calculations varying in width were attempted. The width was determined, when the temperature gradient at the regions of interest did not vary, with increasing width. Similarly, the spread of heat in the direction of welding also influenced the length of the mode. Ideally, modelling in-service welding would require a complete cylindrical mesh. Such a model, while closest to reality, would require significant computing resources. Alternatively, a portion of a cylinder, for example only revolving around the axis of symmetry by $60^o$, can produce accurate results. The length of the model is strongly dependent on the boundary conditions applied, and also of the type of analysis being calculated. A transient model

requires a different mesh from that required by a quasi-steady-state model; both types of mesh, and the development of each will be discussed in later sections, along with the choice of length and boundary conditions.

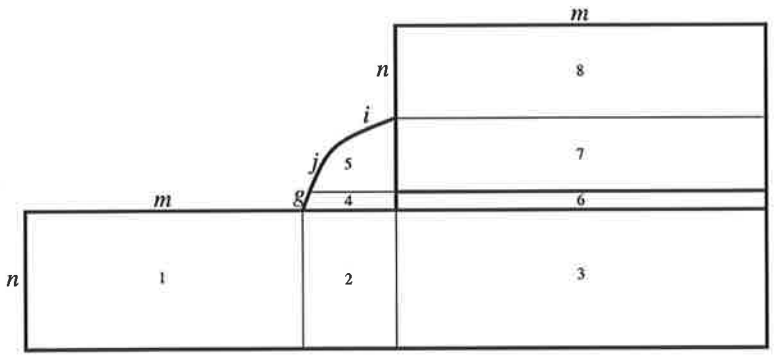


**Figure 3.4:** Circumferential fillet weld, mesh generation parameters.

To aid the development of a mesh generation method, the cross-section of the circumferential fillet weld model is defined by the unison of 8 regions ( labelled 1-8 in Figure 3.4 ): 3 regions $(1-3)$ defining the pipe , 2 regions $(4-5)$ defining the weld bead, 1 region (6) defining the air gap, and finally, 2 regions $(7-8)$ defining the sleeve.

The versatility of the meshing system was enhanced further by the introduction of several control parameters, which were used to control mesh density, and other mesh related qualities, for example aspect ratio. The parameters, $i$, $j$, $m$, $n$, $g$, reflect the number of elements along each respective edge, as can be seen in Figure 3.4. For example, Region 1, is defined by a rectangular region which consists of $m$ elements in width and $n$ elements in height; with a total of $n * m$ elements in the region.

While the aforementioned parameters controlled the number of elements in the mesh, or in a particular region, another set of parameters was introduced to control the distribution of element size along a particular direction. The elements in region 1, 3, 6, 7, and 8 were graded in the horizontal direction, or $Z - axis$, using the following equation:

$$W_n = \frac{\frac{e^{n\ln(R_f)}}{N-1}}{\sum_{i=0}^{i=N-1} \frac{e^{i\ln(R_f)}}{N-1}} \tag{3.1}$$

where $N$ is the total number of elements in the width of a region, and, $R_r$, the reducing

factor corresponding to the ratio $W_1/W_N$, or the ratio of the width of the first element to the width of the last element.

Regions 3, 6, 7, and 8 were graded in the same manner for the horizontal direction, or $Z-axis$, by substituting $R_r = R_f$, where $R_r$ being the reducing ratio for the right side of the model. Similarly, region 1 was graded in the horizontal direction using Equation 3.1, except substituting $R_l = R_f$, where $R_l$ is the reducing ratio for the left side of the model.

Grading in the vertical direction of the cross-section was included for regions 1, 2, 3 and 8. The elements in regions 1, 2, and 3 were graded in the vertical direction using Equation 3.1, except substituting $R_b = R_f$, where $R_b$ is the element reducing ratio for the vertical direction, for all elements in the main pipe. Similarly, elements in region 8 were graded in the vertical direction, by using Equation 3.1, except substituting $R_a = R_f$, where $R_a$, is the vertical reducing ratio for all elements in region 8.

The bead shape was calculated using an empirically derived model; the discussion and development of the model is found later in Section 4.4. Briefly, the empirical model provides the sleeve leg-length, and pipe leg-length dimensions, for a given heat input and and electrode diameter. The weld bead profile was assumed to be parabolic.

The elements in the weld bead were not graded in a logarithmic manner, as was proposed for the previously discussed regions. Instead, the elements were spaced linearly between the parabolic weld bead profile, and the remaining boundaries of the weld bead; an example of which can be seen in Figure 3.5.

In general, the principal reason for grading the mesh, using exponential spacing in some regions, while using linearly spacing in others, was to increase mesh density in regions where large thermal gradients were expected. Such regions, in in-service welding, are found typically surrounding the weld bead, including the fusion zone and HAZ. In Figure 3.6, the application of mesh grading for a 2D cross-section, can be seen.

There are several advantage gained by implementing a parametric system to mesh generation. Firstly, regardless of the values chosen for any of the element control parame-

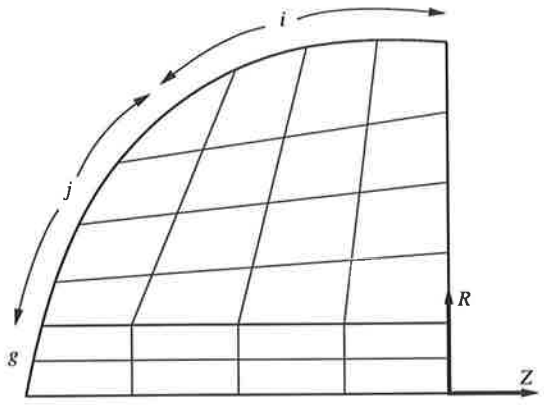


**Figure 3.5:** An example of mesh in the weld bead: parameters are $i = 2$, $j = 2$, $g = 2$.

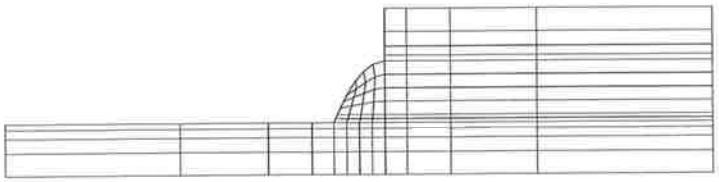

**Figure 3.6:** An example of the cross-section of a circumferential fillet weld mesh.

ters, or element distribution parameters, the model will always be generated without any discontinuities. Secondly, fine mesh may be strategically placed; e.g. at locations near the weld bead, while coarser mesh may be used at regions further away, simply by assigning appropriate parametric values. With such a system, an optimal mesh can quickly be created. The creation of a three-dimensional finite element mesh suitable for transient heat transfer analysis is presented in Section 3.2.3.2, while the three-dimensional finite element mesh suitable for a quasi-steady-state analysis is presented in Section 3.2.4.2.

## 3.2.3 Transient analysis

### 3.2.3.1 Introduction

Applying a transient thermal analysis to a circumferential fillet weld, appears to be unnecessary at first, considering that a quasi-steady-state thermal analysis, already provides much of the relevant and necessary information pertinent to problems associated with in-

service welding. However, a number of interesting and important aspects of in-service welding, can only be analysed using a transient thermal analysis. For example:

- examining the effects associated during the start-up and stopping of welding
- studying the effects of varying arc voltage, current, speed, or heat input during welding.

The next few sections will describe the methods developed, for analysing a circumferential fillet weld, using a transient thermal analysis. The first sections will describe the type of mesh, considered suitable for the task. The second section, will provide details of the method in which the heat from the welding arc, was approximated as a heat flux boundary condition, in the finite element thermal analysis. In particular, the motion of the moving heat source, was critical in the calculation of the heat flux. Finally, the calculation and application of the remaining boundary conditions, associated with in-service welding, is provided. The application of the convective boundary condition, due to the flowing pressurised natural gas is discussed; followed by remaining boundary conditions, relating to the heat transfer due to ambient conditions.

#### 3.2.3.2 Mesh generation

An example of a mesh used for the transient analysis of in-service circumferential fillet welding can be seen in Figure 3.7. Previous research [76] into the numerical modelling of welding, has suggested that the element spacing in the heat source should not be greater than 2mm per element. Such fine element density is required due to the large thermal gradients in the weld pool. Clearly, such an element density can result in a large number of elements and nodes. However, using appropriate assumptions, a full circumferential model is rarely required to calculate the thermal fields due to in-service circumferential fillet welding. Moreover, the size of the main pipe typically found on in-service applications is sufficiently large to enable the use of smaller models. In general, the size of the model

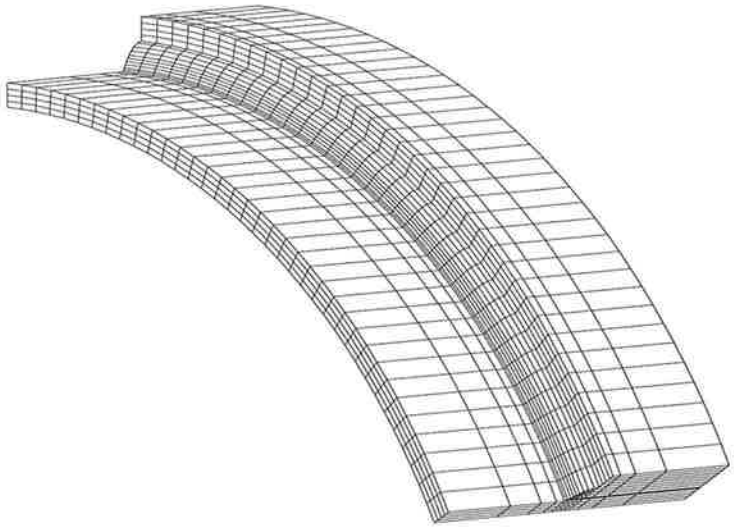

**Figure 3.7:** An example of mesh suitable for the transient thermal analysis of circumferential fillet in-service welding.

is largely dictated by the thermal conductivity or the speed of thermal diffusion within the material.

Applying small sectioned models to in-service welding, for example a model where mesh is essentially a cross-section which has been revolved by 60° around the axis of symmetry, e.g. as seen in Figure 3.7, intrinsically places an adiabatic boundary condition at the start and end faces, for a transient analysis. When such a boundary condition is applied, the choice of location, for the start and end positions of welding, becomes important. If welding were to commence at the edge of the model, large unrealistic thermal gradients would be produced; a similar situation would occur if welding were to finish at the end face of the model. When performing a numerical simulation of in-service welding by ignoring weld pool convection with a conduction only approach, the start and stop locations of welding relies heavily, on the speed of diffusion of heat in the material.

Additional mesh was added to the model behind the start location (front face of the model) and ahead of the stop location (rear face of the model). The amount of mesh added was found to be sufficient by examining the calculated thermal fields for a given weld; if for a given length and width, the temperature gradient at regions of interest did not vary with increasing length and width, the assumption was considered valid and

acceptable. However, if the assumption was found not to hold true, the start and end locations were shifted further inwards, and the width and length were increased.

An investigation was initiated, to determine an appropriate element for the problem of transient thermal heat conduction due to in-service welding. The two elements proposed for the analysis were the 8-noded linear hexahedron, and the 20-noded parabolic hexahedron. In general, performing a FEA calculation using higher order elements creates a solution with smoother results and greater stability. An investigation involving comparing the results of identical welds, differing only in the element types suggested using 8-noded linear elements. Initial investigation had found that smoother thermal contours were noticed in models using parabolic elements. However, applying further mesh refinement to the linear models had resulted in very little discrepancy between the calculated temperature fields. A convergence tolerance of 0.1% was applied to all simulations.

#### 3.2.3.3 Calculation of heat flux

The heat from the welding arc is mathematically represented as an arbitrary distribution; a review of heat sources which are applicable to in-service welding is given earlier in Section 2.3.4. A heat source was developed for low-hydrogen MMA electrodes; the details of which are given later in Section 3.5. The heat distribution can be applied by two methods using the NISA thermal finite element solver; as a boundary condition on a node, or a boundary condition on an element. The unit of heat flux using either method is $energy/(time.volume)$.

The heat flux calculated from the heat source was applied as a boundary condition at a node for the transient thermal models. The accuracy attained by using nodal heat was found to be marginally better, than that found when using element heat; which can be seen in Figure 3.8. Clearly, with greater mesh refinement, approximating the heat source using element heat generation, would have the same accuracy as applying node heat generation. However, such a degree of mesh refinement would require vast amounts of computing resources and solution time. Approximating the heat from the heat source

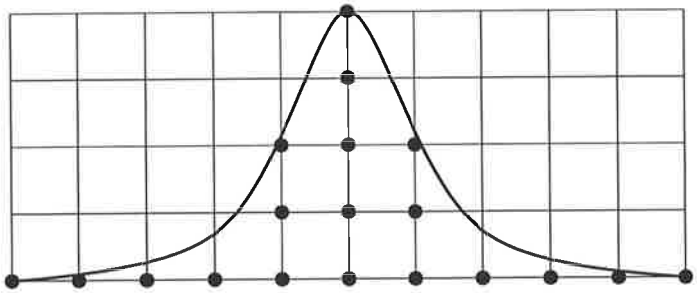

**(a)** Heat applied to the nodes

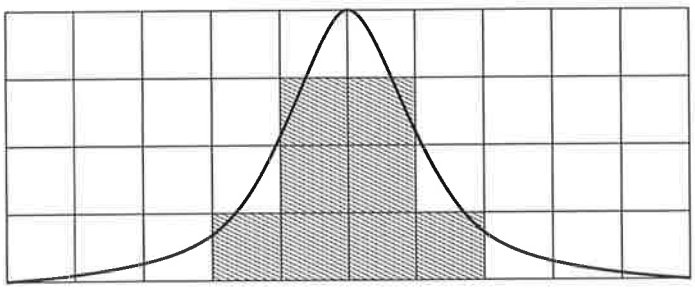

**(b)** Heat applied to the elements

**Figure 3.8:** A comparison between approximating the heat transfered to the model from the arc, as an element boundary condition, or a boundary condition at the node.

using node heat generation, provides the best compromise between accuracy and speed of solution, for the transient analysis of in-service circumferential fillet welding.

A computer program was written to approximate the heat from the welding arc as a heat flux boundary condition for a finite element model. The inputs for the program were:

- dimensions of the circumferential sleeve fitting
- parameters describing the heat source
- welding run parameters: such as the length of the weld, start and end locations, and welding speed.

The first step involved in calculating the heat flux was to determine the start, and end locations, of the welding path, along with the weld path itself.

It was assumed, that the heat source travelled in an arc, of radius $R_{arc}$ in the $x-z$ plane, as displayed in Figure 3.9, for the transient in-service circumferential fillet welding thermal models.

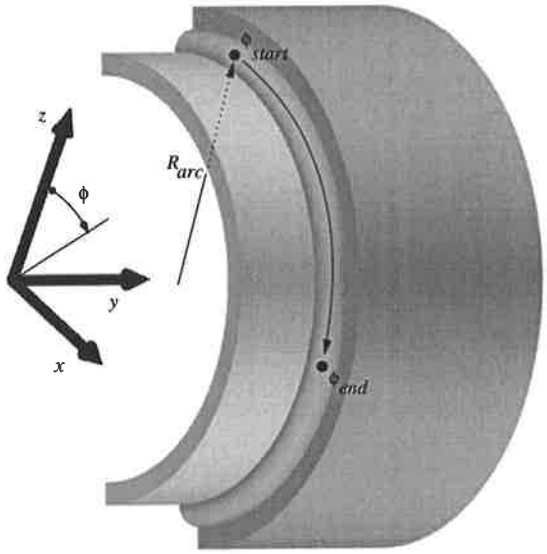


**Figure 3.9:** Path along which welding is deposited.

The location of the arc can be expressed by the following equation:

$$x^2 + z^2 = R_{arc}^2 \tag{3.2}$$

The coordinate of the starting location for welding is

$$\begin{aligned}(x,y,z)_{start} &= (R_{arc}sin(\phi_{start}), 0, R_{arc}cos(\phi_{start})) \\ (x,y,z)_{end} &= (R_{arc}sin(\phi_{end}), 0, R_{arc}cos(\phi_{end}))\end{aligned}$$

Once the path of the heat source was found, the next step was to determine the number of segments in which the welding path is discretized. Assuming a constant welding speed, $w_s$, the following expression was used:

$$N > \frac{R_{arc}\,(\phi_{end} - \phi_{start})}{0.1 w_s} \tag{3.3}$$

where $N$ is a real positive integer. The expression was derived such that length of any segment would require the arc to travel for $0.1s$, at the welding speed, $w_s$. The value of $0.1s$, as discussed earlier in Section 3.1.4, represented a convenient time step, which avoided significant errors due to heat diffusion, and avoided requiring large computing resources and solution times.

Once $N$ is determined, the time steps for the transient analysis is then calculated using the following expression:

$$t_n = n\left(\frac{\phi_{end} - \phi_{start}}{Nw_s}\right) \tag{3.4}$$

The following expression was then used to calculate the location of points from the discretized welding path:

$$\begin{aligned} \phi(n) &= \frac{\phi_{end} - \phi_{start}}{N} + \phi_{start} \\ (x, y, z)_n &= (R_{arc}sin(\phi(n)), 0, R_{arc}cos(\phi(n))) \end{aligned}$$

where, $N$, is a real positive integer which satisfies $0 \leq n < N$.

For each point, which also corresponds to an instant in time, the heat flux due to the welding arc was calculated. The first step involved in the calculation of the heat flux, was to determine the coordinate system of the heat source. The application of the heat source, or power density distribution function, was achieved using a datum plane as seen in Figure 3.10. The sleeve and pipe leg-lengths were then used to calculate the sleeve and pipe datum points; as seen in Figure 3.11 . The line $DSLL - DPLL$ was assigned the same slope, as a straight line joining $SLL$ to $PLL$. The line $DSLL - DPLL$ was assumed to be the line which intersected the parabolic weld bead at one location, as seen in Figure 3.11. The datum points $DSLL$ and $DPLL$ were 5/4 times bigger than $SLL$ and $PLL$ respectively. If the weld bead was considered to be triangular; i.e. to not have any reinforcement, then the datum points $DPLL$ and $DSLL$ would equal $PLL$ and $SLL$.

Once the two datum points, $DSLL$, and $DPLL$, were calculated, the third datum

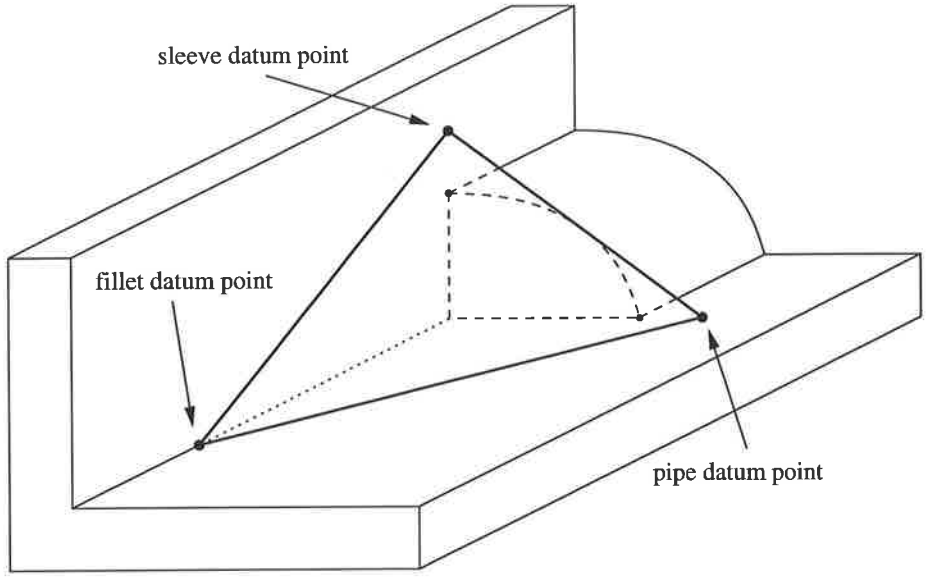


**Figure 3.10:** Heat source datum plane for circumferential fillet welding.

point, $DF$, as seen in Figure 3.12, was calculated using trigonometry. The origin of the heat source, or point $HSO$, is known from the discretized path of the welding heat source; therefore $\phi_{HSO}$ is known. As seen in Figure 3.12, the datum plane is defined by the following three points: $DSLL$, $DPLL$ and $DF$. The datum plane, as viewed from a plane perpendicular to the axis of the pipe, can be seen in Figure 3.13. When defining the datum plane, it was assumed that: $\phi_{DSLL} = \phi_{DPLL}$. From the definition of a given heat source, the values, $c_f$, the length ahead of the heat source origin, and $c_b$ the length behind the heat source's origin, as seen in Figure 3.12, is known. For example, for a hemispherical heat source, the expression $c_f = c_b$ would hold true. For the DEHS, the values $c_f$ and $c_b$ are known.

The x-axis of the heat source, $L_x$, is calculated from the vector expression $\overrightarrow{HSO - DF}$. The z-axis of the heat source, is the vector normal to the plane bounded by the points $DF$, $DSLL$, and $DPLL$. Finally the y-axis of the heat source, $L_y$ is calculated using a cross-product of the x-axis and z-axis, or mathematically using the expression : $L_y = L_z \times L_x$. The origin of the heat source, $HSO$, was now obtained by further trigonometry.

The heat flux was calculated for every time step as follows. For a given time step, the heat source was assigned a local coordinate system, $L_{x,y,z}$, with axes $L_x$, $L_y$, and $L_z$

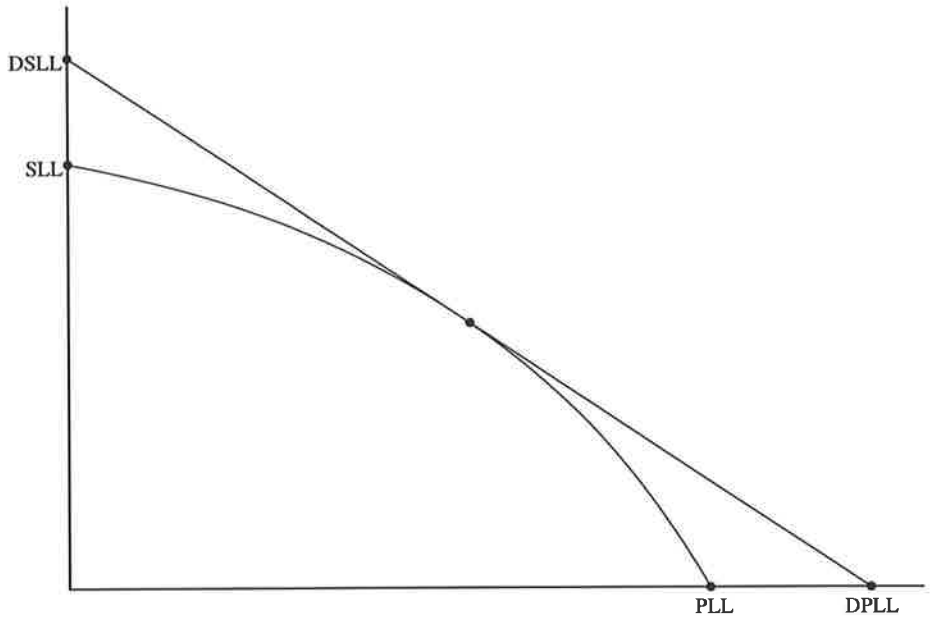


**Figure 3.11:** Pipe and sleeve leg length datum points.

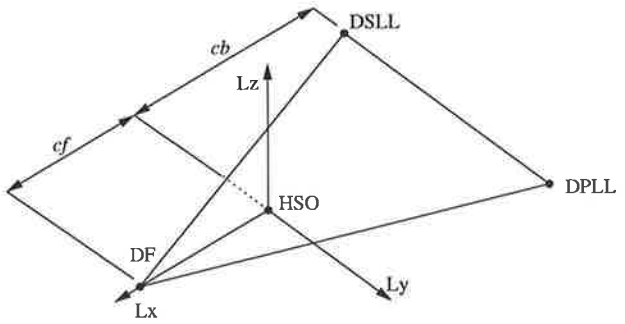


**Figure 3.12:** Circumferential fillet welding heat source coordinate system.

as seen in Figure 3.12. After the origin of the heat source is found for a given time-step, the nodes of the model which lie within the volume of the heat source are determined. Coordinate transformation, is applied at each time step to convert the positions of all nodes in the general coordinate system, to the local coordinate system of the heat source.

Once all the heated nodes are found, the heat flux is calculated for each node using the given distribution. Once all the values of heat flux is calculated for all nodes within the volume of the heat source, for a given time step, the total amount of heat applied to the mesh, for that time step is calculated; i.e. for an 8 noded element, the total heat

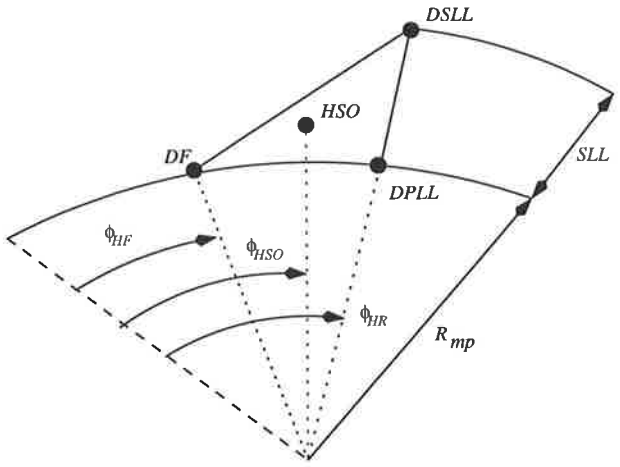


**Figure 3.13:** Datum plane for circumferential fillet welding heat source.

applied to the mesh is evaluated using the following expression:

$$\sum_{n=0}^{n=h_{total}} q_{node} V_c \tag{3.5}$$

where, $h_{total}$, is the number of heated nodes for the time step, $q_{node}$, is the value of heat flux initially calculated for the node $n$; and $V_c$, is the characteristic volume occupied by all elements which contain node $n$. The characteristic volume of a node, is the sum of the volume of all elements which contain the node, divided by eight. The volume of the element was calculated, by approximating the element as consisting of 6 tetrahedron. The volume of a tetrahedron was calculated using vector methods.

The volume required by the heat source was usually found to be slightly different to that calculated using the finite element mesh (as discussed earlier). The difference is due to the discretization of the geometry, however it was overcome using a correction factor, $f_c$, calculated using the following expression:

$$f_c = \frac{\eta V I}{\sum_{n=0}^{n=h_{total}} q_{node} V_c} \tag{3.6}$$

The correction factor was then multiplied to the heat flux value of all heated nodes so that the correct amount of heat was applied for a given time step.

#### 3.2.3.4 Boundary conditions

In addition to the heat flux boundary condition discussed earlier in Section 3.2.3.3, two further distinct boundary conditions are placed on the model:

- heat loss to ambient surroundings due to natural convection
- heat loss to the pressurised flowing natural gas through forced convection.

The heat loss to the atmosphere was approximated as forced convection; airflow at $2m/s$ over $0.2m$ square plate. From Holman [42], a value of $12W/m^2K$ was used for the transient heat transfer analysis. Such a value was considered to be an average value anticipated in typical field in-service welding conditions. The calculation of heat transfer due to the flowing pressurised natural gas, is found later in Section 3.4. The convective heat transfer due to the flowing gas was approximated as a heat transfer coefficient, and applied to the inside surface of the pipe. A typical example, of the boundary conditions placed on a transient heat transfer analysis can be seen in Figure 3.14. The heat loss to the atmosphere by convection was placed on the element faces which are in contact with the atmosphere: namely the outer surface of the weld bead, the outer surface of sleeve, and the outer surface of the main pipe. The heat loss to the flowing pressurised natural gas was applied to all element faces which form the inside surface of the main pipe.

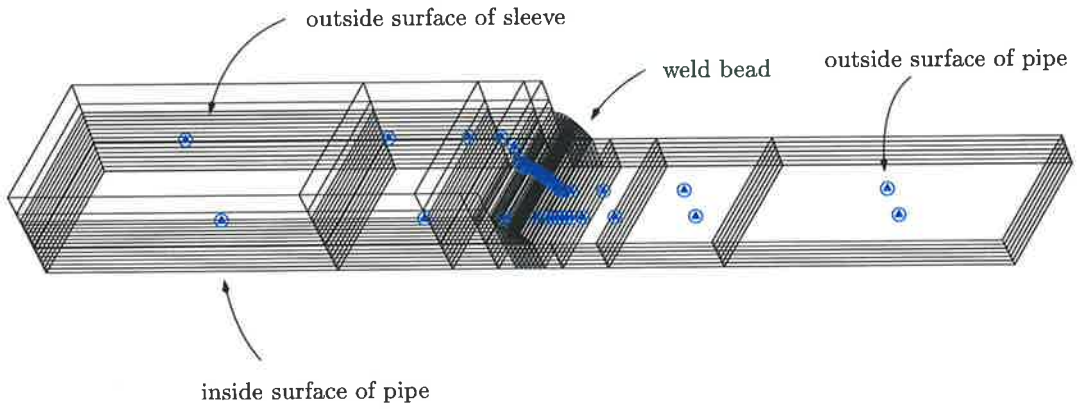


**Figure 3.14:** An example of boundary conditions placed on a transient finite element thermal analysis of in-service circumferential fillet welding.

Heat loss due to radiation, was initially considered for the heat transfer analysis. However, a number of comparisons between solutions which are identical, except for the radiation boundary condition, revealed unnoticeable differences in the temperature field at regions of interest. The relatively small welding pool size, and low peak temperatures is considered to be the primary reason for the insignificant effect of radiation heat transfer.

### 3.2.4 Quasi-steady-state analysis

#### 3.2.4.1 Introduction

The quasi-steady-state analysis, has in the past, as discussed in the literature review in Section 2.3.3, been a popular method of simulating welding processes. While the quasi-steady-state analysis is unable to be used to study certain phenomena in welding as discussed in Section 3.2.3.1, it has many benefits which are useful for the heat transfer analysis of in-service circumferential fillet welding. A transient analysis, requires mesh refinement at all regions where the heat source is expected to travel, and a mesh with significantly larger number of nodes is created as a result. However, a quasi-steady-state analysis, intrinsically avoids such a problem, as the heat source is considered stationary while the mesh has a velocity associated with it. Mesh refinement for quasi-steady-state models, is only required to be fine at one location; within and surrounding the region of the weld pool. Moreover, unlike a transient analysis, where the solution is required to be solved for many time steps, the quasi-steady-state analysis only requires the solution for effectively one time step.

The following sections, will provide details of how the quasi-steady-state assumption, was used for the prediction of temperature fields, due to in-service circumferential fillet welding. The first section, will provide details on the type of finite element mesh which was used during the development of the quasi-steady-state model, along with how it was created. At the next section, the method in which the welding heat source was applied, as a boundary condition in the finite element model is discussed. At the third section,

a discussion on how the quasi-steady-state assumption was applied using a incompressible computational fluid dynamics (CFD) solver, is given; with a detailed examination on the material properties assigned for each specific material. Finally, a discussion on the remaining boundary conditions; ambient and forced convection due to the flowing pressurised natural gas is presented.

#### 3.2.4.2 Mesh generation

The mesh used for the quasi-steady-state thermal analysis of in-service welding was developed with the benefits of a quasi-steady-state solution in mind. Unlike a transient analysis mesh, a quasi-steady-state mesh does not require mesh refinement for a considerable portion of the mesh. An example of a typical mesh used for the quasi-steady-state analysis of circumferential in-service welding can be seen in Figure 3.15(a) and 3.15(b). As can be

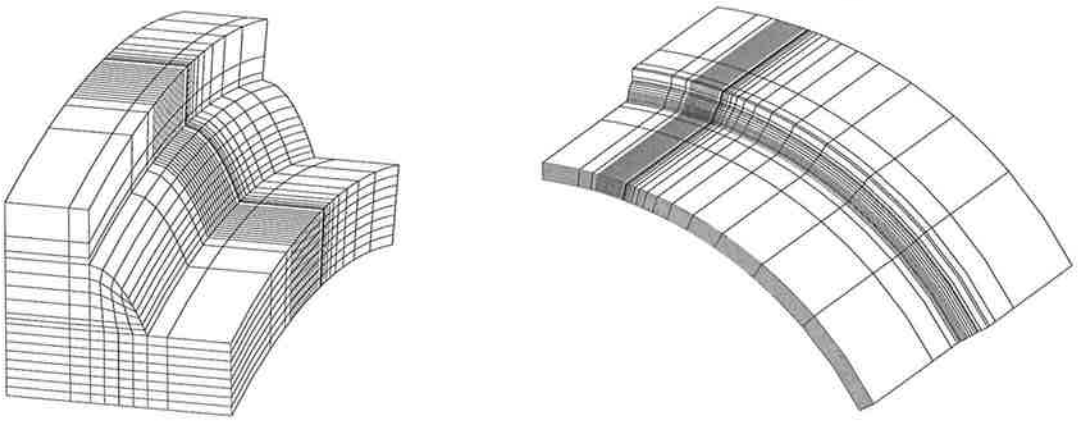

(a) View of weld bead and adjacent regions

(b) View of entire mesh

**Figure 3.15:** Typical mesh used for the quasi-steady-state thermal analysis of in-service circumferential fillet welding.

seen in Figure 3.15(a), considerable mesh refinement was included at regions where large thermal gradients are anticipated. The region where the heat is applied, and the local pipe wall adjacent to the heated region, benefit from the high mesh density. Typically, between 4 and 8 elements spanned the thickness of the pipe; the number of elements used in the thickness was a function of the thickness of the main pipe. A total of 20 elements

were placed in the cross-section of the weld bead; regardless of the area of the weld bead. Due to the lower number or elements, and nodes, as compared to a transient circumferential fillet welding model, it was considered advantageous to apply quadratic 20-noded elements for the quasi-steady-state model. Attempting a quasi-steady-state analysis using parabolic elements has two significant advantages:

- the solution accuracy is improved over comparative linear 8-noded mesh
- more interestingly, the same mesh can be suitably used for a stress-analysis for the study of burnthrough, as discussed later in Chapter 6.

The grading of the mesh was designed to minimise elements with large aspect ratios, at regions where large thermal gradients are anticipated. Typically, at regions far removed from the heat source or weld pool, for example, near the outer edges of the mesh, using elements of moderately large aspect ratios is acceptable. The dimensions of the model, namely width and length were chosen in a manner similar to that proposed for the transient thermal modelling of in-service welding, discussed earlier in Section 3.2.3.2. Briefly, a number of models with increasing dimensions for length and width were calculated, while a width was chosen when the temperature field and thermal gradients at regions of interest did not vary with increasing width and length.

#### 3.2.4.3 Calculation of heat flux

The calculation of heat flux, due to heat from the welding arc, is essentially the same as the calculation of heat flux for the transient heat transfer analysis of in-service circumferential fillet welding, as discussed in Section 3.2.3.3. The calculation of the datum plane, and associated points are identical. However, as a greater amount of mesh density can be used for a quasi-steady-state analysis, in comparison with a transient analysis, the heat flux was calculated and assigned per element, rather than at nodes within the heat source.

The first step in calculating the heat flux, was to determine the elements within the

boundary of a given heat source. If the centre of the element was found to lie within the volume of a given heat source, a value of heat flux, based on the coordinate of the centre of the element was calculated. The process was repeated until all elements were exhaustively searched. On completion of the search, the total amount of heat applied to the mesh was calculated. For a 20-noded element, the volume of the elements was calculated based on the 8 corner nodes of the element. The volume of the element was calculated in a manner identical, to that proposed for the calculation of element volume for the transient analysis of circumferential fillet in-service welding, as discussed in Section 3.2.3.3. The total heat applied to the mesh was then calculated using the following expression:

$$\sum_{n=0}^{n=h_{total}} q_{element} V_{element} \tag{3.7}$$

where, $h_{total}$, is the number of heated elements, $q_{element}$, is the value of heat flux initially calculated for the element and, $V_{element}$, is the volume of the element.

The idea of calculating the total heat, and multiplying by a correction factor, is very similar to that proposed for the transient analysis of in-service circumferential fillet welding, as discussed earlier in Section 3.2.3.3. The initially calculated heat flux value was then multiplied by a correction factor, $f_c$, for all heated elements, so that the correct total amount of heat was applied to the mesh. The correction factor was calculated using the following expression:

$$f_c = \frac{\eta V I}{\sum_{n=0}^{n=h_{total}} q_{element} V_{element}} \tag{3.8}$$

#### 3.2.4.4 Material properties

The quasi-steady-state thermal analysis, used the incompressible computational fluid dynamics solver, developed by *EMRC*. The elements which form the weld bead are assigned either of two material properties. Any elements which lie beneath the heat source and behind the heat source were assigned the same material properties as the main pipe and sleeve. The weld bead region ahead of the heat source was assigned the same material

property as the remaining weld bead, however, the thermal conductivity was reduced to minimise the amount of heat dissipating to the front of the model due to diffusion. The remaining material properties for the weld bead region, main pipe and sleeve are identical to the values used for the thermal modelling of in-service circumferential fillet welding in general, as discussed earlier in Section 3.1.3. An example of such a mesh, with different materials can be seen in Figures 3.16(a) and 3.16(b).

#### 3.2.4.5 Boundary conditions

The quasi-steady-state solution is based on the problem being formulated for an Eulerian reference frame; in comparison a transient analysis as proposed for in-service circumferential fillet welding, is solved using a Lagrangian reference frame. However, the velocity field for all materials, in a quasi-steady-state analysis, is required to be defined as the velocity of the heat source; as in a quasi-steady-state analysis, the velocity of the heat source velocity is zero. In comparison, the transient analysis proposed earlier in Section 3.2.3, is formulated with a moving heat source and a stationary mesh. The velocity of all nodes in the quasi-steady-state mesh was assigned with the velocity of the welding arc. In addition to the velocity of the nodes being initially specified, the temperature of the material entering the mesh was also assigned. The flow of material heat; or solid advection can significantly affect the downstream thermal field; as was reported by Goldak [30]. All nodes at the inlet face of the mesh were assigned an ambient temperature or set to a given preheat temperature.

The remaining boundary condition relating to ambient conditions, and forced convection due the flowing pressurised natural gas, were applied in a manner identical to the transient heat transfer problem; as discussed earlier in Section 3.2.3.4.

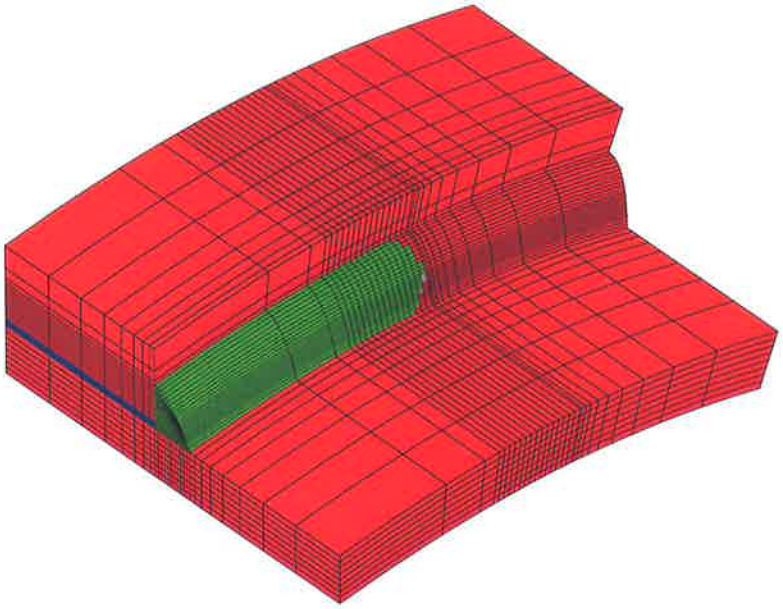

(a) Weld bead in from of heat source coloured green

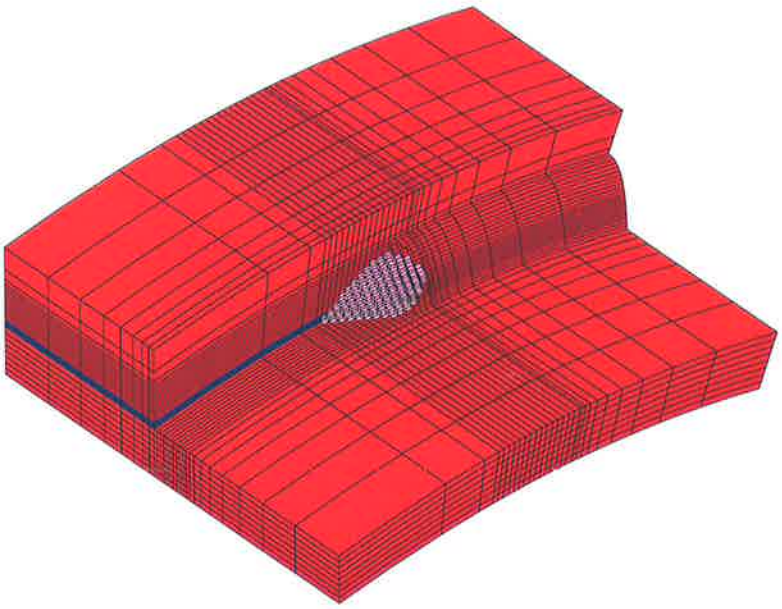

(b) Heated elements coloured pink

**Figure 3.16:** Typical mesh used for the quasi-steady-state thermal analysis of circumferential in-service welding; pipe and sleeve coloured red, air gap coloured blue.

## 3.3 Branch on pipe welding

### 3.3.1 Introduction

The model proposed to calculate weld thermal history due to in-service branch on pipe welding, is essentially identical, to that proposed for the calculation of thermal history of in-service circumferential fillet welding using a transient heat transfer analysis, as discussed earlier in Section 3.2.3. The idea of approximating the heat transfer problem, to only consider conduction, ignoring weld pool convective heat transfer, is common to both. However, the geometry encountered in branch on pipe welding, is considerably more complex than that found in in-service circumferential fillet welding.

The results of the literature review revealed that very little work has been published, relating to the heat transfer analysis of in-service branch on pipe welding. The only notable published work, was by Battelle [49], where the branch on pipe weld was analysed by using two-dimensional approximations. Battelle considered, that the most important regions to examine the thermal fields due to branch on pipe welding, was at the top and bottom position, as previously illustrated in Figure 2.9. The work contained within this thesis represents a significant improvement, over such two-dimensional thermal simulations; the thesis discusses the development of a novel three-dimensional thermal model for in-service branch on pipe welding.

The thermal analysis of in-service branch on pipe welding has two significant difficulties:

- mesh generation
- calculation and application of heat flux to simulate welding

As found in the literature review, no work has been published which attempts either of the aforementioned steps, in successfully calculating thermal fields, due to in-service branch on pipe welding.

A thermal analysis of branch on pipe welding can only be achieved using a transient analysis; unlike circumferential fillet welding, no symmetry exists for branch on pipe welds. The following sections will discuss a model proposed for the transient thermal analysis of branch on pipe welding. The first section will discuss a method developed to generate a finite element mesh, for the thermal analysis of in-service branch on pipe welding. The second section will discuss the method developed, to approximate the heat from the welding arc, as a heat flux boundary condition. The new developed method can accommodate for any variety of electrode and welding angles. The calculated heat flux was applied to a node rather than an element; identical to the approach taken for the transient thermal analysis of in-service circumferential fillet welding, as discussed in Section 3.2.3.3. Finally, the application of the remaining boundary conditions; ambient conditions and forced convection due to the flowing pressurised natural gas, is discussed.

### 3.3.2 Mesh generation

The geometry of a direct branch on pipe weld is complex, and is difficult to reproduce accurately. Several attempts were made to use the commercial program, *DISPLAY III*, to produce a mesh for the thermal analysis of branch on pipe welding. In all attempts, considerable inaccuracy was found, especially at the region where the branch and pipe intersects. The inaccuracy stemmed from the limited manner in which the software dealt with curved surfaces thereby creating inaccurate geometry. The innacuracy was further exacerbated by intersecting two or more curved surfaces such as the region where the branch and pipe intersect. In addition, including the weld bead region accurately within the mesh was found to be almost impossible.

A quarter section of a typical branch on pipe joint can be seen in Figure 3.17. The variation in the cross-section for a branch on pipe joint can be seen in Figure 3.18 where the cross-section is viewed by the plane defined by the expression: $y = tan(\theta)x$.

The dimensions of a typical branch on pipe weld can be seen in Figure 3.19 where

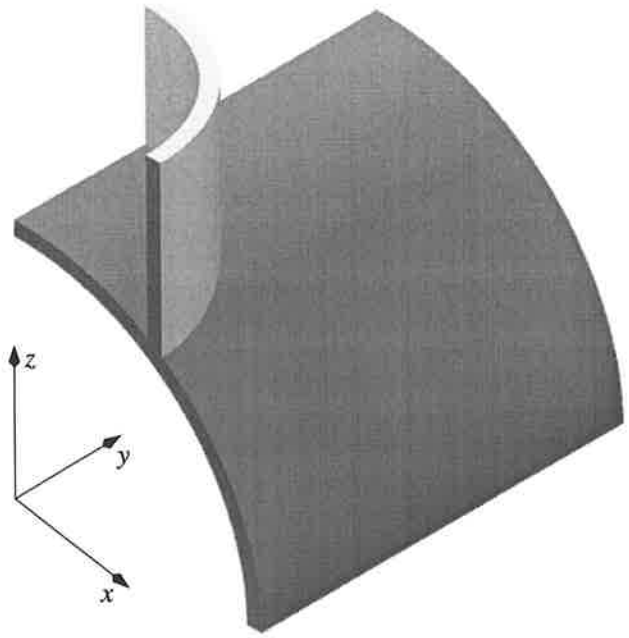


**Figure 3.17:** Quarter section of a typical branch on pipe weld.

(a) $\theta$ =0° (b) $\theta$ =30° (c) $\theta$ =60° (d) $\theta$ =90°

**Figure 3.18:** Cross-section variation of branch on pipe joint, revolving around z-axis.

$R_{branch}$ is the outside diameter of the branch connection, $T_{branch}$ is the thickness of the branch connection, $R_{main}$ is the outside radius of the main pipe and $T_{main}$ is the wall thickness of the main pipe. As branch on pipe welds were rarely discussed in the examined literature, and in addition, were insignificant in the proportion of hot-taps applied within industry, the shape of the weld bead was assumed to be similar to that found for in-service circumferential fillet welding. In addition, little information was found relating to branch on pipe weld preparation.

Due to the changing geometry, as viewed by a plane, $y = tan(\theta)x$, if the pipe and branch leg-lengths of a given weld bead were kept constant, the area of the weld bead

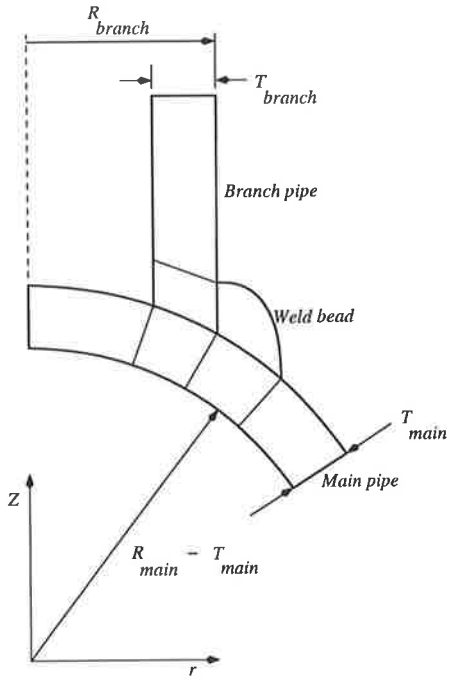


**Figure 3.19:** Typical cross-section of a branch on pipe weld.

would vary with $\theta$. For a given in-service branch on pipe welds, the weld bead area was assumed to remain constant with $\theta$. Including the weld bead for a finite element mesh, was considerably difficult with *DISPLAY III*. Significant inaccuracies in geometry, resulted in a weld bead which was not constant in area. Moreover, including a parabolic profile for the weld bead, was highly difficult, when using *DISPLAY III*. A new method of generating a finite element mesh, was therefore developed.

The branch on pipe mesh was formed by dividing the geometry into N radial slices, positioned around the z-axis. For each slice, the nodes and elements were created for the cross-section, in a manner similar to the approach taken for mesh generation of circumferential fillet welding. To aid mesh generation, the cross-section was divided into several regions, as illustrated in Figure 3.20. Regions $1-4$ for the main pipe, region 5 for the branch pipe adjacent to the weld bead, region 6 for the weld bead, and finally, region 7 for the remaining section of the branch pipe. The process of calculating the nodes and elements is similar to the method proposed for calculating the finite element mesh for the numerical thermal analysis of in-service circumferential fillet welding; as discussed earlier in Section 3.2.2.

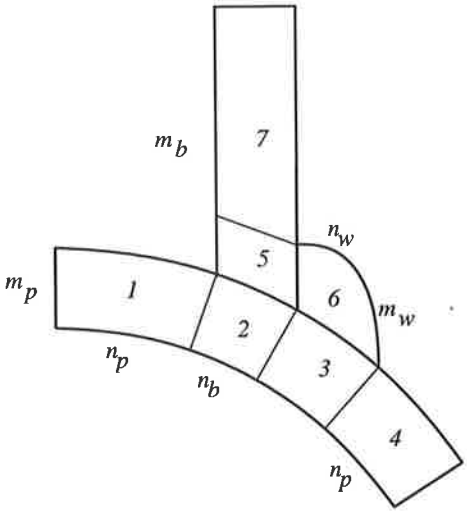


**Figure 3.20:** Division of cross-section to aid and improve the mesh generation program for branch on pipe welds.

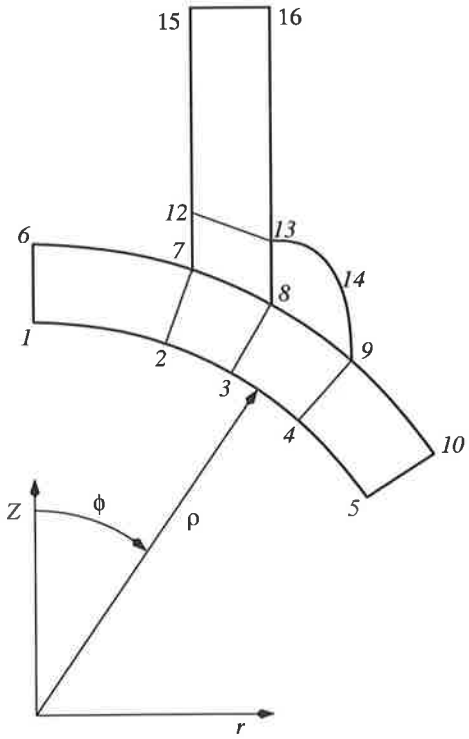


**Figure 3.21:** Parametric definition of branch on pipe cross-section.

Each region is defined by a series of control points, as seen in Figure 3.21; the points are initially defined, and in combination with analytical equations describing the surface of the pipe, weld bead and branch geometry, allow the calculation of coordinates all nodes for a given mesh. Once the coordinates of the node have been defined, the element connectivity is also then defined.

Each region is defined by a number of elements in width and in thickness, as can be seen in Figure 3.20. Regions $1-4$ are defined as having $m_p$ elements in thickness, regions $5-6$ have $m_w$ elements in thickness, while region 7 has $m_b$ elements in thickness. Regions 1 and 4 have $n_p$ elements in width, while regions 3 and 6 have $n_w$ elements in width. Finally, regions 5 and 7 have $n_b$ elements in thickness. The elements spacing for regions 1 and 4 were set using a logarithmic expression, similar to Equation 3.1, discussed earlier for the the mesh generation of in-service circumferential fillet welds, as mentioned in Section 3.2.2. Similarly, the element spacing in the $z$ direction of the remaining branch pipe was calculated using a logarithmic function.

The following expressions were assumed when creating the finite element mesh:

$$\begin{aligned} \phi_1 &= \phi_6 \\ \phi_2 &= \phi_7 \\ \phi_3 &= \phi_8 \\ \phi_4 &= \phi_9 \\ \phi_5 &= \phi_{10} \end{aligned}$$

The value of $\phi_1$, $\phi_6$, $\phi_5$ and $\phi_{10}$ were chosen so as to minimise the impact of model geometry on the temperature field at regions of interest. The following expressions were appropriately chosen:

$$\begin{aligned} \phi_1 &= \phi_6 = 5\frac{\pi}{180} \\ \phi_5 &= \phi_{10} = 2\phi_9 + \left(\frac{\pi}{2} - 2\phi_9\right) cos^2(\theta) \end{aligned}$$

All points along the inside surface of the pipe, or points (1) to (5), and the points along the outside surface of the pipe, or points (6) to (10) were calculated using the following

expression:

$$\rho_i = \frac{R}{\sqrt{\cos^2(\theta) sin^2(\phi_i) + cos^2(\phi_i)}} \tag{3.9}$$

$$\phi_i = \sqrt{\frac{1}{\left(\frac{R}{r}\right)^2 + sin^2(\theta)}} \tag{3.10}$$

where $R = R_{pipe}$ for points (6) to (10), and $R = R_{pipe} - T_{pipe}$, for points (1) to (5).

The intersection of the branch pipe and the main pipe, was defined as the curve between points (7) and (8). The following expressions were used to calculate their locations:

$$r_7 = R_{branch} - T_{branch}$$

$$r_8 = R_{branch}$$

The points used in generating the mesh in the branch pipe were, (15), (16), (12), (13), in addition to the previously defined (7) and (8). The aforementioned points were defined using the following expressions:

$$z_{12} = z_7 + PLL$$

$$z_{13} = z_8 + PLL$$

$$z_{15} = z_{16} + z_7 + BRHT$$

$$r_{12} = r_{15} = r_7$$

$$r_{13} = r_{16} = r_8$$

where $PLL$, is the pipe leg-length associated with the weld bead, and $BRHT$ is the total height of the branch pipe.

There are three methods for calculating the coordinate of point (9). The calculation of the coordinate of point (9), is achieved in an iterative manner. All of the three methods require the cross-sectional area of the weld bead to be known. The weld bead area is calculated by integrating the region between the parabolic weld bead profile, and the

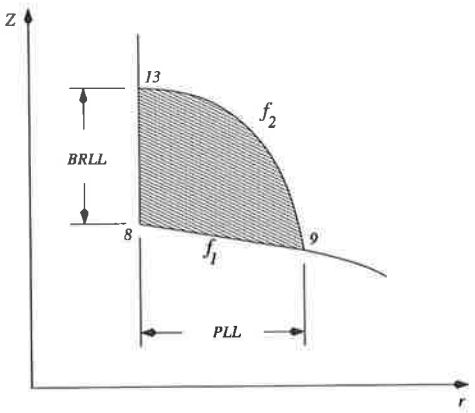


**Figure 3.22:** Parabolic weld bead profile for a branch on pipe weld.

main pipe surface, as can be seen in Figure 3.22. The area is calculated using the following expression:

$$\text{Area} = \int_{r_8}^{r_9} f_{(2)} - f_{(1)} dr \tag{3.11}$$

The three different methods of calculating the coordinate of point (9) are:

1. branch leg-length and pipe leg-length are equal, both need to be calculated
2. branch leg-length dimension is known; therefore, pipe leg-length dimension is to be calculated
3. pipe leg-length dimension is known, therefore branch leg-length dimension is to be calculated

The detailed variation of branch on pipe weld bead geometry with position, or $\theta$ is unknown. For the development of the in-service branch on pipe thermal model, the second option was chosen.

Initially, a value for the pipe leg-length dimension was chosen. The calculation of point (9), involves calculating the intersection of the parabolic weld bead with the main pipe. The equation of the parabolic weld bead in the $r - Z$ plane is defined using the following expression:

$$z = -\frac{BRLL}{PLL}(r - r_8)^2 + BRLL + z_8 \tag{3.12}$$

The pipe surface is then defined using the following expression:

$$z = \sqrt{R_{main} - r^2 cos^2(\theta)} \tag{3.13}$$

Attempting to solve the two equations simultaneously requires the solution for a quartic polynomial. Of the 4 possible solutions, two are real and the remaining two are imaginary. The two real solutions are checked, and the correct and appropriate solution is chosen.

If the calculated area was larger than the desired value, the value of the pipe leg-length dimension was decreased; or alternatively, the value of the pipe leg-length was increased if the calculated area is found to be smaller than desired. Once the area is within 0.01% of the desired value, the program then moves to the next stage of the mesh generation.

The last control point to be calculated is point (14). The point is defined by the intersection of a hypothetical line, parallel to the $r - z$ plane, passing through point (8), with a gradient of $tan(\alpha)$; as shown in Figure 3.23.

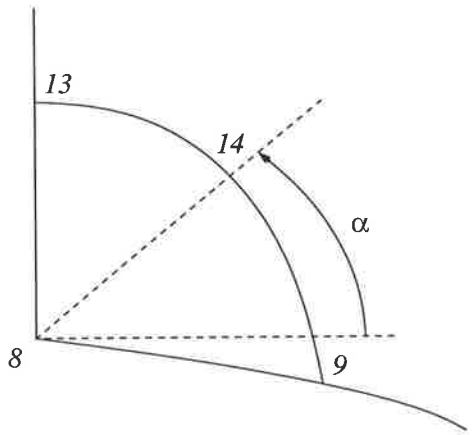


**Figure 3.23:** The calculation of the parabolic weld bead profile control point (14).

The following expressions were solved for simultaneously:

$$z_{14} = tan(\alpha)(r_{14} - r_8) + z_8 \tag{3.14}$$

$$r_{14} = tan(\alpha)(r - r_8) + z_8 \tag{3.15}$$

Solving the two equations yields the following equation for calculating $r_{14}$:

$$r_{14} = \frac{-tan(\alpha) + \sqrt{tan^2\alpha + 4\frac{BRLL^2}{PLL^2}}}{2\frac{BRLL}{PLL^2}} \tag{3.16}$$

Next, the following expression was used to calculate $z_{14}$:

$$z_{14} = tan(\alpha)(r_{14} - r_8) + z_8 \tag{3.17}$$

The points which define the mesh for each slice are now completed. The calculation of the nodes and elements for each region, as seen in Figure 3.20, for the cross-section is then performed.

The node and element calculation follows a procedure similar to the calculation of the mesh, for in-service circumferential fillet welding, as discussed previously in Section 3.2.2. The mesh generation program creates a finite element mesh with either linear or parabolic elements. A linear element was selected if only a thermal analysis was required. However, if a elastic plastic stress analysis was subsequently required, a thermal analysis using quadratic elements was calculated. Moreover, the identical mesh was used for both thermal and stress analysis.

An example of a mesh generated for branch on pipe welds can be seen in Figure 3.24. The example is for a $300mm$ diameter main pipe with a wall thickness of $4.8mm$, with a branch pipe of $150mm$ diameter and $6.4mm$ wall thickness. The bead area was $6mm^2$.

## 3.3.3 Transient analysis

### 3.3.3.1 Introduction

As stated earlier in Section 3.3.1, the thermal analysis of in-service branch on pipe welding, is only possible using a transient thermal analysis. The thermal analysis is identical, in

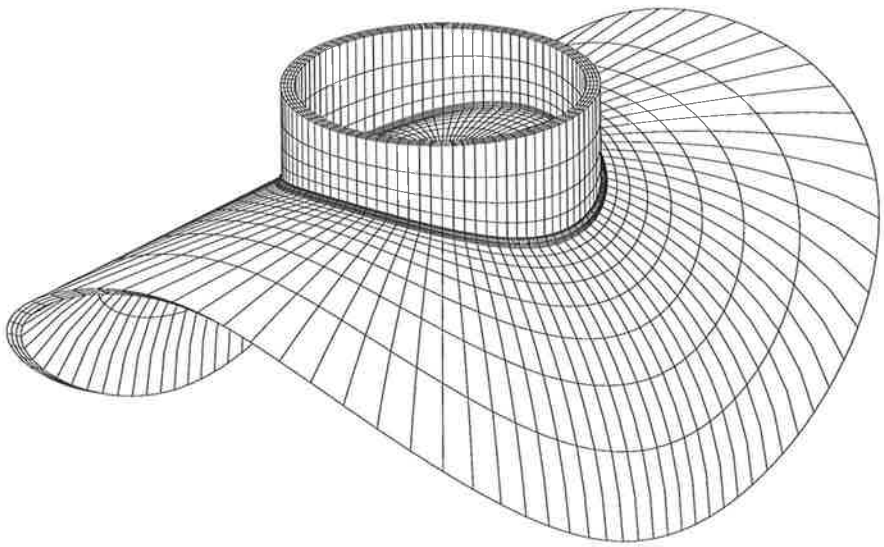

**Figure 3.24:** Example of typical branch on pipe mesh.

theory, to the transient thermal analysis of circumferential fillet welding, discussed earlier in Section 3.2.3. A moving heat source is used to calculate nodal heat flux, which is applied as a boundary condition in a finite element analysis, allows the simulation of branch on pipe welding. The remaining boundary conditions, natural and forced convection are also approximated in a similar manner to that proposed for thermal analysis of circumferential in-service welding. Naturally, the location of the boundary conditions being the principal difference.

#### 3.3.3.2 Mesh

The welding of direct branch on pipe connections rarely occurs with one single pass weld; often multiple welds are required to complete a root pass weld. The transient thermal analysis of in-service branch on pipe welding, benefits greatly from this, as the simulation does not ever need to consider the entire geometry. Smaller sectioned models will be quicker to solve. In total, there are three different root pass weld scenarios which may occur for a given field branch on pipe weld; which can be seen in Figure 3.25, and these are as follows:

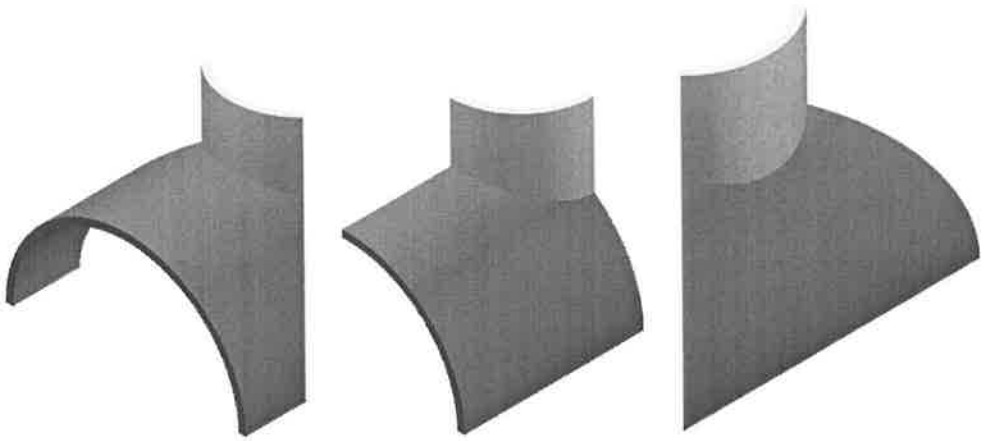

(a) Top (b) Middle (c) Bottom

**Figure 3.25:** Typical branch on pipe weld scenarios.

- a weld which passes through the top position of the intersection between the branch on pipe weld, as seen in Figure 3.25(a)
- a weld which passes through the mid position of the intersection between the branch on pipe weld, as seen in Figure 3.25(b)
- a weld which passes through the bottom position of the intersection between the branch on pipe weld, as seen in Figure 3.25(c)

The finite element solution is only required to calculate temperature fields for each aforementioned weld scenario; therefore significant savings in mesh size and computation time can be attained. However, since a adiabatic boundary condition is assumed at the edges of the model, the size of the meshed zone must be sufficiently large. A similar assumption, was made relating to the influence of the model width and length, on the temperature field and thermal gradient at regions of interest, for the thermal analysis of circumferential fillet in-service welds, proposed earlier in Section 3.2.2. The size of the branch on pipe model must be sufficiently large to minimise the influence on the temperature field and thermal gradients at regions of interest. For a given weld, the size of the mesh was increased until the temperature field and thermal gradients at points of interest did not change with increasing model size. The location of the start and stop

positions for a given weld also influenced the analysis; a few degrees of pipe material, $\theta$ as rotated about the z-axis, were added if required. In addition, the location of the end points, (5) and (10) also influence the results and had to be sufficiently far from the regions of interest.

A typical finite element mesh used for either of the weld scenarios can be seen in Figure 3.26; Figure 3.26(a) for the top position, Figure 3.26(b) for the middle position, and finally, Figure 3.26(c) for the bottom position. The advantage of using such specific mesh geometry is clearly obvious; however, if welds lengths were larger than the either of the three scenarios, a specific mesh could be easily created.

#### 3.3.3.3 Calculation of heat flux

The values of heat flux calculated from a given heat source distribution, was applied as a heat flux boundary condition at the node. As a temperature field due to branch on pipe welds can only be calculated using a transient thermal analysis, the mesh density must not be overly fine, as the solution would require vast amounts of computing resources and time to complete. Such a justification was previously made for the transient heat transfer analysis of in-service circumferential fillet welding, as seen in Section 3.2.3.3. Reiterating, for moderate mesh densities, the heat flux from the welding arc was better represented using nodal boundary conditions, as compared to element heat flux.

A computer program was written to approximate the heat from the welding arc as a heat flux boundary condition for a finite element model. The inputs for the program were:

- dimensions of the branch on pipe fitting
- parameters describing the heat source
- welding run parameters: such as the length of the weld, start and end locations, and welding speed.

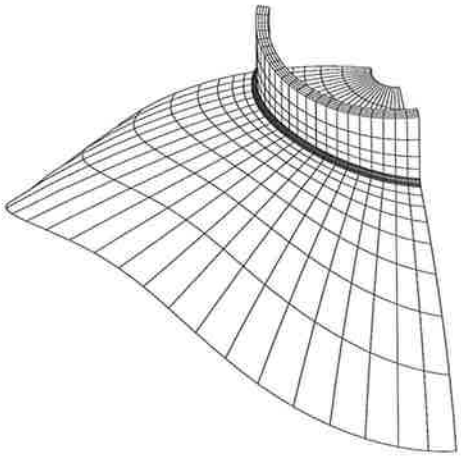

(a) Top

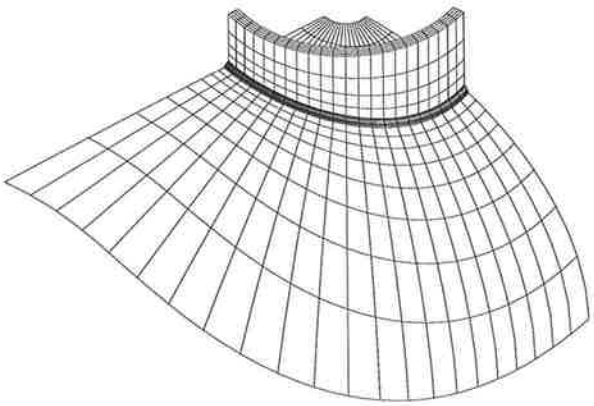

(b) Middle

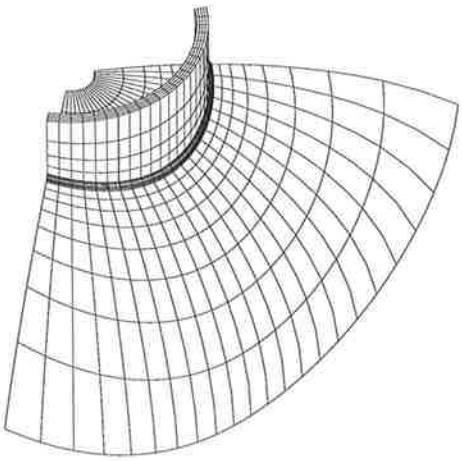

(c) Bottom

**Figure 3.26:** Examples of typical mesh used for the thermal analysis of branch on pipe in-service welds.

The first step in calculating the heat flux was to determine the start and end locations of the welding path, along with the welding path itself. The path of the electrode during branch on pipe welding is largely unknown; no published information was found in the examined literature.

Early development of the branch on pipe transient models assumed that the centre of the heat source was to move around the intersection of the branch, and main pipe. Mathematically, the motion of the centre (and origin) of the heat source, $(x_o, y_o, z_o)$, was as follows:

$$x_o = R_{branch} cos\theta \tag{3.18}$$

$$y_o = R_{branch} sin\theta \tag{3.19}$$

$$z_o = \sqrt{R^2_{branch} - R^2_{main} cos^2\theta} \tag{3.20}$$

The heat source coordinate system was set so that the electrode was perpendicular to the branch surface at all times, while the electrode angle, $\alpha$, could be set to any required angle between the pipe surface to the branch surface. However, due to the limited data available for branch on pipe welds in the literature, the welding angle was selected to bisect the angle of created by the fillet.

The coordinate system for the heat source was defined using the following expressions:

$$i^* = \left[\frac{cos(\theta)tan(\alpha)}{\sqrt{tan^2(\alpha)+1}}, \frac{sin(\theta)tan(\alpha)}{\sqrt{tan^2(\alpha)+1}}, \frac{1}{\sqrt{tan^2(\alpha)+1}}\right] \tag{3.21}$$

$$j^* = [-sin(\theta), cos(\theta), 0] \tag{3.22}$$

$$k^* = i^* \times j^* \tag{3.23}$$

$$\alpha = \frac{\pi}{2} + \frac{\frac{\pi}{2} + acos\left(\frac{y_i^2+y_j^2}{y_i^2+y_j^2+y_k^2}\right)}{2} \tag{3.24}$$

However, the shape of the weld bead also played a significant role in the calculation of heat flux; as the datum points for the heat source was assumed to be tied to the bead

shape geometry, as can be seen in Figure 3.27.

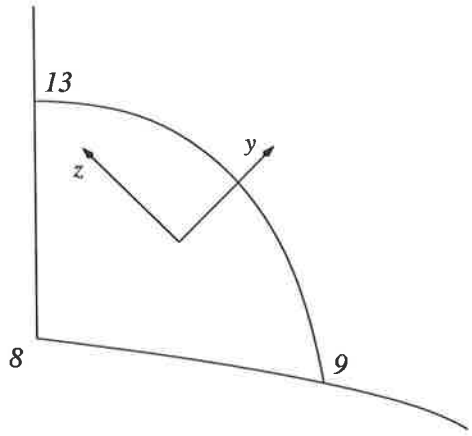


**Figure 3.27:** Datum points for branch on pipe thermal analysis models.

A new set of equations allowed the calculation of the heat source coordinate system. The centre of the heat source was replaced with the following expressions:

$$x_o = \frac{r_9 + r_{13}}{2} cos(\theta) \tag{3.25}$$

$$y_o = \frac{r_9 + r_{13}}{2} sin(\theta) \tag{3.26}$$

$$z_o = \frac{z_9 + z_{13}}{2} \tag{3.27}$$

Next, the coordinate system axes were defined using the following expressions:

$$x_i = -sin(\theta) \tag{3.28}$$

$$x_j = cos(\theta) \tag{3.29}$$

$$z_k = 0 \tag{3.30}$$

$$\alpha = \frac{\frac{\pi}{2} + tan^{-1}\left(\frac{z_9 - z_8}{r_9 - r_8}\right)}{2} \tag{3.31}$$

$$z_i = cos(\theta)cos(\alpha) \tag{3.32}$$

$$z_j = sin(\theta)cos(\alpha) \tag{3.33}$$

$$z_k = sin(\alpha) \tag{3.34}$$

$$y = x \times z \tag{3.35}$$

As the heat source trajectory, and coordinate system is known, a process similar to that proposed to calculate heat flux for circumferential fillet welding was applied. First, the simulation is discretized into $N$ time steps. Next, the location of the heat source is calculated. Using basic trigonometry, the time taken for the heat source to travel from one time step to the next is calculated. The following expressions were used to calculate $\theta$, the centre of the heat source, and the corresponding time associated with the location of the centre of the heat source:

$$\begin{aligned}
\theta_n &= \frac{n}{N}(\theta_{end} - \theta_{start}) + \theta_{start} \\
x_n &= 0.5(x_9 + x_{13})cos(\theta_n) \\
y_n &= 0.5(y_9 + y_{13})cos(\theta_n) \\
z_n &= 0.5(z_9 + z_{13}) \\
t_o &= 0 \\
t_n &= t_{n-1} + \frac{\sqrt{(x_n - x_{n-1})^2 + (y_n - y_{n-1})^2 + (z_n - z_{n-1})^2}}{w_s}
\end{aligned}$$

where: $\theta_{start}$, corresponds to the start location of welding, $\theta_{end}$, corresponds to the end location of welding, $n$, is an integer which satisfies: $0 < n < N$, and finally, $t$, is time.

The next step, is to use the equations stated earlier, to calculate the heat source local coordinate system. Using coordinate system transformation, for a given time step, all nodes in the mesh were converted from the general coordinate system, to the local coordinate system of the heat source. Next, each node is individually checked, to find if it is within the volume, of the given heat source. If the node was found to lie within the given volume, the heat flux value was calculated for the node. The process was continued until all nodes were searched. Finally, a summation of the total heat was calculated, identical to that proposed for the transient heat transfer analysis of in-service circumferential fillet welding as discussed earlier in Section 3.2.3.3 and seen in Equation 3.5. Next, the calculation of a correction factor was achieved using Equation 3.6 which was then applied to all nodes which had a heat flux boundary conditions applied to them. The calculation of

heat flux was then repeated for all of the remaining time steps for the transient analysis.

#### 3.3.3.4 Boundary conditions

The remaining boundary conditions placed on the branch on pipe thermal model are the heat loss to ambient surroundings, and the heat loss to the pressurised flowing natural gas through forced convection. The calculation of heat loss boundary conditions is identical to that proposed for the transient analysis of in-service circumferential fillet welding as discussed earlier in Section 3.2.3.4. In short, both heat losses were approximated as a heat transfer coefficient. However, the location and placement of the boundary conditions were obviously different due to the different geometry; a typical example of boundary conditions of the typed discussed can be seen by Figure 3.28. The heat loss to the atmosphere by convection was placed to the element faces which are in contact with the atmosphere: namely the outer surface of the weld bead, the outer surface of the pipe and the outer and inner surface of the branch pipe. The heat loss due to the flowing pressurised natural gas was applied to all element faces which form the inside surface of the main pipe.

The heat loss due to radiation was disregarded; the reasons for which are identical to those discussed for the application of radiation boundary conditions for the transient thermal analysis of circumferential fillet welding, found earlier in Section 3.2.3.4. In short, the effect was tested and found to be negligible.

## 3.4 Internal pipe convection

### 3.4.1 Introduction

Maintaining the flow of natural gas, is the principal reason why the hot-tapping procedure was developed. In addition, the pressure from the fluid applies a challenging task for welding to be deposited without the risk of pipe wall burnthrough. If the flow were static,

the hot-tapping problem would be reduced to one of welding onto a pressure vessel. However, in most cases in the field, the gas is flowing. In a gas pipeline, the flow of gas is significantly large so that it causes a strong quenching effect on the weld. While the quenching may be useful for avoiding pipe wall failure, as discussed earlier in Section 1.3, the enhanced cooling produces microstrucutures which are harder, and therefore more susceptible to hydrogen assisted cracking. The gas flow and its cooling effect is therefore significant, and must be included in any thermal models of in-service welding.

The addition of convection due to flowing fluid to a finite element calculation is a

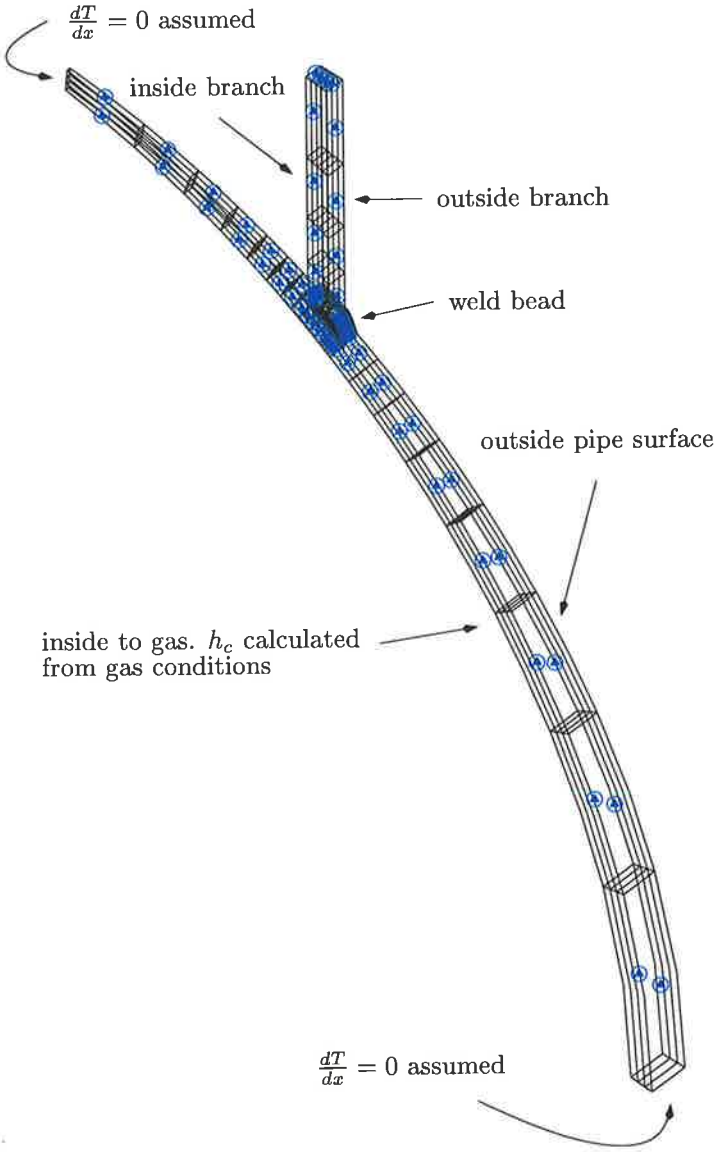


**Figure 3.28:** Boundary conditions for heat loss to ambient surrounding by convection, and heat loss to flowing pressurised natural gas by forced convection.

challenging task. The following sections will discuss the method used to approximate convection on a numerical thermal simulation of in-service welding. The first section will discuss the analysis of the flow regime of the fluid; the results of the analysis offer an insight into the best possible manner to include the thermal heat transfer effect of flowing pressurised natural gas to a thermal analysis of in-service welding. The next section discusses the use of a non-dimensional method to calculate the heat transfer coefficient suitable for a conduction only thermal model of in-service welding as proposed earlier in Chapter 3. The last section discusses the attempts made to involve a CFD calculation with proposed thermal analysis. A CFD approach is considered to offer potentially greater accuracy; details of how to implement and improve such a model using such a technique is given with the last section.

### 3.4.2 Flow regime

The range of pressure found in a typical in-service welding situation is broad; the diameter and strength of the pipe influence the upper operating pressure limit; such a limit is defined as the $MAOP$ described in Section 1.3. Such a limit is defined by Equation 1.1.

The lower limit of gas flow is arbitrary, and only reflects the flow of gas which the operating pipelines experiences; commercial factors or gas demand are the principal determining factor. For example, in some instances, the pressure can be as low as $1.0MPa$ or lower. Therefore, a typical range of pressure, for low pressure pipeline to high pressure capacity pipelines is from $0MPa$ to $MAOP$.

In order to determine the type of convection which is likely to occur for a given in-service weld, the Reynolds number, $Re$, for a range of in-service welding conditions typically found in the field was calculated. The equation to calculate the Reynolds number for flow in a circular duct can be seen in Equation 3.36:

$$Re_d = \frac{\rho V D}{\mu} \tag{3.36}$$

where $\rho$ is density, $V$ is the bulk velocity, $D$ is the diameter of the duct, and finally $\mu$ is the viscosity of the fluid. In order to calculate the Reynolds number, a number of physical properties of natural gas were required to be determined, namely density, $\rho$, and viscosity, $\mu$.

As the primarily constituent of natural gas is Methane, the calculation of various parameters related to fluid dynamics and heat transfer were achieved by approximating natural gas as Methane. A number of empirically derived methods to calculate viscosity of gas at low pressure, were compared against experimental results [69]; the Reichenberg method, displayed the least error for Methane gas for pressure between 40 and 500$bar$. The values of viscosity for a range of pressure and temperature for Methane can be seen in Figure 3.29.

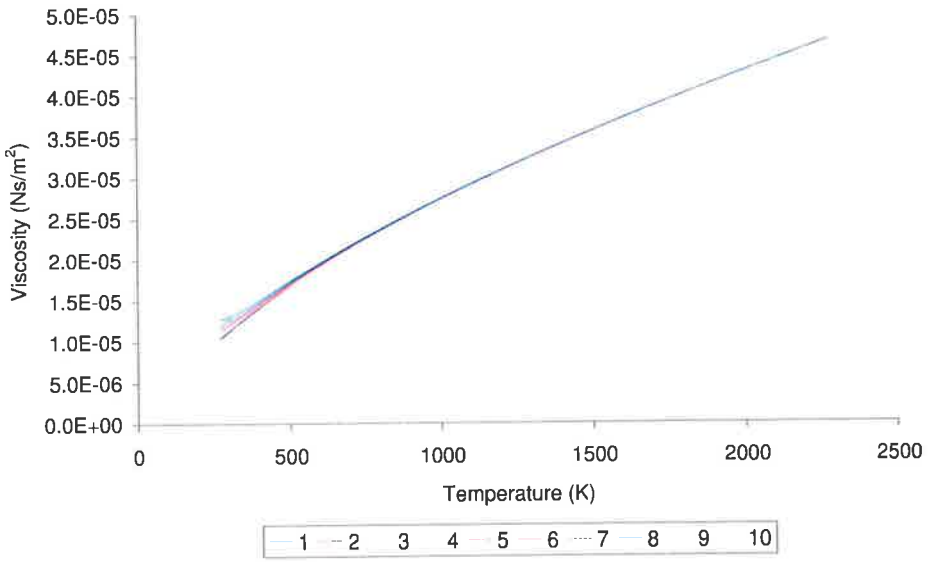


**Figure 3.29:** The calculation of viscosity was achieved using the Reichenberg method. The graph shows the variation of the viscosity of Methane for a range of pressure ($MPa$) and temperature ($K$).

The density of natural gas was calculated on the assumption that natural gas can be considered to be an ideal gas. The ideal gas equation, as seen in Equation 3.37 was used to calculate the density of natural gas. The ideal gas equation used for the calculation was as follows:

$$\rho = \frac{P \times 16.043}{kT_b} \tag{3.37}$$

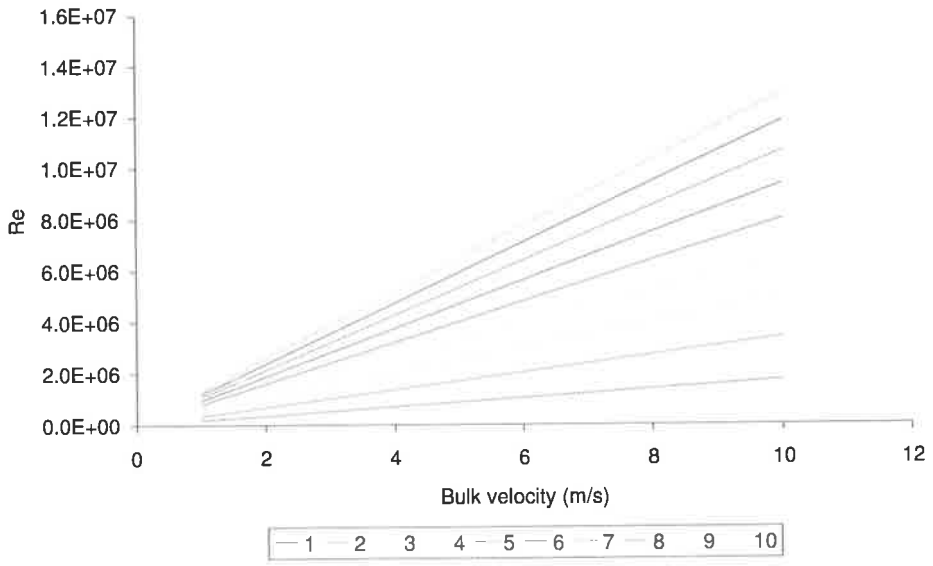


**Figure 3.30:** Variation of Reynolds number with velocity and pressure; $T_b = 300K$, $D = 0.3m$.

where, $k$, is the ideal gas constant and, $T_b$, is the bulk temperature of the fluid.

The flow field predominantly found during in-service welding is considered fully developed and turbulent. In most practical in-service welding situations, the combination of flow rate and pipe diameter results in a Reynolds number exceeding 10000. For example, on a $300mm$ diameter pipe containing natural gas, a flow rate of $1m/s$ with an operating pressure of $1MPa$ results in $Re = 171262$. Moreover, a calculation of Reynolds number for a range of flows typically expected for in-service welds can be seen in Figure 3.30. Finally, the flow in a constant area pipe or duct is said to be fully developed if the shape of the velocity profile is the same at all cross-sections [29]. Additionally, the length of duct required for flow to be fully developed and turbulent is expressed by the following expression:

$$\frac{L_e}{D} \approx 25 \tag{3.38}$$

for typical engineering flows ($10^4 < Re < 10^5$). As the length of the pipeline usually exceeds $L_e$, the flow is considered to be fully developed.

### 3.4.3 Non-dimensional estimation of heat transfer coefficient

#### 3.4.3.1 Introduction

The Sieder & Tate approximation was used to calculate the heat transfer coefficient due to the flowing pressurised natural gas. This relationships was chosen after examining a number of options documented by Holman [42]. Earlier work by Battelle [26] in an effort to develop software to predict cooling rates and maximum inside temperatures for in-service had also used a variation of the Sieder & Tate non-dimensional relationship.

#### 3.4.3.2 Calculation of heat transfer coefficient

The non-dimensional relationships proposed by Sieder & Tate can be seen in the following expression:

$$Nu_d = 0.027 Re_d^{0.8} Pr^{1/3} \left(\frac{\mu_b}{\mu_w}\right)^{0.14} \tag{3.39}$$

where, $Nu_d$, is the Nusselt number, $Re_d$, the Reynolds number, $Pr$, the Prandtl number, $\mu_b$, the bulk viscosity of the fluid, and $\mu_w$, the viscosity of the fluid near the pipe wall. The heat transfer coefficient is then calculated using the following expression:

$$h_c = \frac{kNu_d}{D} \tag{3.40}$$

Interestingly, the work by Battelle had used the following relationship:

$$\frac{h_c}{C_p.V.\rho} = 0.023 Re^{-0.2} Pr^{-2/3} \left(\frac{\mu_b}{\mu_w}\right)^{0.14} \tag{3.41}$$

The significant difference between the two methods is the slight change in coefficient. The work by Battelle had involved using heat transfer coefficient which was slightly lower than that calculated for the present work.

To calculate the heat transfer coefficient, the additional calculation of the Prandlt

number, using the following expression is required:

$$Pr = \frac{\mu C_p}{K} \tag{3.42}$$

where, $\mu$, is viscosity, $C_P$, is specific heat and, $K$, is thermal conductivity. As a result, the calculation of thermal conductivity and specific heat for natural gas for a range of temperatures and pressures is also required.

An expression for calculating thermal conductivity of gases was found contained within the work by Reid [69]. The effect of pressure on the thermal conductivity of gases was found to be insignificant; increasing by less than 1% per bar. The thermal conductivity was calculated using the following equation:

$$\lambda = A + BT + CT^2 + DT^3 \tag{3.43}$$

where $A = -1.869E-3$, $B = 8.727E-5$, $C = 1.179E-07$, $D = -3.614E-11$, and, $\lambda$, is the thermal conductivity with units $W/m.K$. Additionally, the specific heat of Methane was calculated using the following equation based on the work by Reid:

$$C_p = a + b \times 10^{-3}T + c \times 10^{-6}T^2 + d \times 10^{-9}T^3 \tag{3.44}$$

where $a = 19.887$, $b = 50.252$, $c = 12.686$, $d = -11.011$, and, $C_p$, is the specific heat with units $J/g - molK$.

The calulation of heat transfer coefficient using the method proposed by Sieder & Tate for a range of pipe flow and pressures typical found in in-service welding can be seen in Figure 3.31.

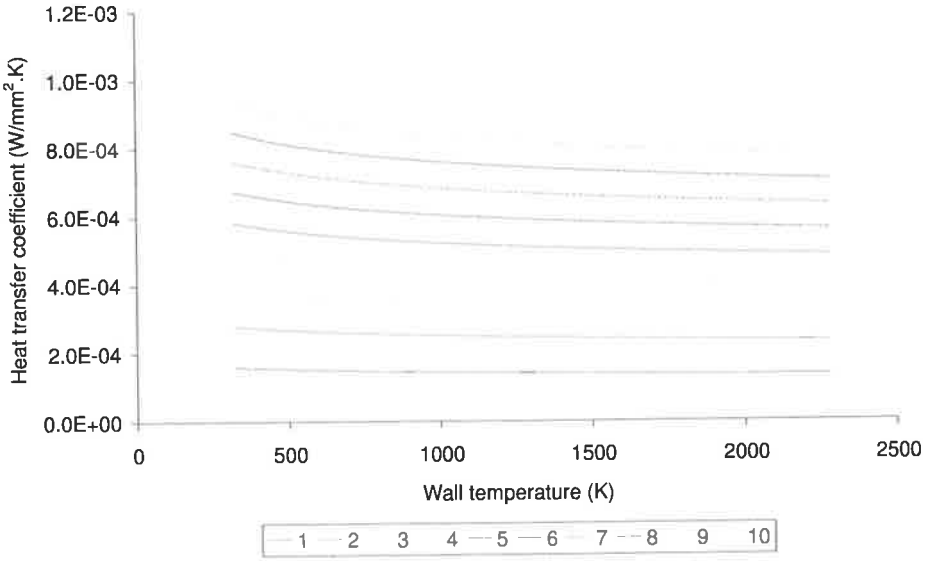


(a) Pressure=$5MPa$,Bulk temperature=$300K$, velocity varying from $1-10m/s$.

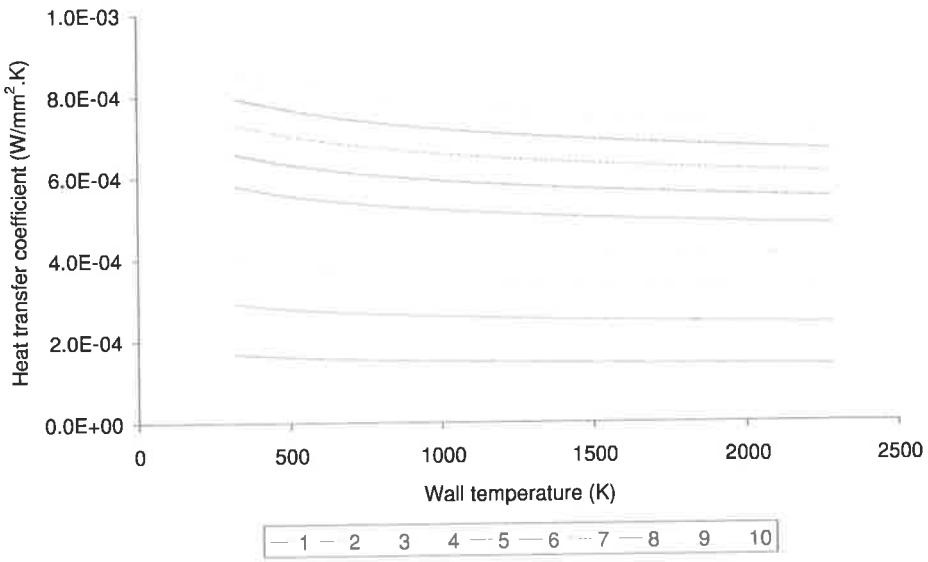


(b) Bulk velocity=$5m/s$,Bulk temperature=$300k$, pressure varying from $1-10MPa$.

**Figure 3.31:** Heat transfer coefficient based on Sieder & Tate for typical in-service welding flow conditions.

#### 3.4.3.3 Sensitivity analysis of thermal models to Sieder & Tate non-dimensional approximation

The accuracy of the Sieder & Tate method to determine the heat transfer coefficient for turbulent fluid low in a circular duct was estimated at ±25% by Holman [42]. While such large variations may be considered to be a mediocre estimation at best, the sensitivity of the predictions from the thermal model was unknown; a sensitivity analysis was therefore performed.

A test case involving welding onto a $4.8mm$ wall thickness pipe with a high flow-rate and under high operating pressure, was used to determine the sensitivity of the predictions of the thermal model, to the heat transfer coefficient. It is considered that the lower wall thickness chosen will allow for a greater rate of heat transfer to the fluid by convection simply due to the reduced thermal mass; it is considered that above a certain wall thickness, the primary method of heat transfer for in-service welding is diffusion. The reduced wall thickness will result in higher wall temperatures at the inside surface of the pipe, further increasing the sensitivity of the model to the heat transfer coefficient.

The test cases for determining the sensitivity of the model can be seen in Table 3.2: where $B$ was the nominal case. The results from the test can be seen in Table 3.3: The

| Test | % variation in $h_c$ | $h_c$ $(W/mm^2.K)$ | Heat input $(kJ/mm)$ | Wall thickness $(mm)$ |
|---|---|---|---|---|
| A | +25% | 6.51 | 1.0 | 4.8 |
| B | 0% | 5.21 | 1.0 | 4.8 |
| C | −25% | 3.91 | 1.0 | 4.8 |

**Table 3.2:** Test cases for Sieder & Tate model sensitivity analysis.

| Test | FZD $(mm)$ | HAZD $(mm)$ | $t_{8/5}$ $(s)$ | % FZD | % HAZD | % $t_{8/5}$ |
|---|---|---|---|---|---|---|
| A | 0.60 | 3.40 | 5.58 | $< 0.1$ | +3.0 | +4.0 |
| B | 0.60 | 3.51 | 5.81 | | | |
| C | 0.60 | 3.62 | 6.04 | $< 0.1$ | −3.0 | −4.0 |

**Table 3.3:** Results from Sieder & Tate model sensitivity analysis.

results from the sensitivity analysis are encouraging. The variation of weld cooling rate

was found to be ±4.0%, while the variation of maximum HAZ depth was ±3.0%. The variation of penetration depth was negligible. As the sensitivity analysis was performed on a case where the largest variations were expected, the minor variation of the results from the model suggests that the accuracy of the non-dimensional approach is adequate for the thermal analysis of in-service welding.

### 3.4.4 Numerical approach

#### 3.4.4.1 Introduction

An alternative method is to include the calculation of the flow field associated with the flowing pressurised natural gas with the heat conduction problem of in-service welding. In such a calculation, the heat flow from the welding arc, through the thickness of the pipe wall, and finally dissipated through the flow field is intrinsically included in the simulation. With the advent of numerical methods to solve complex differential equations, the study of fluid flow using CFD has largely been invaluable. Numerical analysis software which offers CFD for engineering analysis is becoming increasingly readily available; NISA not being an exception. The thermal effects of flowing natural gas in a pipeline was considered to be a challenging problem in which CFD could be applied. The next few sections will discuss the method which was developed to apply CFD to the in-service welding problem, in addition to the problems encountered during the formulation of the problem. Unfortunately, due to the relatively lack of sophistication in NISA's fluid solver, the approach was abandoned; however, a number of key ideas for future development are discussed.

#### 3.4.4.2 Analysis

Two approaches for the CFD simulation of convection due to pressurised flowing natural gas in the pipeline were considered. The first approach considered was the fully coupled approach. In this model, the temperature and velocity field of the gas was calculated as it was heated within a pipe due to welding. The second approach is the decoupled approach.

In this method, only the velocity field of the gas is calculated; the any thermal effects due to welding is ignored. The calculated velocity field is then applied as a boundary condition to a new model where the effects of heat transfer in the pipe wall due to welding is considered. The temperature field is then calculated for a given weld. The decoupled approach was favoured over the coupled approach for a number of reasons. The primary reason was computational efficiency. The fully coupled approach was considered to be far too expensive for the minor gain in accuracy over the non-dimensional approach. Secondly, any variation in the fluid velocity field near the pipe wall and boundary layer was assumed to be largely unaffected by the heating due to welding. This assumptions was made as the size of the heated zone is usually small compared to the diameter of the pipe; the effects of pipe flow is considered to override any effects due to the heating of the pipe wall. Finally, as the direction of welding is perpendicular to the direction of flow, the effects of high wall temperatures on the fluid flow is also considered to be minimal.

The first step of the decoupled approach was therefore to calculate the velocity field. The flow regime, as discussed earlier in Section 3.4.2 was found to be turbulent and fully developed. In addition, the flow was assumed to be incompressible. The velocity profile calculated using the CFD approach must therefore assume a method of approximating turbulent flow conditions. The two turbulent models available with the NISA are:

- k-$\epsilon$
- RNG (Renormalization Group)

The first step in simulating the heat transfer effects of the flowing gas is select the appropriate turbulence model. The calculation of the velocity field by choosing an appropriate turbulent model reveals the first difficulty in implementing a CFD approach to the thermal modelling of natural gas in in-service welding. The accuracy in which the turbulence models approximate such flows is unknown and is difficult to determine. While the velocity field of the core can be readily approximated, the velocity field of the fluid near the wall including the boundary layer is difficult to calculate. In addition, the velocity field

near such regions experience fluctuations; the effect on the heat transfer properties of the fluid can be considerable.

Once the velocity field is calculated, the convective transfer of heat is either directly calculated using the coupled approach, or is indirectly calculated using a further calculated; based on the model proposed whereby the velocity field is applied as a boundary condition.

A significant problem occurs with the method proposed so far. The added effects involved with turbulent heat transfer is not included in the thermal calculation. While the velocity field is calculated, the effect of turbulent convective heat transfer is not included. As a result, the NISA solver is strongly driven by the predicted velocity field.

Such a calculation requires further computing resources while is less stable compared to the non-dimensional approach. Moreover, the fluid flow within the pipe is usually highly turbulent; numerical simulation of turbulent flows in its own right is complex and largely difficult to implement, while as stated earlier, the accuracy of the prediction is difficult to determine.

A number of models were used to examine the advantages of using a CFD approach in order to avoid the use of non-dimensional relationships. However, it was established that to obtain results it was necessary to artificially increase the thermal conductivity of the gas in the region near the pipe wall to allow for the enhanced heat exchange during turbulent flow. This somewhat arbitrary scaling was not better than the application of the Sieder & Tate non-dimensional relationship. In addition, as discussed earlier in Section 3.4.3.3, it was established that the sensitivity of the model outcomes to variations in gas flow and pressure were not high, hence a tolerance to some uncertainty in the heat transfer coefficient was considered acceptable. In this work the difficulties of accurately representing heat transfer in turbulent flow, and the sensitivity of the gas flow to the thermal field in the pipe, ultimately led to the adoption of the non-dimensional approach in favour of the CFD approach.

#### 3.4.4.3 Future work

The additional heat transfer effects associated with turbulent heat transfer is unknown. In addition, a method of implementing them, via modifications to the energy equations, or approximating them, by suitably modifying the thermal conductivity or specific heat of the material close and adjacent to the pipe wall, for example, could yield considerable accuracy. Finally, the accuracy of the CFD approach is also required to be known. Comparisons with experiments involving, for example an EWI test, as discussed earlier in Section 2.2.1 with numerical simulations will allow the accuracy to be measured.

### 3.4.5 Conclusions

The accuracy of the non-dimensional approach was considered to be adequate for the thermal simulation of in-service welding. The sensitivity of the resulting in-service welding thermal model to slight changes in heat transfer coefficient is considered to be minor, further justifying the use of a non-dimensional method. Clearly, involving CFD methods to calculate and simulate the convection due to the flowing pressurised natural gas can yield better accuracy. However, in view of other unknowns and practical variations in welding heat input and uncertainties in exact joint form, it is doubtful that such additional complexity is merited.

## 3.5 Heat source development

### 3.5.1 Introduction

Representing the MMA welding process in a manner which is suitable for solving the heat conduction equation by finite element methods is challenging. Due to the non-linear complex nature of welding, a strategy commonly employed has been to represent the welding process as an arbitrary defined mathematical distribution of heat flux or heat

source and also to ignore any fluid motion within the weld pool. The heat source is unique to every welding process and very little research is available in literature to determine a feasibly accurate MMA welding heat source.

The effect of the aforementioned assumptions is to reduced the problem to the calculation and solution of the time dependent heat conduction equation. Some thermal models have used anisotropic thermal conductivity to simulate the effect of weld pool convection. The lack of weld pool modelling inherently removes an important mechanism of heat transfer. The convective heat transfer mechanism due to the swirling weld pool is commonly approximated. Many researchers compensate for the weld pool convective heat transfer with an artificially high thermal conductivity for the metal in the weld pool. Alternatively, compensation for these effects can be built into the formulation of the heat source.

The following sections will discuss the development of a heat source suitable for the numerical thermal analysis of in-service welding. The first section will discuss the derivation of the heat source; a review of earlier heat sources is made which allowed the derivation to be made. In addition, the effect of the weaving motion is attempted to be included in the formulation of the heat source. The second section will discuss the results from numerical experiments of the heat source. The last section offers the conclusions and discusses the best parameters to be used for the thermal analysis of in-service welding.

### 3.5.2 Derivation

A number of heat source definitions have been proposed over the years for the numerical analysis of welding process in general [76]. In particular, two specific heat source definitions were identified as having qualities which were suitable for the thermal analysis of in-service welding. A well known example of a heat source distribution is the DEHS developed by Goldak et al. [32]; which defines the heat flux Q ($kJ/mm^3$) for a point within the volume defined by the heat source.

The DEHS has been often used to represent common non-autogenous welding processes. However, these are usually simple welds deposited in the 'down hand flat position', i.e. welding horizontally in a straight line on a horizontal flat plate with the electrode perpendicular to the plate. A number of modifications to the formulation of the DEHS need to be made to improve the accuracy of the thermal analysis of out-of-position low-hydrogen MMA welding process.

The MMA welding process used for in-service welding is applied using a 'weave' technique. Such a welding technique along with the characteristics of low hydrogen electrodes often generate shallow penetration which suggests a heat distribution which is flatter and more evenly distributed than Gaussian. The heat source definition proposed by Pavelic [67] is considered to have excellent prospects as it is a two-dimensional surface heat source. However, the heat from the electrode is such that a three-dimensional volumetric heat source offers the least amount of compromise and greatest accuracy for a numerical thermal simulation. As concluded earlier in the literature review, it was considered that a modification to the DEHS would yield a heat source suitable for in-service welding. A new modification to the DEHS distribution, to introduce some flexibility, was made by changing an exponential term and a coefficient. The new equation is:

$$q(x,y,z) = Q_f exp\left[-3\left(\frac{x}{c_f}\right)^2 - 3\left(\frac{y}{a}\right)^{n_2} - 3\left(\frac{z}{f.a}\right)^2\right] \tag{3.45}$$

where $n_2 \geq 2$ and a real positive even integer, and $f$ a real positive number and $0 < f \leq 1$.

The constant, $-3$, was chosen in the same manner as Goldak et al. [32], by requiring that the value of heat flux at the boundary is $0.05Q_{max}$. In this case, the boundary is not ellipsoidal but corresponds such that:

$$\left(\frac{x}{c_f}\right)^2 + \left(\frac{y}{a}\right)^{n_2} + \left(\frac{z}{f.a}\right)^2 = 1 \tag{3.46}$$

The value of $Q_f$ is determined by numerical integration as follows:

$$\eta V I = Q_f \sum_{\text{vol. of source}} exp\left[-3\left(\frac{x}{c_f}\right)^2 - 3\left(\frac{y}{a}\right)^{n_2} - 3\left(\frac{z}{f.a}\right)^2\right] \tag{3.47}$$

A visual comparison of heat flux between Gaussian and $n_2 = 10$ can be seen in Figure 3.32(a) and Figure 3.32(b). Increasing the power, $n_2$, above 2, spreads the distribu-

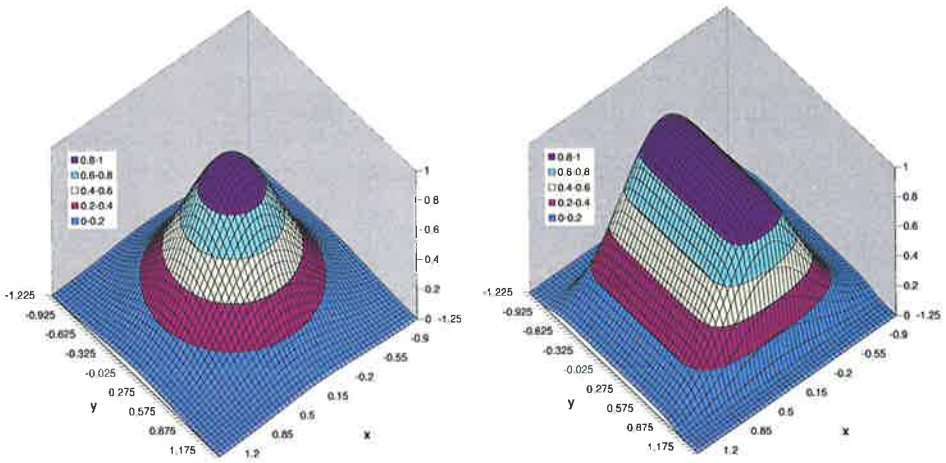


**(a)** $n_2 = 2$. **(b)** $n_2 = 10$.

**Figure 3.32:** Heat source distribution for proposed in-service welding MMAW heat source.

tion in the y-direction. The spread of heat arising from higher values of $n_2$ effectively flattens the distribution; the effect of weld weaving was approximated in this manner. In addition, the depth of the heat source, or the coefficient $f.a$, can be reduced to produce a shallow penetration weld. The reduction of the depth of the heat source, in addition to the increase in the coefficient $n_2$ was considered a method to produce a wide and shallow weld pool. The resulting predicted HAZ depth and penetration depth was thought to be similar to that found for low hydrogen in-service MMA welding. To determine the effects of the aforementioned modifications to the DEHS, and to determine a configuration suitable for the thermal modelling of in-service welding, the heat source was tested by solving a given welding condition with various values of $n_2$ and $f$. The results and discussion is given in the next section.

### 3.5.3 Discussion

The results from a series of numerical experiments to test the validity of the proposed heat source can be seen in Figure 3.33, 3.34 and 3.35. All tests were conducted under identical heat input, weld bead geometry, welding speed, internal pipe convection boundary condition and material properties. The parameters which were changed for each test were related to the heat source definition as follows: $n_2$ and $f$. For each test, a plot of maximum temperature for the cross-section of the pipe can be seen in Figures 3.33 and 3.34. A plot of the variation of maximum HAZ depth and maximum penetration depth with heat source parameters $n_2$ and $f$ can be seen in Figure 3.35.

As the depth of the heat source, or parameter $f$, was increased with the distribution related parameter $n_2 = 2$, the predicted maximum penetration depth was found to increase. However, for $n_2 = 8, 14, 20$, the maximum penetration depth had only increased as $f$ was increased to $f = 0.75$ and then decreased for $f = 1.0$. It can be observed that for these tests, the shape of the fusion zone approaches that of a rectangular shape; clearly such a fusion zone is unrealistic and unlike those typically found for in-service MMA welding. The observed decreasing maximum penetration depth for $f > 0.75$ and $n_2 = 8, 14, 20$ is considered to be an artifact resulting from the near rectangular fusion zone. Moreover, the near rectangular fusion zone profile displays a lack of heat transfer to the weld bead. Clearly as $n_2$ is increased, less of the weld bead has exceeded molten temperature. A similar trend can also be observed as $f$ is increased. The level of penetration into the root of the weld was also observed to decrease as $n_2$ was increased; this trend is most significant for $n_2 = 0.1$, while diminishing as $f$ is increased from $f = 0.25$ to $f = 1.0$.

The assumption that increasing the power $n_2$ would produce shallow penetration welds is clearly not evident in the results of the numerical experiments. For $f = 0.1, 0.25, 0.5$, clearly the trend is in-fact the opposite. However for $f = 0.75, 1.0$ the trend from the experiment is suggested to be a result of the unrealistic fusion zone shape. However, the difference in predicted fusion zone depth for $f = 0.75, 1.0$ is small. Clearly, the heat source definition which produced an acceptable weld bead molten region, acceptable root

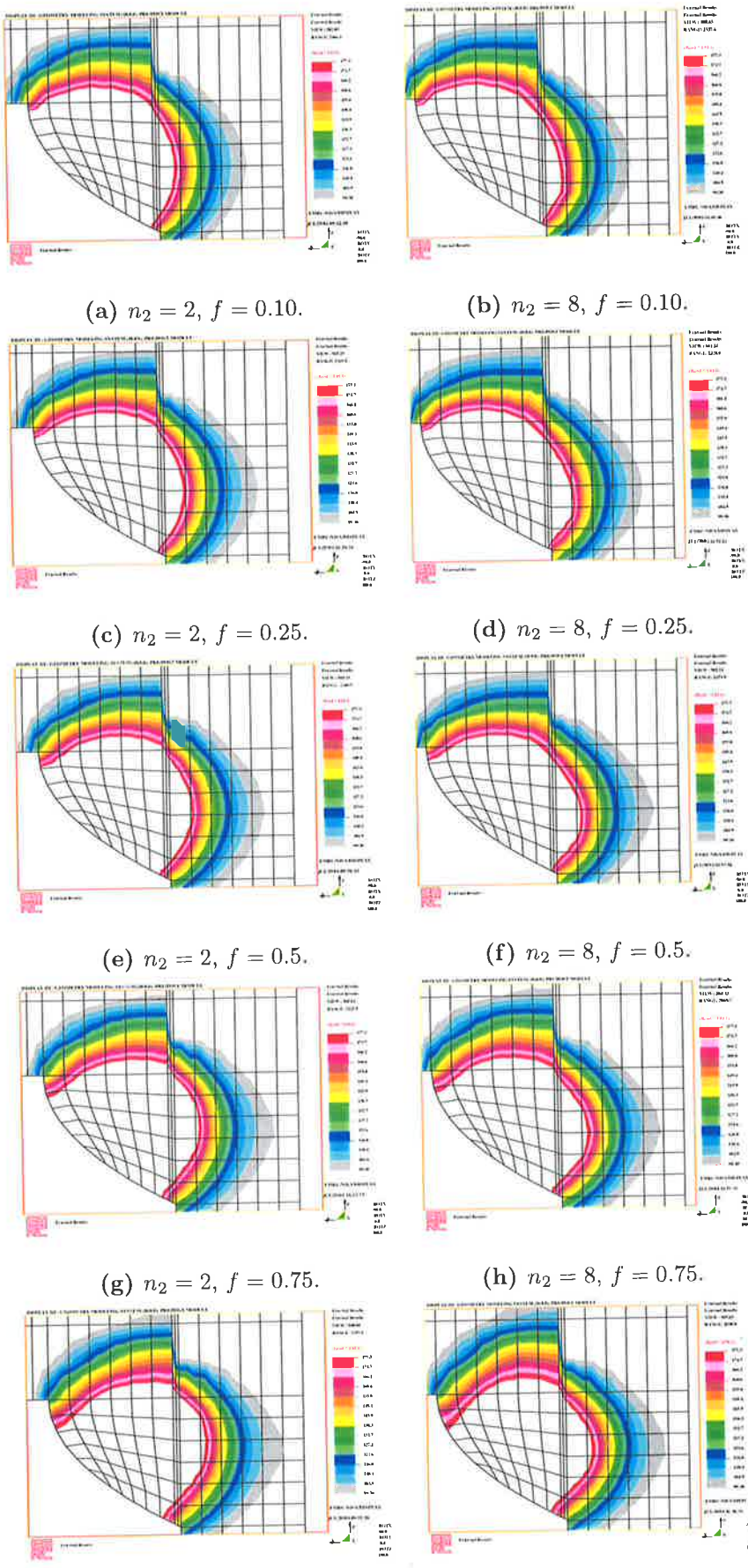

(a) $n_2 = 2$, $f = 0.10$. (b) $n_2 = 8$, $f = 0.10$.

(c) $n_2 = 2$, $f = 0.25$. (d) $n_2 = 8$, $f = 0.25$.

(e) $n_2 = 2$, $f = 0.5$. (f) $n_2 = 8$, $f = 0.5$.

(g) $n_2 = 2$, $f = 0.75$. (h) $n_2 = 8$, $f = 0.75$.

(i) $n_2 = 2$, $f = 1.0$. (j) $n_2 = 8$, $f = 1.0$.

**Figure 3.33:** Plot of maximum temperature for a heat source with the parameters: $n_2 = 2$ and $n_2 = 8$.

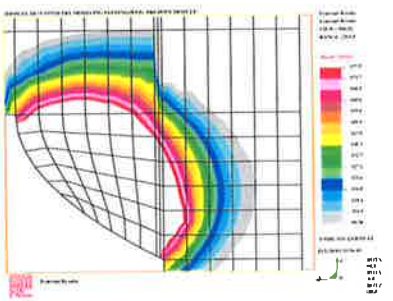

(a) $n_2 = 14$, $f = 0.10$.

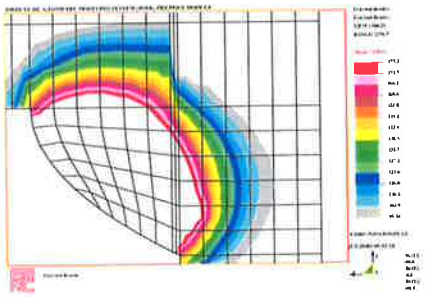

(b) $n_2 = 20$, $f = 0.10$.

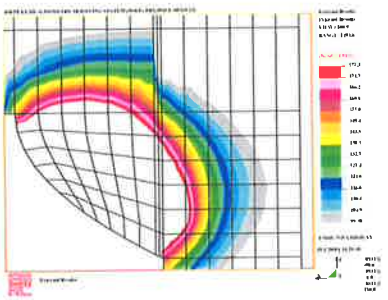

(c) $n_2 = 14$, $f = 0.25$.

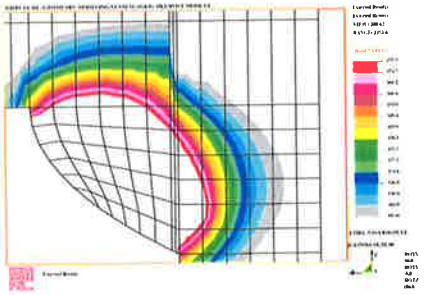

(d) $n_2 = 20$, $f = 0.25$.

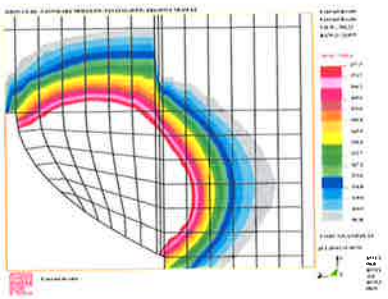

(e) $n_2 = 14$, $f = 0.5$.

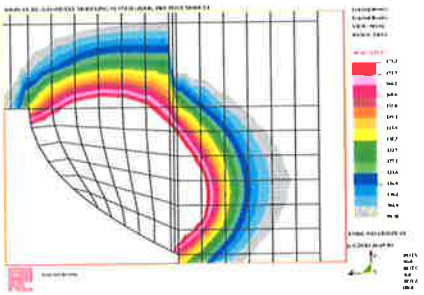

(f) $n_2 = 20$, $f = 0.5$.

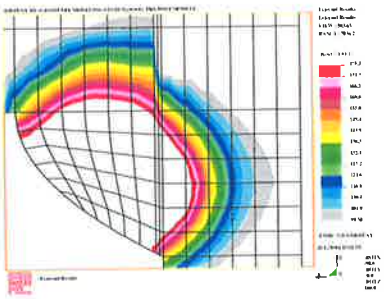

(g) $n_2 = 14$, $f = 0.75$.

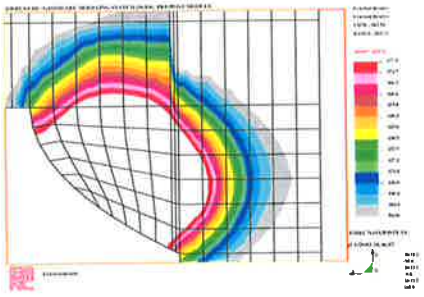

(h) $n_2 = 20$, $f = 0.75$.

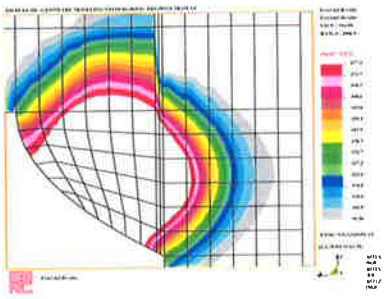

(i) $n_2 = 14$, $f = 1.0$.

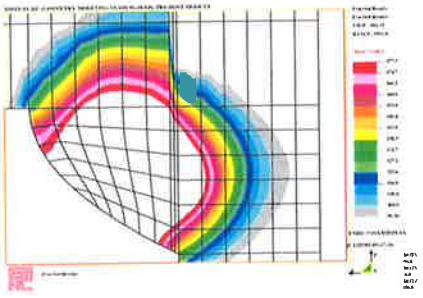

(j) $n_2 = 20$, $f = 1.0$.

**Figure 3.34:** Plot of maximum temperature for a heat source with the parameters: $n_2 = 14$ and $n_2 = 20$.

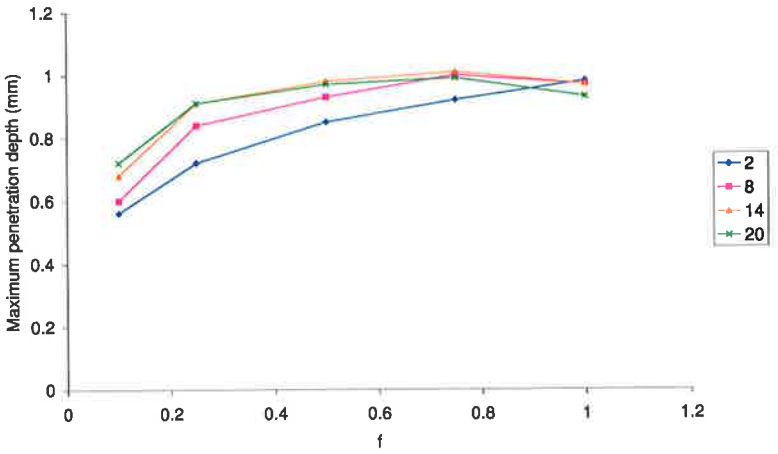


(a) Penetration depth variation.

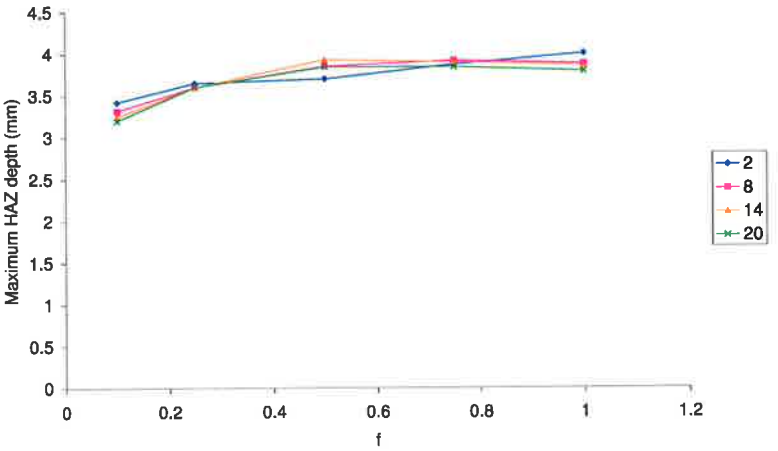


(b) Heat affected zone depth variation.

**Figure 3.35:** Plot of maximum penetration and heat affected zone depth for various heat source configurations: $n_2 = 2, 8, 14, 20$, $f = 0.1, 0.25, 0.5, 0.75, 1.0$.

fusion, while producing the least penetration for a given heat input was for the heat source parameters: $n_2 = 2, f = 0.1$.

The trend observed for predicted maximum HAZ depth is similar to that found for maximum penetration depth. For $n_2 = 2$, as $f$ was increased, the predicted HAZ depth was found to increase. However, for $n_2 = 8, 14, 20$, the predicted HAZ depth was observed to increase with $f = 0.1, 0.25, 0.5$. However, the predictions then began to drop as $f$ was increased from $f = 0.75$ to $f = 1.0$. In addition, for $f = 0.1$, as $n_2$ was increased, the resulting HAZ depth was observed to decrease. This observed trend was the goal for the original formulation of the heat source, involving raising heat source parameter

$n_2$ to produce a shallow fusion and HAZ depth. The trend is different for the values $f = 0.25, 0.5, 0.75$. However, for $f = 1.0$, the predicted HAZ depth was also found to decrease. However, in general, the difference between predicted HAZ depth for all $f = 0.1, 0.25, 0.5, 0.75, 1.0$ is small.

### 3.5.4 Conclusions

In summary, the DEHS with the parameters $f = 0.1, n_2 = 2$ is considered to be reflect the low penetration and HAZ depth due to an in-service MMA welding. However, further work is required to formulate a heat source for vertical up welds. The current definition of the heat source does not consider the diameter of the electrode or the applied welding current; further studies will aid and improve the accuracy of the existing heat source model. Perhaps a change in the shape of the heat source or a change in the distribution of the heat flux can be used to approximate the effect of welding current. However, the proposed modification to the DEHS is considered to be accurate for the purpose of the thermal analysis of in-service welding. Clearly, the reduced penetration depth and HAZ depth found for vertical down in-service welding has been reproduced by the proposed modifications of the DEHS.

# Chapter 4

# Experiments

## 4.1 Introduction

The development of numerical thermal models, in isolation, purely from scientific theory, is almost impossible. Often, many parameters required for such thermal models, can only be determined using empirically derived data. In relation to in-service welding, the required data, as concluded in Section 2.2.1.1 of the literature review, is either unavailable, or incomplete. For example, published data relating to in-service welding experiments, may quote $t_{8/5}$ cooling times, but other significant parameters, such as weld penetration, HAZ shape, and bead shape are not available.

Accurate description of many important parameters for the thermal models required data gathered from experiments. Examples include: the possible variation of heat input with position for circumferential fillet welds, the variation of heat input with welding angle, and the differences in heat input found with electrode type. For example used with numerical models, such experimental data allows verification of heat source type and confirmation of the suitability of boundary conditions. Any experiments aimed at investigating in-service welding and link with numerical model development consequently needs to generate a more complete data set, as the principal objective. The results of the

literature review, and work aimed at determining the most commonly used practice in industry, highly recommended using low hydrogen controlled electrodes. Such electrodes, were therefore chosen for the experiments.

The data recorded from the experiments were required to accurately describe important parameters within the thermal models, such as the possible variation of heat input with:

- position around a circumferential fillet weld
- welding angle
- electrode type.

Specifically, the objectives of the experiments were to:

- establish any significant variation of heat input with welding position for in-service circumferential fillet welds
- measure the deposition rate and weld bead geometry
- establish any characteristic variation of weld bead geometry with position for in-service circumferential fillet welds
- establish empirical relationships between bead volume, shape and weld process parameters, for example, heat input
- examine the differences in behaviour between welds in the vertical-up and vertical-down position, on a range of typical pipe steels
- generate specific data on fusion zone shape, HAZ shape for comparison with numerical models for a rage of welding conditions and pipeline flow conditions
- generate $t_{8/5}$ cooling times to verify accuracy of model predictions
- generate HAZ hardness to facilitate suitability of CE relationship between $t_{8/5}$ , composition and hardness.

The following sections will discuss the experiments, that were conducted during the course of the research. In total, three separate experiments were attempted. The initial experiment involved a mechanised welding system, while the remaining two experiments were attempted using welders qualified in in-service welding. The first two experiments, were essentially laboratory based, and the cooling influence of flowing natural gas was simulated using flowing water. The last experiment, was carried out on a temporary flow-loop established at Duke Energy's metering facility at Gladstone, Queensland.

## 4.2 Laboratory simulation

To date, the approach commonly taken for testing in-service welding is to weld on a small section of pipe which is artificially cooled [12, 21]. While such a system simulates the increased cooling rate due to in-service welding, it does not consider or simulate a pressurised system. While experiments relating to in-service welding onto a pressurised pipe have been reported [84], only a limited number of experiments have involved welding onto a flow-loop, or a by-pass, where conditions, gas flow-rate and pressure, are similar to operational pipelines [17, 23]. Moreover, the published data from such experiments are considered to be incomplete. For obvious safety reasons, the majority of the experimental work, relating to in-service welding, have been undertaken using an artificially cooled system.

A number of experiments, involving welding onto an artificially cooled pipe material, using a variety of fluids have been carried out by EWI [12]. The fluids used for the artificial cooling included motor oil, water and air. The $t_{8/5}$ cooling time attained when welding with a given heat input, using different cooling fluids can be seen in Figure 4.1(a) and Figure 4.1(b). In both figures, the relationship between cooling rate when welding onto an operational pipeline is compared with similar welds deposited on test pipes cooled with water, motor oil, or air. It can be observed that using water, in general, returns welds with the lowest $t_{8/5}$ cooling time, or the fastest cooling rate, for a given heat input.

In comparison, using air as the cooling medium results in welds with the slowest cooling rate, or highest $t_{8/5}$ cooling time. Moreover, motor oil produces cooling rates between air and water. The cooling times obtained using pressurised flowing natural gas lie between air and water. The difference in cooling rates between the four fluids is found to be more significant when welding onto thinner walled pipes; as can be seen by comparing Figure 4.1.

Alternatively, the differences in heat transfer, for each type of fluid, can be determined, by calculating the heat transfer at the inside surface of the pipe wall. For example, the convective heat transfer coefficient, $h_c$, can be calculated by using an established non-dimensional relationship, such as Dittus Boelter [42]:

$$Nu_d = 0.023 Re_d^{0.8} Pr^{0.4} \tag{4.1}$$

where, $Nu_d$, is the Nusselt number, $Re$, the Reynolds number, and $Pr$, the Prandtl number; all evaluated for fluid flow in a duct. Such a relationship, as seen in Equation 4.1 calculates the effective heat transfer coefficient, for a given fluid, simply from the thermal properties and velocity field of the fluid.

A calculation of heat transfer coefficient for various fluids at selected velocities; methane under typical flow pipeline flow-rates and pressures, air at low pressure, water and two types of oil, can be seen in Figure 4.2. To achieve the same heat transfer characteristics as Methane at $8MPA$, flowing at $3.2m/s$, would require ambient air at a flow-rate of over $296m/s$. When using oil as the cooling fluid, the flow-rate is a somewhat more manageable $9.0m/s$. However, if such flow-rates were considered for experiments, large quantities of fluid would be required along with a large capacity pump. If oil was chosen as the cooling fluid, such an experimental set-up would he highly impractical. However, if water were the chosen cooling fluid, very low flow-rates, between $0 - 1m/s$ would be sufficient. While such a flow-rate is feasible for experimentation, water is troublesome as it can potentially boil at such low flow-rates. The added heat transfer induced due to boiling phase change is significant and difficult to monitor and control; such a phase

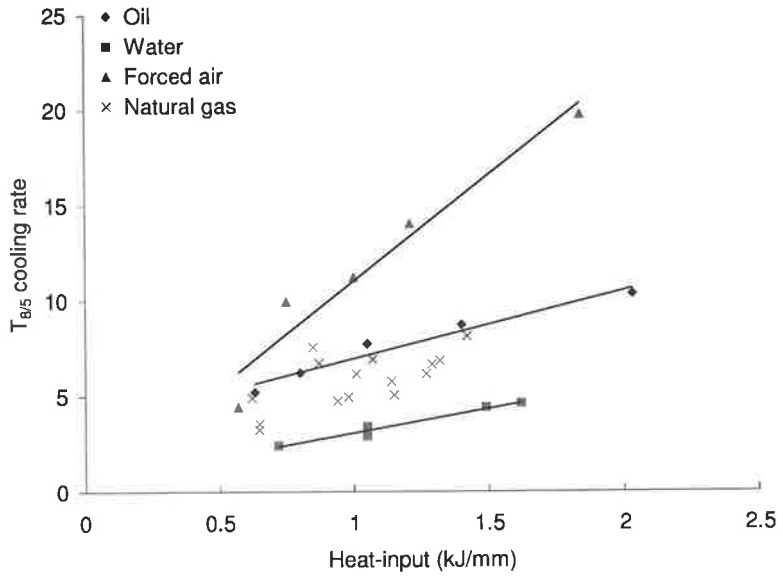


(a) 4.8mm.

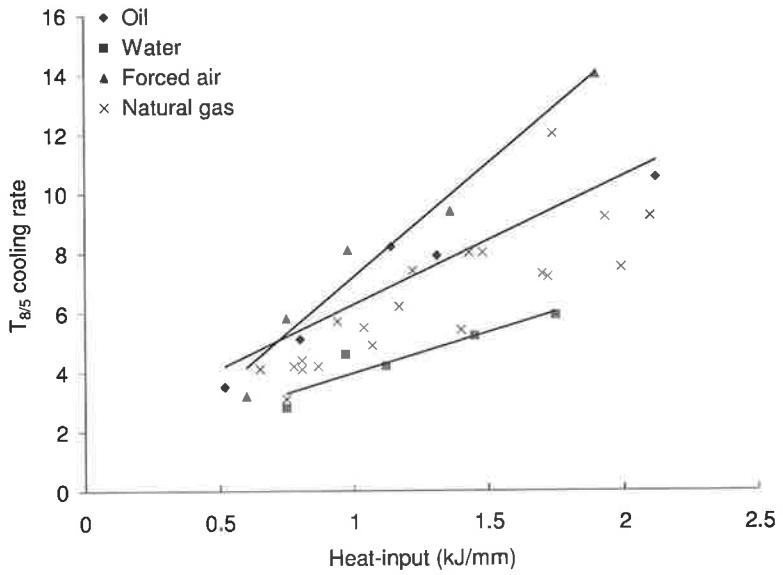


(b) 6.4mm.

**Figure 4.1:** Comparison between weld cooling rates using different cooling fluids on $4.8mm$ and $6.4mm$ thick pipe.

change effect is not included in Figure 4.2.

In general, existing weld procedure development methods have generally accepted these difficulties and used water as the cooling fluid. The argument proposed is that if welds deposited on water cooled testing facilities exhibit a satisfactory $t_{8/5}$ cooling time, then the cooling rate when depositing on a live gas pipeline will be lower. Conse-

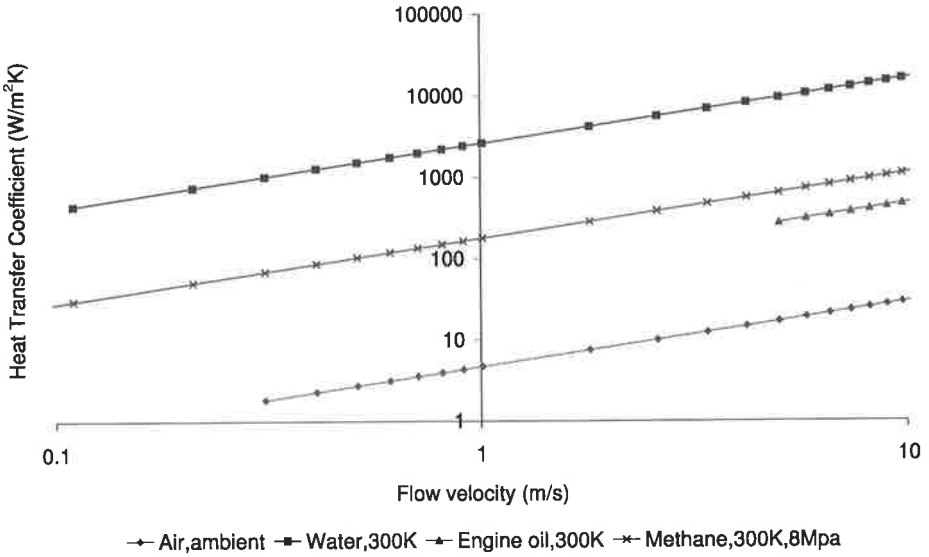


**Figure 4.2:** Predicted convective heat transfer coefficients for different flowing fluids compared with values calculated for methane gas under typical operational conditions.

quently, the level of post-weld hardness will be the same as the test weld, if not lower. The test weld conditions are therefore considered to be conservative, which is favourable when considering hydrogen assisted cracking. However, the possibility of burnthrough is now potentially increased, as heat input may be higher than needed when welding onto operational pipelines. It is evident that burnthrough is not directly considered by test procedures which involve unpressurised fluids such as oil, air or water.

### 4.2.1 Initial experiment: mechanised welding

The automated MMA welding machine, used in initial experiments into in-service welding, can be seen in Figure 4.3. In principal, the automated welding machine provided an excellent experimental set-up; allowing for constant heat input, out-of-position welds to be deposited. As can be seen in Figure 4.3, the welding machine consisted of a moving table, an electrode feeder, and a voltage controller. The angle of the frame and table could be set to any desired angle, while in combination, the angle of the electrode feeder could also be independently set to any desired angle. Such versatility, enabled the simulation of out-of-position welding with any desired trailing and leading angle. The feed rate of

**Figure 4.3:** Autorun mechanised welding system.

the electrode could be controlled to a give desired value of arc voltage.

An external welding generator enabled the constant steady supply of current for a given amperage, while a welding control system restricted the electrode feed rate to provide a constant given arc voltage. In addition, the speed of welding, or the speed of the traverse, was able to be set for a given speed. In combination, the mechanised welding machine was able to deposit welds for a wide range of heat input.

To simulate in-service welding, a simple cooling chamber, as seen in Figure 4.4 was manufactured. The chamber used water as the cooling fluid, while the flow-rate was controlled by a pair of valves; the flow was supplied by a electric pump. A given steel plate, could be attached on top of the cooling chamber; essentially sealing the unit while being cooled from the underside by the flowing water. The angle of the cooling chamber, in relation to the surface of the traverse was also variable. The angle of the fillet, or the electrode angle could therefore be set to a desired value.

While the mechanised welding machine provided many controllable parameters, un-

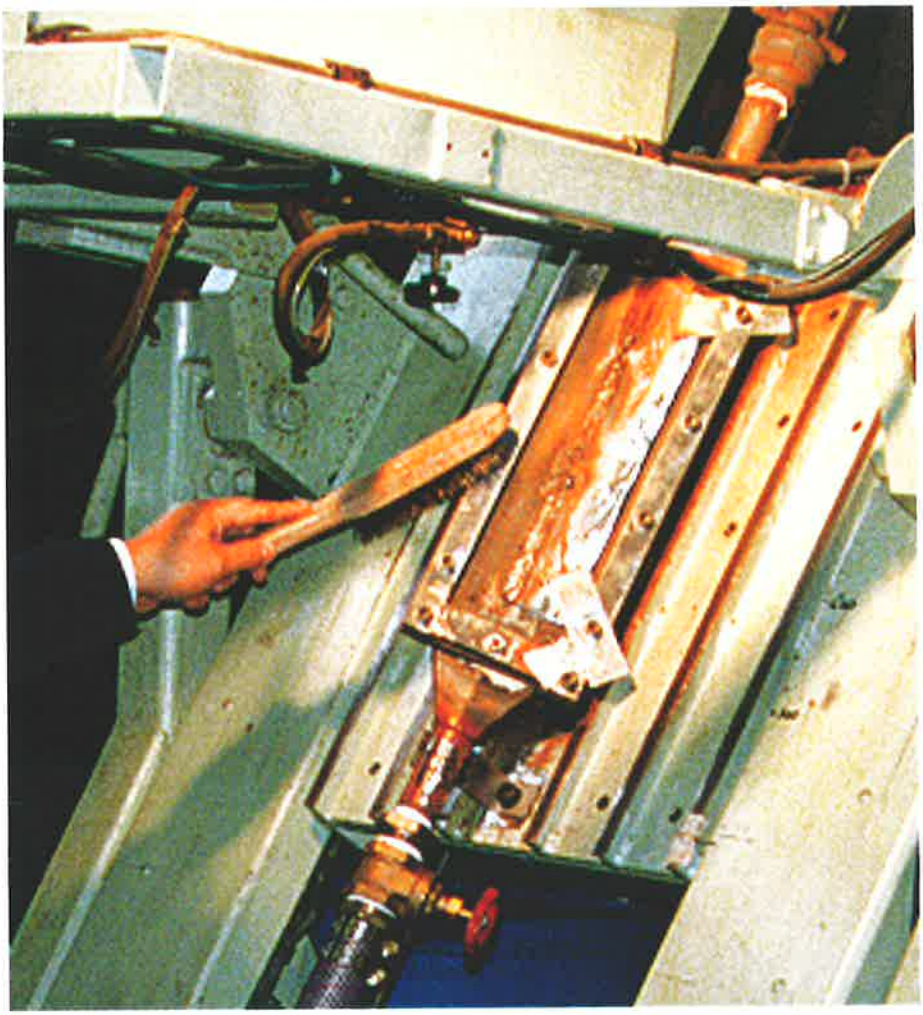

**Figure 4.4:** Water cooled weld chamber.

fortunately, a number of unresolved problems eventually caused the approach to be abandoned. The problems which arose from lengthy trials included:

- good consistent quality welds could not be obtained
- with thin $\phi 2.5mm$ diameter electrodes, the position of the tip could not be held in a stable position
- the electrode feeder failed to operate satisfactorily.

As the speed of the traverse was constant, it was found that a satisfactory weld was unable to be deposited. For satisfactory weld quality, it was found that the welding speed was required to be adjusted depending on the simulated position. The electrodes

chosen were required to be operated under a restricted range of current and voltage. Any deviation from the range, for a given electrode, would cause a compromise in the quality of the deposited weld. The speed of welding was therefore controlled by the heat input and the position of welding; resulting with a limited range of operation. Clearly, satisfactory welds had occurred in only a few instances; suggesting that the approach should be abandoned.

The electrode feeder, at best, worked with limited success. For thin, 2.5$mm$ diameter electrodes, the force at which the electrode feeder would apply, caused the electrode to buckle. The problem was not found when welding with larger, 3.2$mm$ diameter electrodes. The electrode feeder, also began to behave erratically as the weld was deposited for unknown reasons. It is suggested, that the principal reason for the failure of the experiments, is that out-of-position welding, for MMA electrodes, requires far more sophisticated feed control and voltage control, than a machine, such as the mechanised welding system, could provide. It appears, that MMA welding is a highly dynamic welding process, requiring constant adjustment by the welder.

It was concluded that welds of acceptable 'industry standard' quality could not be obtained with this equipment. Therefore it was abandoned and replaced with experiments involving manually welding onto water cooled pipe segment, with an experienced welder qualified in in-service MMA welding.

### 4.2.2 Manual in-service welding laboratory simulation

#### 4.2.2.1 Experimental equipment

An experiment involving welding onto artificially cooled pipe, was attempted with a welder qualified in in-service MMA welding. The equipment consisted of a half section of pipe with a water jacket clamped to the inside surface, as seen in Figure 4.5(a). The cross-sectional area of the jacket was kept small to maintain a high linear flow-rate, and avoid boiling and reduce the total throughput required. Circumferential fillet welding was sim-

ulated by attaching a second segment of pipe, $100mm$ in width, on top of the test pipe as seen in Figure 4.5(b). With such a configuration, all welding positions encountered during circumferential fillet in-service welding could be simulated. An array of thermocouples were attached at various locations, as seen in Figure 4.6, to measure cooling histories near the region of the weld. A data acquisition module, as seen in Figure 4.5(b) was used to the record temperature history of the weld, at a frequency of 10 samples per second.

In addition, a welding monitor, as seen in Figure 4.5(b), was used to record arc voltage and current at 1 second intervals. The time taken to complete each weld was also measured, using a hand operated stop-watch. By measuring the length of a completed weld, the average welding speed was then calculated, and in combination with the arc current and voltage recorded from the welding monitor, allowed the calculation of average weld heat input.

Initial trials were attempted using a combination of sheathed thermocouples, $1mm$ in diameter, and type-k thermocouples. The sheathed thermocouples, as seen in Figure 4.6, were attached to holes drilled into the inside surface of the test pipe, in an attempt to measure the HAZ temperature history due to welding. Additionally, type-k thermocouples were harpooned, as seen in Figure 4.7, into the molten weld pool behind the arc during welding, in an attempt to record the temperature history of the weld bead. While the molten weld pool would occasionally melt and destroy the thermocouple, further attempts generally returned consistent results.

The application of the sheathed thermocouple proved to be difficult. Welding under accelerated cooling produces HAZ regions which are very small compared with those in welds which cool under ambient conditions. In some instances, the thickness of the HAZ in the pipe due to in-service welding was less than $1mm$. Consequently, the positioning of the thermocouple required tight tolerances. Moreover, as in-service welding is a manual process, the size of the HAZ region can also fluctuate significantly. As a result, the application of the sheathed thermocouple proved unworkable, and was abandoned. Temperatures cycles were therefore measured by applying the harpoon technique, as seen

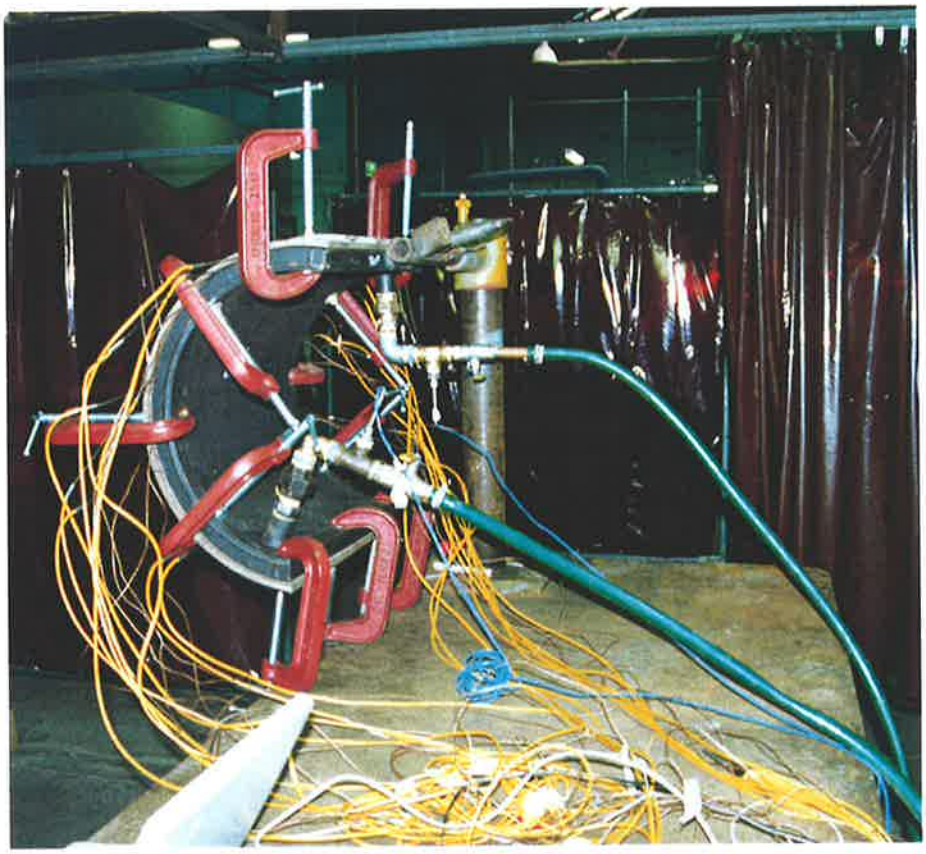

(a) Photograph displays cooling jacket and thermocouple wires.


(b) Photograph displays the simulated in-service pipe segment, along with data acquisition module, and laptop computer.

**Figure 4.5:** Laboratory experiment apparatus.

**Figure 4.6:** Sheathed thermocouples used in laboratory experiments.

in Figure 4.7, using type-k thermocouples.

#### 4.2.2.2 Experimental plan

The experiments were conducted using two types of electrodes:

- E8018G, used in the vertical-down position
- E7016 used in the vertical-up position.

Three diameters were chosen for each type of electrode: $2.5, 3.2$ and $4mm$. To determine appropriate welding parameters, for each electrode, a number of tests were performed by depositing circumferential single pass welds, on a uncooled pipe. The results of the tests are found in Table 4.1.

A total of eight types of pipe, varying in diameter, wall thickness and material grade were selected for the study, as seen in Table 4.2. The selection was chosen to reflect the typical range of pipe materials used in current and future Australian pipelines.

**Figure 4.7:** Thermocouple harpooning.

| Test No | Electrode type | Diameter (mm) | Welding direction | Volts | Amps | Time (min) | Weld Length (mm) | Heat Input (kJ/mm) |
|---|---|---|---|---|---|---|---|---|
| 1 | E7016 | 2.5 | VU | 22.0 | 66.0 | 1.43 | 205 | 0.61 |
| 2 | E7016 | 2.5 | VU | 24.5 | 87.0 | 1.58 | 205 | 0.99 |
| 3 | E7016 | 3.2 | VU | 22.0 | 92.0 | 1.18 | 200 | 0.72 |
| 4 | E7016 | 3.2 | VU | 27.0 | 120.0 | 0.95 | 200 | 0.92 |
| 5 | E7016 | 4.0 | VU | 22.0 | 118.0 | 0.90 | 190 | 0.74 |
| 6 | E7016 | 4.0 | VU | 26.0 | 132.0 | 1.12 | 195 | 1.18 |
| 7 | E8081G | 2.5 | VD | 21.0 | 80.0 | 1.00 | 205 | 0.49 |
| 8 | E8081G | 2.5 | VD | 22.0 | 106.0 | 1.10 | 195 | 0.79 |
| 9 | E8081G | 3.2 | VD | 19.0 | 92.0 | 0.97 | 170 | 0.60 |
| 10 | E8081G | 3.2 | VD | 23.0 | 158.0 | 0.70 | 170 | 0.90 |
| 11 | E8081G | 4.0 | VD | 20.0 | 150.0 | 0.95 | 210 | 0.81 |
| 12 | E8081G | 4.0 | VD | 22.0 | 194.0 | 0.77 | 210 | 0.93 |

**Table 4.1:** Welding Parameter Sets established for E7016 & E8018G Electrodes.

| Pipe | Diameter (mm) | Wall Thickness (mm) | Material Grade |
|---|---|---|---|
| 1 | 508.0 | 8.6 | API 5LX60 AGL |
| 2 | 406.0 | 8.6 | API 5LX70(Nippon)AGLPWA |
| 3 | 406.0 | 7.8 | API 5L X60 AGLPQ |
| 4 | 323.9 | 5.2 | API 5L X42 AGLPQ |
| 5 | 323.9 | 5.2 | API 5L X52 |
| 6 | 168.0 | 3.6 | API 5L X42 |
| 7 | 558.0 | 9.5 | API 5L X42 AGL |
| 8 | 406.0 | 7.8 | X80 |

**Table 4.2:** Pipe materials used in the laboratory trials.

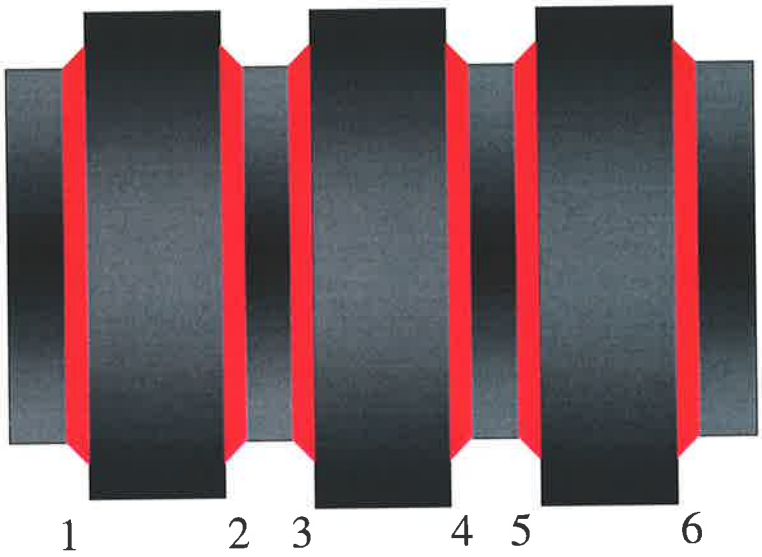


**Figure 4.8:** Welding sequence for laboratory tests.

| Weld Number | Electrode type | Welding direction | Heat input | Number of weld runs | Cooling water flow-rate $(m/s)$ |
|---|---|---|---|---|---|
| 1 | E8018G | VD | LHI | Multi-pass | 3 |
| 2 | E8018G | VD | HHI | Multi-pass | 3 |
| 3 | E7016G | VU | LHI | Multi-pass | 3 |
| 4 | E7016G | VU | HHI | Multi-pass | 3 |
| 5 | E8018G | VD | LHI | Single-pass | 3 |
| 6 | E7018G | VU | LHI | Single-pass | 17 |

All electrodes were $3.2mm$ in diameter.

**Table 4.3:** Test welding sequence.

A standard test pattern of welds was established as shown schematically in Figure 4.8 and in Table 4.3. For each weld, the welding conditions were monitored and the heat input was calculated. Additionally, the $t_{8/5}$ weld cooling time was measured from harpooning thermocouples. Once the test was completed, each weld was radially sectioned and macrographs were taken. Measurements of HAZ shape, fusion zone shape, and weld bead shape, were then taken from the photographs.

### 4.2.3 Analysis of experimental results

#### 4.2.3.1 Variation of heat input with welding position

The data recorded using the welding monitor, arc voltage and current, combined with the average speed, allows the calculation of heat input, for a given welding run. A typical plot, of the variation of heat input with position around the pipe, can be seen in Figure 4.9. Five electrodes (five individual weld runs) were required to complete the 180$^o$ root pass. The discreet, stepped variation in heat input, is a direct result of recording the average speed for a given weld, rather than recording continuously. There was a significant variation in heat input for each weld run, as can be seen in Figure 4.9. However, the variation in welding current and voltage was found to be minor; suggesting that the in-service welding heat input is primarily controlled by welding speed.

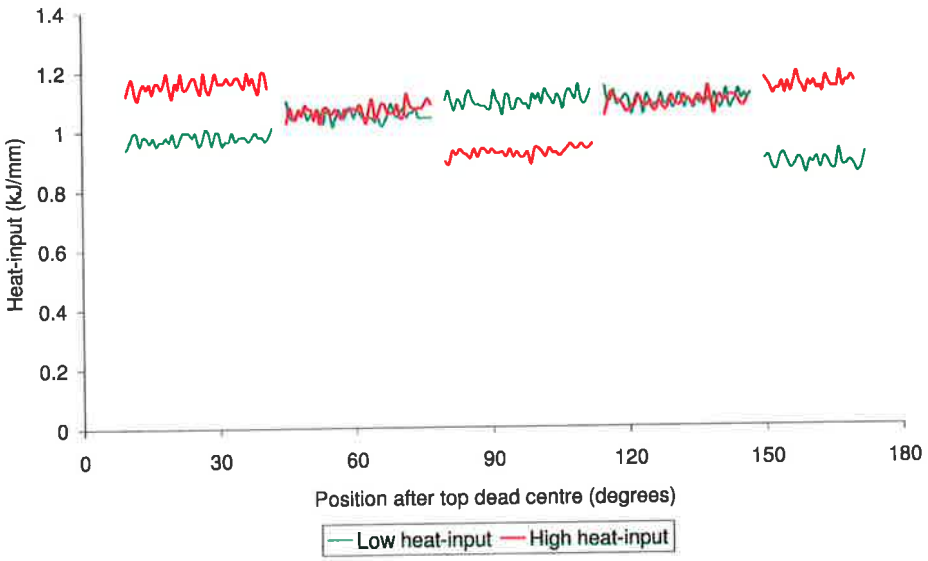


**Figure 4.9:** Typical variation in heat input for two different circumferential fillet root pass welds carried out during the laboratory tests.

Since in-service welding is a manually operated process, it is understandable for some variation to exist. However, the variation was found to be significant, and is conservatively estimated to be ±20%. Such a trend was evident in every weld which was deposited in the experiment. Due to such variation in heat input for all welding runs, it is difficult to form rigorous statements, with respect to the variation of heat input, for circumferential

fillet welding with position around the pipe.

Consider the variation of heat input with position recorded by experiment, seen in Figures 4.10, 4.11, 4.12, 4.13. An obvious trend is not immediately evident. However, in all cases, there does exists a trend where heat input is greater at the 5 o'clock position than at the 1 o'clock position; vertical-up E7016 electrodes exhibit greater variation in comparison to the vertical-down E8081G electrodes. Examining both electrodes, revealed that heat input had increased between $0 - 30\%$, between the 1 o'clock position and 5 o'clock position.

The existence of such significant variation implies that any trends should only be notionally taken as a guide. Clearly, the significant variation in heat input of in-service welding, is primarily due the process requiring manual operation. Moreover, while such variation may be acceptable for thick-walled pipes, such variation when applied to thinner walled pipes could compromise the quality of the weld, along with the structural integrity of the pipe. Clearly, a method of assisting the welder to control the welding heat input within tighter tolerances is highly desirable.

#### 4.2.3.2 Variation of weld penetration with welding position

A number of macrographs were taken at predefined positions around the pipe; 5 equally spaced sections from the 1 o'clock to the 5 o'clock position. Firstly, radial sections for each single pass weld were taken for each pipe tested. The sections were then mounted, polished, etched and finally, macrographs were taken. An example is illustrated in Figure 4.14. The depth of penetration was readily measurable from the macrographs, and therefore the variation of weld penetration with welding position was considered.

The variation of weld penetration with welding position, for both E8018G vertical-down, and E7016, vertical-up electrodes, can be seen in Figures 4.15(a) & 4.15(b). The data was gathered from welds deposited on six types of line pipe. On initial examination, considerable scatter is evident for both electrodes. However, increased weld penetration is

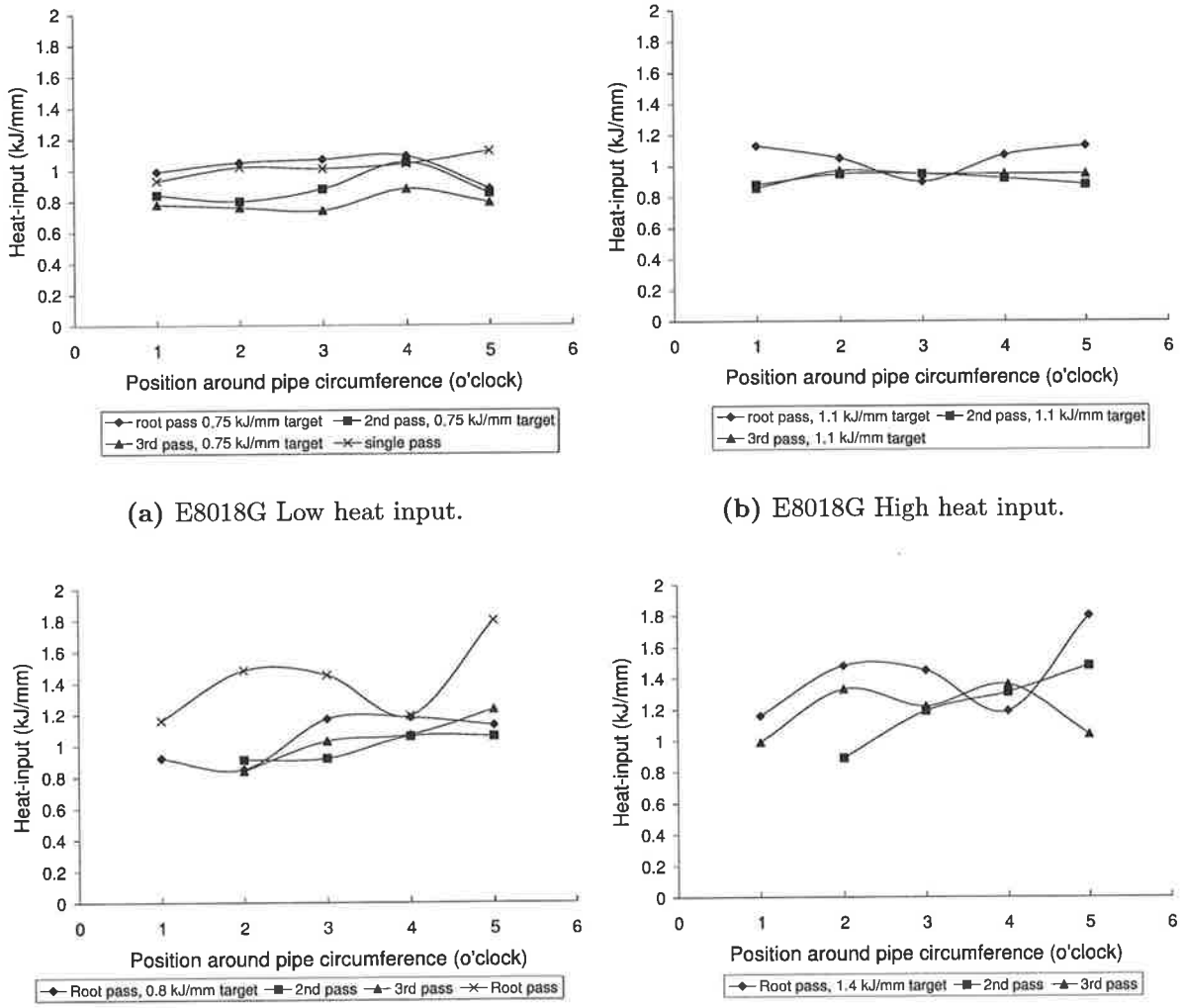


(a) E8018G Low heat input.

(b) E8018G High heat input.

(c) E7016 Low heat input.

(d) E7016 High heat input.

**Figure 4.10:** The variation of heat input with circumferential angular position from top-dead-centre for pipe AGL 01.

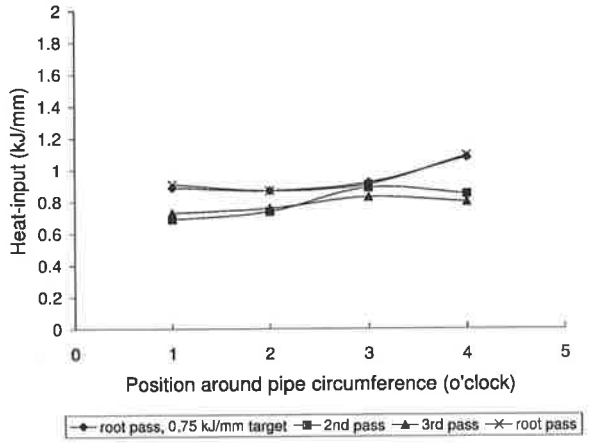


(a) E8018G Low heat input.

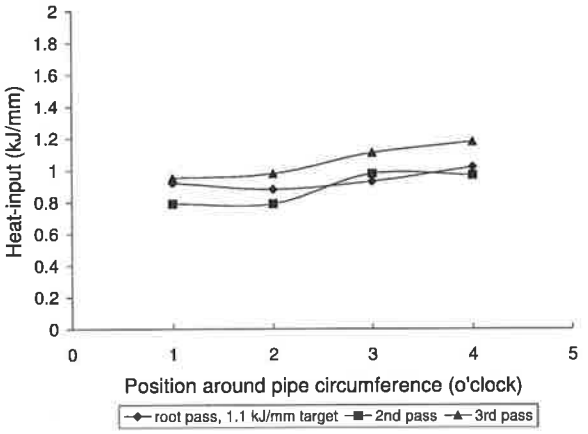


(b) E8018G High heat input.

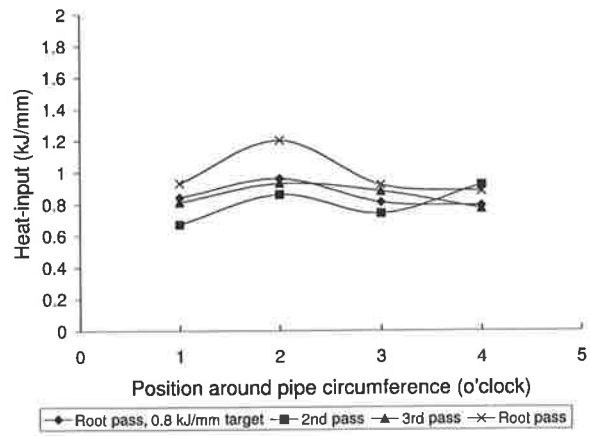


(c) E7016 Low heat input.

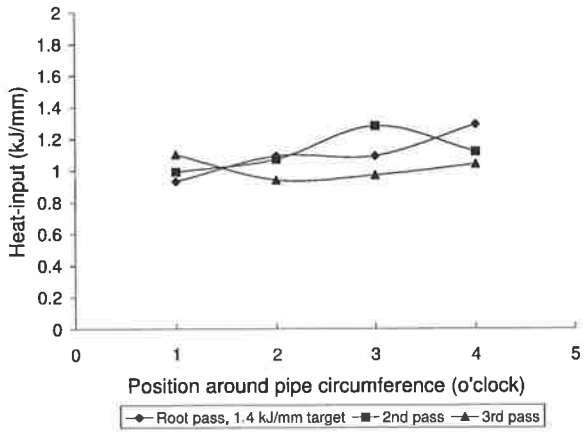


(d) E7016 High heat input.

**Figure 4.11:** The variation of heat input with circumferential angular position from top-dead-centre for pipe AGL 02.

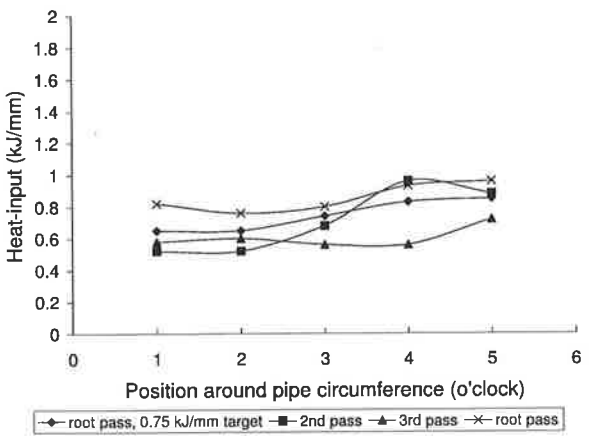


(a) E8018G Low heat input.

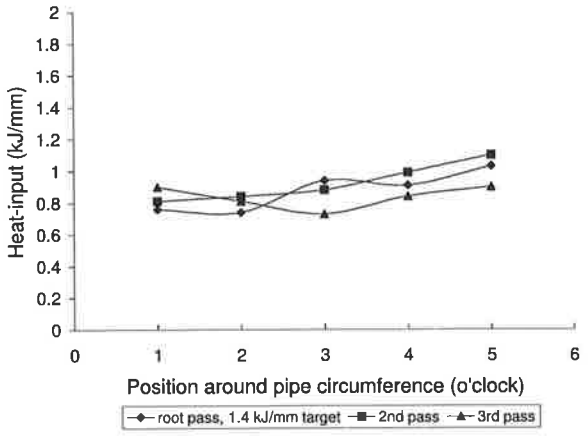


(b) E8018G High heat input.

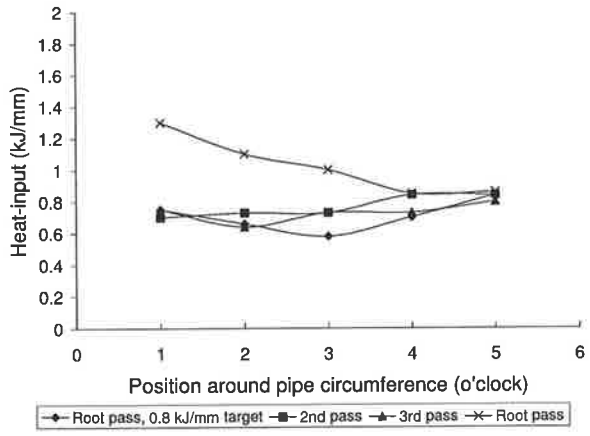


(c) E7016 Low heat input.

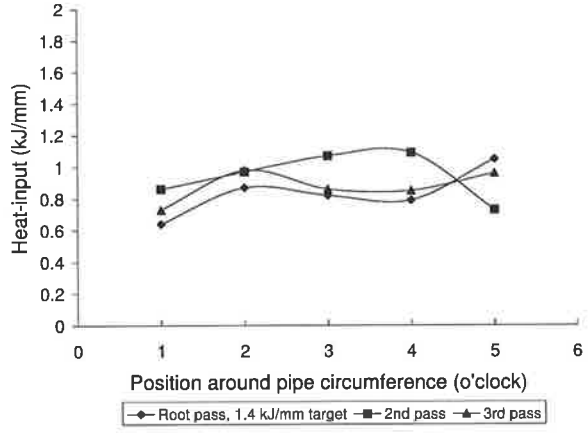


(d) E7016 High heat input.

**Figure 4.12:** The variation of heat input with circumferential angular position from top-dead-centre for pipe AGL 12.

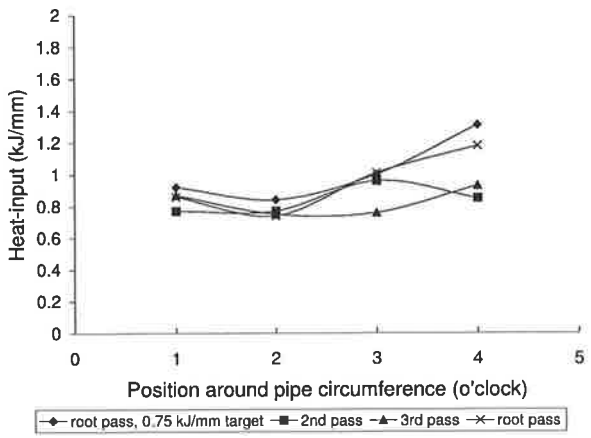


(a) E8018G Low heat input.

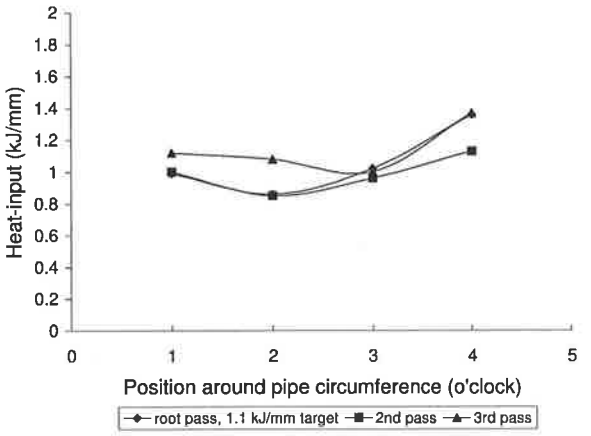


(b) E8018G High heat input.

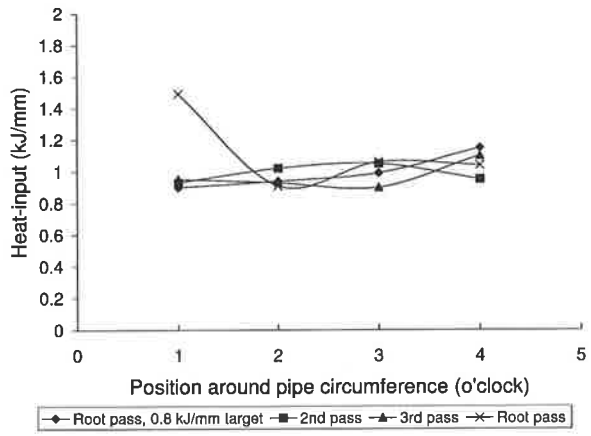


(c) E7016 Low heat input.

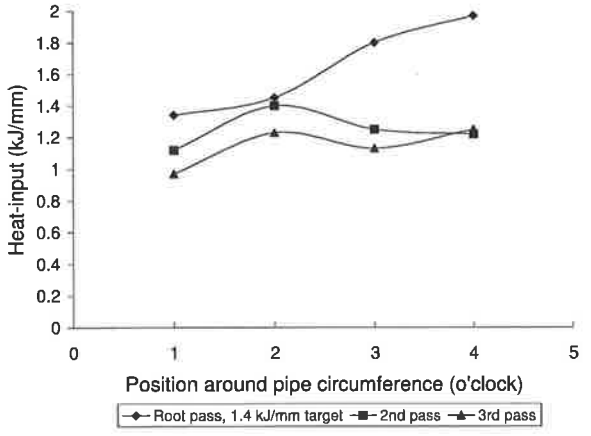


(d) E7016 High heat input.

**Figure 4.13:** The variation of heat input with circumferential angular position from top-dead-centre for pipe AGL 15.

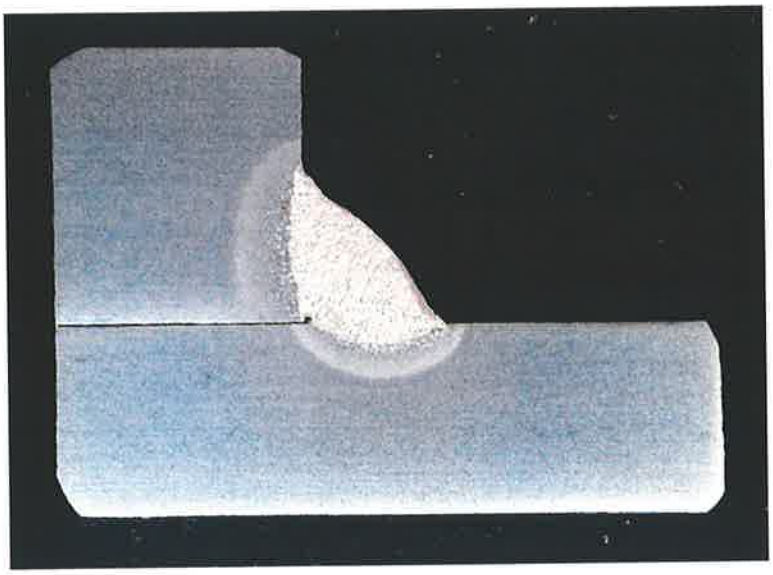

**Figure 4.14:** Sample macro taken from laboratory experiments.

apparent at the 5 o'clock position for the E8018G vertical-down electrodes; no such trend was evident for the E7016 vertical-up electrode. The experiment data, revealed that E7016 vertical-up electrodes produced greater penetration, on average, in comparison to the E8018G vertical-down electrode; which is in agreement with work reported by Phelps et al. [68].

#### 4.2.3.3 Variation of weld penetration with heat input

The variation of penetration with heat input was also considered. The results from experiments is shown in Figure 4.16(a) for E8081G electrodes, and Figure 4.16(b) for E7016 electrodes. Considering simple heat transfer principles, penetration into the pipe is expected to increase with greater heat input. The results contain a fair degree of scatter, and so can only give an approximate indication of the relationship between penetration and heat input. No relationship between penetration and heat input was found; broadly for this range of heat input, weld penetration was the same. As the welding was deposited using manual techniques, a significant degree of variation in heat input may introduce such scatter.

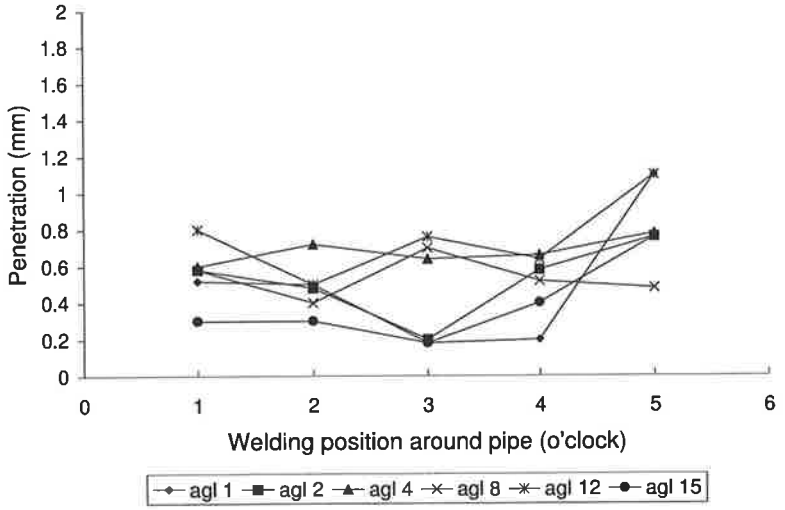


(a) E8018G.

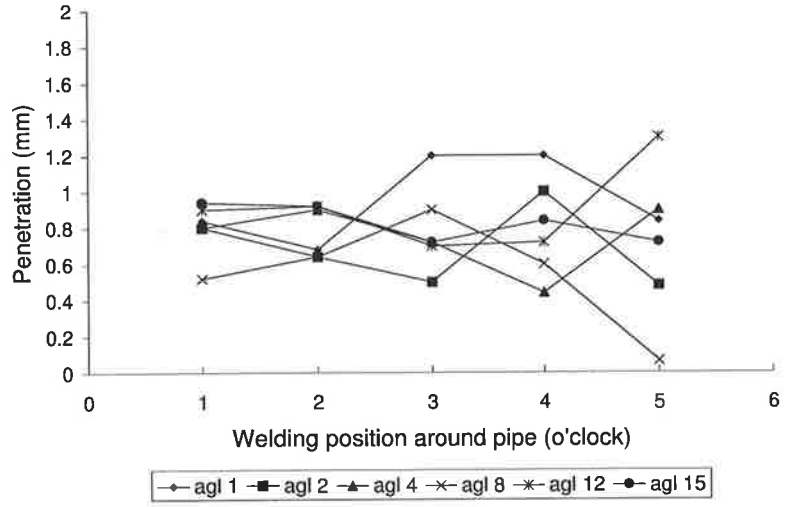


(b) E7016.

**Figure 4.15:** Weld penetration variation with position around circumference of pipe.

### 4.2.4 Conclusions

The analysis of welding conditions and welds produced using pipe cooled with a water jacket to generate a rapid quench, gave the following results:

1. Penetration into the run pipe was generally greater when using the E7016 electrode in the vertical-up position rather than with E8018G in the vertical-down.

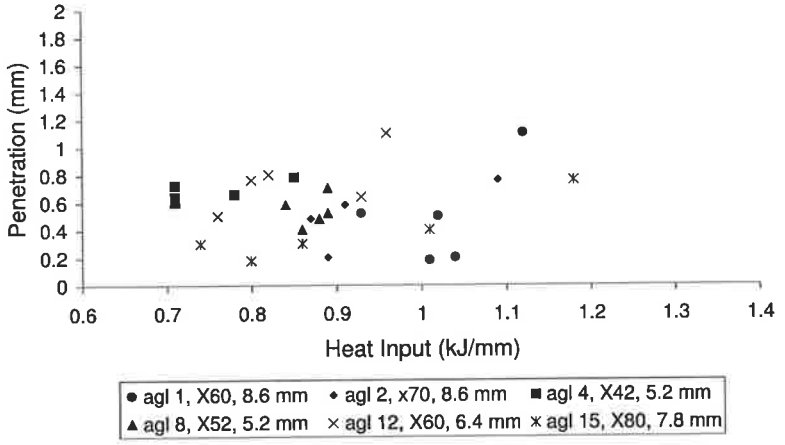


(a) E8081G.

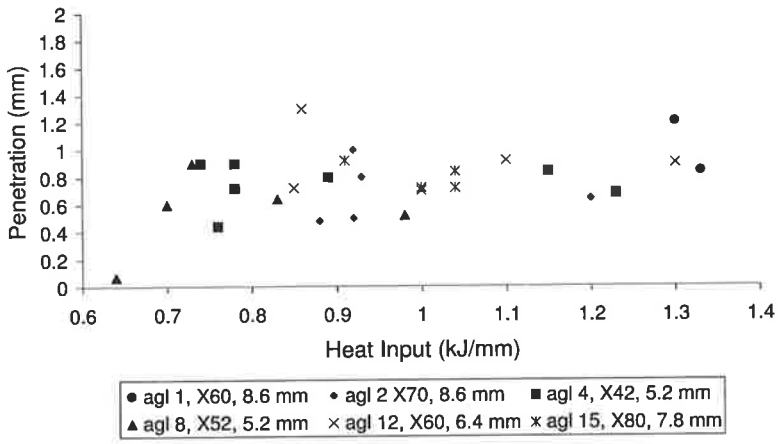


(b) E7016.

**Figure 4.16:** Weld penetration variation with heat input.

2. Penetration into the run-pipe slightly increased with increasing heat input although this effect was largely swamped by a significant variability at a given heat input. At a nominal heat input of about $1kJ/mm$ this variability was approximately, $0.2 - 0.8mm$ with E8018G and $0.5 - 1.0mm$ with E7016 electrodes.

3. The presence of scatter in the results is suggested to be largely due to the significant variation of heat input with position.

The implications of these observations to the thermal modelling of in-service welding is discussed later in Chapter 5.

## 4.3 Field experiments

### 4.3.1 Introduction

A significant proportion of experiments related to in-service welding, has been achieved using simulated laboratory work; where, for example, oil or water is the cooling fluid. However, difficulty arises when attempting to simulate field conditions using a laboratory simulation. Cooling fluids, as stated earlier in Section 4.2, have limited range, where they can reproduce cooling characteristics of flowing pressurised natural gas in an operating pipeline. While there exists a small amount of published data relating to field in-service welding experiments, often, many important parameters, for example, penetration and HAZ depth, are not included.

An apparatus, commonly used for field in-service welding experiments, is the flow-loop; referred to earlier in Section 1.4. Recapping, a flow-loop, as seen in Figure 4.17, is a section

**Figure 4.17:** Flow-loop facility.

of pipeline which operates in parallel to an existing pipeline. Commonly, a flow-loop, is controlled at either end using valves to adjust flow-rate and pressure. An experiment using a flow-loop clearly includes the gas flow and heat loss due to flowing natural gas, and is the closest possible simulation of operational conditions. Once the experiments have been completed, the section of pipe can be removed, allowing specimens to be sectioned from

the pipe for metallographic related work.

Due to the overall complexity, logistics involved, and costs related to the operation of a flow-loop facility in the course of this work, only one trial, over an 8 hour period was attempted. The use of the flow-loop was kindly provided by Duke Energy. The trial consisted of depositing a number of circumferential fillet welds on specially constructed length of pipe, 300$mm$ in diameter, under known pipe flow.

The objectives of the trial were:

1. To measure the arc energy, arc current and voltage for a range of in-service welding conditions.
2. To measure the welding speed.
3. To measure the thermal cycle for each weld from which $t_{8/5}$ cooling times could be extracted
4. To take a metallographic section of each weld and measure:
    - the maximum depth of weld penetration
    - the maximum depth of HAZ penetration
    - characteristic weld bead dimensions.

### 4.3.2 Test material

The specially constructed pipe, used for the flow-loop experiments, consisted of three individual types of line pipe, joined end-to-end together, as seen in Figure 4.18

Two of the three pipes had identical material grade, *X70*; a classification used in the pipeline industry stating the yield strength of the pipe. The two pipes were 4.8$mm$ and 5.6$mm$ in wall thickness. The remaining pipe was 6.4$mm$ in wall thickness and was of the material grade, *Ultrapipe*. Each individual pipe was approximately 3$m$ in length,

**Figure 4.18:** Pipe attached to flow-loop facility.

giving a total length of approximately $9m$. The chemical compositions, as measured using spectroscopy, are given in Table 4.4. To simulate in-service circumferential fillet welding, further pipe, $9mm$ thick of material grade Ultrapipe was saw-cut, to a width of $100mm$, and placed on top of the test pipe to simulate a typical sleeve joint. The sleeve was attached to the pipe prior to welding, by welding the four corners of sleeve to the pipe.

| | %C | %Si | %Mn | %Cu | %Ni | %Cr | %Mo | %V | %B | %Nb | %Ti |
|---|---|---|---|---|---|---|---|---|---|---|---|
| 4.8mm X70 | 0.065 | 0.34 | 1.42 | 0.014 | 0.029 | 0.023 | 0.107 | 0.005 | 0.001 | 0.076 | 0.02 |
| 5.6mm X70 | 0.065 | 0.31 | 1.32 | 0.01 | 0.024 | 0.011 | 0.106 | 0.005 | 0.001 | 0.062 | 0.019 |
| 6.4mm Ultra-pipe | 0.137 | 0.12 | 1.03 | 0.018 | 0.031 | 0.009 | 0.01 | 0.005 | 0.001 | 0.005 | 0.005 |

**Table 4.4:** Chemical composition of test pipe used in flow-loop trials.

### 4.3.3 Experiment methodology

A total of 45 test welds were deposited on a flow-loop over an 8 hour period. Photographs of the site with the test pipe attached are shown in Figure 4.17. Further photographs of the deposited welds are shown in Figure 4.18.

The apparatus used for the flow-loop experiment can be seen in Figure 4.19. The test welds were deposited as a single root-pass, circumferential fillet weld. Welds were deposited between top dead centre, $0^o$, and bottom dead centre, $180^o$, for the $300mm$ diameter pipe. The weld preparation for each fillet was $90^o$; each simulated sleeve was saw-cut, and then placed on top of the pipe to form the fillet.

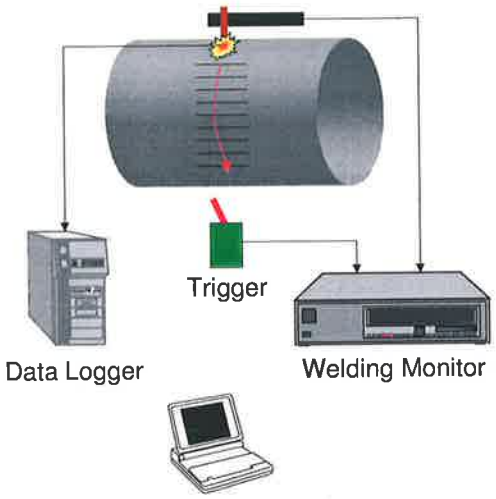


**Figure 4.19:** Schematic of apparatus used for flow-loop tests.

All welds were deposited using low-hydrogen controlled E8018G electrodes; and electrode specifically used for vertical down welding. Two diameters were chosen for the test: $2.5mm$ & $3.2mm$. The pressure and flow-rate were recorded at 1 minute intervals by the operator of the flow-loop facility. While it was not possible to achieve largely varied flow-rates and pressures, the option of operating under two flow conditions was provided. The first 27 test welds were deposited under high pressure $(5.5-6MPa)$, while the latter 18 test welds were deposited under low pressure, $(2.5-3MPa)$. The flow rate varied from $52-59kscm/h$.

The conclusion of the laboratory trials as discussed earlier in Section 4.2.4, revealed that the welding heat input, was found to vary significantly; primarily due to a variation in weld travel speed. Measuring the speed of a manually operated welding process is quite a difficult task; especially if accurate data is required. A new technique was therefore

employed; which involved recording the time at which the weld had passed a series of points, 25mm apart on the surface of the pipe.

The time at which a weld had passed a point on the pipe was recorded by activating a hand operated electronic trigger. The trigger was attached to the welding monitor, which recorded voltage at a frequency of 10Hz on a specially programmed channel. The trigger had two states: high and low voltage. Whenever the switch was triggered, the welding monitor would record the respective voltage. Therefore, during the a given weld, the resulting signal was similar to a square waveform. The time at which the trigger had occurred was simply when the voltage has switched from low to high, or *vica versa.* The remaining channels of the welding monitor recorded arc voltage and current, at a frequency of 1Hz, for each test weld.

The thermal history of a given weld, was measured indirectly by recording the temperature history of the weld pool. The method employed was to harpoon thermocouples into the weld pool during welding; a data acquisition module then measured the temperature at a frequency of 10Hz. The harpooning method is identical to the type used for the laboratory simulation.

### 4.3.4 Analysis data collection

After the experiment was completed, the first task was to process the data recorded from the welding monitor and the data acquisition module. An example of the raw data from the data acquisition module can be seen in Figure 4.21; similarly, voltage and current measured using the welding monitor can be seen in Figure 4.20(a), and Figure 4.20(b) for the square waveform showing when the weld had traversed a distance of $25mm$.

A typical result from the thermocouple harpooning, as seen in Figure 4.21, displays the difficulty in measuring weld cooling rates, while welding. Harpooning thermocouples in to a weld pool is not an easily controlled technique, and considerable scatter and erroneous results were obtained. The data was filtered according to a number of rules:

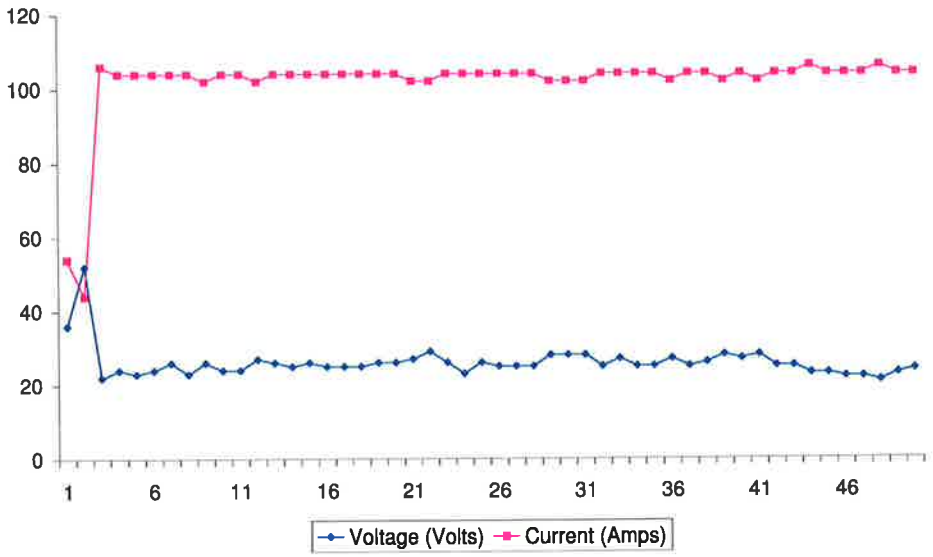


(a) Data measured from the welding monitor.

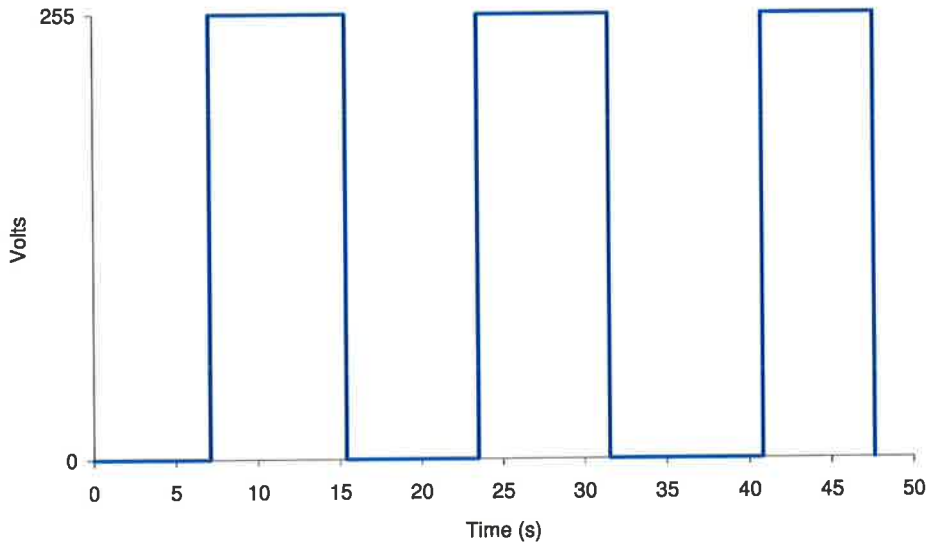


(b) Square waveform which was used to measure time between predetermined intervals.

**Figure 4.20:** Typical data measured from welding monitor.

- noise - any noise in curves resulted in the cooling rate being discarded - the integrity of the measurement was compromised - an example is given Figure 4.21(a)
- too steep a slope - curves should be reasonably smooth - an example is given in Figure 4.21(b).

An example of a cooling curve considered, smooth and acceptable can be seen in the

purple line in Figure 4.21(b)

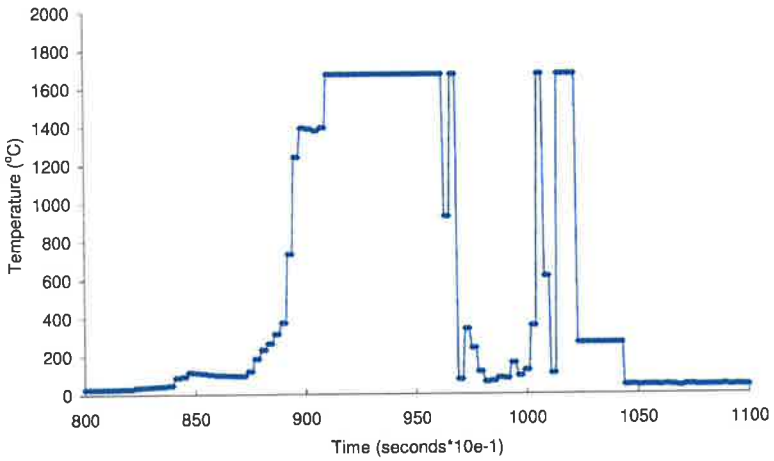


(a) Data exhibiting a significant amount of noise.

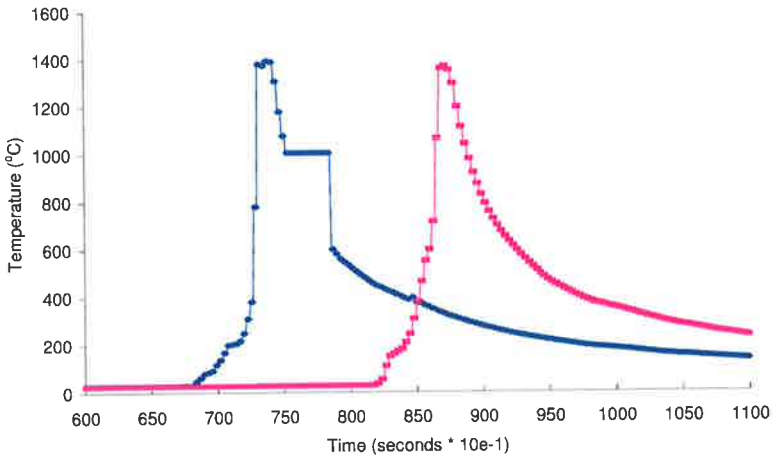


(b) Data exhibiting both unusable and smooth results from harpooning thermocouples into weld pool.

**Figure 4.21:** Example of data recorded using thermocouples and a data acquisition module with a total sampling frequency of $10Hz$.

An example of the variation of welding speed, for a given welding run, can be seen in Figure 4.22. Using a spreadsheet, the locations of each change in waveform was calculated. Next, average speed, for all $25mm$ lengths was calculated. In combination with the recorded values of voltage and current, a calculation of heat input for the duration of a given weld pass was achieved. An example of the variation of heat input for a given weld deposited in the field trials can be seen in Figure 4.23.

The aim of the flow-loop field trials was to validate and test the proposed in-service

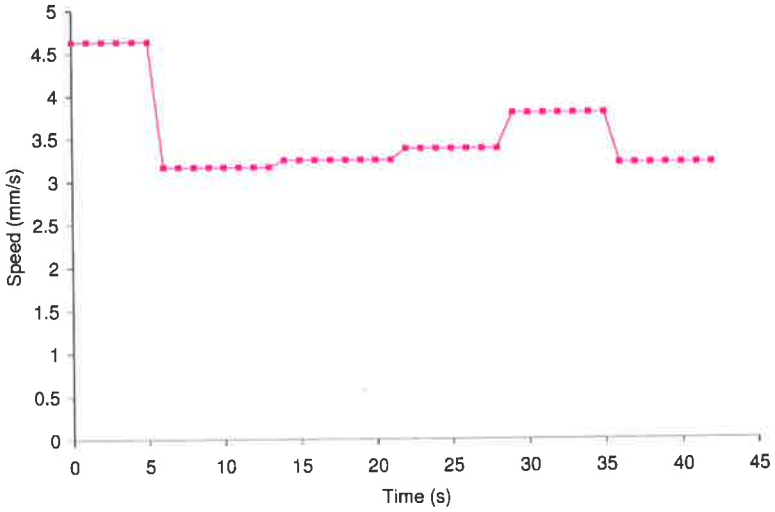


**Figure 4.22:** Example of typical variation of speed for a given weld run.

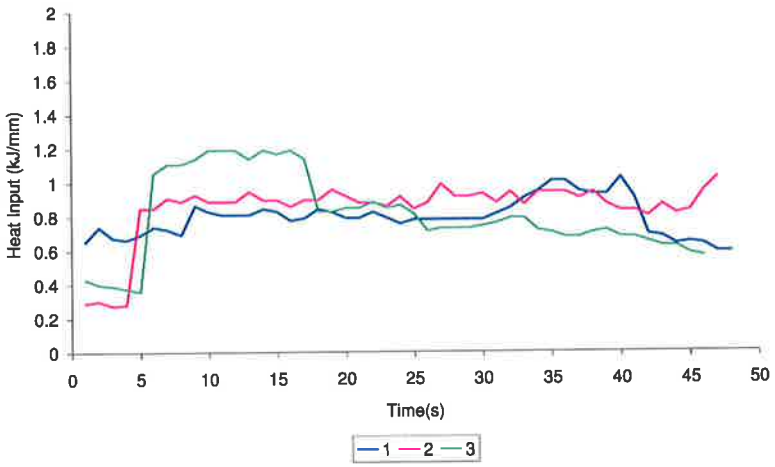


**Figure 4.23:** Typical variation of heat input during a weld pass recorded during the field experiments.

welding circumferential fillet welding model. As mentioned earlier in Section 4.3.1, a total of 45 test welds were deposited on a pipe attached to a flow-loop test facility. While all 45 test welds were deposited with intentions to allow comparison with the proposed circumferential fillet welding thermal models, a number of test welds fell outside of the range in which the proposed model was developed. It is suggested that the broad variability found within the 45 samples was largely due to welding being deposited manually. To aid the analysis of the results from the field experiments, each weld was examined using a number of tests to determine if it was a result of acceptable in-service welding practice. The following paragraphs provide justification for the exclusion of various test

welds; in addition to defining some of the limits of the proposed thermal circumferential fillet welding model.

The range of heat input in which the proposed circumferential fillet welding model can provide accurate predictions for is limited due to the use of the empirically derived weld bead area model. The development of a weld bead geometry model for use with the thermal models is discussed later in Section 4.4. As the weld bead area model was only developed from data spanning a limited range of heat input, the accuracy in which bead area and shape can be predicted for a given heat input is also limited. As the proposed in-service circumferential fillet welding model was developed for a restricted range of heat input, the accuracy of predicting the fusion zone and HAZ size, shape, and maximum depth for heat inputs outside the range is compromised. The resulting predicted maximum penetration and HAZ depth based on the restricted range of heat input must therefore also be correspondingly in a restricted range. The measured maximum penetration and HAZ depth from the flow-loop field trials was therefore used as a criteria for the selection of samples in which to validate the proposed thermal model. Moreover, the size and shape of the fusion zone and HAZ also allowed samples to be discarded from the validation.

The effect of the varying apportionment of heat from the welding arc to the sleeve and pipe is seen in Figure 4.24. The size of the HAZ and pronounced fusion zone in the sleeve, and the low penetration depth and fusion zone in the pipe, suggests that the greater proportion of total heat was applied to the sleeve, for the two welds displayed in Figure 4.24. This observation is clearly significant and emphasises the variation of heat during a given weld pass and the resulting variation in pipe fusion zone and HAZ. As the proposed circumferential fillet welding model is developed for a restricted range in welding technique, the types of macrographs displayed under Figure 4.24 are outside the range of values predicted by the model. In principle, the proposed in-service welding models can account for any known variation in welding angle or heat input, but clearly can not practically incorporate all random manual variations. The models therefore adopt one welding angle and a constant heat input. Weld samples which displayed excessive

sleeve fusion and HAZ along with relatively minor fusion zone in the pipe were therefore discarded.

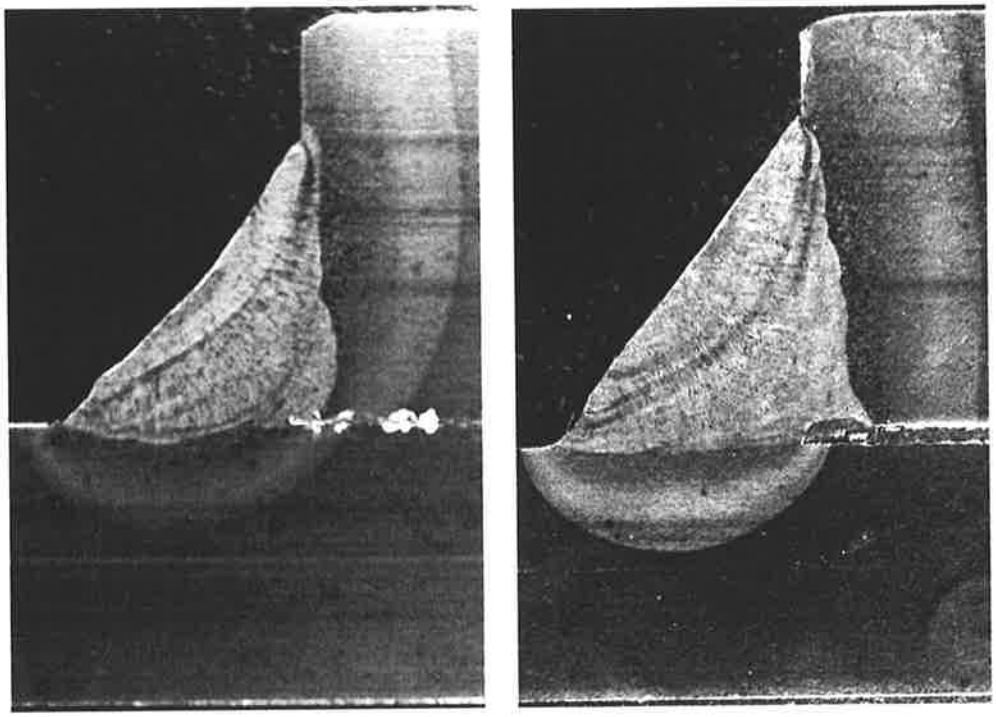

(a) 11 (b) 19

**Figure 4.24:** Excessive sleeve HAZ size for flow-loop field trials: $1kJ/mm$ heat input.

In some welds, the level of penetration was significantly low; the level of penetration was considered to be unrealistic for a real in-service weld. As can be seen in Figure 4.25(a), very little fusion is seen into the main pipe. A number of welds had exhibited penetration depth which are considered to be uncharacteristic; especially considering the heat input with which the weld was deposited. Any welds which exhibited unlikely penetration for a given heat input, was considered suspect and was discarded. For example, consider the welds as can be seen in Figure 4.25. Both macrographs are of welds which were deposited under identical heat input using identical electrode types and diameter. However, clearly the resulting pipe penetration depth and HAZ depth are vastly different. Welds which displayed significantly low pipe penetration depth and small HAZ were therefore discarded.

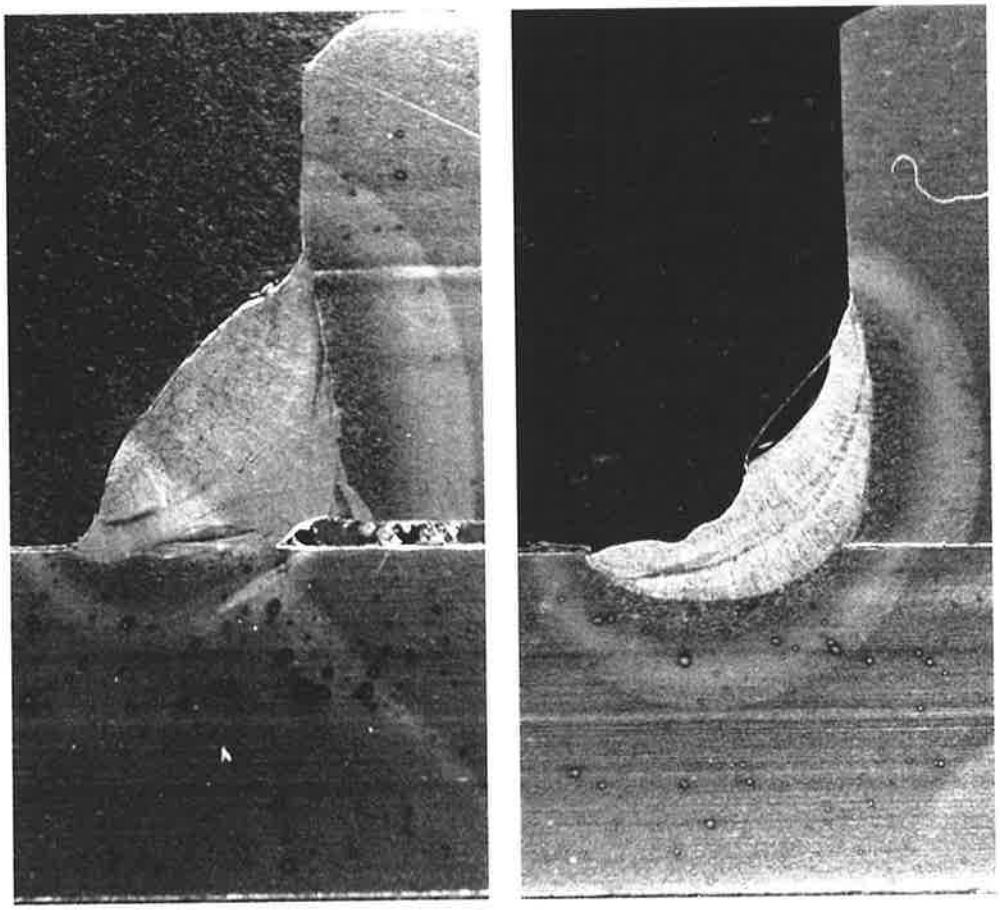

(a) 29 (b) 28

**Figure 4.25:** Variation in penetration for flow-loop field trials: $1kJ/mm$ heat input.

A number of welds were discarded from the validation as the insertion of the thermocouple wire was thought to significantly affect the resulting microstructure of the pipe. When thermocouple wire is inserted into weld pool, the weld pool begins to solidify, or cool down significantly, as heat is required to melt the thermocouple wire. The welder, in reaction, applies further heat to maintain a weld pool. The additional heat influences the HAZ and penetration depth.

The effects of the insertion of thermocouple wire into the weld pool is, as stated earlier, considered to be significant. The additional volume creates an unrealistic weld bead, while the additional heat applied by the welder creates unrealistic fusion zone depth and HAZ depth, and possibly shape. Examples of welds which were considered to be contaminated by the thermocouple wire are seen in Figures 4.26(a) and 4.26(b). The regions of the

weld bead, featuring a distinctively shiny, lighter coloured regions are thought to be due to the thermocouple wire.

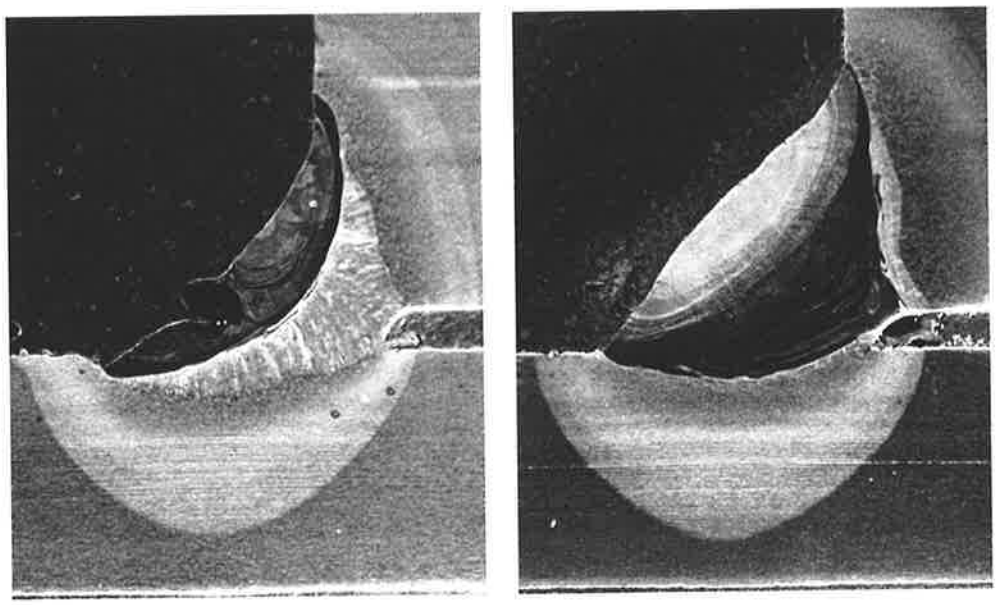

(a) 04 (b) 31

**Figure 4.26:** Examples of welds contaminated by thermocouple wire.

Interestingly, in most cases where the thermocouple bead is thought to have significantly altered the pipe microstructure, the resulting HAZ depth in the pipe was significantly larger, compared with other welds deposited under identical conditions. It is believed, the additional heat applied by the welder in maintaining the molten weld pool, is a strong reason.

The measurement of traverse speed in the field welding trials, as mentioned earlier in Section 4.3.3 has the potential for a significant amount of error. However, determining if the error is in existence for a given weld is difficult. A method for determining the possibility of error in the measurement of speed was developed. The method, a simple yet reasonable idea, involves plotting the variation of travel speed with time for a given weld; for example as seen in Figure 4.27. In all welds, the variation in speed was considered to be minor; if a sudden change were to occur, the particular event was documented. In all 45 welds, such an event did not occur. The possibility of error was based on the variation

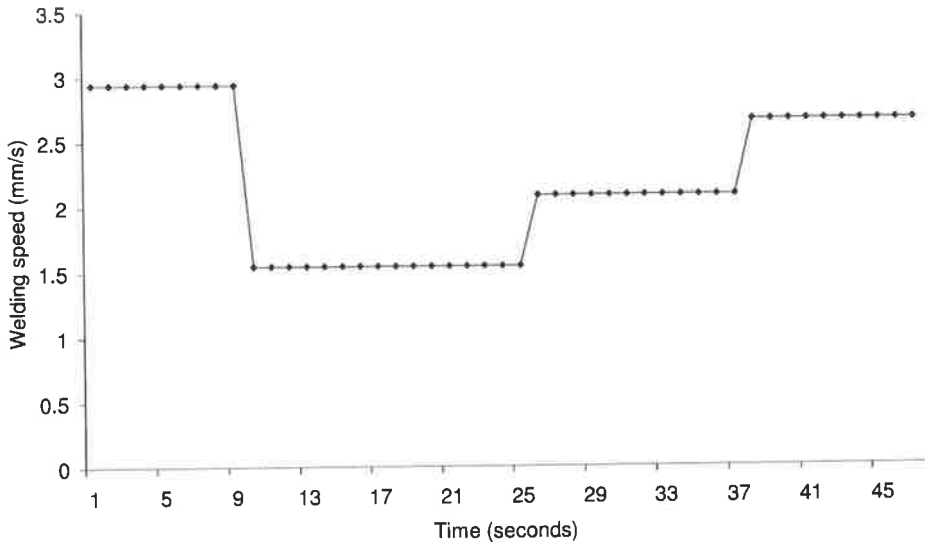


**Figure 4.27:** Typical example of the variation of welding speed for a given weld.

of speed with time for a given weld. If a weld were to vary significantly by over 25%, the weld was considered to have a great risk of having recorded the travel speed incorrectly. Possible inaccuracies include the improper activation of the switch, the misjudgement of the location of the markers by the welder, and any time delays in the activation of the switch; the severity of these events were difficult to determine independently. However, in the few instances where the weld travel speed had varied significantly in a short period of time, the result was thought to be due to either the weld monitor not recording an event or a combination of the aforementioned inaccuracies. Only such a combination of events was thought possible for such large sudden variations in welding speed.

Errors associated with the welding monitor were also used as the basis for discarding some welds from the analysis. As the welding monitor had a limited amount of storage for voltage, current and speed trigger, a few welds were deposited without the knowledge that the welding monitor's memory was full. In these cases, the welding monitor stopped short of recording the voltage, current and speed trigger for the duration of the weld.

Finally, the proposed weld bead geometry model as discussed later in Section 4.4, was developed and validated for $2.5mm$ diameter low hydrogen vertical-up and vertical-down electrodes. A number of welds deposited during the flow-loop field trials used $3.2mm$ diameter electrodes. The reason for which was to gain some understanding on the

penetration characteristics of larger diameter electrodes. However, the majority of the experiment was conducted using 2.5$mm$ diameter electrodes; all samples using 3.2$mm$ diameter electrodes (9 in total) were discarded from the set used for validation.

## 4.3.5 Data analysis

### 4.3.5.1 Variability of heat input

The microstructure of a given in-service weld, as stated earlier in Section 1.3 is significantly dependent on the heat input of the welding process. Moreover, as in-service welding is a manual process, concern is placed on the potential variation of heat input for a given weld. The two main concerns relating to heat input for in-service welding are:

- variation of heat input for a given weld
- variation of heat input around the circumference of the joint

Laboratory simulation, as stated earlier in Section 4.2.3 had identified the variation of welding heat input during the length of a weld. In addition, considerable variation was also noted around the circumference of the pipe.

The variation of welding heat input for all welds deposited during the field trials is shown in Figure 4.28. For each weld, the maximum, minimum and average heat input is plotted. The variation in heat input for a given weld, in some cases is considerable. The variation of heat input, for a given wall thickness, can also be seen in Figure 4.28, however, the variation is more easily visible in Figure 4.29. The variation of heat input between welds for a given wall thickness is greatest for 6.4$mm$ wall thickness pipe.

The variation of heat input around the circumference of the pipe can be seen in Figure 4.29(a), Figure 4.29(b) and Figure 4.29(c). In most cases, as recorded in the field trials, a total of three welds is required to complete a circumferential fillet root pass weld; from top dead centre to bottom dead centre. The sequence of welding can be obtained from

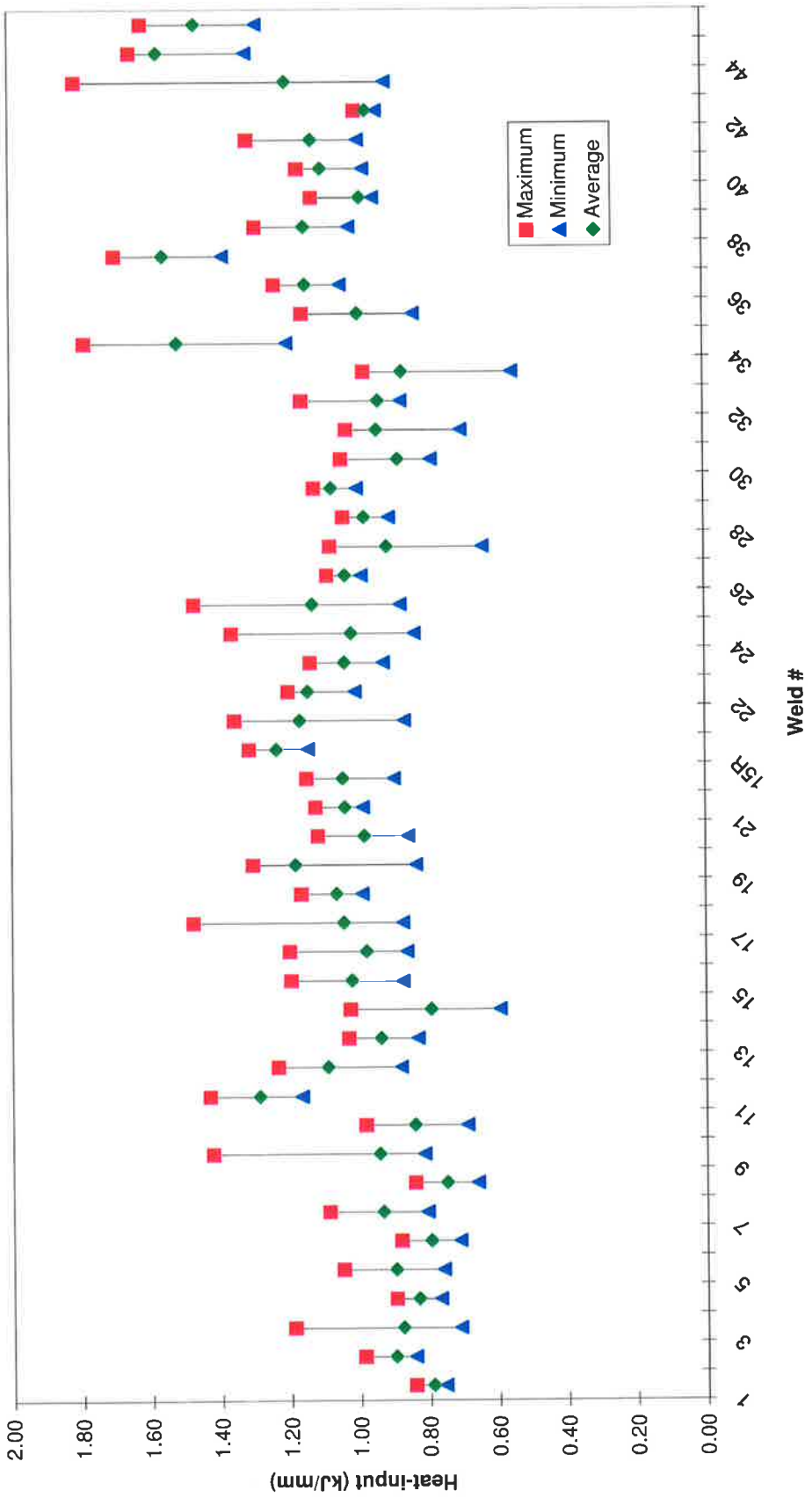


**Figure 4.28:** Variation of heat input for flow-loop field tests.

Table 4.5 for welds deposited on 4.8$mm$ wall thickness pipe, Table 4.6 for welds deposited on 5.8$mm$ wall thickness pipe, and finally, Table 4.7 for welds deposited on 6.4$mm$ wall thickness pipe. A significant variation of heat input around the circumference of the

| | | | | |
|---|---|---|---|---|
| Top dead centre | 4 | 14 | 31 | 14R |
| | 5 | 15 | 32 | 15R |
| Bottom dead centre | 6 | 16 | 33 | 16R |
| | | 17 | | |

**Table 4.5:** 4.8$mm$ wall thickness pipe - weld order.

| | | | | | |
|---|---|---|---|---|---|
| Top dead centre | 7 | 18 | 25 | 34 | 40 |
| | 8 | 19 | 26 | 35 | 41 |
| Bottom dead centre | 9 | 20 | 27 | 36 | 42 |
| | | 21 | | | |

**Table 4.6:** 5.6$mm$ wall thickness pipe - weld order.

| | | | | | | |
|---|---|---|---|---|---|---|
| Top dead centre | 1 | 10 | 22 | 28 | 37 | 43 |
| | 2 | 11 | 23 | 29 | 38 | 44 |
| Bottom dead centre | 3 | 12 | 24 | 30 | 39 | 44 |
| | | 13 | | | | |

**Table 4.7:** 6.4$mm$ wall thickness pipe - weld order.

pipe is noted for many welds, and this is the dominant feature which probably swamps any variation with welding position. The most notable trends are that heat input was found to increase from the 12 o'clock position to the 3 o'clock position for the majority of welds deposited on 4.8$mm$ wall thickness pipe. Furthermore, heat input was measured and found to decrease from the 3 o'clock position to the 6 o'clock position for the majority of welds deposited on 6.4$mm$ wall thickness pipe. Based on the results relating to the variation of heat input, the concern for controlling heat input for in-service welding is clearly obvious. A conservative estimate of the range of variation is $\pm 15\%$ of the nominal value; however there are examples where the heat input varied by 1.5 times the nominal value.

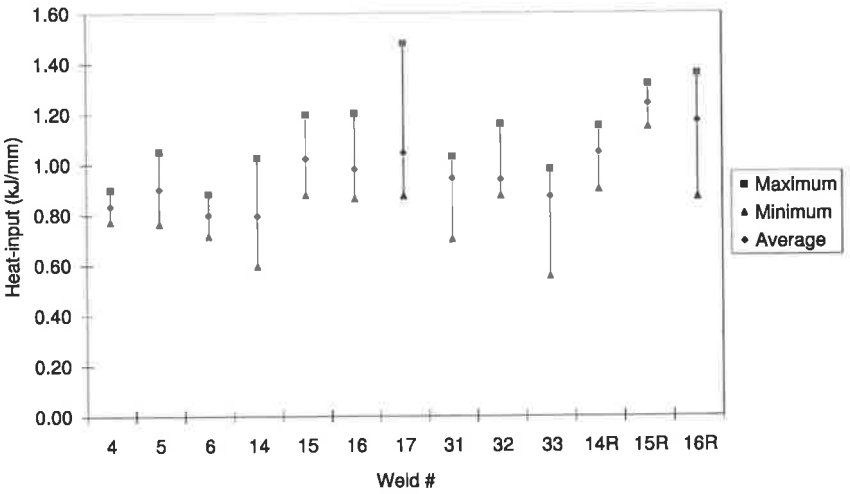


(a) 4.8$mm$.

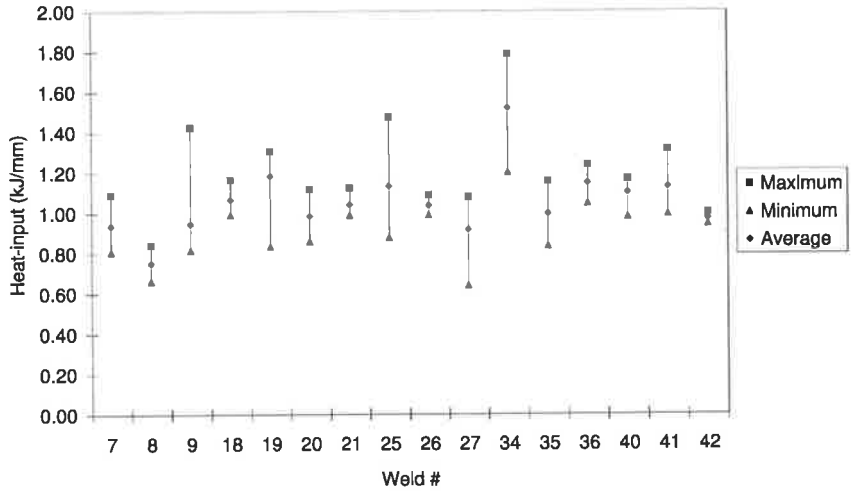


(b) 5.6$mm$.

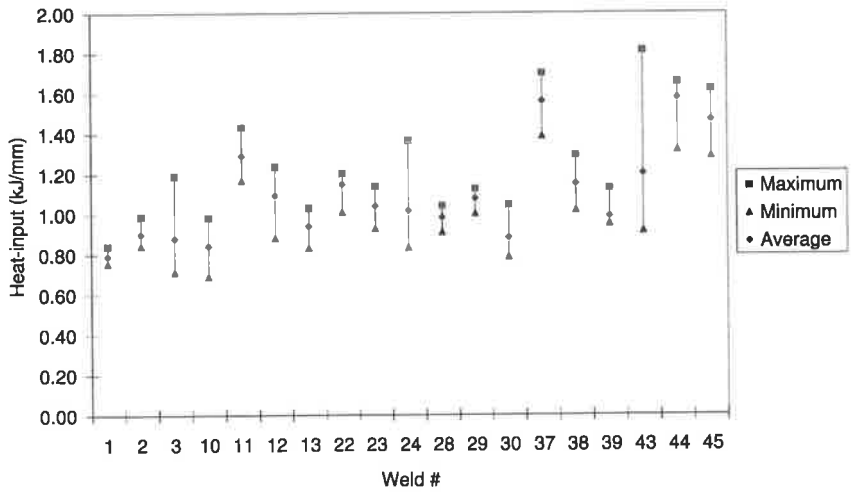


(c) 6.4$mm$.

**Figure 4.29:** Variation of heat input for welds deposited on 4.8$mm$, 5.6$mm$ and 6.4$mm$ pipe during field trials.

#### 4.3.5.2 Maximum penetration depth variation with heat input

The variation of penetration depth with heat input for all welds deposited in the field trials can be seen in Figure 4.30; the results of welds deposited on $4.8mm$ wall thickness pipe can be seen in Figure 4.30(a), welds deposited on $5.6mm$ wall thickness pipe in Figure 4.30(b), and $6.4mm$ wall thickness pipe in Figure 4.30(c). Clearly, in all welds deposited on either $4.8mm$, $5.6mm$ or $6.4mm$ wall thickness pipe, variability is high and no systematic relationship between heat input and penetration can be observed. The severe variation of maximum penetration depth is suggested to be largely due to the welding technique employed. The measurement of heat input is not without error and is also suggested to have a minor influence on the results. The variation of maximum penetration depth for welds deposited under near identical heat input is alarming: in the case of welds deposited with a heat input of $0.8kJ/mm$ on $4.8mm$ wall thickness pipe, the resulting penetration depth varied from $0.5mm$ to $0.9mm$. For welds deposited on $5.6mm$ wall thickness pipe with a heat input of $0.85kJ/mm$, the resulting penetration depth varied from $0.5mm$ to $1.3mm$. Finally, welds deposited on $6.4mm$ wall thickness pipe with a heat input of $0.9kJ/mm$ resulted in penetration depth varying from $0.1mm$ to $1.0mm$. Clearly, such variation has significant bearing on avoiding burnthrough. Such variation can have disastrous effects when welding on pipes of wall thickness $4.8mm$ or less.

Selecting the data points which represent welds that were considered to be a result of an acceptable in-service weld, as discussed previously in Section 4.3.4, from the full set displayed earlier in Figure 4.30, the variation of maximum penetration depth with heat input for these selected data points can be seen in Figure 4.31. While welds were deposited under a similar range of heat input, flow conditions and electrodes type for the three different pipes, the effect of wall thickness on maximum penetration depth is not obvious. It is suggested that any effect which wall thickness may have had on the weld HAZ and fusion zone was largely overridden by the variation of heat input during a given weld pass. However, for a very similar range of heat input, the mean penetration depth

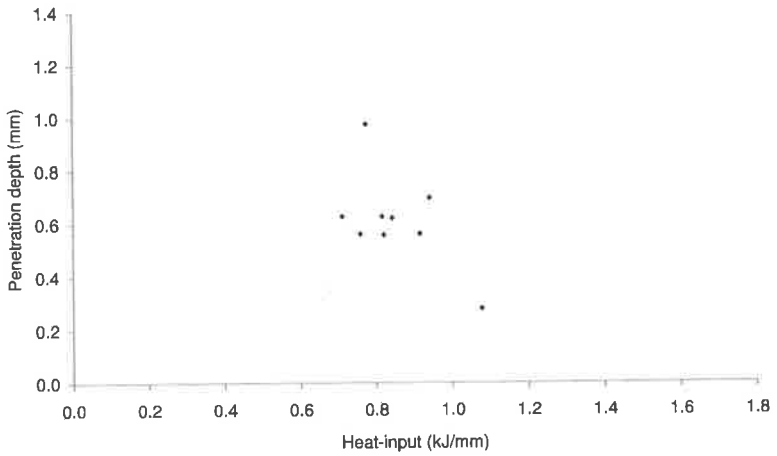


(a) $4.8mm$.

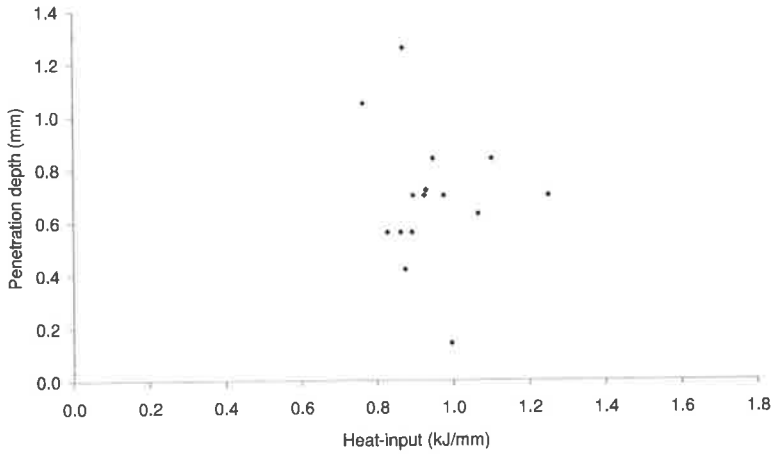


(b) $5.6mm$.

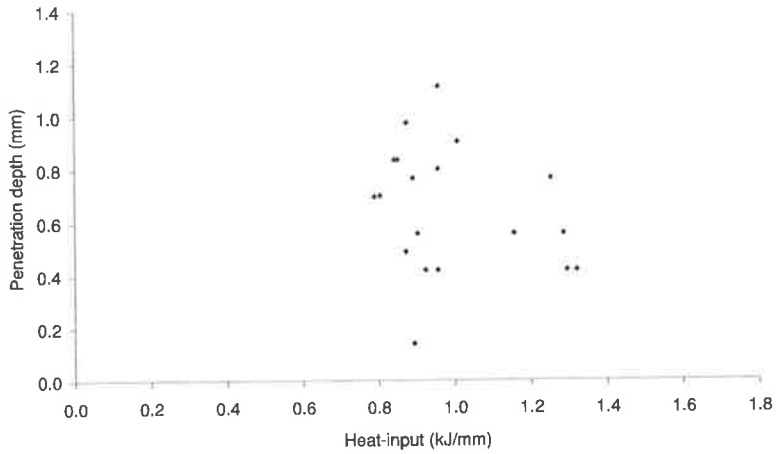


(c) $6.4mm$.

**Figure 4.30:** Maximum penetration depth variation with heat input for different wall thickness pipe.

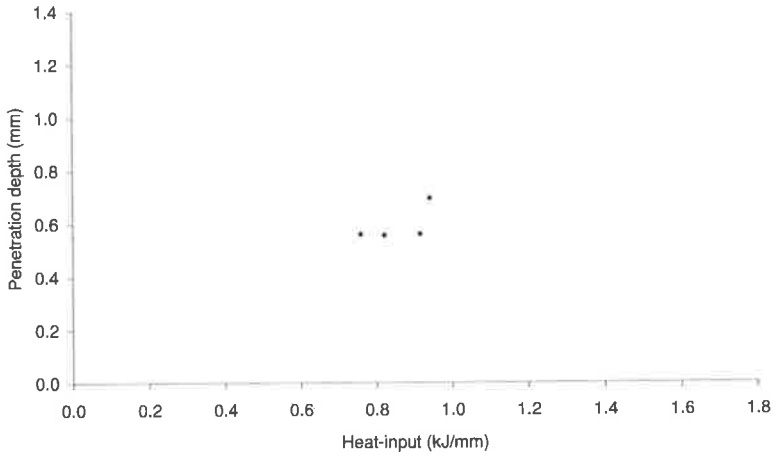


(a) 4.8$mm$.

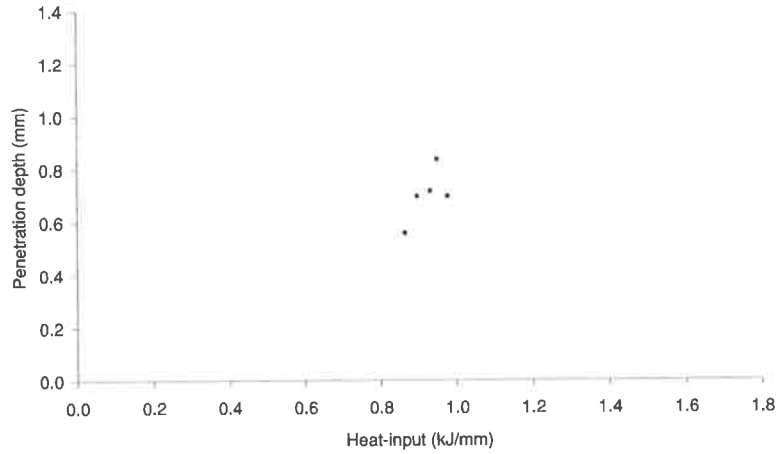


(b) 5.6$mm$.

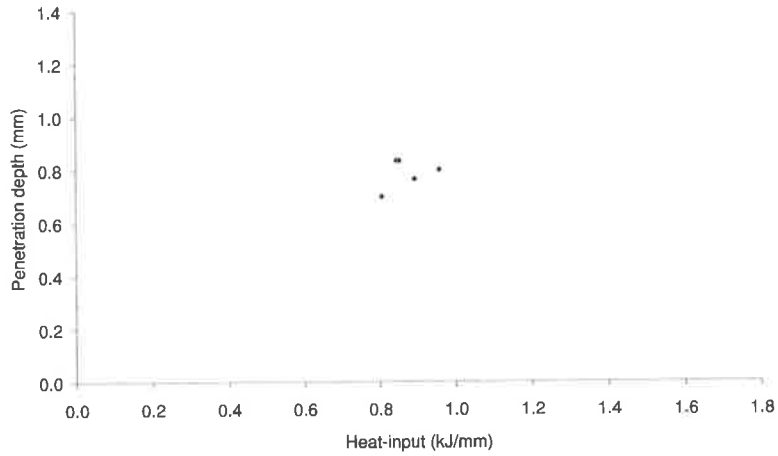


(c) 6.4$mm$.

**Figure 4.31:** Maximum penetration depth variation with heat input for different wall thickness pipe.

was found to increase with wall thickness : $0.59 \pm 0.06mm$ for $4.8mm$ wall thickness pipe, $0.70 \pm 0.07mm$ for $5.6mm$ and finally, $0.79 \pm 0.04mm$ for welds deposited on $6.4mm$ wall thickness pipe.

#### 4.3.5.3 Maximum HAZ depth variation with heat input

The variation of maximum HAZ depth with heat input for all welds deposited in the field experiments can be seen in Figure 4.32; the results of welds deposited on $4.8mm$ wall thickness pipe can be seen in Figure 4.32(a), welds deposited on $5.6mm$ wall thickness pipe in Figure 4.32(b), and $6.4mm$ wall thickness pipe in Figure 4.32(c). The results for all wall thicknesses display a fair degree of scatter, however some trends are evident. The increase in HAZ depth with increasing heat input is greatest with $4.8mm$, then $5.6mm$ and finally $6.4mm$ wall thickness pipe. The total proportion of heat transfer due to diffusion and convection can be considered to be a significant reason for the observations. As pipe wall thickness is increased for a given welding heat input, a greater proportion of heat is removed by diffusion rather than by convection due to the flowing pressurised natural gas. As a result, the size of the HAZ is decreased for thicker wall thickness in-service welding; as the heat transfer for diffusion is far greater than heat transfer by convection. As wall thickness is decreased, the relative proportion of heat transfer by convection is rising; and therefore the reduced heat transfer by diffusion produced a larger HAZ.

Selecting the data points which represent welds that were considered to be a result of an acceptable in-service weld, as discussed previously in Section 4.3.4, from the full set displayed earlier in Figure 4.32, the variation of maximum HAZ depth with heat input for these selected data points can be seen in Figure 4.33. Minor variation of HAZ depth with heat input was observed for welds deposited on $6.4mm$ wall thickness pipe. In addition, results from welds deposited on $5.6mm$ wall thickness display a considerable amount of scatter. Interestingly, the depth of the HAZ was found to be on average (for a similar range of heat input), increasing with welds deposited on decreasing wall thickness pipe: $2.85 \pm 0.13mm$ for $4.8mm$ wall thickness pipe, $2.85 \pm 0.22mm$ for $5.6mm$ and finally,

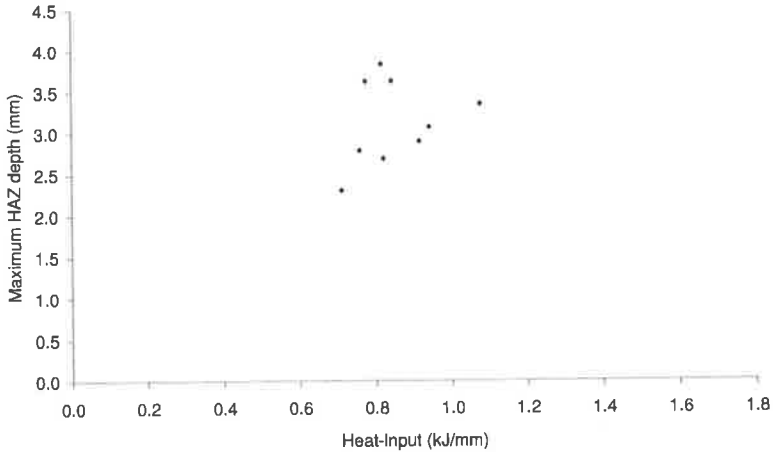


(a) 4.8$mm$

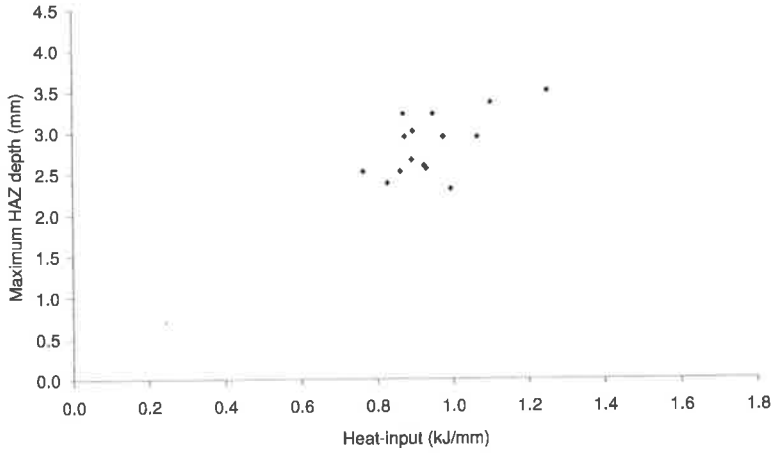


(b) 5.6$mm$

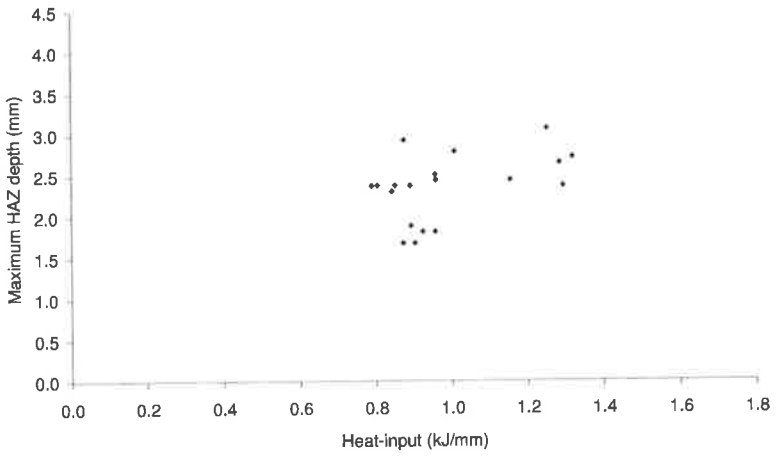


(c) 6.4$mm$

**Figure 4.32:** Maximum HAZ depth variation with heat input for different wall thickness pipe.

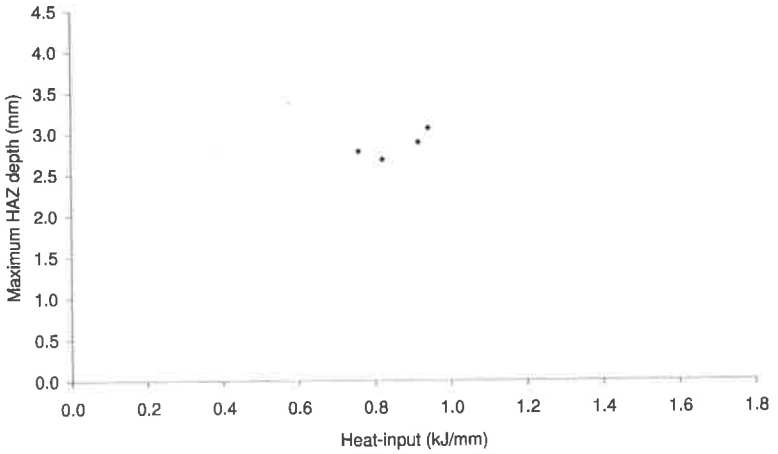


(a) 4.8$mm$.

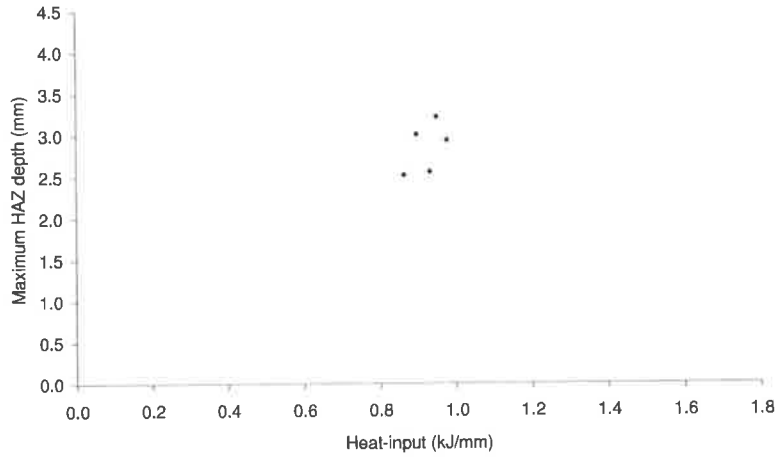


(b) 5.6$mm$.

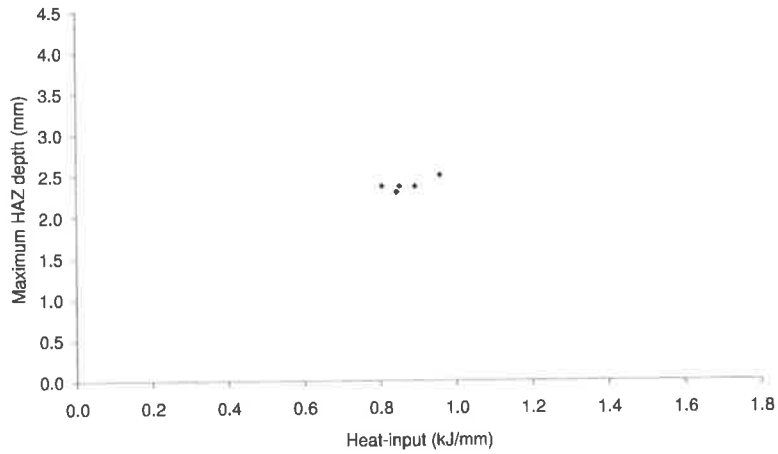


(c) 6.4$mm$.

**Figure 4.33:** Maximum HAZ depth variation with heat input for different wall thickness pipe.

$2.38 \pm 0.05mm$ for welds deposited on $6.4mm$ wall thickness pipe. This trend appears to be in contrast to the trend observed for the variation of penetration depth with heat input as discussed earlier in an Section 4.3.5.2. The observed trend appears to agree with the earlier argument that as wall thickness is decreased, the relative proportion of heat transfer by conduction is decreased due to the reduced mass. Moreover, the contrast to the observed trend with penetration depth suggests that the HAZ depth is not as sensitive to significant fluctuations in heat input during a given weld.

#### 4.3.5.4 Weld cooling time variation with heat input

The variation of $t_{8/5}$ cooling time with heat input for all welds deposited in the field trial experiments can be seen in Figure 4.34; the results of welds deposited on $4.8mm$ wall thickness pipe can be seen in Figure 4.34(a), welds deposited on $5.6mm$ wall thickness pipe in Figure 4.34(b), and $6.4mm$ wall thickness pipe in Figure 4.34(c). The level of scatter found in the comparison of $t_{8/5}$ with heat input is surprisingly moderate considering the variability of the measuring process. However, the inherent problems associated with employing the harpooning technique is evident; for example, the difference in measured $t_{8/5}$ for a given weld pass can be observed by examining the purple and blue points in Figure 4.34. As discussed earlier in Section 4.3.3, for each weld pass, two measurements of weld cooling rate were attempted. The blue data points reflect the $t_{8/5}$ time measurement by the first thermocouple while the second measurement is found by the pink data point. If both thermocouples were successful, the two readings can be seen vertically aligned on the charts for an identical heat input. Moreover, if for a given weld, the measurement of weld cooling rate was successful for both attempts, the variation of $t_{8/5}$ during a given weld pass may also be observed; the difference in cooling rate between the two data points will exhibit the variation.

The variation in weld cooling rate is possible due to the varying location of thermocouple placement. As stated by Oddy [62], a minor change in the location of the thermocouple can significantly change the measured values. In addition, the variability

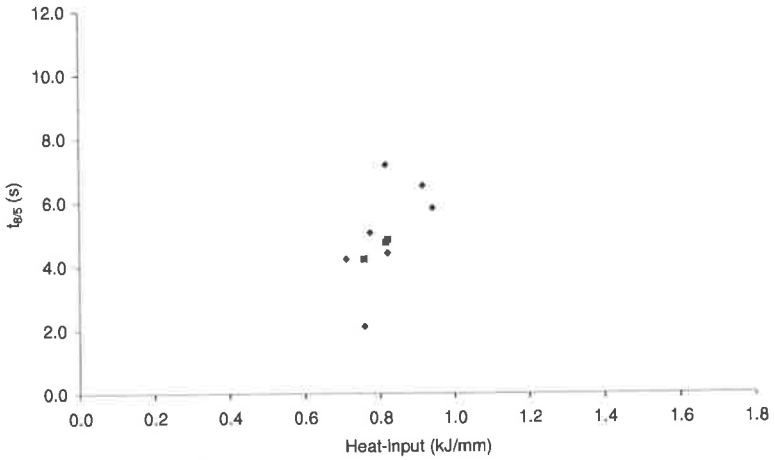


(a) $4.8mm$.

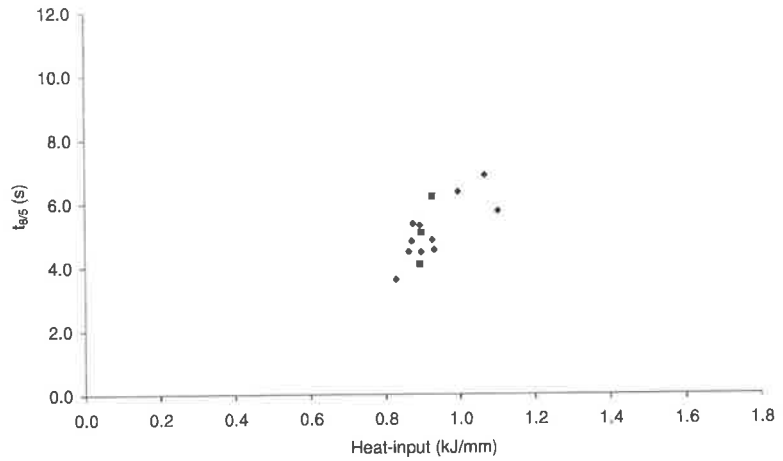


(b) $5.6mm$.

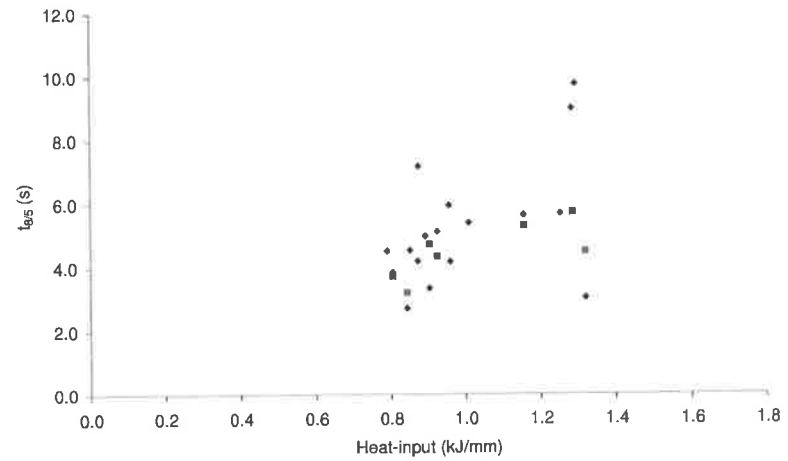


(c) $6.4mm$.

**Figure 4.34:** Weld cooling time variation with heat input for different wall thickness pipe.

of the manual welding technique can further exacerbate the observed variation. As heat input was found to vary with position and welding technique during both laboratory and field experiments, the variation of weld cooling rate is also highly likely. Broadly, the increase in $t_{8/5}$ with welding heat input is greatest with $4.8mm$ wall thickness pipe, followed by $5.6mm$ and finally $6.4mm$ wall thickness pipe. However, the scatter found particularly in the values obtained during welding onto $6.4mm$ wall thickness pipe does not allow for accurate conclusions. It is likely that the decreasing cooling rate, or increasing $t_{8/5}$ with increasing heat input is greatest with the thinner pipe as less heat is being transfered by diffusion as compared to the thickness pipe, therefore producing a larger HAZ.

Selecting the data points which represent welds that were considered to be a result of an acceptable in-service weld, as discussed previously in Section 4.3.4, from the full set displayed earlier in Figure 4.34, the variation of $t_{8/5}$ weld cooling time with heat input for these selected data points can be seen in Figure 4.35. A moderate amount of scatter can still be observed in the results from the field experiments. Moreover, a limited amount of samples make defining a trend almost impossible.

The largest variation of $t_{8/5}$ for welds deposited under a similar range of heat input was observed for those deposited on $4.8mm$ wall thickness pipe; welds deposited on $6.4mm$ had slightly lower while those deposited on $5.6mm$ had the lowest. The lowest average $t_{8/5}$ was measured for welds deposited on $6.4mm$ wall thickness pipe, $3.59 \pm 0.51s$, with welds deposited on $5.6mm$ having the next highest average, $4.63 \pm 0.25s$, and finally welds deposited on $4.8mm$ having the highest average, $4.63 \pm 1.02s$. This trend appears to follow the argument that decreased wall thickness causes reduced weld cooling rates for welds deposited for a similar range of heat input.

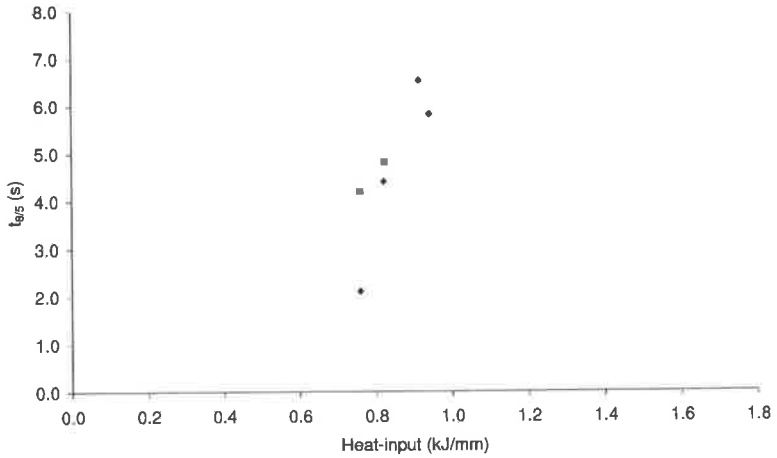


(a) $4.8mm$.

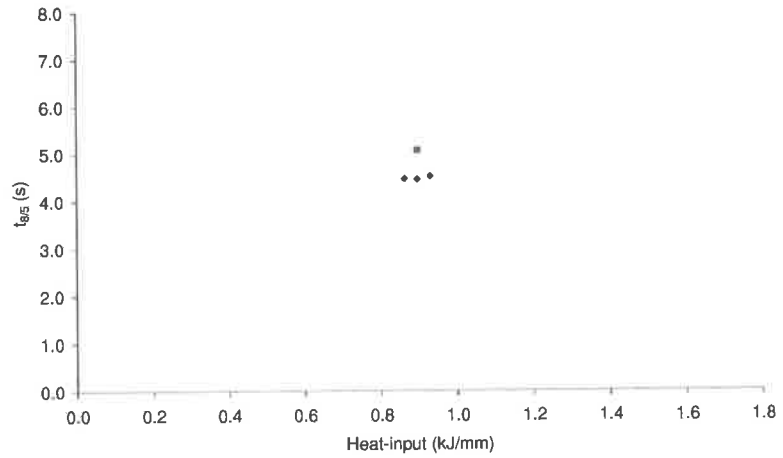


(b) $5.6mm$.

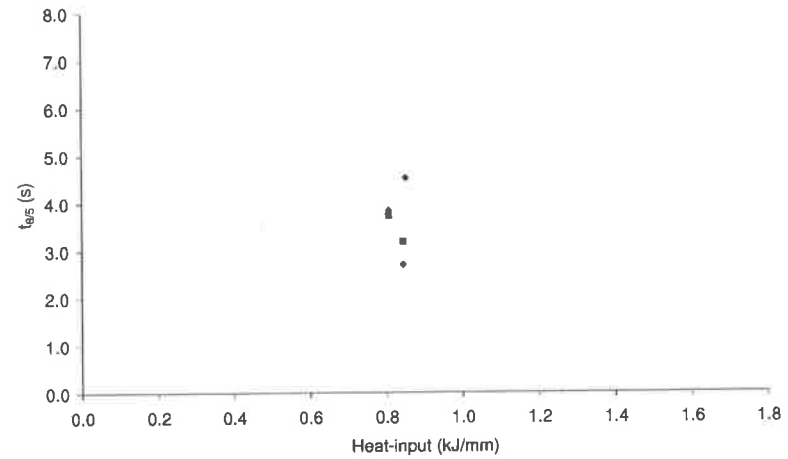


(c) $6.4mm$.

**Figure 4.35:** Weld cooling time variation with heat input for different wall thickness pipe.

### 4.3.6 Variation of HAZ and penetration depth with position

#### 4.3.6.1 Maximum HAZ depth variation with position

The variation of HAZ depth with position around the circumference can be seen in Figure 4.36; the variation of HAZ depth on 4.8$mm$ wall thickness pipe in Figure 4.36(a), 5.6$mm$ wall thickness pipe in Figure 4.36(b), and the variation on 6.4$mm$ wall thickness pipe in Figure 4.36(c). Due to the diameter of the pipeline which was used for the in-service welding experiments, often, 3 to 4 welds were required to complete a weld from top dead centre to bottom dead centre. The sequence and position of each weld is tabulated in Table 4.5 for welds deposited on 4.8$mm$ wall thickness pipe, Table 4.6 for 5.6$mm$ and finally Table 4.7 for welds deposited on 6.4$mm$ wall thickness pipe. The variation of HAZ depth with position may be observed by examining, for example, welds 18-21. The variation of HAZ with position is clearly difficult to analyse. For welds deposited on 4.8$mm$ wall thickness pipe, no clear trend is evident; clearly, the limited number of test welds deposited on 4.8$mm$ wall thickness pipe attribute greatly to this. The trend of HAZ depth with position for welds deposited on 5.6$mm$ wall thickness pipe is again difficult to analyse. In some cases, the variation of HAZ depth with position is insignificant, while for others, a sudden large variation is observed. In two welds runs, the HAZ depth is significantly reduced at the 3 o'clock position. The trend observed for welds deposited on 6.4$mm$ wall thickness pipe is more evident. There is a trend for the majority of the samples to have reducing HAZ depth with position. However, the variation in the remainder of the samples is minor.

#### 4.3.6.2 Penetration depth variation with position

The variation of penetration depth with position around the circumference can be seen in Figure 4.37; the variation of penetration depth on 4.8$mm$ wall thickness pipe in Figure 4.37(a), 5.6$mm$ wall thickness pipe in Figure 4.37(b), and the variation on 6.4$mm$ wall thickness pipe in Figure 4.37(c). The level of scatter found when comparing measured

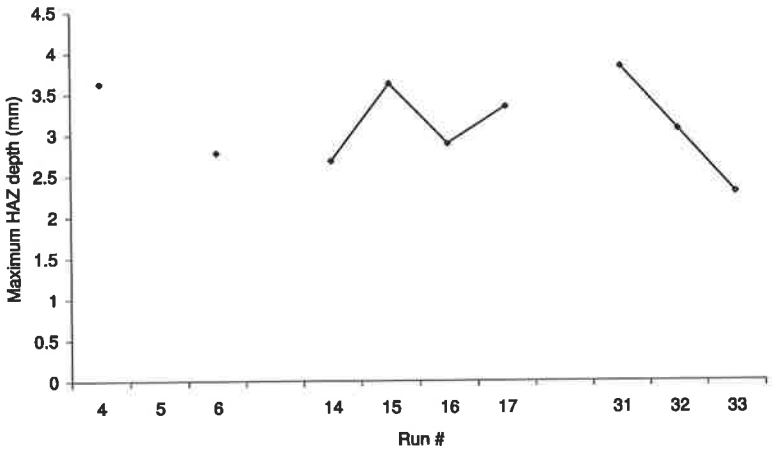


(a) 4.8$mm$.

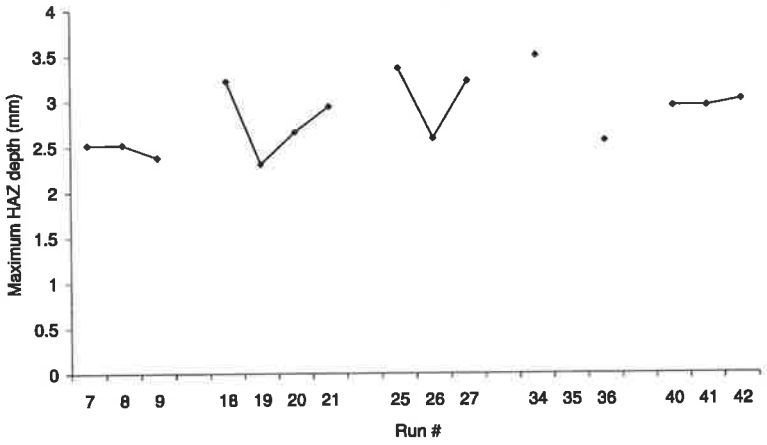


(b) 5.6$mm$.

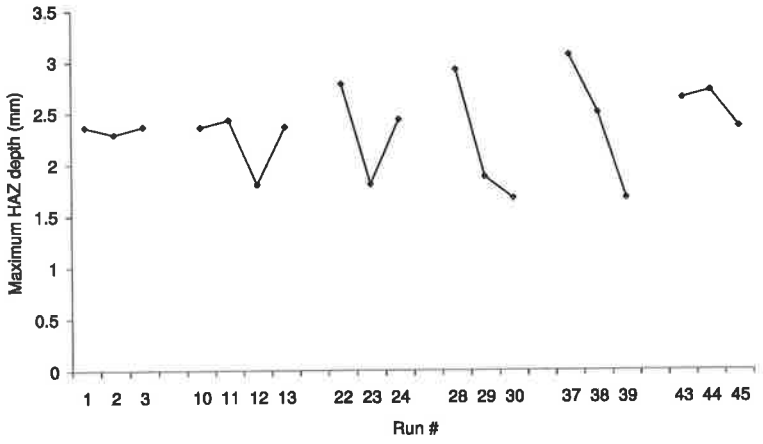


(c) 6.4$mm$.

**Figure 4.36:** Maximum HAZ depth variation with welding position for different wall thickness pipe.

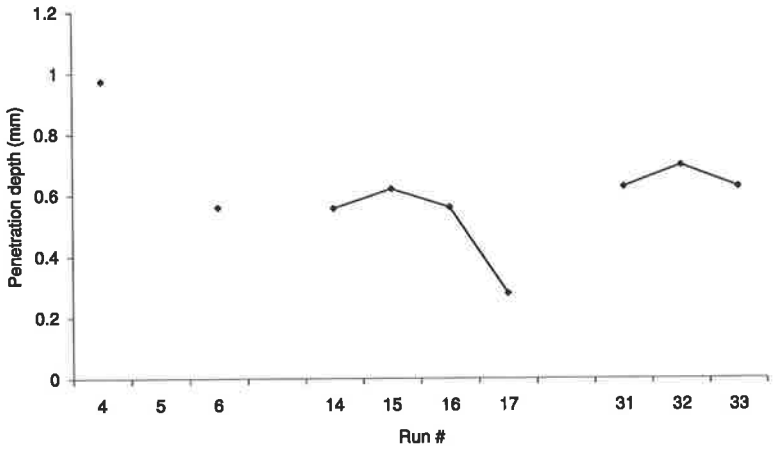


(a) 4.8$mm$.

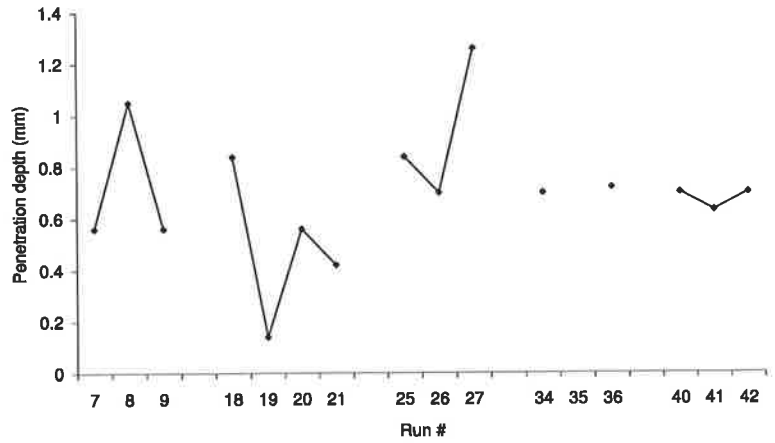


(b) 5.6$mm$.

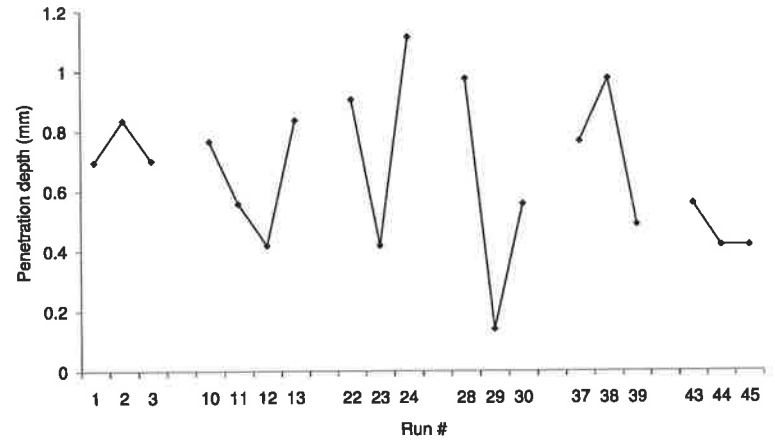


(c) 6.4$mm$.

**Figure 4.37:** Maximum penetration depth variation with welding position for different wall thickness pipe.

penetration depth with measured heat input is of similar magnitude with the previous comparison of HAZ depth with welding position. It is suggested that the variability of the manual process is further exacerbated by out-of-position welding. The most notable trend was found for welds deposited on $6.4mm$ wall thickness pipe; in the majority of completed weld passes, a reduction in penetration depth at the 3 o'clock position was measured. As discussed earlier, in Section 4.3.5.2, while the variation can have a significant impact on the likelihood of burnthrough when welding on a $4.8mm$ or less wall thickness pipe, the variation of penetration was observed to be reducing as wall thickness was decreased.

#### 4.3.6.3 Variation of HAZ and penetration depth for a given weld pass

The variation or HAZ and penetration depth for a given weld pass was observed by viewing longitudinal macrographs; a few samples of which can be seen in Figure 4.38. The macrographs illustrated in Figure 4.38 are for welds deposited on $4.8mm$ wall thickness pipe with a heat input of $1.0kJ/mm$; the welds were deposited from right to left for those illustrated. The variation of HAZ and penetration depth for a complete weld pass may be observed by Figures 4.38(b) 4.38(c): Figure 4.38(b) illustrates the weld from near top-dead-centre to approximately halfway, while Figure 4.38(c) displays the bottom portion of the same weld pass. Clearly, the variation of HAZ depth and penetration depth is significant. Measurement of the maximum and minimum penetration and HAZ depth revealed that the penetration depth can vary by $\pm 0.23mm$ while the HAZ depth can vary by $\pm 0.46mm$ for a given weld. The variation was determined by the average of three welds deposited on $4.8mm$ wall thickness pipe under similar weld positions for identical target heat input. The variation of penetration and HAZ depth is considered to be significant as the weld was considered to be deposited under a tight tolerance of heat input. The variation of the manual process is clearly obvious.

(a) 32T.

(b) 33T.

(c) 33B.

**Figure 4.38:** Variation of HAZ and penetration depth with position during single weld pass.

### 4.3.7 Conclusions

The analysis of circumferential fillet welding on a flow-loop under a variety of flow rates and operating pressures using low hydrogen E8018G vertical down electrodes gave the following results:

1. The apportionment of heat from the arc to the weldment was observed and the effects of which were found to be highly indicative of the resulting weld microstructure. Moreover, the variability of the manual welding technique and its effect on

weld microstructure was observed. Clearly, the variability of pipe penetration depth and HAZ depth during a weld pass is significant. Macrographs of weld cross-sections revealed that penetration into the pipe had varied from a nominal value to virtually nil while the weld was deposited under a given heat input. This variation is considered to be principally due to the variation of the arc and welding technique, while to a lesser degree the position at which welding had occurred.

2. The variation of fusion depth and HAZ depth during a given weld pass was observed and measured by slicing a circumferential fillet weld pass in the radial plane. The variation of penetration depth for a weld deposited on a $4.8mm$ wall thickness pipe with a heat input of $1.0kJ/mm$ was estimated at $\pm 0.23mm$ from a nominal value; the corresponding variation of HAZ depth was estimated at $\pm 0.46mm$. This variation is again considered to be due to the welding technique and the motion of the electrode and arc rather that the position at which welding had occurred.

3. The variation of heat input for a given weld pass was estimated at $\pm 15\%$ of the nominal value. However, there are examples where the heat input varied by 1.5 times the nominal value.

4. The study of the variation of penetration depth and HAZ depth due to welding position had difficulty with establishing trends from the results. However for welds deposited on $6.4mm$ wall thickness pipe, the trend was for HAZ depth to be decreasing with position, and a reduction in penetration depth after the 3 o'clock position.

5. An immediately clear trend for the variation of heat input with position was not found. However, the reduction on heat input for welds deposited on $6.4mm$ wall thickness pipe, and the increase in heat input for welds deposited on $4.8mm$ wall thickness pipe was found. A further study involving using smaller increments to measure welding speed may provide more accurate results.

The implications of these observations to the thermal modelling of in-service welding is discussed later in Chapter 5.

## 4.4 Weld bead geometry model

### 4.4.1 Introduction

In order to develop a complete in-service welding model, only fundamental parameters should be required as inputs. While the proposed in-service welding thermal models, depend on many parameters, as discussed earlier Section 2.2.1.1, all of the parameters are further dependent on the following basic parameters:

- heat input
- electrode diameter
- pipe flow conditions
- pipe geometry.

Previously, Graville & Read [36], and the Battelle Memorial Institute [20], developed empirical models to calculate bead shape geometry, as a function of heat input, electrode diameter and electrode type. In particular, Graville & Read produced a model to predict the sleeve leg-length for submerged arc welding, while the software developed by Battelle had predicted the deposited area for welds deposited using E7018, E7010 and stainless rod MMA electrodes. However, both research groups did not develop bead shape models for low hydrogen (E8018G) MMA electrodes, which is commonly used for vertical-down and vertical-up in-service circumferential fillet welding.

The following sections will discuss the model developed for calculating weld bead geometry, for in-service vertical-up and vertical-down circumferential fillet welding.

### 4.4.2 Derivation of model

The development of a model, to predict the weld bead geometry for circumferential in-service welding, deposited using low-hydrogen electrodes, was required due to the limited published information. As stated earlier in Section 4.4.1, while previous attempts were made at developing similar models, e.g. Battelle [20], Graville & Read [36]; no information was found for in-service circumferential fillet welding using low-hydrogen electrodes in the available literature. The results attained from the laboratory simulations, as mentioned in Section 4.2, were principally used for the development of the weld bead geometry model suitable for the thermal heat transfer analysis of in-service circumferential fillet welding. Secondly, the results from the field experiments, as discussed in Section 4.3, enabled the validation and improvement of the in-service circumferential fillet welding weld bead geometry model. After comparing the results from the laboratory and field experiments, a number of interesting aspects were also found relating to the subtle difference in the method a welder had chosen for welding onto a live pipeline, compared to welding on a simulated laboratory test. The results of the comparison are given later in Section 4.4.3.

Work by Battelle, as stated in the literature review (Section 2.3.4), led to the development of a 2D finite difference based software package aimed at predicting peak inner surface temperature and weld cooling rate. For the thermal models, the bead area was calculated using empirically derived functions; the relationships were established experimentally from sections taken through welds. The bead area was approximated to be a linear function of heat input and electrode type. The equations for calculating weld bead area for the three electrode types are of the form:

$$\text{Deposited area} = A \times X + B \tag{4.2}$$

where $A$ and $B$ are dependent on the type of electrode, as can be seen in Table 4.8, and, $X$, the welding heat input in $kJ/inch$. The shape of the bead was assumed to be triangular; the relationship between pipe leg-length and sleeve leg-length being made by

| Electrode type | A | B |
|---|---|---|
| E7018 | 0.0008754 | -0.003556 |
| E7010 | 0.0008283 | 0.001109 |
| Stainless | 0.0008495 | -0.00165 |

**Table 4.8:** Coefficients for weld bead area model for various electrodes proposed by Battelle [20].

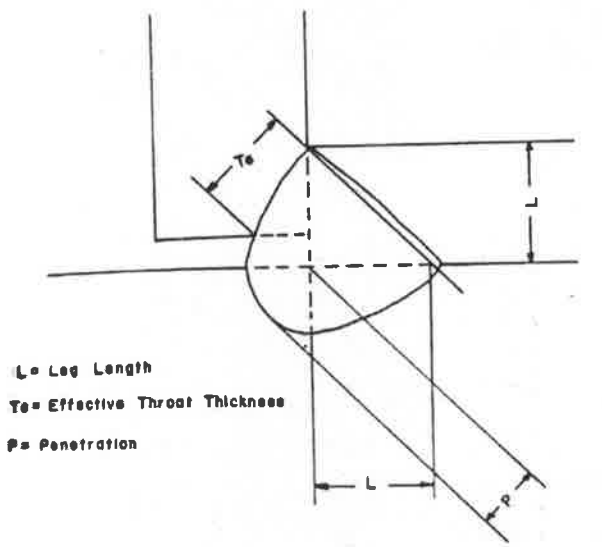


**Figure 4.39:** Dimensions of the various weld dimensions; Graville & Read [36].

bead area and the angle of the electrode between the sleeve and the pipe, or electrode angle.

While one may argue, that the linear relationship chosen by Battelle for their software, may be somewhat simple and possibly unrealistic, previous work by Graville & Read [36] support such a linear relationship. As stated in the literature review (Section 2.2.1), Graville & Read attempted to establish a relationship between the size of a given fillet weld, and the resulting HAZ hardness. Experiments involving depositing MMA welds at various heat input revealed a linear relationship between leg-length and heat input. Additionally, another weld geometry parameter, 'effective throat thickness', was also found to have a linear relationship with leg-length. The effective throat thickness, sleeve leg-length and pipe leg-length for a given weld can be seen in Figure 4.39. While, the work by Graville & Read was undertaken for MMA welding using E7018 electrodes, GMA and submerged

arc welding processes, it is probable that a similar relationship could be established for E8018G MMAW electrodes.

It is unclear if the models proposed by Battelle, and Graville & Read, took into consideration the position at which welding was deposited. The available literature from both authors does not consider or mention comments relating to position; it is assumed that the models were developed under a flat welding position. It is likely that welding position highly influences the welding process and therefore the resulting weld bead geometry. However, the study of the variation of weld bead geometry with position was considered to be out of the scope the present study.

#### 4.4.2.1 Parabolic reinforcement

The development of a weld bead geometry model for MMA welding is clearly difficult. As the welding process is deposited manually, a significant variation in the weld bead profile is highly likely. As a result, the weld bead geometry model developed for circumferential fillet welding is not overly complex; however, it does provide adequate information for accurate thermal field calculation of in-service welding using the finite element method. The work by Battelle, and Graville & Read, suggest to disregard the additional weld bead volume presented due to reinforcement of the weld bead. Both models clearly propose a triangular weld bead geometry.

Initial development of the weld bead geometry model, began with the assumption that the weld bead may be approximated as a triangle with an additional reinforcement region; as can be seen in Figure 4.40. However, the new additional parameter, 'reinforcement length', or in addition the prediction of the reinforcement length for a given weld, was not found in the available open literature. Clearly, as welding is deposited manually, a high degree of variation is likely to exist in the reinforcement length parameter. Based on the macrographs of weld deposited in the laboratory and field experiments, those which were consistent with acceptable in-service weld quality, had a shape nearing that of a parabola. The effect of assuming either a parabolic or triangular weld bead on thermal models was

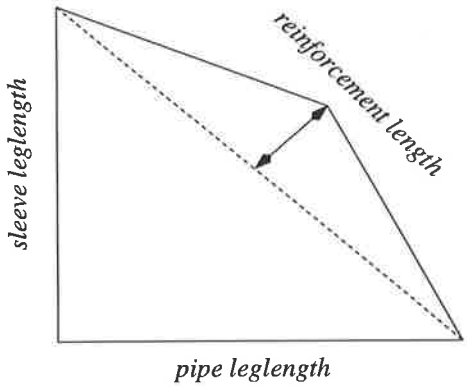


**Figure 4.40:** Initial weld bead geometry model.

examined by comparing the results of two predictions based on the same weld, however differing only in the shape of the reinforcement. The reinforcement length was chosen so that both calculations had identical weld bead area. The results from the comparison can be seen in Table 4.4.2.1. Clearly, the affect of assuming a parabolic reinforcement

| Reinforcement type | Penetration depth | HAZ depth | $t_{8/5}$ |
|---|---|---|---|
| Parabolic | 0.63mm | 3.25mm | 2.21s |
| Triangular with additional reinforcement | 0.66mm | 3.30mm | 2.17s |

**Table 4.9:** Comparison of predictions of a given weld using two different weld bead shapes.

is insignificant to the predictions made using the thermal model developed for in-service welding. The literature review revealed that previous work by Pardo & Weckman [66] (1989) had attempted thermal modelling using weld beads which were assumed to have a parabolic reinforcement. The method developed to calculate the parabolic weld bead profile geometry was loosely based on the equations developed by the authors.

#### 4.4.2.2 Weld bead area

A number of measurements of the weld bead geometry were taken from the laboratory experiments. To perform a numerical simulation of in-service welding, often, the shape of the bead must be known. The data gathered from the laboratory experiments, allows such bead shape information to be included in the numerical analysis. In addition, the

shape of the bead, is often used as a datum point for the heat source.

The dimensions of the weld bead were measured as illustrated in Figure 4.14. In addition, the cross-sectional area of the weld bead was determined by approximating the closed region as an n-sided polygon; the greater the value of n, the better the accuracy of the resulting calculation. The relationship between bead shape geometry and heat input, for both E8018G vertical-down, and E7016 vertical-up electrodes is displayed in Figures 4.41 & 4.42. Basic linear regression relationships were established for weld bead area, and welding angle for both electrodes. The relationships seen in Figures 4.41 & 4.42 are not precise, due to the limited data and evidence of scatter. However, the accuracy is satisfactory for the intended use. The relationships derived for calculating the weld bead area for E7016 and E8018G electrodes can be seen in Equation 4.3 & 4.4.

$$\text{Area} = 16.918 \times \text{Heat Input (E8018G)} \tag{4.3}$$

$$\text{Area} = 13.302 \times \text{Heat Input (E7016)} \tag{4.4}$$

#### 4.4.2.3 Welding angle

The angle of the electrode, between the sleeve and the pipe, significantly alters the apportionment of heat between the sleeve and the pipe. The welding angle was found by the following simple expression:

$$\alpha = tan^{-1}\left(\frac{\text{sleeve leg-length}}{\text{pipe leg-length}}\right) \tag{4.5}$$

where $\alpha$ is the welding angle. Hypothetically, a welding angle of 90 degrees would provide the sleeve with the significantly greater amount of heat, whereas a welding angle of 0 degrees would provide the pipe with the largest amount of heat. The variation of the welding angle for vertical-up and vertical-down welding can be seen in Figure 4.42(a) and Figure 4.42(b) respectively.

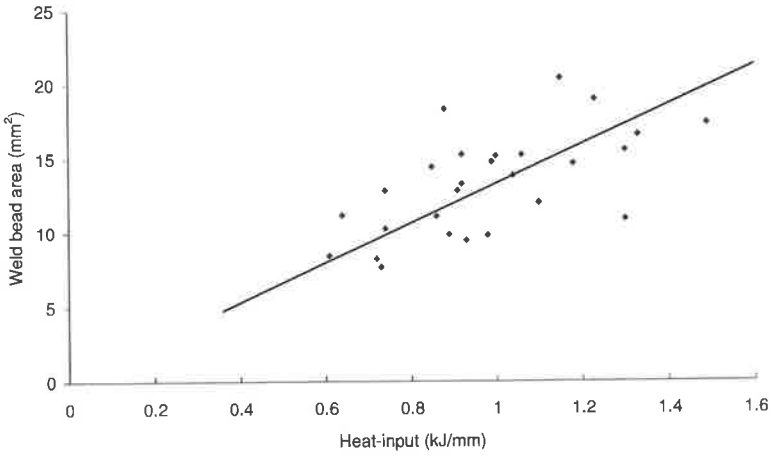


(a) E7016.

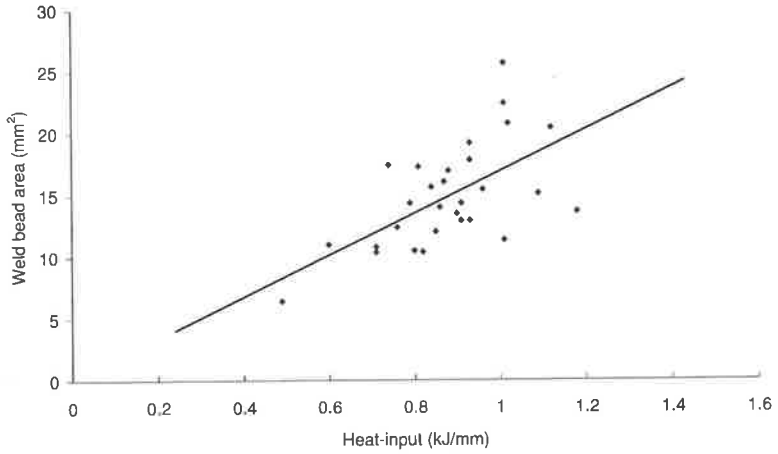


(b) E8018G.

**Figure 4.41:** Variation of weld bead area with heat input for laboratory experiments.

While a degree of scatter is evident for both vertical-up and vertical-down electrodes; a general trend is evident. When welding with vertical-down electrodes, the welding angle was found to be approximately defined by Equation 4.6, and Equation 4.7 for vertical-up welding.

$$\alpha = -4.1041 \times \text{Heat Input} + 49.417 \text{ (E8018G)} \tag{4.6}$$

$$\alpha = -1.7104 \times \text{Heat Input} + 44.716 \text{ (E7016)} \tag{4.7}$$

The trend evident when welding with either electrode is for the welding angle to decrease with increasing heat input. Such a trend appears to be inconsistent with avoiding burnthrough; since as heat input is increased, a greater ratio of heat is applied to the

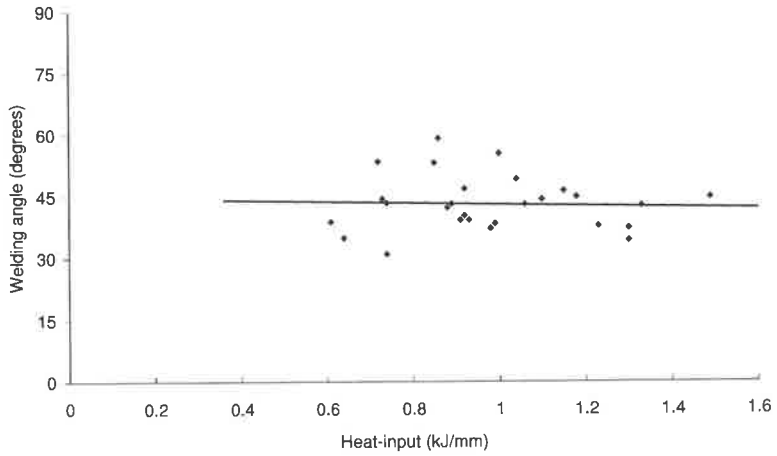


(a) E7016.

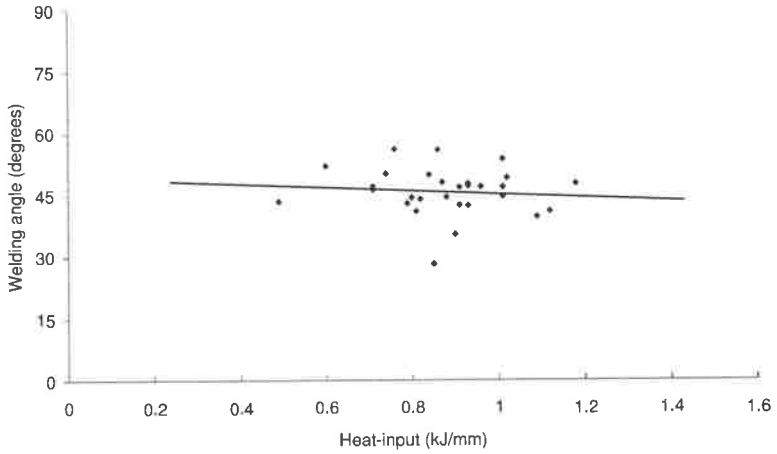


(b) E8018G.

**Figure 4.42:** Variation of welding angle with heat input for E7016 and E8018G electrodes from laboratory experiments.

pipe which potentially increases the penetration or fusion depth. As Figure 4.42(a) and Figure 4.42(b) suggest, the trend appears to be stronger with E8018G electrodes than with E7016 electrodes; welding with E7016 electrodes invariably results in more heat applied to the pipe than the sleeve, whereas with E8018G, the trend is to gradually apply a greater proportion of total heat to the pipe with increasing heat input. For a typical range of heat input used for in-service welding, $(0.6 - 1.2kJ/mm)$, welding with E8018G electrodes results in greater proportion of total heat being applied to the sleeve compared with E7016 electrodes.

### 4.4.3 Comparison with field tests

#### 4.4.3.1 Introduction

The model was tested and improved upon by comparing the predictions with the field results attained from the flow-loop experiments. While the field trials consisted of 45 test welds, not all of the welds were deposited in a satisfactory manner, and a number of these welds were discarded; the justification and explanation is given earlier in Section 4.3.4.

#### 4.4.3.2 Weld bead geometry: field experiments

For all 45 test welds deposited in the field trial, the measurements of pipe leg-length, and sleeve leg-length were taken; the measurements were taken in a manner similar to the laboratory tests as discussed earlier in Sections 4.4.2.2 & 4.4.2.3. The variation of welding angle with heat input is discussed in Section 4.4.3.3, while the variation of weld bead area with heat input is discussed in Section 4.4.3.4.

An immediate trend is not obvious, due to the significant presence of scatter. The laboratory tests also displayed a similar degree of scatter, therefore, a conclusive statement regarding the possible differences in bead shape between the experiment and the field trial is not easily made. However, a number of interesting trends are evident; the details of which are discussed in the following sections.

#### 4.4.3.3 Welding angle

A comparison of the welding angle predicted from the weld bead model with those derived from the field trials can be seen in Figure 4.43. The removal of weld samples from the analysis for reasons discussed in Section 4.3.4 had reduced the level of scatter. A degree of scatter still remains, however, the results are encouraging. The most notable difference in the comparison is that the welding angle for the field trials increases with heat input, whereas the welding angle as predicted by the weld bead geometry model decreases with

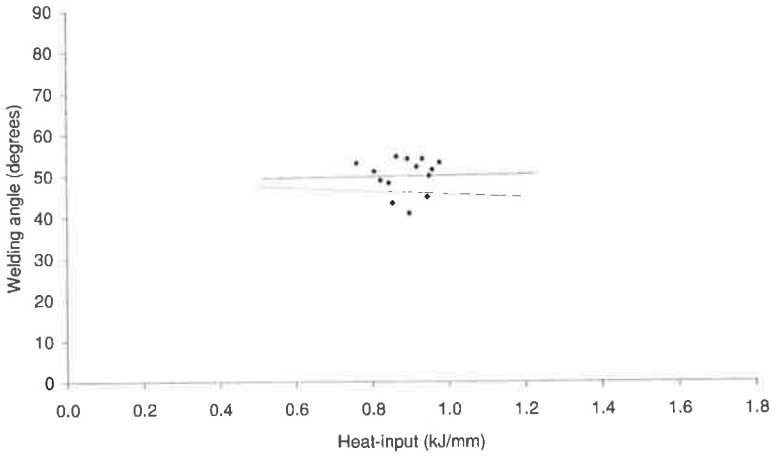


**Figure 4.43:** Welding angle predicted from model derived from laboratory experiments (pink line) is compared with welding angle calculated from field experiments (blue points and black line).

heat input. In addition, the welding angle of the field trials is such that the greater proportion of total heat is applied to the sleeve. The welding angle measured from the field trials is described by the following equation:

$$\alpha = 1.3801 \times \text{heat input} + 48.096 \tag{4.8}$$

While the accuracy of the measurement of heat input can potentially account for some of the discrepancy, the results indicate the variability of the manual welding process to account for the majority of the discrepancy. The application of a greater amount of heat into the sleeve on a live operating pipelines, compared with the same weld on a unpressurised water cooled laboratory test may also account for the discrepancy. In addition, both experiments were undertaken with different welders, and therefore the difference in welding technique might differ would account for the discrepancy. The results from the field experiments is in agreement with the argument proposed for the analysis of welding angle as earlier discussed in Section 4.4.2.3; in that to avoid burnthrough, a greater proportion of heat is applied for the sleeve with increasing heat input.

Finally, the sensitivity of the proposed thermal in-service welding model to welding angle was determined by comparing the predictions of a number of models, differing only in welding angle, sleeve and pipe leg-length. The results from the analysis can be

seen in Table 4.4.3.3. The analysis was performed for a hypothetical $0.96kJ/mm$ welds

| Angle | Penetration depth | HAZ depth | $t_{8/5}$ |
|---|---|---|---|
| +5 | 0.64mm | 3.04mm | 2.31s |
| 0 | 0.66mm | 3.30mm | 2.17s |
| -5 | 0.72mm | 3.65mm | 2.34s |

**Table 4.10:** Comparison of predictions of a given weld varying in welding angle.

onto a $4.8mm$ wall thickness pipe with a gas flow similar to that found during the field experiments. The nominal welding angle was 45.5 degrees. The range of welding included in the analysis is considered to be broader that that observed for the laboratory and field experiments. The sensitivity of welding angle on the thermal model is evident; with decreasing welding angle, the predicted fusion and HAZ depth had increased. However the magnitude of the effects on the results of the thermal model is considered to be minor.

The welding angle predicted by the proposed weld bead geometry model may be sufficiently accurate for the purpose of thermal field prediction of in-service welding by numerical methods. However, it is suggested that future work aimed at improving the proposed thermal model and weld bead model, in particular, an attempt to decouple the datum plane of the heat source from the leg-lengths of the weld bead may be beneficial. The present thermal model assumes that the angle of the electrode is based on the relationship of leg-lengths of the weld bead. However, it is possible that the instantaneous welding angle used in the thermal models, is not that reflected by the ratio of the leg-lengths from the resulting weld bead. The justification for this statement is due to the manual welding technique. A solution to this problem may arise from a study on the motion of the electrode during welding, or more importantly, the apportionment of heat to the sleeve and pipe during welding. Such a study would effectively decouple the heat source datum plane and definition from the weld bead geometry. It is suggested that the sensitivity of the thermal model is strongly dependent on definition of the heat source, principally influenced by the datum plane of the heat source, rather than the geometry of the weld bead, for a given weld bead area.

#### 4.4.3.4 Weld bead area

A comparison between the deposited area of 2.5$mm$ and 3.2$mm$ diameter electrodes from the field experiments can be seen in Figure 4.44. A fair degree of scatter is once again

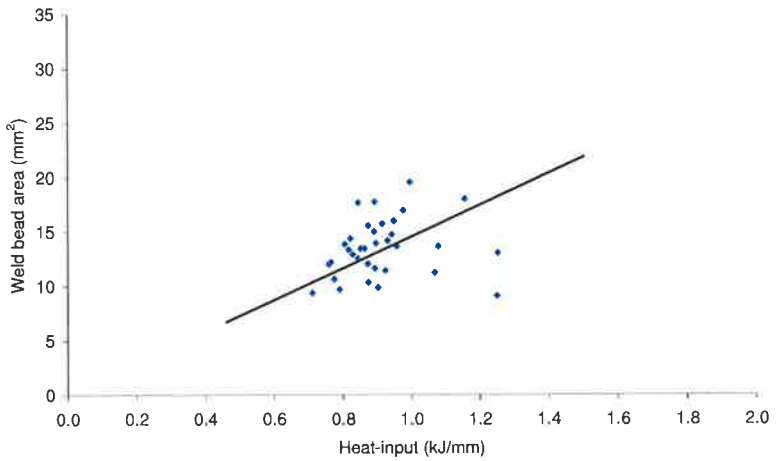


(a) 2.5$mm$.

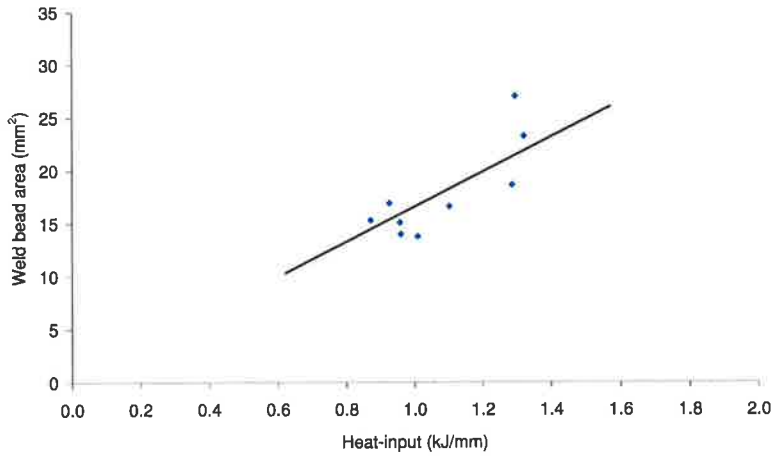


(b) 3.2$mm$.

**Figure 4.44:** Weld bead area measured from field trials for both 2.5$mm$ and 3.2$mm$ diameter E8018G electrodes.

present in the results, however, the general trend exhibited by comparing both electrodes, suggest that the deposition area of 3.2$mm$ diameter electrodes is greater than 2.5$mm$ diameter electrodes for a given heat input. The amount of scatter found for 2.5$mm$ diameter electrodes is considered to be mainly due to the manual welding technique, in particular the degree of weaving employed. In-service circumferential fillet welding with

MMA electrodes usually incorporates weaving to some degree; the observations from both the laboratory and field experiments confirm this.

A comparison between the weld bead area for the flow-loop field trials and the proposed weld bead geometry model can be seen in Figure 4.45. The removal of weld samples from

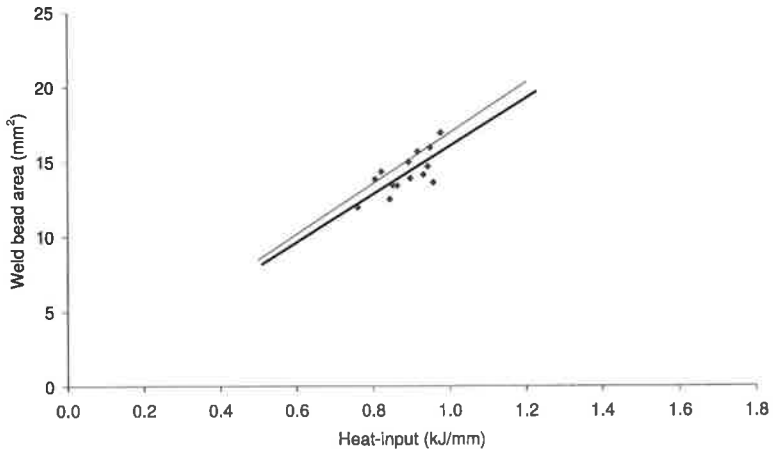


**Figure 4.45:** Comparison of predicted weld bead area based on laboratory experiments with those measured from field experiments for $2.5mm$ diameter E8018G electrodes.

the analysis as discussed in Section 4.3.4 had reduced the level of scatter considerably. The relationship between weld bead area and heat input for welds of acceptable quality deposited in the field experiments using $2.5mm$ diameter electrodes is described by the following equation:

$$\text{Weld bead area} = 16.051 \times \text{heat input} \tag{4.9}$$

With 90% confidence, the mean error between the weld bead area measured from the field experiments, and that predicted from the proposed weld bead geometry model for $2.5mm$ diameter electrodes was between 3% and 9%. The difference in welding technique employed by the two different welders for the field and laboratory simulations, is suggested to account for a substantial portion of the aforementioned discrepancy between the predictions from the weld bead geometry model and the field experiments. In addition, any errors which may have arisen when measuring heat input for both experiments, may also have influenced the discrepancy. While a fair amount of scatter still remains in the data, the resulting trend line based on the flow loop experiments appears to be similar to the

predictions based on the proposed weld bead geometry model as found in Section 4.4.2.2. However, the accuracy of the weld bead geometry model is considered to be reasonable, for the purpose of the heat transfer problem.

### 4.4.4 Conclusions

As stated earlier in Section 4.4.1, there are very few models which predict the geometry of the weld bead for MMA welding. Moreover, there is even less information published relating to the weld bead geometry for in-service welding using low-hydrogen electrodes. The model developed is not overly complex nor sophisticated. While the proposed weld bead geometry model is based on an earlier concept, proposed by Battelle, and Graville & Read, it does provide adequate information, namely pipe leg-length, sleeve leg-length for in-service vertical down circumferential fillet welding using low hydrogen electrodes.

The proposed weld bead geometry model is simple, and effective for its intended purpose to provide geometric information for the heat transfer analysis of circumferential fillet in-service welding. In the development of the model, a difference was found for welds deposited under laboratory conditions, and those which were deposited onto a live pipeline. As in-service welding is a manual process, the observed scatter and measured variation is believed to be primarily due to the manual process. A study into the technique of in-service welding, and its effect on the weld bead geometry, may yield increased accuracy to the proposed in-service welding thermal model. As suggested earlier in Section 4.4.3.3, a thermal model where the datum plane of the heat source is defined independently to the geometry of the weld bead may yield increased accuracy in the predictions from the in-service welding thermal model.

A number of improvements are suggested to the proposed weld bead geometry model:

1. The proposed model does not consider the effect of welding position on weld bead geometry. A study on the effect of welding position would yield tremendous benefits not only in order to derive a more accurate weld bead geometry model, but also to

study the variation of heat input for a given in-service circumferential fillet weld.

2. The proposed model does not consider the variation of welding angle, or the influence of weaving during welding. The study of weaving on heat input and weld bead geometry would considerably improve the present model's predictions. The present model suggests a linear relationship between welding angle and heat input; such a relationships, while effective, is most likely to be overly simple and unsophisticated. The study of the effect of weaving to the apportionment of heat to the sleeve and pipe would yield considerable accuracy to the proposed thermal models. A study on the change in the apportionment of heat between the sleeve and pipe during welding, with position, and during weaving, would be highly beneficial.

# Chapter 5

# Validation of in-service welding thermal model

## 5.1 Introduction

The prediction of post-weld hardness due to in-service welding is a significant improvement to traditional in-service weld procedure development. As stated earlier in Section 1.3, the three dominant factors which influence post-weld cracking due to in-service welding are: the existence of hydrogen in the cooling weld, a brittle HAZ microstructure in the pipe wall, and the existence of residual stresses in the HAZ microstructure. The principal mechanism of post-weld cracking from in-service welding, is due to the formation of a crack susceptible microstructure within the pipe. Modern pipe steels, consisting of low concentrations of carbon, rarely produce hardness levels in excess of $350HV$ due to in-service welding, even under very fast cooling rates. However, earlier vintages of pipe steels can easily produce hardness in excess of $350HV$ from in-service welding.

Previous research, as discussed earlier in Section 2.2.1, found that welds which contain HAZ hardness in excess of $350-400HV$ are in general, highly susceptible to hydrogen assisted cracking. Therefore, a model which predicts the post-weld hardness of the pipe due

to in-service welding would be sufficient, and highly useful for in-service weld procedure development. The approach taken here is to combine a numerical heat transfer model with hardness/cooling-rate model. For example, a finite element calculation would determine the cooling time for a given in-service weld; which is then used in a hardness/cooling-rate model to calculate hardness. The accuracy of the proposed model, would largely be a result of the accuracy of the predicted thermal field, and the appropriate choice of an empirical hardness/cooling-rate model.

The following sections will discuss the accuracy of the developed thermal model, as proposed in Chapter 3, by comparing predictions of welds deposited in the field experiments, as discussed in Section 4.3 with experimental measurements. The following quantities of a given in-service weld were compared with the results from the thermal models:

- penetration depth into main pipe
- maximum HAZ depth into main pipe
- weld cooling time
- hardness.

The accuracy of predicted penetration depth was determined by comparing it against experimental results; a simple macrograph of a weld would reveal penetration depth easily. Moreover, the penetration depth represents the liquid-solid melting isotherm, which can be easily compared with numerical model results. The comparison of maximum HAZ depth for validation, is of the same rationale. The edge of the HAZ represents a temperature of $720^oC$ for carbon steels. A simple plot of an isotherm representing $720^oC$ from the thermal models would provide a simple, quick and accurate comparison. The cooling time of the weld was again chosen for its simplicity, accuracy, and ease of comparison. As stated earlier in Section 4.3.3, the field trials were supplemented by the insertion of thermocouples in to the molten weld pool to measure weld cooling time. Post-processing the results from the thermal models, as discussed earlier in Section 3.1.5 allows the comparison

between predictions and experimental measurements. Finally, combining an appropriate hardness/cooling-rate model with the results from the thermal model allows for the comparison of predicted hardness with measured hardness from experiments. A number of measurements of hardness of the field welds were made to allow for comparison.

## 5.2 Validation of in-service welding models

### 5.2.1 Introduction

To test the accuracy of the proposed in-service circumferential fillet welding thermal model, a number of welds deposited during the field experiments were used as a comparison. Following the discarding of various welds as discussed in Section 4.3.4, a total of 15 welds were chosen to validate the proposed thermal models. Of the 15, 4 samples were for welds deposited on $4.8mm$ wall thickness pipe, 5 for welds deposited on $5.6mm$ wall thickness pipe, and finally, the remaining 5 were for welds deposited on $6.4mm$ wall thickness pipe. The input parameters for the thermal models are heat input, pipe geometry, gas pressure and flow-rate; these values are identical to that measured for each individual weld being compared for validation.

### 5.2.2 Penetration depth

A comparison between predicted penetration depth and measured maximum penetration depth for in-service welds deposited on $4.8mm$, $5.6mm$ and $6.4mm$ wall thickness pipe can be seen in Figure 5.1: Figure 5.1(a) for welds deposited in $4.8mm$ wall thickness pipe, Figure 5.1(b) for $5.6mm$ wall thickness pipe and finally, Figure 5.1(c) for welds deposited on $6.4mm$ wall thickness pipe. Overall, the thermal model had over predicted the depth of penetration for $4.8mm$ wall thickness pipe. With 90% confidence, the mean error between experimental and predicted penetration depth for welds deposited on $4.8mm$ wall thickness pipe was between $-4.4$ and 33.6%. For welds deposited on $5.6mm$ wall thickness

pipe, the models had in general given reasonable correlation. With 90% confidence, the mean error between experimental and predicted penetration depth for welds deposited on $5.6mm$ wall thickness pipe was between $-14.7$ and 7.3%. Curiously, for welds deposited on $6.4mm$ wall thickness pipe, the models had under predicted the depth of penetration. With 90% confidence, the mean error between experimental and predicted penetration depth for welds deposited on $6.4mm$ wall thickness pipe was between $-22.2$ and $-0.2$%. The general trend is that as wall thickness is increased, the models vary in prediction from over prediction to under prediction. With 90% confidence, the mean error between experimental and predicted penetration depth for all welds compared was between $-10.2$ and 7.8%. From a perspective of avoiding pipe wall failure, the over prediction for $4.8mm$ wall thickness pipe is welcome. The degree of under prediction for $6.4mm$ wall thickness is not considered to be alarming. The variation of penetration depth for a given weld, as discussed earlier in Section 4.3.6.3, is displayed within the error bars found in Figure 5.1. The accuracy in which penetration was predicted is considered to be acceptable, considering the significant effect which the variation in welding technique during a given weld pass has on penetration.

A number of observations are made regarding the experimental measurements and the numerical predictions. While the error of the actual measurement of penetration depth is minor, an inaccuracy may be found if the cross-section of the sample was not perpendicular to the circumference. Considerable effort was made to ensure that all cross-sections of samples were perpendicular, however, it is likely that some samples could potentially not be perpendicular. A further source of inaccuracy is due to the difficulty in determining a location which could be defined as the fusion zone. Clearly, the fusion zone is a narrow region, however, the fusion line was considered to be the middle section of the fusion zone. However, in some samples, the possible inaccurate definition of the fusion zone may introduce further errors. In addition, as discussed earlier in Section 4.3.4, the insertion of thermocouples can also affect the fusion zone depth.

While a number of errors may of be found for the experimental measurements, the

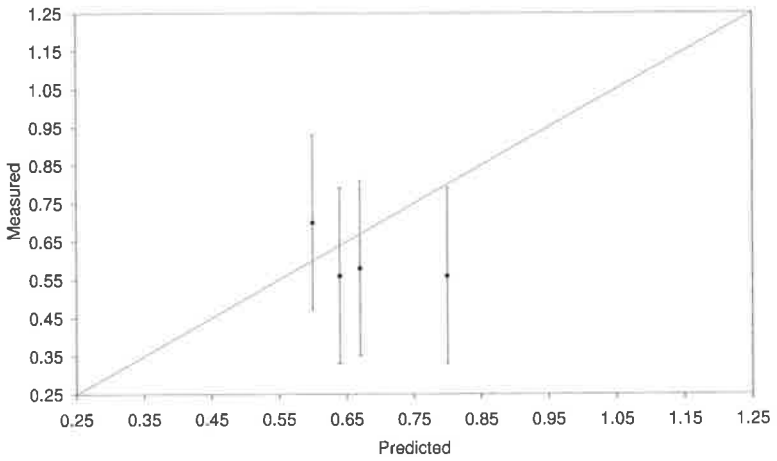


(a) $4.8mm$.

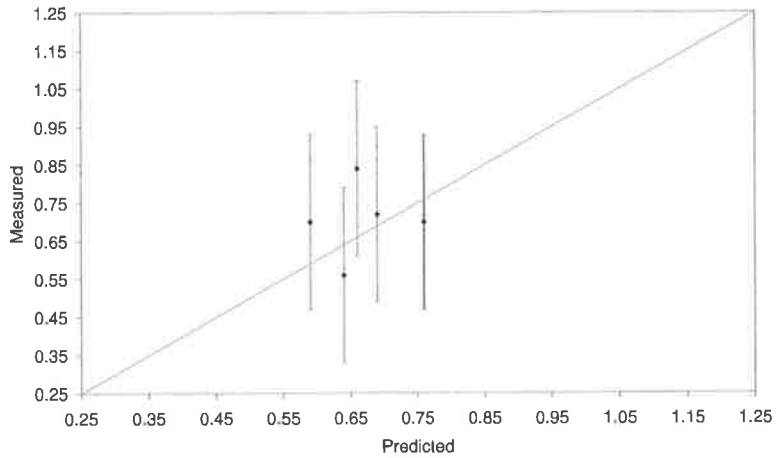


(b) $5.6mm$.

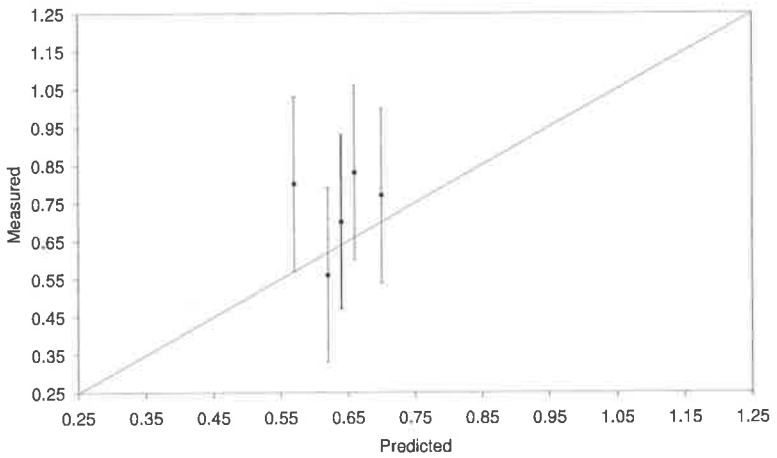


(c) $6.4mm$.

**Figure 5.1:** Comparison of predicted penetration depth with experiments for quasi-steady-state thermal models.

predictions are also not without possible inaccuracy. As the numerical method is an approximate calculation, the size and density of the finite element mesh influences the accuracy of the solution. If the mesh is found to be exceedingly stiff or coarse, the resulting temperature field may in some regions be artificially higher. In particular, if the mesh density in the direction of welding is too low, the predicted penetration depth may be too large. However, the numerical calculations were performed with sufficient mesh density in regions considered necessary; e.g. in the region within and adjacent to the heat source, and all other regions where large thermal gradients were expected. The problem of mesh density in the direction of welding is pertinent to both transient and quasi-steady-state thermal models. Moreover, the time steps chosen for the transient analysis may yet introduce a further error. If the size of the time step is too great, the model may under predict penetration depth; in the extreme case, the model will represent a serious of discrete welds.

A number of observations were made regarding the feasibility of comparing predicted penetration depth with experimental measurements as a measure of the accuracy of the proposed model. Penetration depth is considered to be more a reflection of the instantaneous arc rather than the history of the weld prior. However, clearly this is not the case for weld startup; nor does the model predict the temperature field for weld startup. Laboratory and field experiments had revealed that heat input had varied with position and during a given weld pass. In addition, the variation of voltage and current with time was also observed for both experiments. The variation of the arc is therefore considerable with time and welding position. As a result, the depth of penetration is also highly variable. In contrast, the variation of heat from the arc with time and due to position was not included in the model. However, the formulation of the heat source was to produce a wide and shallow weld pool; the resulting model predicts a cross-sectional temperature field which is considered to reflect the average cross-sectional temperature field for a given weld pass with constant heat input, ignoring weld start and stop conditions.

The effect of weaving is also considered to be a significant source of discrepancy be-

tween experiments and numerical predictions. It is thought that the position of the arc during welding also influences penetration depth. A given weld with a known heat input can have vastly different fusion zone profiles depending on the position of the electrode for a given instant in time. If the electrode is applying a greater proportion of total heat to the sleeve of the joint, then the resulting penetration depth into the pipe is less than if the same electrode were applying a greater proportion of total heat to the pipe; both welds have the same heat input but different penetration depths. The variation in welding angle during welding is not accounted for the model. However as discussed earlier, the distribution of the proposed heat source effectively predicts the average penetration depth into the pipe.

In conclusion, in combination with the compounding errors from the measurement of heat input to the possible inaccuracies of using a numerical model, the predictions are considered to be well within error. However, further studies involving decoupling the heat source datum plane from the weld bead geometry as discussed earlier in Section 4.4.3.3 may further improve the accuracy of the thermal model.

### 5.2.3 HAZ depth

The results from numerical predictions of maximum HAZ depth for selected welds deposited in the field experiments can be seen in Figure 5.2: Figure 5.2(a) for welds deposited in $4.8mm$ wall thickness pipe, Figure 5.2(b) for $5.6mm$ wall thickness pipe and finally, Figure 5.2(c) for welds deposited on $6.4mm$ wall thickness pipe. The thermal models over predicted the maximum HAZ depth for welds deposited on $4.8mm$ and $6.4mm$ wall thickness pipe. With 90% confidence, the mean error between experimental and predicted maximum HAZ depth was between 10.4 and 18.4% for welds deposited on $4.8mm$ wall thickness pipe, while for welds deposited on $6.4mm$ wall thickness pipe, the mean error was between 5.2 and 11.2%. Interestingly, the models had on average provided mixed correlation with welds deposited on $5.6mm$ wall thickness pipe; a degree of scatter is evident, however the model had clearly under and over predicted the maximum HAZ

depth. With 90% confidence, the mean error between experimental and predicted maximum HAZ depth for welds deposited on 5.6$mm$ wall thickness pipe was between $-3.8$ and 12.2%. Of all 14 test samples, only two samples had a larger measured maximum HAZ depth than what was predicted. With 90% confidence, the mean error between all experimental and predicted maximum HAZ depth compared was between 4.5 and 12.5%. The accuracy is considered to be acceptable considering the limited number of samples in which the predictions from the model were compared with. The variation of HAZ depth for a given weld, as discussed earlier in Section 4.3.6.3, is displayed within the error bars found in Figure 5.2. The accuracy in which HAZ depth was predicted is considered to be acceptable, considering the effects of the variation in welding technique during a given weld pass has on the weld microstructure.

A number of similar problems to that found when measuring penetration depth were also found when measuring maximum HAZ depth. The main problem is if the surface of the cross-section is not exactly perpendicular to the circumference. Another source of potential inaccuracy is the exact definition of the HAZ boundary or the 720$^oC$ isotherm. However, the edges of the HAZ was considered to be the 720$^oC$ isotherm. The remaining concerns regarding the accuracy of the experimental measurements are similar to those discussed for penetration depth earlier in Section 5.2.2. They include the variation of welding technique and heat input with position and during a given weld, and to a lesser extent, any additional heat that may have been placed on the weld due to the measurement of weld cooling time by harpooning thermocouples, as discussed earlier in Section 4.3.4. The concerns regarding the accuracy of the numerical predictions are identical to those discussed for penetration depth, found earlier in Section 5.2.2.

The depth of the HAZ is considered to be influenced by the instantaneous heat from the arc, however not to the same degree as was suggested for penetration depth. Moreover, the depth of the HAZ is also influenced by the history of the arc during a given weld. At the actual location of measurement, the HAZ is influenced by the history of the arc up to the point of measurement and also up to a point past the location of measurement. This is

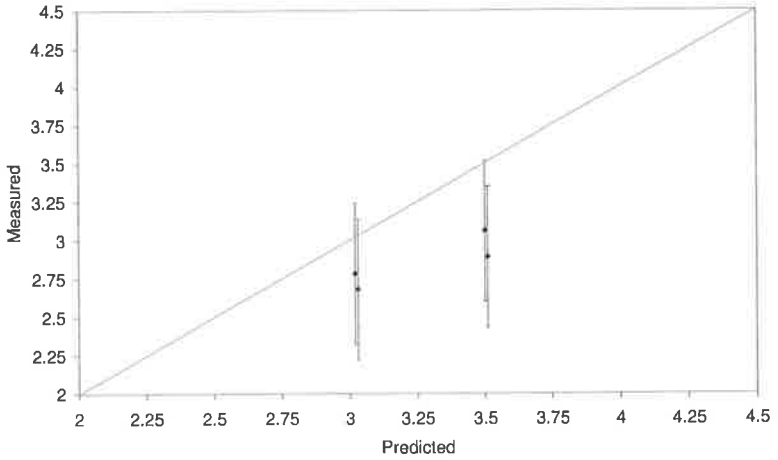


(a) $4.8mm$.

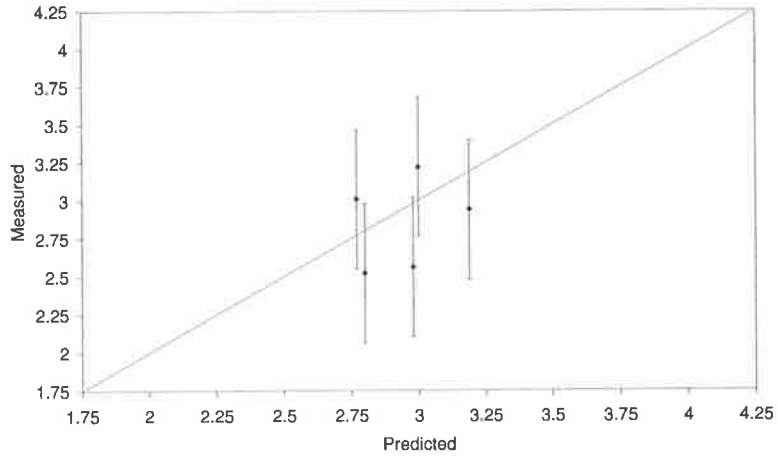


(b) $5.6mm$.

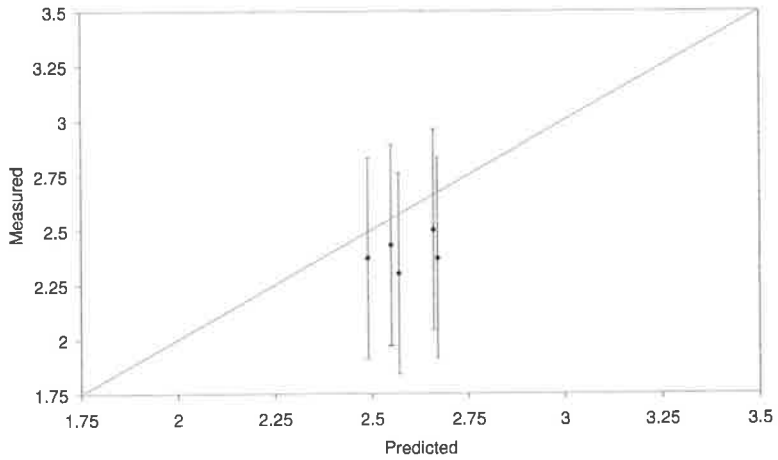


(c) $6.4mm$.

**Figure 5.2:** Comparison of predicted HAZ depth with experiments for quasi-steady-state thermal models.

said to occur as the heat from the arc at locations near the measured point influences the eventual HAZ region. As a result, the depth of the HAZ at a given location is influenced by the instantaneous welding technique, the welding technique and heat input fluctuation prior to and after the point of measurement.

In conclusion, it is considered that in light of all compounding errors previously mentioned, the accuracy of the thermal models based on the results of HAZ depth correlation is sufficient.

### 5.2.4 Weld cooling time

The results from numerical predictions of weld cooling time ($t_{8/5}$ ) for selected welds deposited in the field experiments can be seen in Figure 5.3: Figure 5.3(a) for welds deposited in 4.8$mm$ wall thickness pipe, Figure 5.3(b) for 5.6$mm$ wall thickness pipe and finally, Figure 5.3(c) for welds deposited on 6.4$mm$ wall thickness pipe. The correlation between predictions and experiments was best for welds deposited on 5.6$mm$ wall thickness pipe. With 90% confidence, the mean error between experimental and predicted weld cooling time for welds deposited on 5.6$mm$ wall thickness pipe was between $-4.5$ and 15.5%. The discrepancy between predictions and measurements for welds deposited on 4.8$mm$ and 6.4$mm$ wall thickness pipe is reasonable considering the inaccuracies involved in the measurement of weld cooling time. With 90% confidence, the mean error between experimental and predicted weld cooling time was between $-7.2$ and 22.8% for welds deposited on 4.8$mm$ wall thickness pipe, while for welds deposited on 6.4$mm$ wall thickness pipe, the mean error was between $-27.5$ and 16.5%. With 90% confidence, the mean error between all experimental and predicted weld cooling time compared was between $-5.9$ and 12.1%.

The measurement of the weld cooling time, by harpooning a thermocouple into the weld pool has the potential for significant levels of inaccuracy. As mentioned previously by Oddy & McDill [63] and Goldak [35], a minor change in the location of the thermocouple

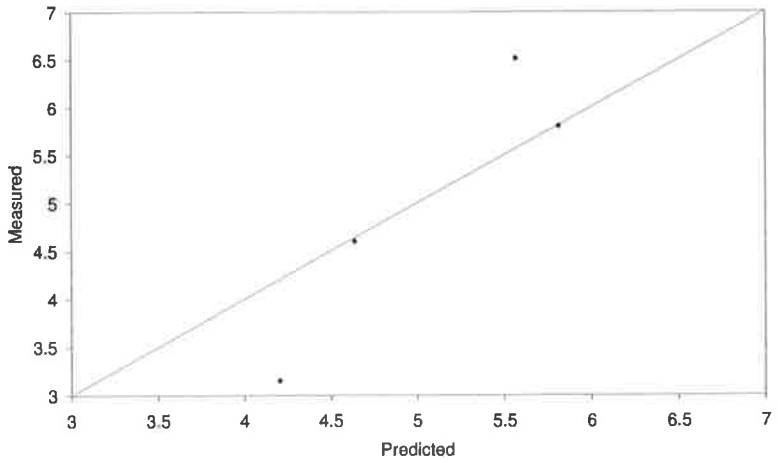


(a) $4.8mm$.

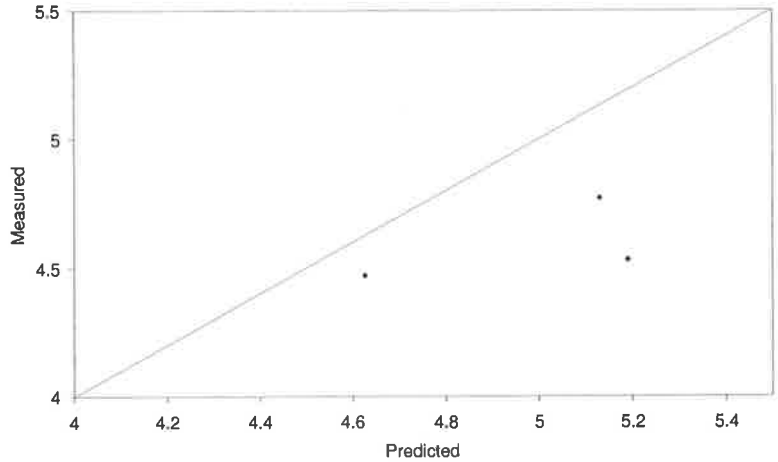


(b) $5.6mm$.

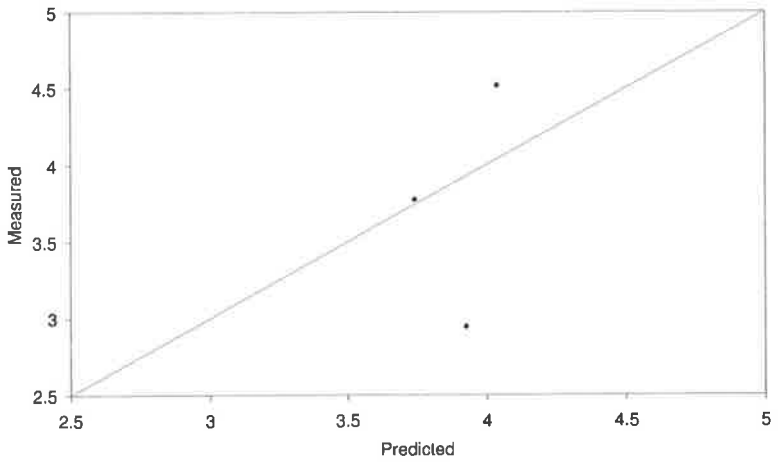


(c) $6.4mm$.

**Figure 5.3:** Comparison of predicted weld cooling time ($t_{8/5}$ ) with experiments for quasi-steady-state thermal models.

can result in a dramatic change in temperature. Oddy & McDill [63] (1999) had found the measurement of peak temperatures on the inner surface of the vessel as a difficult task. Poor placement of the thermocouples had lead to erroneously low measured values. Goldak et al. [35] (1992) found when measuring peak surface temperatures, the results were strongly dependent on the position of the thermocouple. Any error in position, even only a fraction of a millimetre, can be significant near the weld source. The author found that peak predicted inner surface temperatures were likely to be higher than measured values.

A number of concerns were identified regarding the accuracy of measuring weld cooling time using the harpooning method. The quality of the bond between the thermocouple and the weld pool is suggested to be a possible source of experimental error. Moreover, the junction of the wires can further influence the measurement; in some instances, the wire was joined much earlier than at the original junction and point of measurement. In addition, as discussed previously in Section 4.3.4, the insertion of the thermocouple into moderately sized weld pools exerts its own heat transfer effects. Of primary concern is the additional heat introduced to the joint by the welder in an effort to maintain the size of the weld pool, and to compensate for the heat loss due to the introduction of the thermocouple and in extreme cases, where the thermocouple was observed to melt. The additional heat introduced can significantly alter the measured and perceived weld cooling time. While welds exhibiting a microstructure containing foreign material due to a molten thermocouple were discarded, the degree of melting in those samples where visual observation was unable to identify as such is also likely to introduce further errors in measurement. However, no other alternative was available for measuring the cooling time.

A number of concerns regarding the accuracy of the predictions of the numerical model were identified. The level of mesh refinement is considered to influence the accuracy of weld cooling time prediction for quasi-steady-state thermal models. In particular, the mesh density or distribution along the line of welding is important. As the weld cooling

time is measured for the radial cross-sectional plane, the cooling time is related to the distance travelled by the arc, which is related to the length between nodes. The primary concern is that an error due to interpolating between nodes could introduce an inaccuracy in the predicted weld cooling time. Further inaccuracies relating to the general numerical modelling of welding are also applicable to the prediction of weld cooling time.

Observations from experiments also suggests that as there is a variation of heat input with position, then weld cooling time is also likely to vary with position. This variation of weld cooling time with position can also give poor correlation between predictions and experiments. The models had not considered the variation of heat input during a weld run, and therefore can not predict the variation in weld cooling time with position for a given weld run. However, as stated earlier, the proposed heat source definition is formulated to provide a near average 2D cross-sectional temperature field, and resultantly weld cooling time.

In conclusion, the prediction of weld cooling time is adequate, considering the limited number of welds in which the model could be compared against, the variability and difficulties associated with the actual measurement, and the variation of weld cooling time with position and during a given weld.

### 5.2.5 Hardness comparison

The predictions of hardness from the numerical models was achieved by using using established empirical relationships of weld cooling time and hardness. The comparison of 10 different empirical models which calculate hardness from weld cooling time, using the composition of the pipe was reported by Painter & Sabapathy [64] (2000). For each weld deposited in the field trials, a hardness traverse, perpendicular to the surface of the pipe, through the deepest section of the HAZ was performed. Peak hardness from each weld was then compared with the predicted hardness from each of the hardness/cooling time models using the measured $t_{8/5}$ weld cooling time. The results from the work can be seen

in Table 5.1. The work had found that the Beckert relationship would provide the best correlation for the types of steels found in the flow-loop field experiments. The predicted hardness was therefore calculated using the Beckert relationship, predicted weld cooling time, and the chemical composition of the pipes used in the flow-loop experiments; the composition of the pipes can be found earlier in Section 4.3.2 under Table 4.4.

The comparison between model predictions and experiments can be seen in Figure 5.4: Figure 5.4(a) for welds deposited in $4.8mm$ wall thickness pipe, Figure 5.4(b) for $5.6mm$ wall thickness pipe and finally, Figure 5.4(c) for welds deposited on $6.4mm$ wall thickness pipe. The correlation between predictions and experiments was best for welds deposited on $5.6mm$ wall thickness pipe. In general, the model had over predicted hardness for welds deposited on $5.6mm$ wall thickness pipe. With 90% confidence, the mean error between experimental and predicted peak hardness for welds deposited on $5.6mm$ wall thickness pipe was between 1.3 and 7.3%. The model also had, in general over predicted the peak hardness for welds deposited on $4.8mm$ wall thickness pipe. With 90% confidence, the mean error between experimental and predicted peak hardness for welds deposited on $4.8mm$ wall thickness pipe was between 2.3% and 12.3%. The model had over predicted all predictions for welds deposited on $6.4mm$ wall thickness pipe. With 90% confidence, the mean error between experimental and predicted peak hardness for welds deposited on $6.4mm$ wall thickness pipe was between 13.4% and 31.4%. Overall, the model had over predicted peak hardness for all measured welds. With 90% confidence, the mean error between all experimental and predicted peak hardness compared was between 6.6 and 16.6%.

The measurement of peak hardness from the experiments is not without error. The measurement of hardness was achieved by using a automatic micro-hardness indenter. For a given macrograph, the deepest part of the HAZ was identified, and a line perpendicular to the top surface of the pipe was then drawn through the identified point. Measurements of hardness starting from the surface of the pipe down to the deepest part of the HAZ and beyond were then taken every $0.1mm$. The peak hardness of a given weld was therefore

| Measured $t_{8/5}$ | Measured hardness | Suzuki BL70 | Suzuki BL70S (Pcm) | Suzuki BL70S (Pcm) using Ito B* | Suzuki BL70SM Pcm | Suzuki BL70S (CEm) | Suzuki BL70S (CE) | Beckert | Yurioka -1 | Yurioka -2 | Yurioka -3 | Dueren | Terasaki JOM-2 |
|---|---|---|---|---|---|---|---|---|---|---|---|---|---|
| 3.2 | 262 | 308 | 309 | 326 | 307 | 307 | 303 | 300 | 310 | 318 | 318 | 280 | 322 |
| 4.6 | 244 | 294 | 291 | 314 | 289 | 288 | 284 | 266 | 291 | 298 | 298 | 262 | 305 |
| 6.5 | 239 | 277 | 271 | 298 | 268 | 268 | 263 | 228 | 268 | 275 | 276 | 244 | 286 |
| 5.8 | 254 | 283 | 277 | 304 | 275 | 275 | 270 | 240 | 276 | 282 | 283 | 250 | 292 |
| 4.5 | 238 | 284 | 282 | 307 | 276 | 280 | 275 | 252 | 279 | 282 | 284 | 251 | 293 |
| 4.8 | 244 | 281 | 278 | 304 | 272 | 276 | 271 | 244 | 275 | 277 | 279 | 248 | 289 |
| 4.5 | 239 | 284 | 282 | 307 | 276 | 280 | 275 | 252 | 279 | 282 | 284 | 251 | 293 |
| 3.8 | 222 | 323 | 321 | 355 | 299 | 329 | 325 | 274 | 329 | 314 | 318 | 322 | 307 |
| 2.9 | 223 | 345 | 343 | 371 | 323 | 350 | 347 | 318 | 350 | 342 | 345 | 344 | 331 |
| 4.5 | 227 | 307 | 305 | 342 | 283 | 314 | 310 | 244 | 314 | 295 | 301 | 308 | 290 |
| Average error: | | 25% | 24% | 36% | 20% | 25% | 23% | 10% | 25% | 24% | 25% | 16% | 26% |

**Table 5.1:** Comparison of the accuracy of various empirical cooling time/hardness models using measured $t_{8/5}$ and hardness from field experiments.

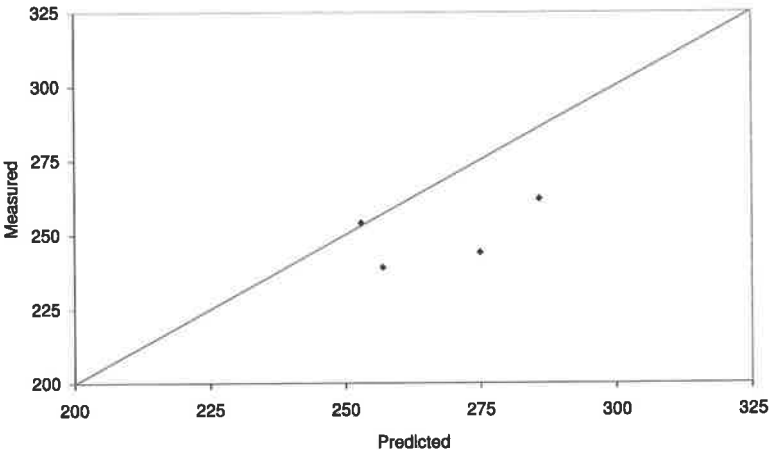


(a) 4.8$mm$.

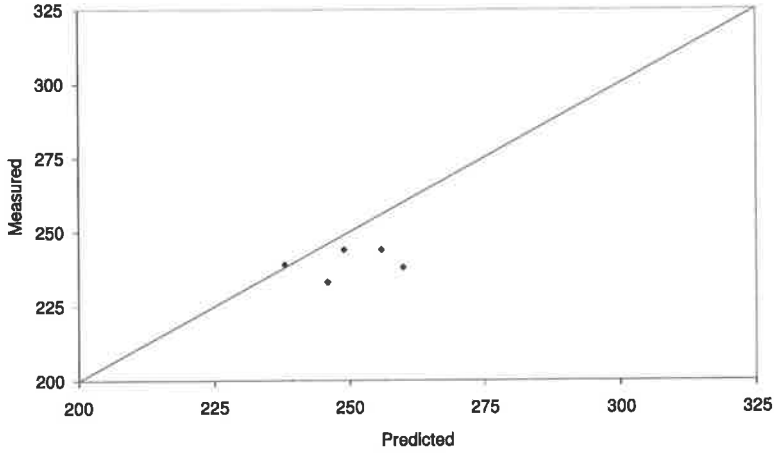


(b) 5.6$mm$.

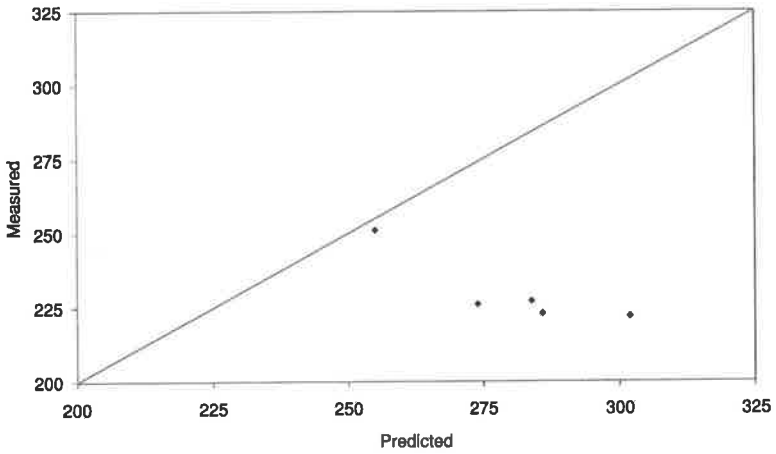


(c) 6.4$mm$.

**Figure 5.4:** Comparison of predicted hardness with experiments for quasi-steady-state thermal models.

considered to be the measurement returning the highest value from the traverse. However, as the measurements were taken in fixed increments, the maximum measured hardness is likely to be lower than actual peak hardness. Further inaccuracies include the definition of the line which is perpendicular to the surface, and errors in the measurement of the size of the indentation.

The concerns regarding the accuracy of the predictions are identical to those discussed previously in Section 5.2.4 for the prediction of weld cooling time. However, in addition, the choice of appropriate empirical hardness/cooling-rate model can further introduce inaccuracies. Moreover, the measurement of the chemical composition of the pipe can also introduce further errors. However, the resulting magnitude of the error is considered to be, at best, minor.

The general trend for the model to over predict peak hardness is considered to be significantly due to the method in which the measurements from the experiments were taken. As measured hardness was lower than actual peak hardness, the resulting trend was for the models to over predict peak hardness. In the case of severe over prediction of peak hardness of welds deposited on $6.4mm$ wall thickness pipe, it is suggested that the method of measurement used to measure peak hardness is to attribute for a significant proportion of the discrepancy. As discussed earlier in Section 4.3.5.3, for a given range of heat input, the range of the resulting HAZ depth for $6.4mm$ wall thickness pipe was found to be lower than that for $4.8mm$ and $5.6mm$ wall thickness pipe. As the measurement of peak HAZ hardness was achieved by fixed incremental measurements, for a weld with smaller HAZ, less measurements of hardness were taken. As the measurement of HAZ hardness was achieved using fixed increments of $0.1mm$, for a weld with smaller HAZ size, less number of measurements would have been taken. Due to less measurements, the probability of measuring actual peak hardness is further decreased. The argument proposed here is that the smaller the size of the HAZ, the greater the chance of not measuring peak hardness, and the greater the disparity of actual peak hardness measurement and measured maximum hardness, due to the measurement using fixed increments. In

conclusion, the model predicts peak HAZ hardness with an acceptable level of accuracy. Future work is suggested to further validate the model by measuring actual peak hardness and also to use smaller sized increments during hardness measurement.

## 5.3 Conclusion

The thermal models provide the best correlation with HAZ depth, followed by peak hardness, penetration depth and finally weld cooling time.

The relatively mediocre correlation of predicted penetration depth with experimental measurements is suggested to be due to the sensitivity of penetration depth with heat input. As discussed earlier, the variation of heat input with position has been observed for the experiments. In addition, the variation of heat input during a given weld has also been observed. However, the most significant observation has been the effect of welding technique to heat input and the apportionment of heat to the joint. Clearly, the effect of the apportionment of heat to the sleeve and the pipe can significantly influence the resulting penetration depth. Future work includes further refinement of the existing method to measure welding speed. However, of primary importance is the study of the variation of the apportionment of heat during manual welding. Predicts of penetration depth is related to the datum plane of the heat source. In turn, the datum plane of the heat source is related to the weld bead geometry. In addition, the relationship of weld bead geometry, especially pipe leg-length and sleeve leg-length is controlled by welding angle. The welding angle strongly influences the apportionment of heat to the sleeve and pipe and therefore strongly controls the prediction of penetration depth. A study aimed at understanding the variation of welding angle, the apportionment of heat due to welding technique and weaving would improve the ability of the model to predict penetration depth considerably.

The accuracy in which the model predicts HAZ depth is considered to be encouraging. While the model in general over predicts the depth of the HAZ, the correlation is

reasonable. Moreover, the reasonable correlation of HAZ depth would also imply that the correlation of HAZ size and shape would also be of acceptable accuracy. The sensitivity of HAZ depth to heat input is not to the same degree as with penetration depth. However, the sensitivity is suggested to play a significant role in the discrepancy between model predictions and experimental measurements. The correlation of predicted peak hardness and measured hardness is also considered to be encouraging. The improvement of peak hardness correlation is as discussed earlier in Section 5.2.5, likely by measuring actual peak hardness. Future work involving measuring hardness with smaller increments is considered to significantly improve correlation; especially as predicted peak hardness is in general greater than experimental measurements. However, the combination of predicting peak HAZ hardness and HAZ depth with reasonable accuracy is considered to be encouraging. The relatively poor correlation of weld cooling time is suggested to be largely due to the problems associated with measuring weld cooling time and the large importance of accurate thermocouple placement. However, as predicted peak hardness was calculated from cooling time, this would suggest that the correlation of weld cooling time in the pipe would be of similar accuracy to the prediction of peak hardness.

In conclusion, with the significant variation of many parameters for a given weld, the end result of a developing a model which predicts peak hardness with acceptable accuracy has been reached. The proposed model combines the use of an empirically based relationship to calculate heat transfer coefficient, and yet another to predict hardness from predicted weld cooling time. Moreover, the proposed model incorporates a heat source to simulate low penetration, low-hydrogen MMA electrodes, and also incorporates a new weld bead geometry model which predicts deposition area and welding angle. The combination of all these innovations results in a model which predicts penetration depth, maximum HAZ depth, weld cooling time and most importantly predicts peak HAZ hardness with good accuracy.

# Chapter 6

# Pipe wall failure

## 6.1 Introduction

Of the two main concerns pertaining to in-service welding, the failure of the pipe wall is by far, the least understood. Burnthrough is the term coined to designate a pipe wall failure or the bursting of the pipe wall during in-service welding. Very few experiments have been attempted, or are published in the open literature, which have studied the various phenomena, or modes of failure associated with burnthrough. The principal reason is notionally suggested to be the considerable safety implications of such an experiment. In addition, there have been relatively few attempts to systematically determine the conditions necessary to avoid burnthrough during in-service welding. Of the few experiments which have been attempted, most have involved remotely depositing welds under wide and varied conditions. Conclusions arising from such experiments tend to provide general directions rather than quantified limits. However, by sensible deduction, combined with some experimental observations, the qualitative causes of burnthrough are known. The principal factors which influence burnthrough can be seen in Figure 2.7.

A review of the work undertaken to directly and indirectly study burnthrough can be found earlier in Section 2.2.2. Recapping, extensive investigation of in-service welding

was attempted experimentally by the Edison Welding Institute [21] and Battelle Memorial Institute [20]. However, the efforts by both research groups were primarily focused on weld cooling rate and had not considered burnthrough limits directly. Only a limited amount of research into the conditions which control the onset of burnthrough during in-service welding is available in the open literature.

Observations of burnthrough generally show significant local plastic distortion of the pipe wall, and a fracture along the weld pool axis. Figure 6.1 reproduces a section across a failure presented by Bruce [15] during a weld repair and this shows the typical features.

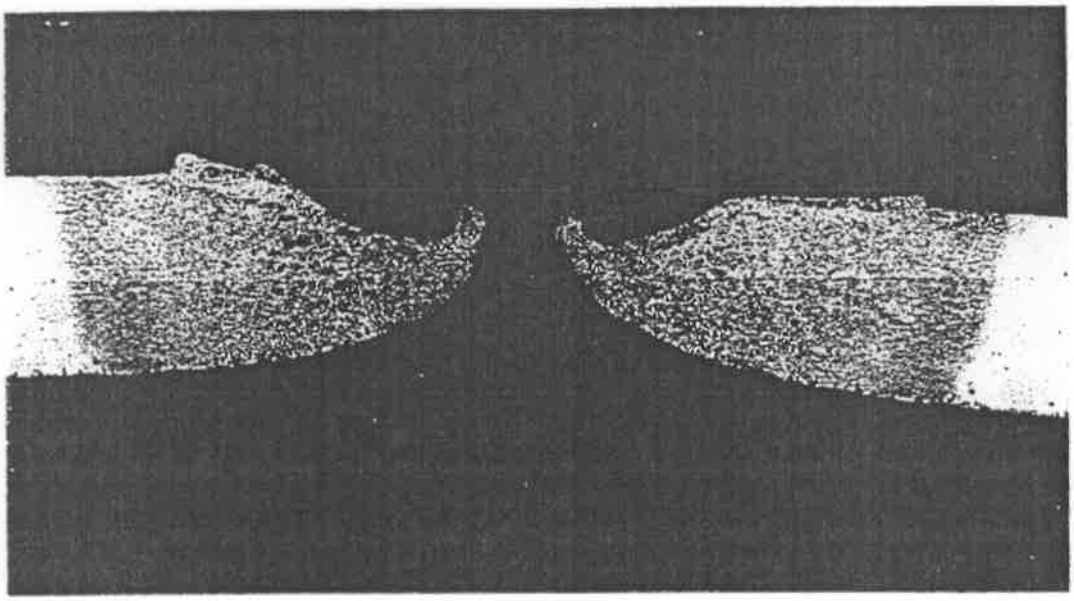

**Figure 6.1:** Example of burnthrough: $2.4mm$ diameter electrode, $80A$, $21V$, $1.9mm/s$ welding speed, $0.88kJ/mm$ heat input.

Clearly, the risk of burnthrough is related to the loss of pipe wall strength in the weld zone, and to its inability to resist local stress, or to retain the internal gas pressure of the pipe during welding. The reduction in wall strength depends on the elevated temperature around the weld, and on the depth of weld penetration relative to the original wall thickness.

The consensus from industry practice and research work is that the dominant factors influencing burnthrough are:

1. Pipe wall thickness.

   Reduced wall thickness increases the risk of burnthrough; other factors being constant. Pipe wall thickness is often used as a cut-off to safe in-service welding, with welding not recommended below a given thickness, often in the $4 - 5mm$ range.

2. Heat input.

   Increased heat input tend to increases burnthrough risk. Most recommended procedures consider specifying some upper limit at a given pipe wall thickness.

3. Internal pressure.

   High internal gas pressure increases the risk of burnthrough and often a pressure limit has been set for welding on thin-walled pipe.

In addition, the typical recommended practices for avoiding burnthrough are:

- a specified lower wall thickness of about $5 - 6mm$ below which welds should not be carried out without significant pressure reductions
- restricted low heat input welds (typically $0.5 - 1.0kJ/mm$), using controlled arc current and welding speeds
- the use of small diameter, low arc current, low hydrogen electrodes in the vertical-down welding position.

The following sections will discuss the application and validation of a novel method proposed by Bout & Gretskii [8] to predict the pressure at which a given in-service weld would be considered to have failed. Briefly, the failure pressure for a given weld is calculated by the assumption that the burnthrough of an in-service weld can be modelled as the failure of an equivalent corrosion cavity for the same wall nominal pipe wall thickness and given internal pressure. Therefore, existing models which provide the maximum pressure which an operating pipeline can withstand for a given corrosion cavity can be used to determine a safe welding pressure.

The first section will examine the definition of pipe wall failure of in-service welding itself; the term burnthrough is used to describe the final stage of failure where the weld pool expulsion has occurred due to the pressurised gas contained within. The next section will then discuss the elastic-plastic model developed for predicting the onset of burnthrough for in-service welding. The thermal elastic-plastic models will be verified using some limited burnthrough related experimental data published by Wade [84]. In addition, the accuracy and limitations of an existing corrosion cavity model will also be discussed. Finally, the validity of the proposed equivalent cavity model will be considered by comparing the predictions with thermal elastic-plastic models.

## 6.2 Examining pipe wall failure

The literature search revealed only a small number of publications relating to pipe wall failure or burnthrough due to in-service welding. The results contained within are for a limited range of welding conditions, gas flow-rates and pressures. Moreover, due to the risks associated with burnthrough, a limited quantity of welds were deposited. The work reported by Bruce et al. [15] for the study of repairing corrosion cavities by in-service direct deposition has also revealed a number of macrographs of welds under various degrees of distortion and failure. The macrographs of interest can be seen in Figure 6.2.

The welds displayed in Figure 6.2 have a number of similarities. The distortion primarily occurs in the radial direction. However, distortion in the longitudinal or axial direction is not able to be determined due to the cross-sectional view only being available. However, the stress field in a pressurised pipe is significant in both hoop and longitudinal directions. The level of radial deflection is greatest at the inside surface of the pipe, while it appears that the radial distortion at the surface of the pipe is the least. It is suggested that the radial distortion varies from a maximum amount from the inside surface of the pipe, to a minimum amount at the outer surface of the pipe.

The second similarity which the macrographs displayed in the above figure have in

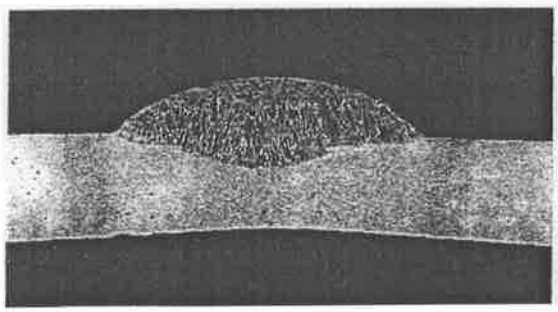

(a) $\phi 2.4mm$, $80A$, $2.7mm/s$, $0.62kJ/mm$.

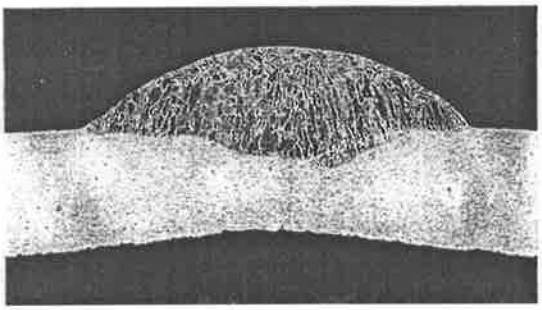

(b) $\phi 3.2mm$, $110A$, $2.2mm/s$, $1.07kJ/mm$.

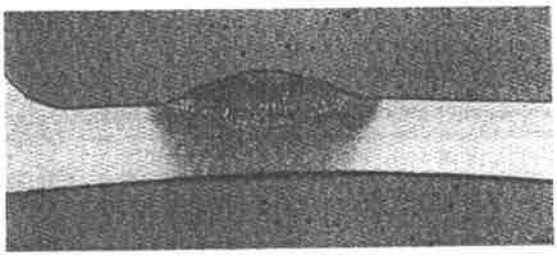

(c) $\phi 3.2mm$, $100A$, $4.4mm/s$, $0.48kJ/mm$.

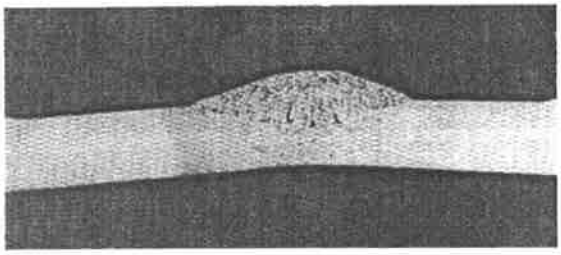

(d) $\phi 3.2mm$, $109A$, $4.4mm/s$, $0.52kJ/mm$.

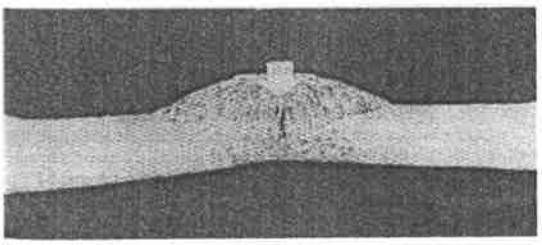

(e) $\phi 3.2mm$, $117A$, $4.3mm/s$, $0.60kJ/mm$.

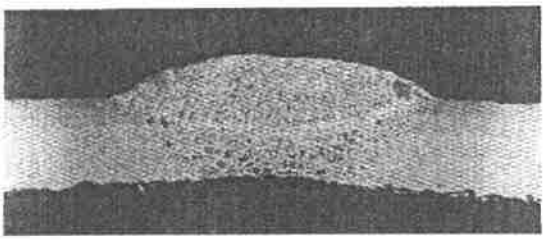

(f) $\phi 2.4mm$, $84A$, $3.1mm/s$, $0.75kJ/mm$.

**Figure 6.2:** Macrographs of various burnthrough test welds [15]; $\phi$ is electrode diameter.

common is the depth of the HAZ. For all these welds, the HAZ depth includes the entire wall thickness. Moreover, the width of the HAZ at the inside surface of the pipe is also considerable, and is of similar width to that at the outer surface of the pipe. While it may be argued that as the welds were deposited in a bead-on-plate manner such a wide HAZ is expected, the resulting HAZ from a fillet welds is considered to be not too dissimilar to that from a bead on pipe weld. However, the size of the HAZ observed in the welds is significant. Clearly, the HAZ is a result of temperature exceeding $720^oC$. The temperature at the edge of the HAZ is $720^oC$ while that in other regions is dependent on other factors. The temperature field due to welding for these welds varies from molten, as seen from the fusion zone boundary to $720^oC$ as seen at the edge of the HAZ. The temperature field in

the HAZ is therefore a distribution from $720^oC$ at the edge to molten at the fusion zone boundary. The significance of this observation to burnthrough is the resulting strength of the material beneath and surrounding the weld. While the penetration depth of all these welds is not overly significant, the size of the HAZ appears to be a significant reason for pipe wall failure. The strength of steel varies considerably with temperature. The yield strength of steel at $800^oC$ is only 4% of that at ambient [8]. Moreover, the elastic modulus of steel is also significantly lower. It is suggested that the significant size of the HAZ, leading to large regions where a considerable loss of strength is evident, is the primary reason for the deflections seen in Figure 6.2. Clearly, full penetration welding is not required for pipe wall failure.

## 6.3 Thermal elastic-plastic stress analysis of in-service welding

### 6.3.1 Introduction

The verification of the proposed in-service safe welding pressure model is clearly difficult as very little experimental data was found in the available open literature. An experiment to produce such data was briefly considered but was eventually not attempted due to the inherent problems with safety and as the financial costs were found to be prohibitive. However, an alternative method whereby simulating the initial stages of pipe wall failure using a thermal elastic-plastic analysis was considered. As simulating the distortion of structures was in general widely simulated using finite element methods, it was considered that with careful assumptions the simulation of in-service welding could also be attempted.

To verify this assumption, it was considered that the thermal elastic-plastic model should be directly compared with some data from experiments. The work undertaken by Wade [84] was compared against the elastic-plastic models to assess the limits of pressure for in-service welds with various heat input. The following sections will discuss the method

used to achieve the comparisons between numerical predictions and the results from the experiments performed by Wade.

### 6.3.2 Analysis

In Wade's [84] work, a number of longitudinal welds were deposited remotely on $300mm$ diameter $X60$ grade pipe with a wall thickness of $9mm$. To simulate the welding on thinner pipe, sections of the pipe were machined out to leave a wall thickness of $3, 5$ and $6mm$. The welds were deposited with 3.2 and $4.0mm$ diameter electrodes with target heat inputs of $1.0, 1.2, 1.6$ and $1.8kJ/mm$.

To determine the accuracy of the thermal elastic-plastic approach, four welds varying in heat input from $1.2 - 1.8kJ/mm$ were analysed using finite element methods. First, the temperature field for a longitudinal weld was calculated using a quasi-steady-state approach similar to that proposed earlier in Section 3.2.4 for the thermal analysis of circumferential fillet welding. A specialised computer program was developed to generate the mesh and apply the boundary conditions for forced and natural convection. The mesh generation used a method identical to that previously discussed for the thermal analysis of branch on pipe welds and circumferential fillet welding. Briefly, the mesh was considered to be a prismatic sweep along the direction of welding. The cross-section of the mesh consisted of material which represented the pipe, weld, reinforcing fin and the air gap between the fin and the pipe. The gap thickness was assumed to be a mean average of $0.25mm$, while the area of the weld bead was determined using empirical relationships of weld bead area and heat input as proposed earlier in Section 4.4. The dimensions of the fin were unknown, however, a width of $10mm$ and height of $50mm$ were assumed. The element type, material property variation with temperature, and solution method used for the analysis was identical to that used for the quasi-steady-state analysis of circumferential fillet welding as discussed earlier in Section 3.2.4.

An example of a typical temperature field resulting from a quasi-steady-state analysis

of a longitudinal weld can be seen in Figure 6.3: the temperature field for the entire joint can be seen in Figure 6.3(a), in addition the temperature field for the pipe alone can be seen in Figure 6.3(b) and 6.3(c).

The calculated thermal field was then used in a thermal elastic-plastic stress analysis. The material for the stress analysis was assumed to fit a linear stress strain relationship with a flow stress dependent on temperature. The analysis does not take into account any stresses developed due to thermal expansion as it was considered that these would not significantly influence the results. The variation of yield strength, $\sigma_y$, with temperature for the types of steels encountered in in-service welding can be seen in Figure 6.4. The numerical analysis was carried out using NISA [25] finite element code. Parabolic elements were used and a full Newton-Raphson iterative solution procedure was adopted. The temperature field was assumed steady and the internal pressure in the pipe was incremented through a range from 0 to $MAOP$. Deformation and stress were calculated at each pressure; a typical plot of radial deflection for a longitudinal welds using a thermal elastic-plastic analysis can be seen in Figure 6.5.

### 6.3.3 Results

The comparison between numerical predictions and experiments was achieved using two values of heat transfer coefficient at the inside surface of the pipe: $300W/m^2.K$ and that of still air. The failure criteria used by Wade was for the height of the bulge to exceed $1mm$; Wade had also measured the pressure at which the failure had occurred. The variation of radial deflection with pressure is readily available from the stress analysis, and was therefore compared with experimental measurements. The comparison between experiments and numerical predictions can be seen in Figure 6.6.

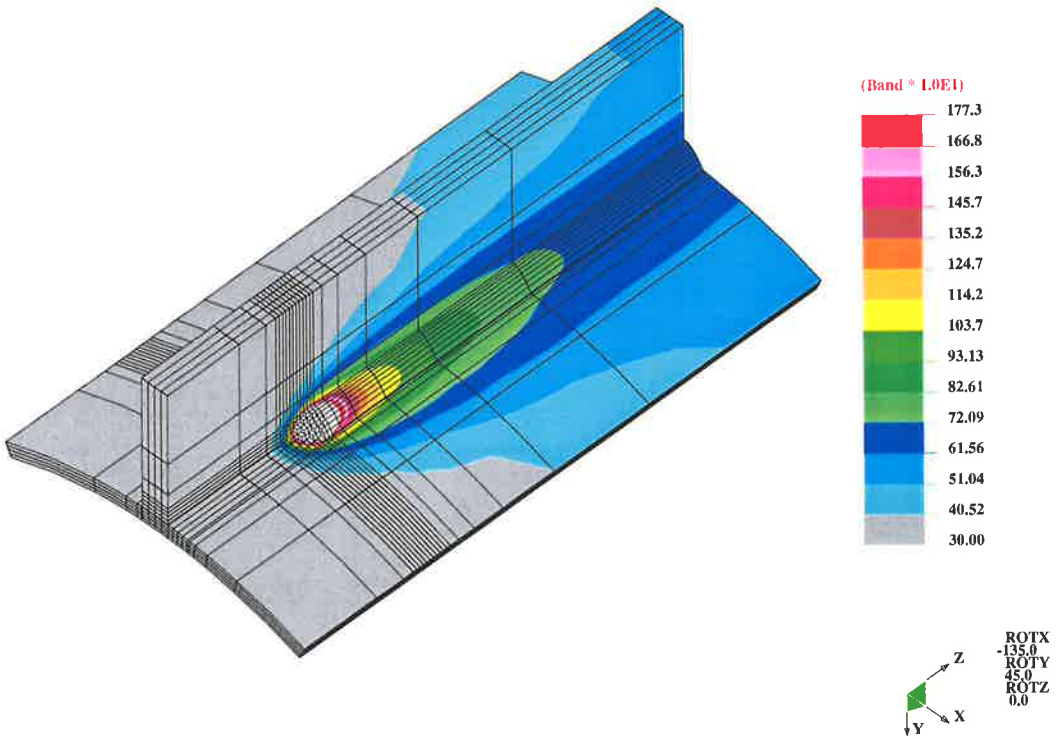


(a) An example of a temperature field due to in-service longitudinal fillet welding.

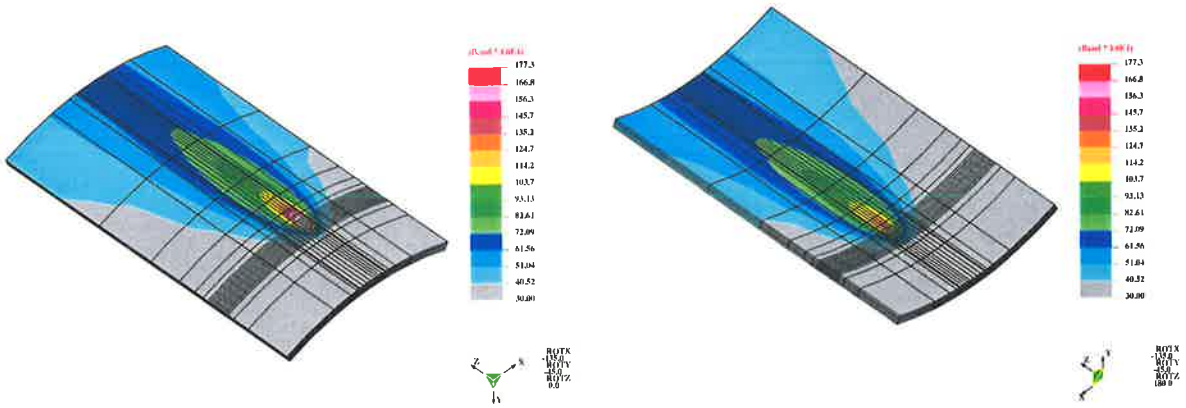

(b) Outside surface.

(c) Inside surface.

**Figure 6.3:** Typical temperature field for in-service longitudinal fillet welding.

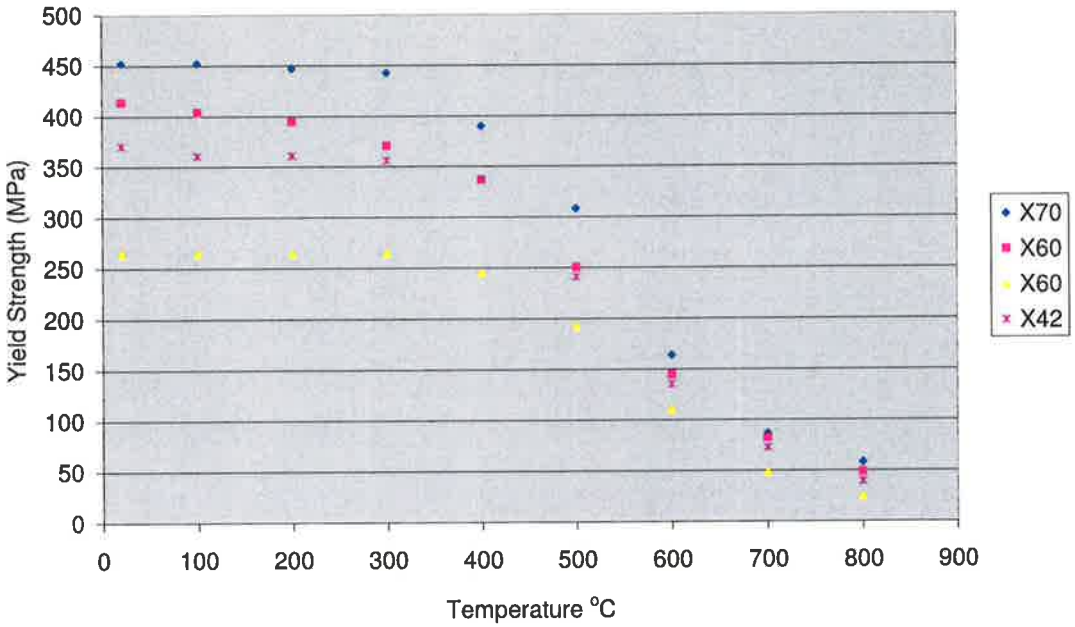


**Figure 6.4:** Variation of yield strength with temperature for different grades of pipeline steel.

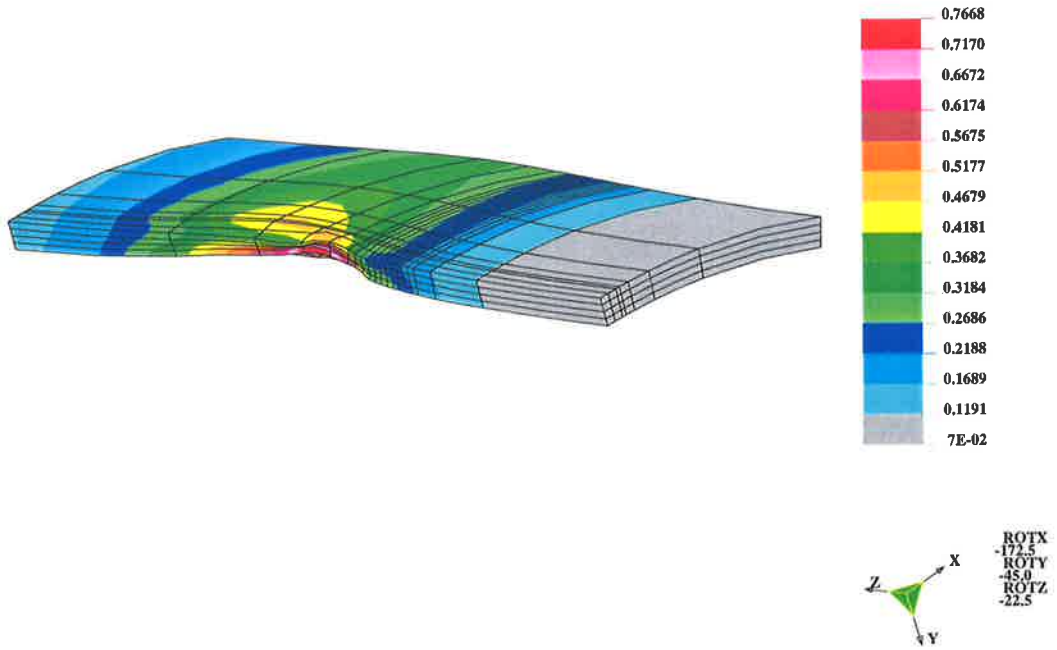


**Figure 6.5:** Typical radial deflection from a thermal elastic-plastic stress analysis of longitudinal welding of the type deposited in the work by Wade [84].

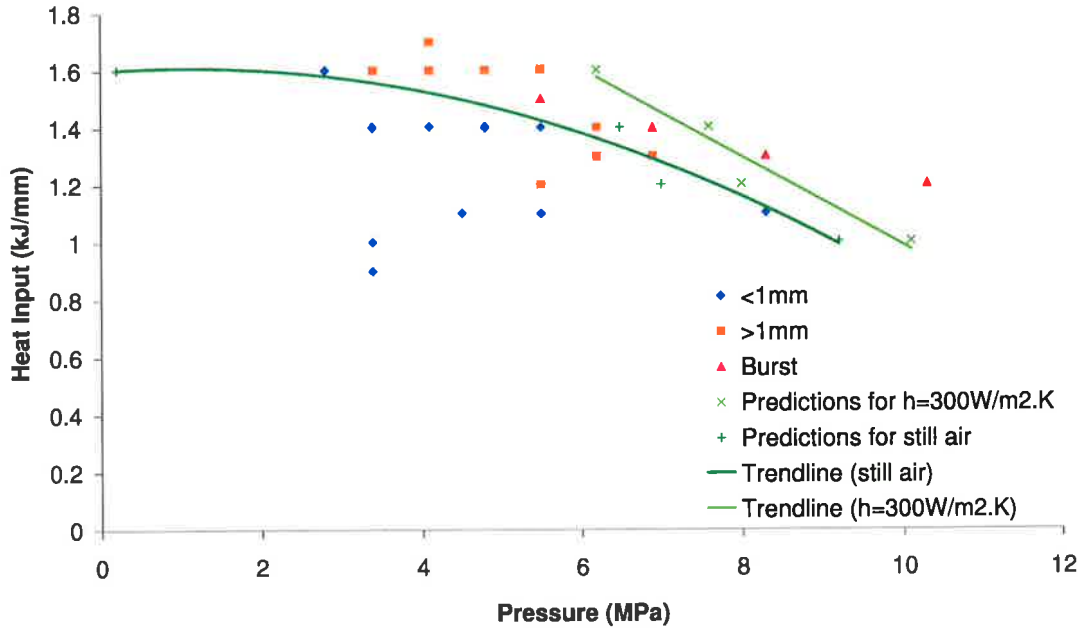


**Figure 6.6:** Comparison of predictions from thermal elastic-plastic analysis of longitudinal welds deposited under the work by Wade.

### 6.3.4 Discussion

The degree of accuracy attained from the numerical predictions is clearly not perfect, however the general trend of the data indicates reasonable accuracy. The effect of the stiffening fin in the model is considered to influence the numerical predictions. Clearly, the larger the width and height of the stiffening fin, the more rigid the structure will become. Moreover, the level of predicted radial deflection for a given pressure will also be influenced. The work reported by Wade does not state the dimensions of the stiffening fin, so some of the discrepancy between numerical predictions and measurements may be due to the stiffening fin. In addition, while the material used in the experimental work by Wade was stated as $X60$ therefore implying a specified minimum yield strength, the variation of yield strength with temperature for the pipe used in the experiments is unknown. The variation of yield stress with temperature chosen for the stress analysis is considered to largely reflect the type of material used in the experimental work by Wade, however, any difference between them is considered to account for a moderate proportion of the discrepancy between numerical predictions and measurements.

### 6.3.5 Conclusions

The used of a thermal elastic-plastic model to simulate in-service welding with reasonable accuracy has clearly been demonstrated. In addition, the combination of a predicted temperature field using a quasi-steady-state analysis with a elastic-plastic stress analysis to form a method of predicting the early stages of pipe wall failure with reasonable accuracy has been demonstrated.

Whilst is has been demonstrated that a thermal elastic plastic model can be used to predict the safe operating pressure to avoid burnthrough, such models are computationally expensive. Solution times are long and they may not yet be a practical tool that welding engineers can use to determine safe welding conditions. Alternatively, approximate methods have been proposed by Bout & Gretskii [8]. These approximate methods seek to make the weakening of the pipe wall during in-service welding equivalent to a localised cavity in the pipe wall. They then used empirical equations such as B31G (relationships between cavity geometry and bursting pressure) to estimate safe operating pressures. The thermal field is used to estimate equivalent cavity dimensions, hence a thermal elastic-plastic stress analysis is avoided. To examine the development, accuracy and potential of this approach, the accuracy of the B31G criteria is assessed.

## 6.4 Verification of B31G corrosion cavity model

### 6.4.1 Introduction

The development of models which predict the safe operating pressure for a pipeline with corrosion cavities has been of significant use for the pipeline industry; a number of models, varying in sophistication have been developed over the years. Of particular note is the B31G model which has been successfully implemented in the American Society for Mechanical Engineers code, and the more recent work by Vieth & Kiefner [82] (1993) in developing their computer program, RSTRENG. In Australia, the B31G code, as found

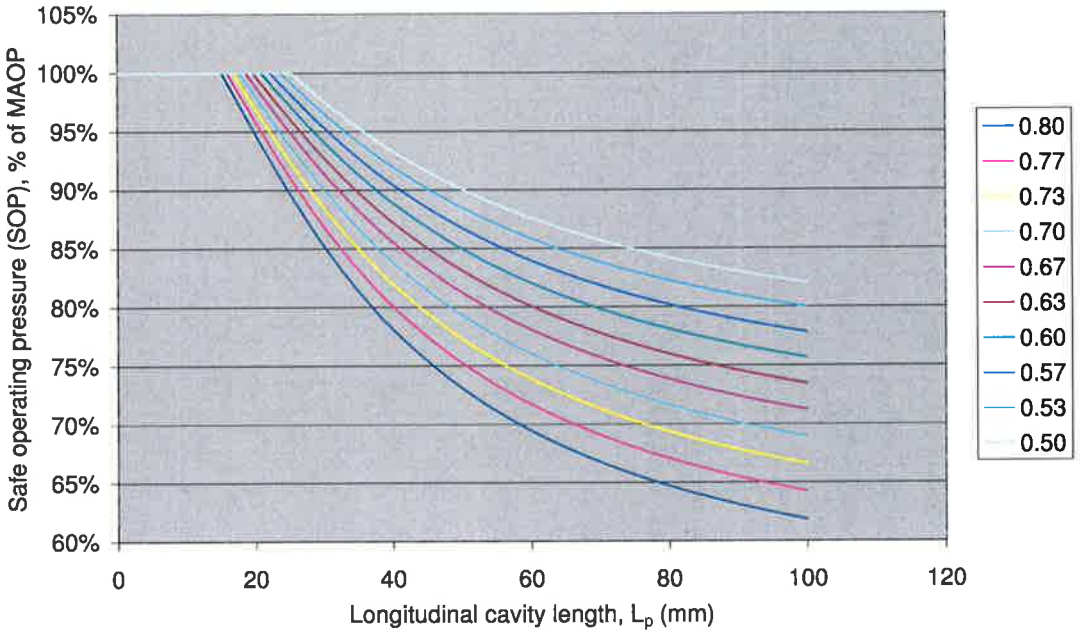


**Figure 6.7:** Variation of B31G (AS2885) corrosion cavity predictions ($SOP$) with cavity depth ratio ($dc/dn$) (coloured lines) and longitudinal cavity length ($L_p$), for a $300mm$ diameter, $3.0mm$ wall thickness pipe.

in AS2885 is successfully used in the field. However, findings by Vieth & Kiefner suggests that the model can be overly conservative. Development of the $RSTRENG$ program resulted in the modified B31G criterion in an effort to remove the conservative nature of the original B31G model. However, as the new model has not yet been incorporated in the standard, the B31G model was chosen to be included in the overall cavity model.

### 6.4.2 Comparison

The range in which the B31G model is suggested to be applied for is for cavity depths less than 80% of the wall thickness of the pipe. In addition, a limit is placed on the minimum dimension of the longitudinal length of a given cavity which, in turn, is a function of pipe diameter; if a given cavity has a longitudinal length below this limit, the B31G model suggests to operate the pipeline at MAOP. The limits in which the model was developed for can be seen in Figure 6.7. The results from the model is the ratio, $pc/pd$, which is the safe operating pressure as a fraction of the MAOP of the pipe.

A number of shortcomings of the B31G model was realised. The exclusion of circumferential cavity dimension was considered to be important. As in-service welding is most often achieved using circumferential filet welding, the resulting cavity dimensions are in general longer in the circumferential direction than the longitudinal direction. The limitations of the B31G model due to the limit in longitudinal cavity length is minor compared to the model's disregard for circumferential cavity length. Clearly, the B31G models does not consider the impact of circumferential cavity length and therefore does not involve the dimensions in the calculation of a safe maximum operating pressure. It is suggested that a cavity which is primarily longitudinal in shape is more likely to cause pipe wall failure than a cavity with identical depth, but larger circumferential dimensions due to the stress field within the pressurised pipe. The B31G model also effectively assumes that for a given cavity, if the longitudinal length of the cavity were below a certain limit (where the limit is a function of diameter, wall thickness and cavity depth), then pressure reduction is not required. With the aforementioned omission of circumferential cavity length it is suggested that the model may in some instances over predict the safe operating pressure; clearly a potentially dangerous situation. Finally, the limitation of the B31G model to cavity depth is considered to be significant to the proposed equivalent cavity model. As discussed earlier in the literature review, Bout & Gretskii had argued that it was possible to weld onto a pipe with dramatically reduced wall thickness provided that adequate support was placed around the region of reduced thickness. The support of the adjacent pipe wall to regions of reduced thickness found in corrosion cavities can be considered as having been reinforced by the surrounding uncorroded material. The B31G model was considered to be conservative to limit the cavity depth.

### 6.4.3 Analysis

To determine the accuracy of the B31G model, a number of corrosion cavities were analysed using a numerical model. The cavities were considered to be ideal as they were of a cosine shape and therefore did not have any distinct edges. The cavity was approximated

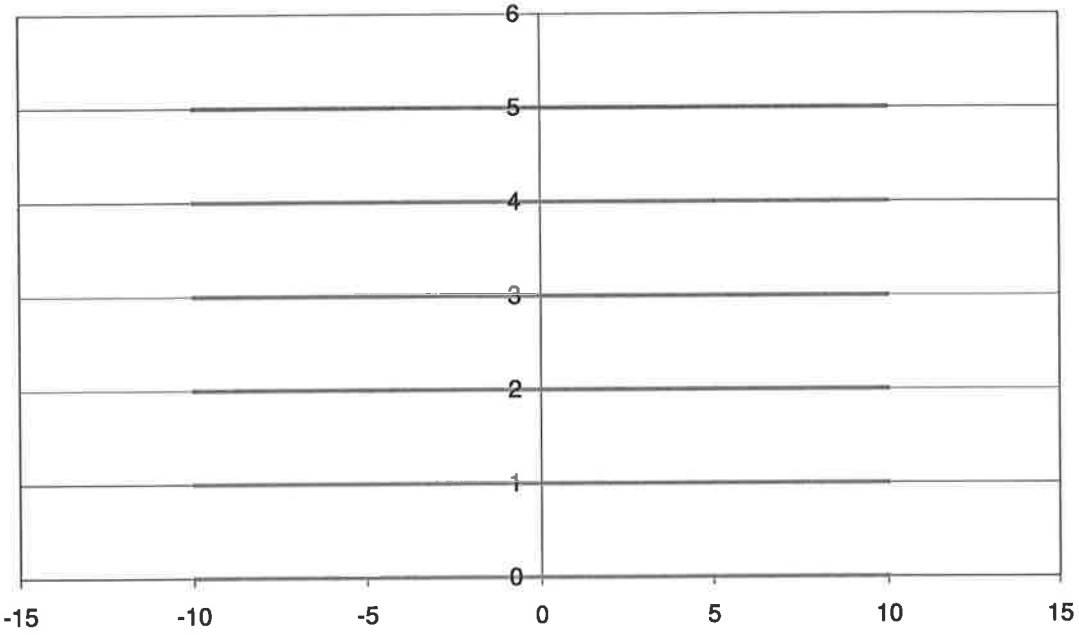


(a) Two-dimensional mesh.

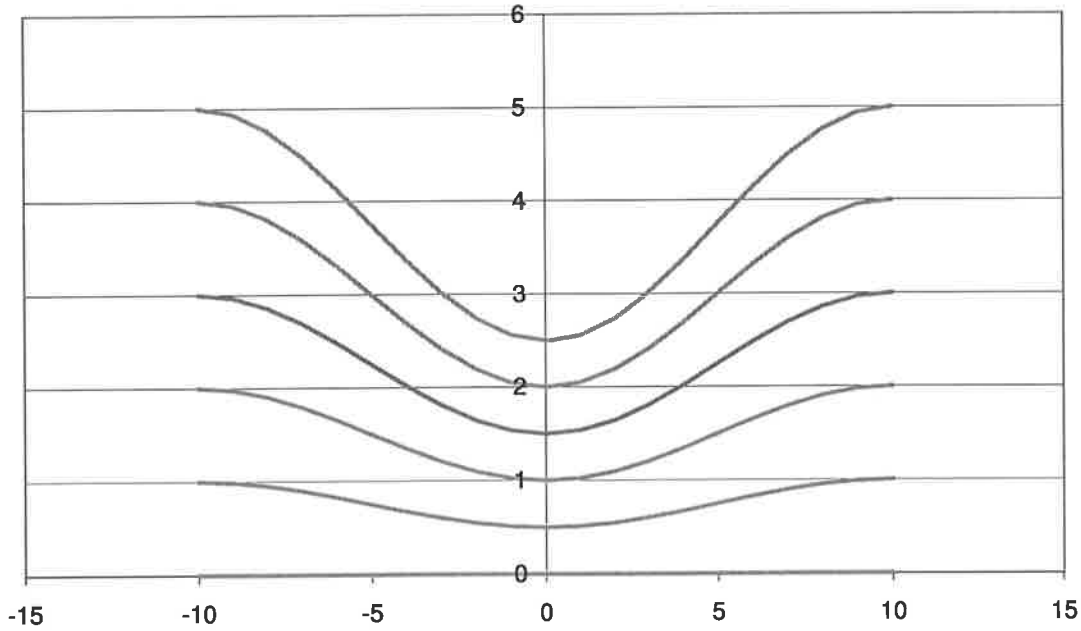


(b) Two-dimensional mesh modified.

**Figure 6.8:** Example of mesh modifications to create a idealised cavity model.

as a finite element mesh of a quarter section of pipe with the idealised cavity. An example of the modifications made to a 2D mesh can be seen in Figure 6.8. A program was written to modify a mesh of a quarter section of pipe by placing in it a cavity of known dimensions. The cavity dimensions which could be specified are circumferential length,

longitudinal length and cavity depth. The finite element mesh was for a quarter section of pipe and consisted of parabolic elements. The distribution of elements in the mesh was such that greater mesh density was found in the cavity and in the surrounding regions were large deformations were expected. An example of a idealised cavity finite element mesh can be seen in Figure 6.9. The element type and solution method used is identical

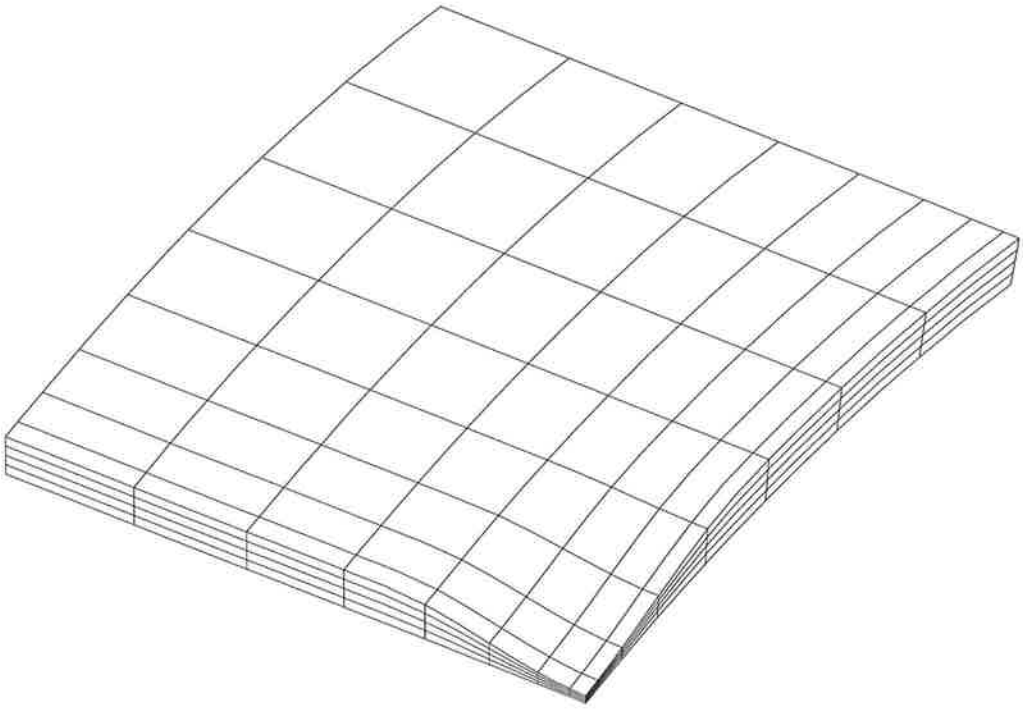

**Figure 6.9:** Example FE mesh for idealised cavity analysis.

to that chosen for the thermal elastic-plastic analysis of longitudinal welds as discussed earlier in Section 6.3.

The deformation of the cavity was determined from the elastic-plastic stress analysis by measuring the maximum radial deflection at the centre of the cavity. While the failure criterion defined by Wade was initially considered, two alternative failure criterion were adopted to examine the accuracy of the B31G calculation. The first criterion can be considered as an effective yield pressure or the point where the model departs from linear behaviour. This criterion was applied by measuring the location where a line of the same slope as the bottom of a given deflection curve, except offset by 0.02%, would intersect

the deflection curve. The second criterion was the pressure at which the von Mises stress at the bottom of the cavity would exceed the yield strength of the pipe.

### 6.4.4 Results & Discussion

#### 6.4.4.1 Varying longitudinal cavity length

The B31G model appears to be primarily developed for corrosion cavities which are in general oriented in the longitudinal direction; i.e. the length of the cavity in the longitudinal direction is the largest dimension. The verification of the B31G model using the proposed idealised cavity analysis was initially achieved by solving for models with a circumferential cavity length of $3.75mm$ and then $26.25mm$; both sets of models has a cavity depth of $dc/dn = 0.8$. The longitudinal cavity length was varied from $15mm$ to $30mm$. The prediction of varying maximum radial deflection with pressure can be seen in Figure 6.10: for cavities with a circumferential cavity length of $3.75mm$, the variation of maximum radial deflection with pressure can be seen in Figure 6.10(a), while the plot of maximum radial deflection against pressure for a cavities with a longitudinal dimension of $26.25mm$ can be seen in Figure 6.10(b).

The results indicate that as the longitudinal length of the cavity is increased, so does the increase in radial deflection for a given pressure. The models indicate clearly a very small increase in radial deflection with pressure for a cavity with a circumferential cavity length of $3.75mm$. However, for models with a circumferential cavity length of $26.25mm$, the change in maximum radial deflection with pressure is clearly more obvious and dramatic. The resulting trend from the finite element idealised cavity analysis model is in agreement with that predicted by the B31G model.

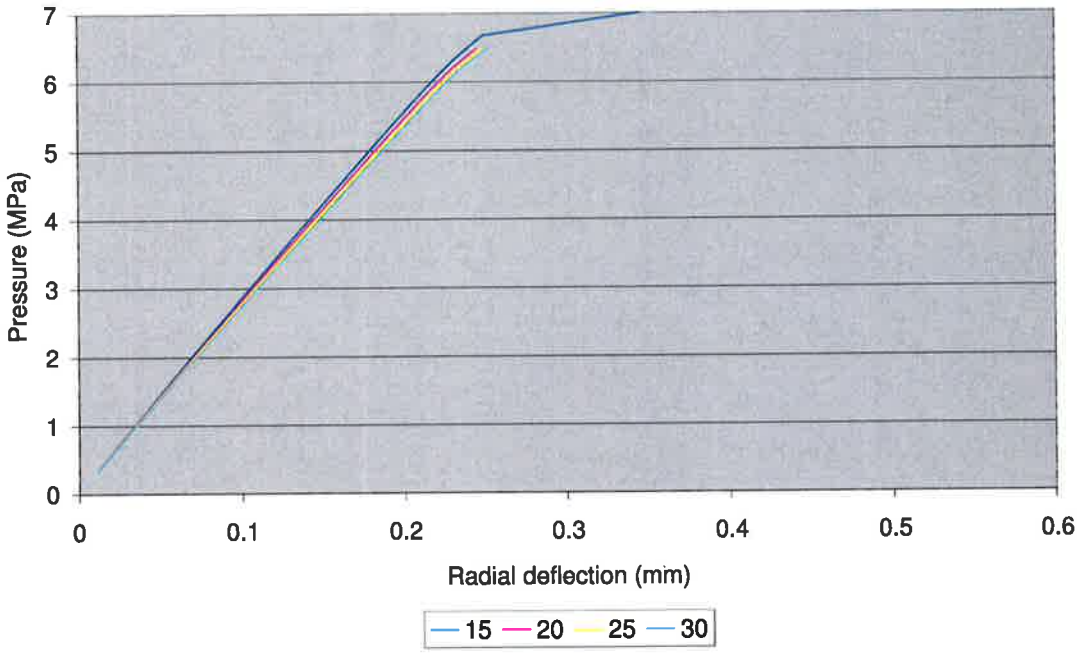


(a) $L_c = 3.75, dc/dn = 0.8.$

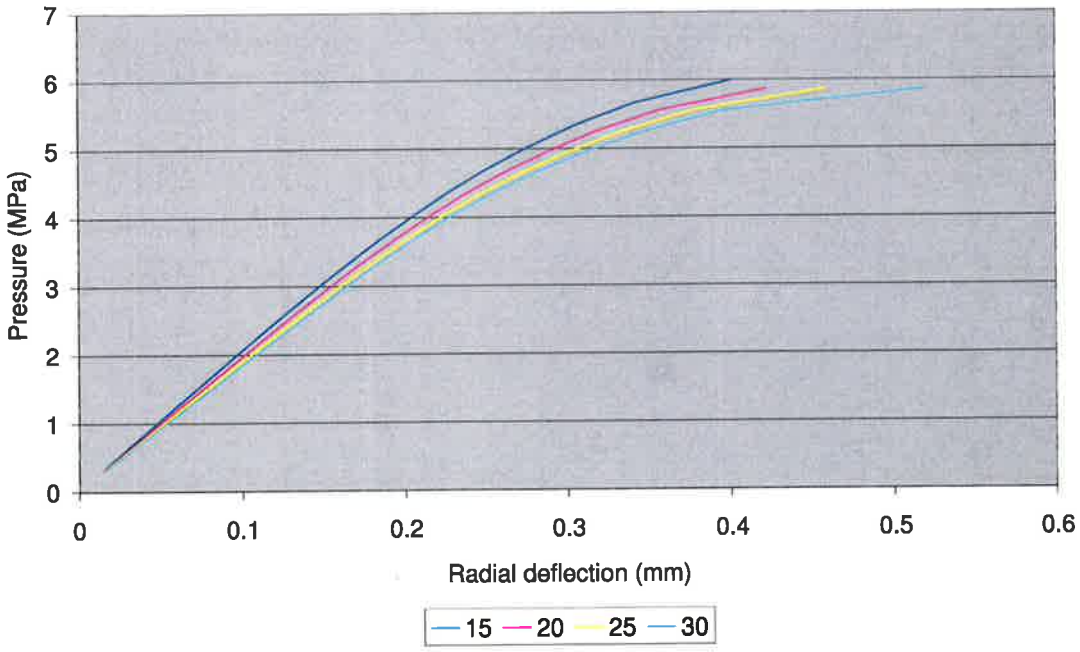


(b) $L_c = 26.25mm, dc/dn = 0.8.$

**Figure 6.10:** Variation of radial deflection with internal pressure for different longitudinal (coloured lines (mm)) and circumferential cavity lengths ($L_c$).

#### 6.4.4.2 Varying circumferential cavity length

The variation of maximum radial deflection with pressure for a cavity with longitudinal dimension of $12.5mm$, cavity depth of $dc/dn = 0.8$ and varying circumferential cavity length was initially determined using the idealised cavity analysis. The motivation was to examine the level of optimism which the B31G model may have had. The circumferential length of the cavity was varied from $5mm$ to $50mm$. The resulting plot of predicted maximum radial deflections against pressure can be seen in Figure 6.11. Clearly the

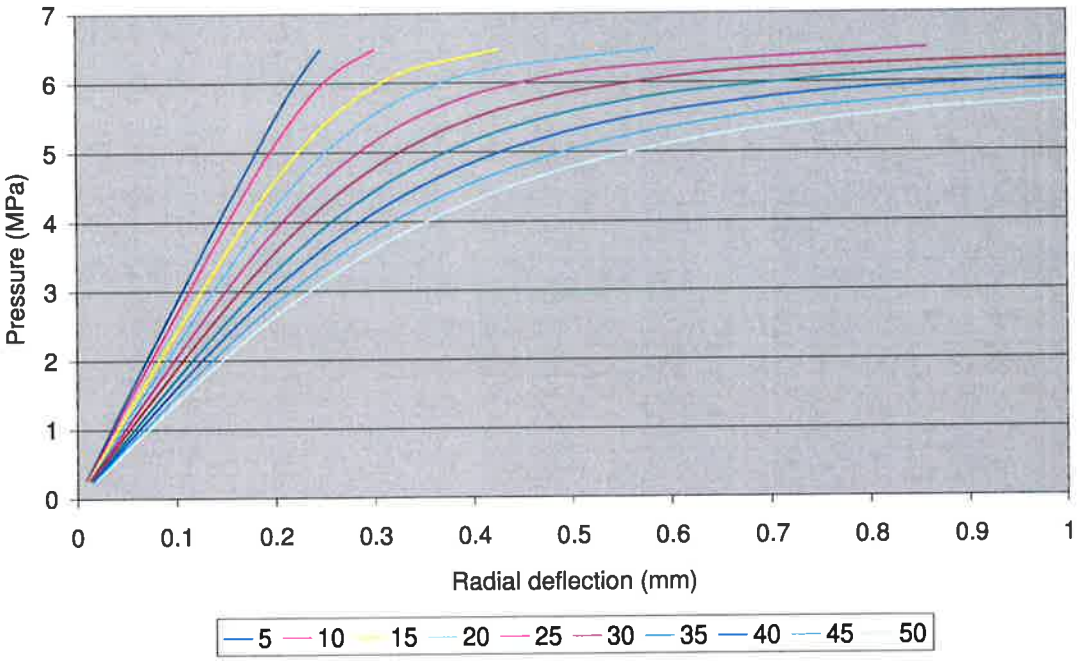


**Figure 6.11:** Variation of radial deflection with pressure and circumferential cavity length (coloured lines ($mm$)) for cavities with longitudinal length, $L_p = 12.5mm$, and cavity depth, $dc/dn = 0.8$.

influence of circumferential cavity length on the deformation of the cavity is significant. As the size of the circumferential dimension of the cavity is increased, the level of radial deflection is also increased for a given pressure.

The behaviour of a cavity for varying circumferential cavity length was also determined for cavities which had a longitudinal length of 15 and $30mm$, with a cavity depth of $dc/dn = 0.8$. For these models, the circumferential cavity length was varied from $3.75mm$ to $26.25mm$. The variation of maximum radial deflection with pressure can be

seen in Figure 6.12. For cavities with a longitudinal length of $15mm$, the variation in maximum radial deflection with pressure can be seen in Figure 6.12(a), while the variation in maximum radial deflection with pressure for cavities with a longitudinal length of $30mm$ can be seen in Figure 6.12(b). As observed with the earlier analysis, the deformation of the cavity is significantly influenced by its circumferential length.

Two criteria defining failure are proposed: the pressure where the von Mises stress exceeds the yield stress, and the pressure where the radial deflection is considered to have departed from linear behaviour. A straight line with the slope equal to that at the start of a given radial deflection curve, except offset by 0.02% or a millimetre is superimposed on the graph; for example, consider the hypothetical example seen in Figure 6.13. Where the radial deflection curve intersects the line is considered to be the point where the departure from linear behaviour had occurred. The pressure at the intersection is defined as the failure pressure based on the linear departure failure criteria.

The comparison of the safe operating pressure calculated using the B31G relationship and that predicted using the idealised cavity analysis can be seen in Figure 6.14. Clearly, with increasing circumferential cavity length, the safe operating pressure is diminished. The optimistic nature of the B31G models has clearly been demonstrated.

#### 6.4.4.3 Cavity depth

A number of calculations involving pressurised idealised cavities with depths exceeding $dc/dn = 0.8$ was attempted to further investigate the level of potential conservatism within the B31G model. A set of calculations were initiated involving an idealised cavity with a longitudinal length of $12.5mm$ and a cavity depth of $dc/dn = 0.95$. The circumferential cavity length was varied from $5 - 50mm$. The results showing the variation of maximum radial deflection with pressure for the tests can be seen in Figure 6.15. The trend observed for the cavities is similar to that discussed for idealised cavity experiments with a depth of $dc/dn = 0.8$ earlier in Section 6.4.4.2

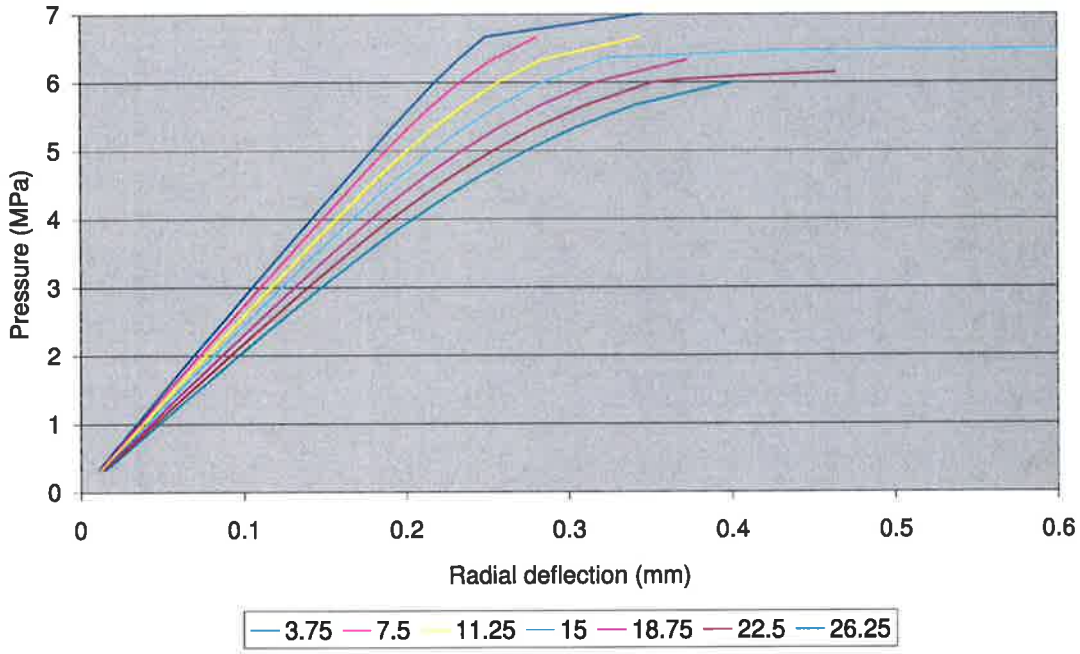


(a) $L_p = 15mm, dc/dn = 0.8$.

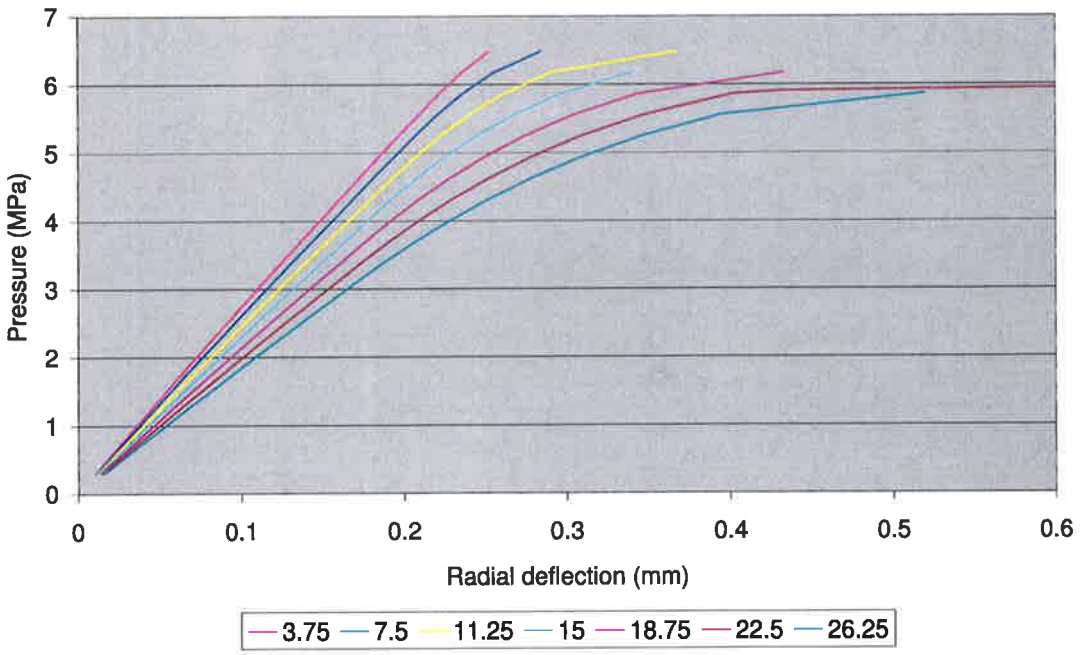


(b) $L_p = 30mm, dc/dn = 0.8$.

**Figure 6.12:** Variation of radial deflection with internal pressure for different longitudinal, $L_p$, and circumferential cavity lengths, $L_c$ (coloured lines ($mm$)).

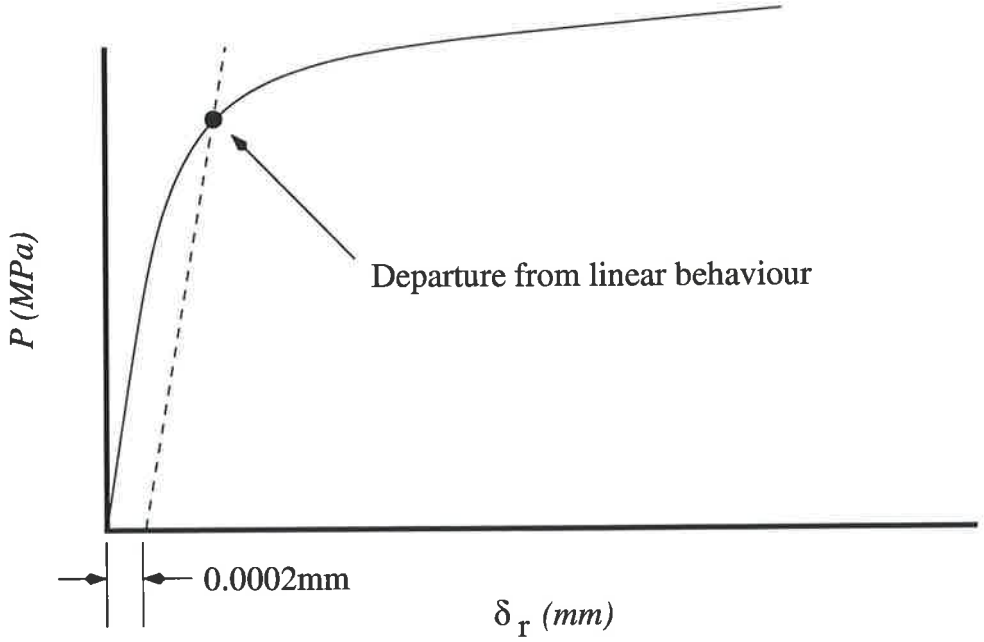


**Figure 6.13:** Linear departure failure criteria.

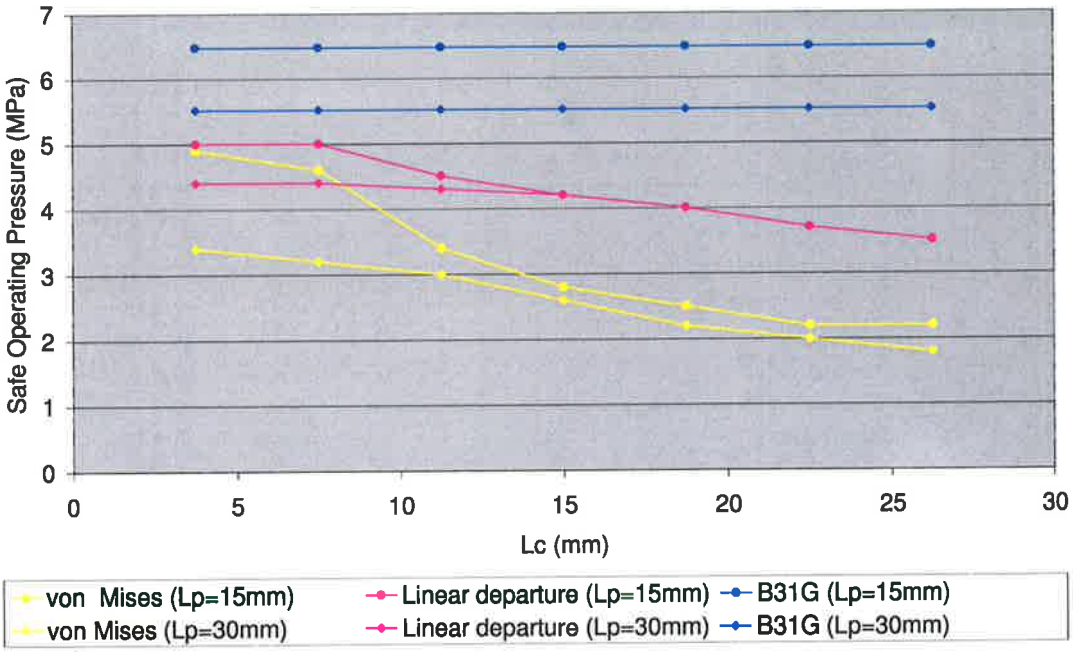


**Figure 6.14:** Comparison of safe operating pressure predicted using B31G criterion and the idealised cavity models for a cavity with $dc/dn = 0.8$.

A second set of calculations determined the strength of a cavity for different cavity depths; with cavity depth varied from $dc/dn = 0.8$ to $dc/dn = 0.95$. The cavity length in the longitudinal directions was fixed at $12.5mm$ while the circumferential cavity length was either $5mm$ or $50mm$. The results from these calculations may be found in Figure 6.16: for

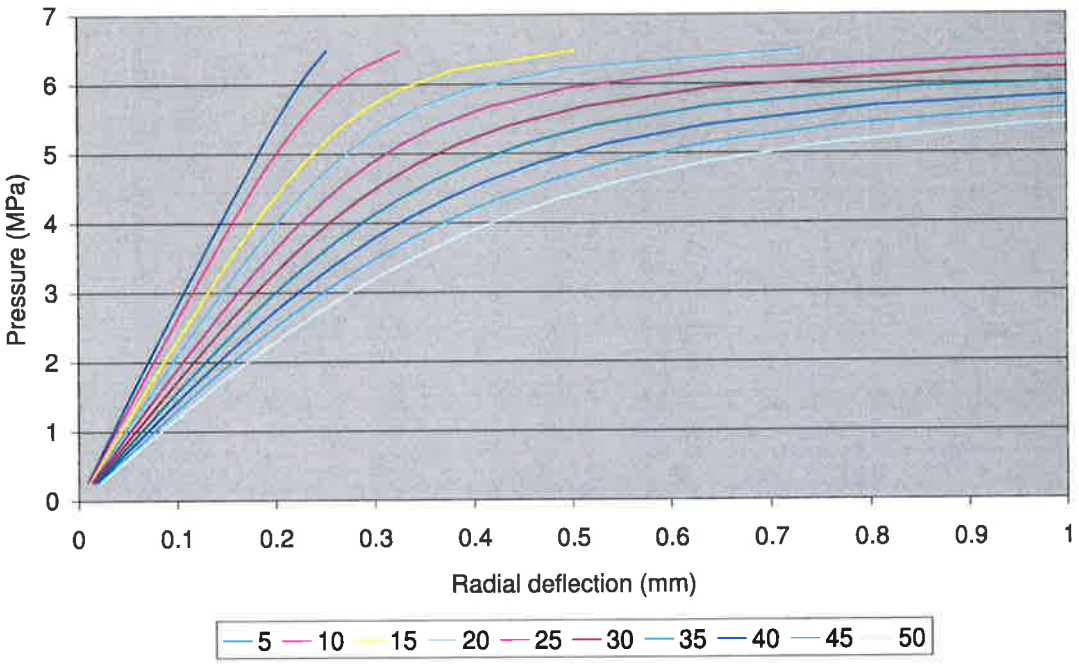


**Figure 6.15:** Variation of radial deflection with pressure and circumferential cavity length, $(L_c)$ (coloured lines $(mm)$), for cavities with longitudinal length, $L_p = 12.5mm$, and cavity depth, $dc/dn = 0.95$.

a cavity with a circumferential length of $5mm$, the variation of maximum radial deflection with pressure for different depths, $dc/dn$, can be seen in Figure 6.16(a), while similarly the results for a cavity with a circumferential length of $50mm$ can be seen in Figure 6.16(b). The variation of maximum radial deflection with cavity depth was negligible for a cavity with a circumferential length of $5mm$. The variation of maximum radial deflection with cavity depth was more prominent for a circumferential cavity length of $50mm$. With increasing circumferential cavity length, the corresponding maximum radial deflection for a given gas pressure is increased, and the safe operating pressure is reduced. Again the B31G model does not account for increased circumferential length and would predict a constant safe operating pressure for these cavities; in this case, the maximum allowable operating pressure.

An example of the predicted safe operating pressure for cavities with $dc/dn = 0.95$ using the idealised cavity analysis can be seen in Figure 6.17. Clearly, there does exist some scope for safe operation of a hypothetical pipeline with a cavity depth of $dc/dn = 0.95$.

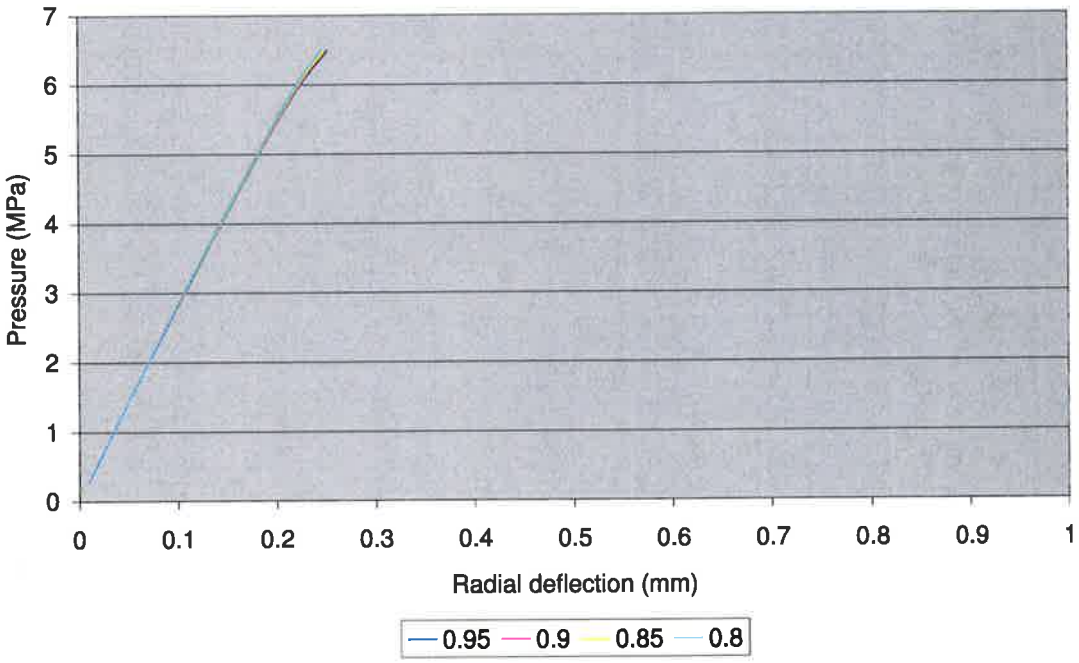


(a) $L_p = 12.5mm, L_c = 5mm.$

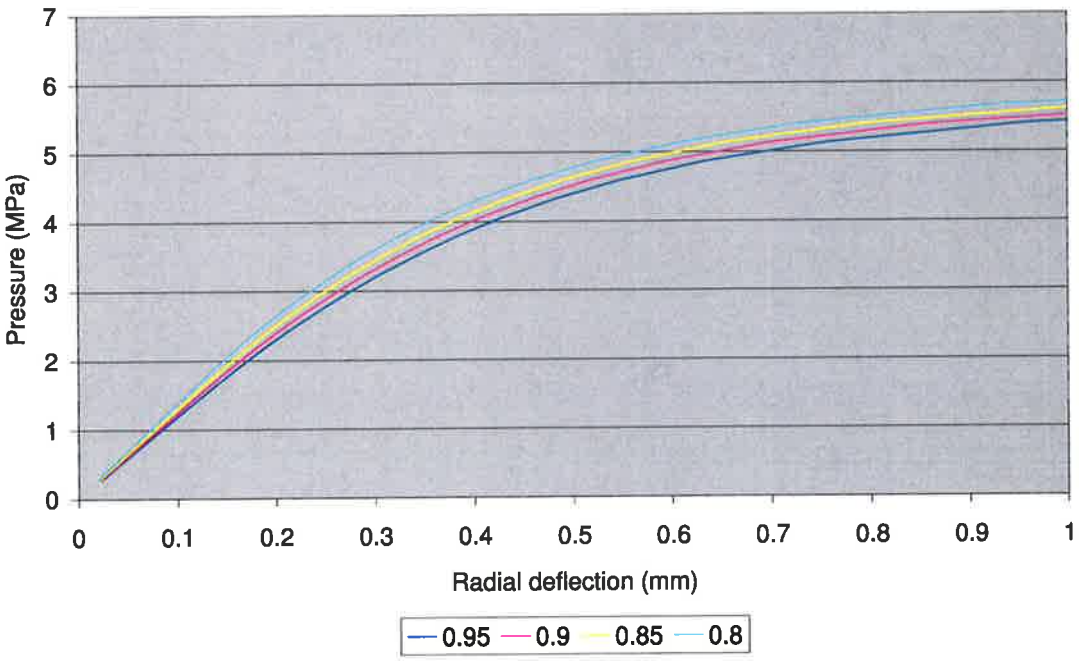


(b) $L_p = 12.5mm, L_c = 50mm.$

**Figure 6.16:** Variation of radial deflection with internal pressure for different cavity depths ($dc/dn$) (coloured lines).

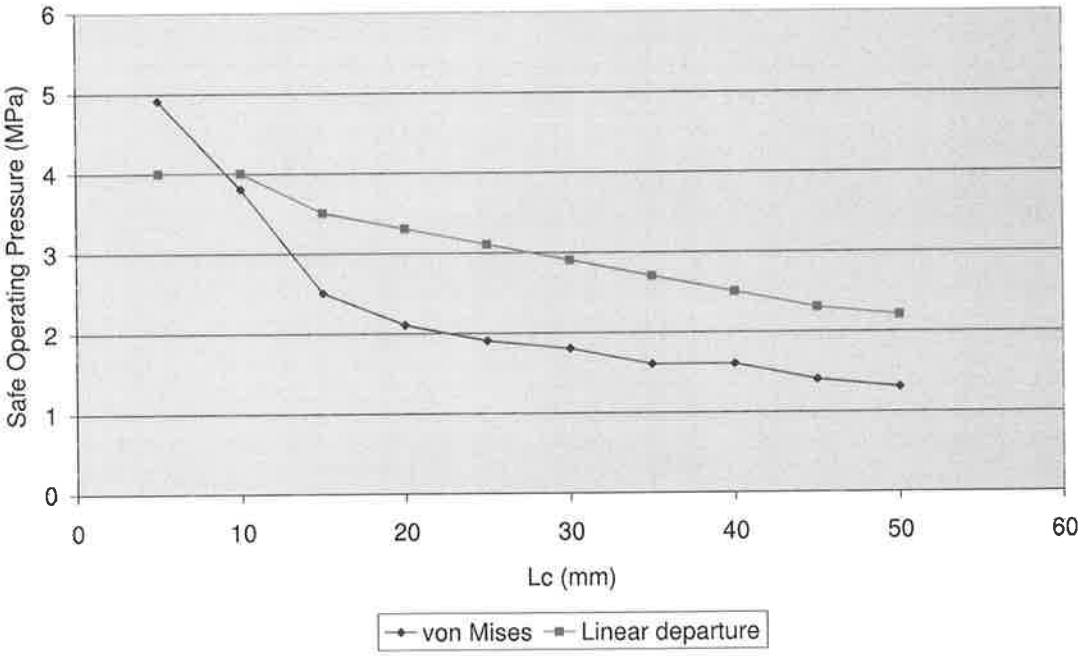


**Figure 6.17:** Predicted safe operating pressure for cavities with $dc/dn = 0.95, L_p = 12.5mm$.

### 6.4.5 Conclusions and recommendations

The comparison of predictions of safe operating pressure using the B31G analysis with those using elastic-plastic stress analysis models has demonstrated that the B31G model can clearly over predict the safe operating pressure as the circumferential cavity length is not included. It has been observed that as circumferential cavity length is increased, the accuracy of the B31G model is decreased. However, the conservative nature of the B31G model has also been demonstrated; clearly the operation of a pipeline with a cavity exceeding $dc/dn = 0.8$ has been demonstrated. The results indicate that the safe operating pressure of a pipe containing a single cavity will depend on:

- the remaining wall thickness
- the cavity width perpendicular to the hoop stress
- and the circumferential length.

Because the B31G criteria does not account for circumferential length, it may over predict safe operating pressures; clearly examples of this occurring has been demonstrated within

this thesis.

## 6.5 Verification of equivalent cavity model

### 6.5.1 Introduction

Predicting the onset of burnthrough, in general, requires a reasonably involved calculation. Historically, as discussed earlier in Section 2.2.2, a number of models have been proposed, in an effort to minimise and simplify such a calculation. However, each of the proposed models has significant disadvantages, a summary of which can be found earlier in Section 2.2.2.1. Predicting the onset of burnthrough is possible using the generally accepted finite element thermal elastic-plastic stress analysis. However, such a model is highly computationally intensive. The equivalent cavity model allows the calculation of a failure pressure, purely on the thermal field of a given in-service weld. Such a thermal field, can be easily and quickly calculated, using either of the models proposed earlier in Chapter 3. The equivalent cavity model, in addition to existing aforementioned maximum pressure pipeline defect models, allows the calculation of a maximum pressure, at which welding is considered safe, for the given thermal field, or, heat input of welding. The following sections will discuss the results of tests using thermal elastic-plastic models of in-service welds to assess the accuracy of the equivalent cavity model.

### 6.5.2 Results & comparison

A number of welds varying in heat input were chosen to form a comparison between thermal elastic-plastic models and the equivalent cavity model. The equivalent cavity model was calculated by excluding all material above $980°C$, or as illustrated in Figure 6.18, while the thermal elastic plastic analysis was achieved using the method discussed earlier in Section 6.3. The temperature field was calculated from a quasi-steady-state analysis of a circumferential fillet weld. An example of a typical temperature field resulting from a

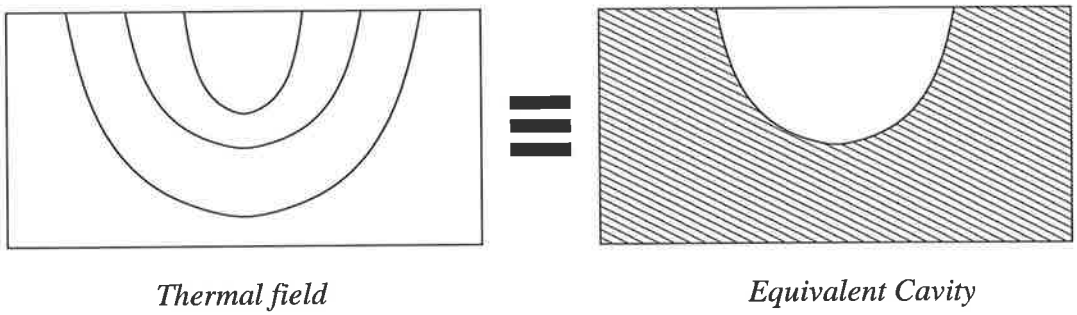


**Figure 6.18:** Equivalent cavity model.

quasi-steady-state analysis can be seen in Figure 6.19: the temperature field for the entire joint can be seen in Figure 6.19(a), in addition the temperature field for the pipe alone can be seen in Figure 6.19(b) and 6.19(c).

An example of a typical result from a thermal elastic-plastic stress analysis of an in-service weld can be seen in Figure 6.20, while the corresponding result of a elastic-plastic stress analysis of the corresponding equivalent cavity of the same weld can be seen in Figure 6.21.

The comparison of six welds with increasing heat input can be seen in Figure 6.22. The graphs shows the variation of radial deflection against pressure for a node which displayed the greatest deflection in each respective calculation. In addition, to aid comparison and discussion, a similar plot is also presented for a pipe at ambient temperature and without a cavity.

The results indicate that in general, the cavity model over predicts the level of radial deflection for a given pressure. Moreover, with increasing heat input, this trend is more significant. A significant observation is the difference in behaviour between the equivalent cavity and thermal elastic-plastic models during the initial application of pressure ($0 - 4MPa$). There is very little difference in the variation of radial deflection with pressure, with different heat input, for the thermal elastic-plastic models. However, the influence of heat input is significant on the variation of radial deflection with pressure for the cavity model, during this initial application of pressure. Moreover, this difference in behaviour between the two models is clearly more pronounced during the latter application

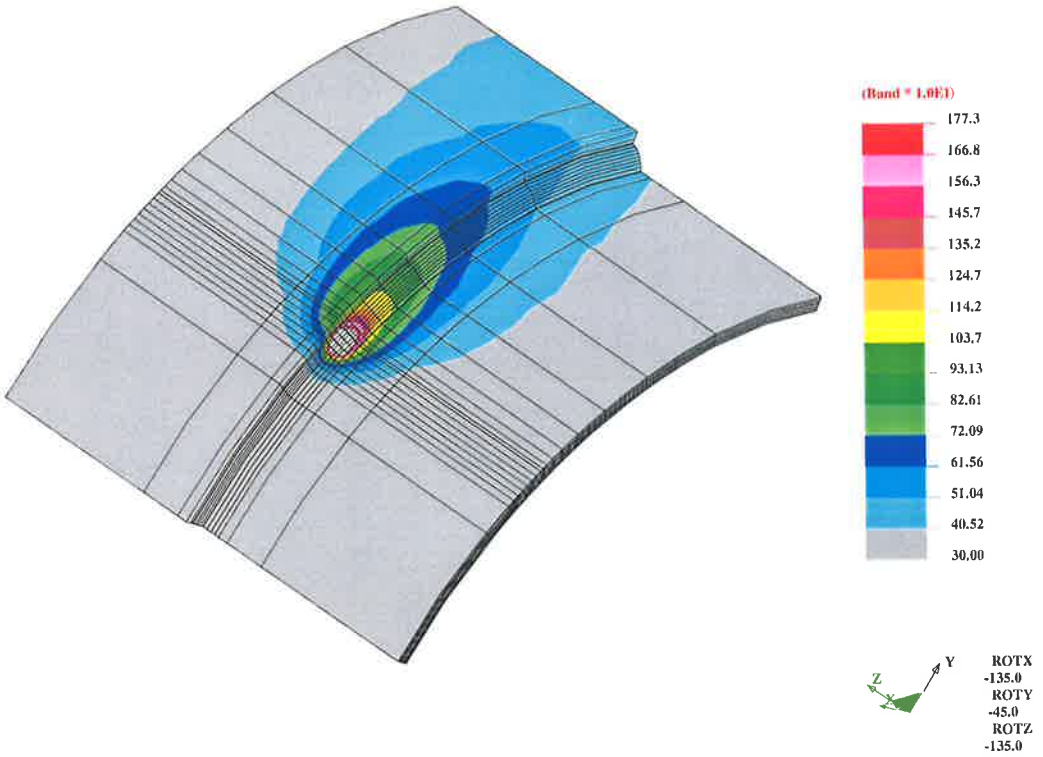


(a) An example of a temperature field due to in-service circumferential fillet welding.

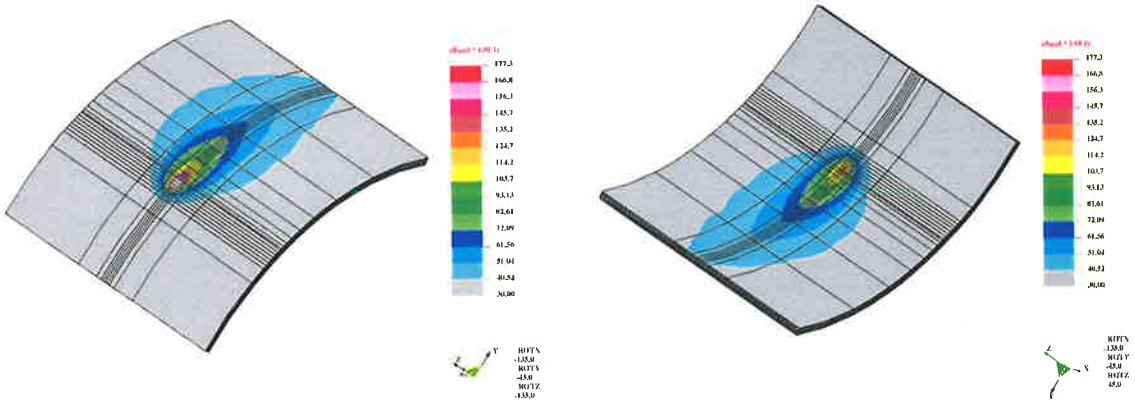

(b) Outside surface.

(c) Inside surface.

**Figure 6.19:** Typical temperature field for in-service circumferential fillet welding.

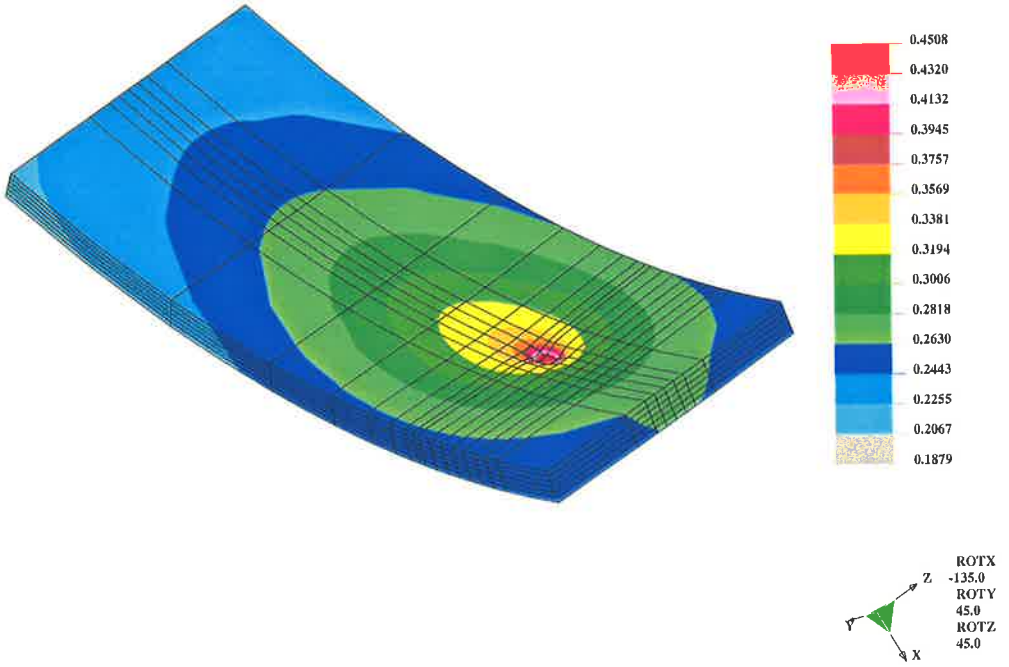


(a) Inside view

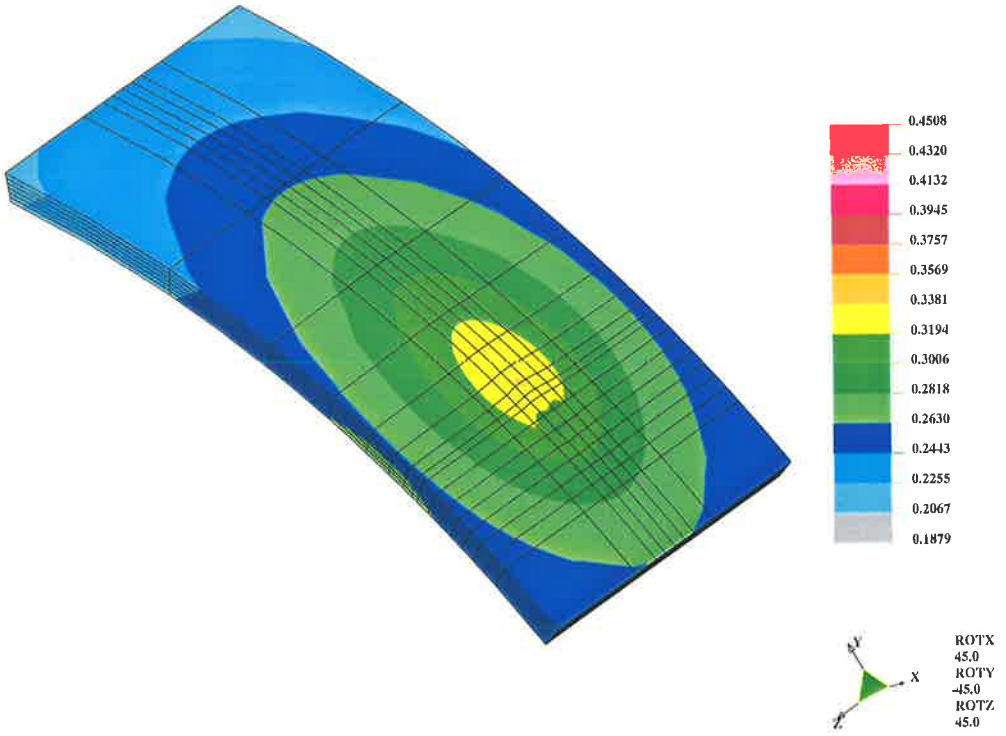


(b) Outside view

**Figure 6.20:** Example plot of radial deflection from thermal elastic-plastic FEA models.

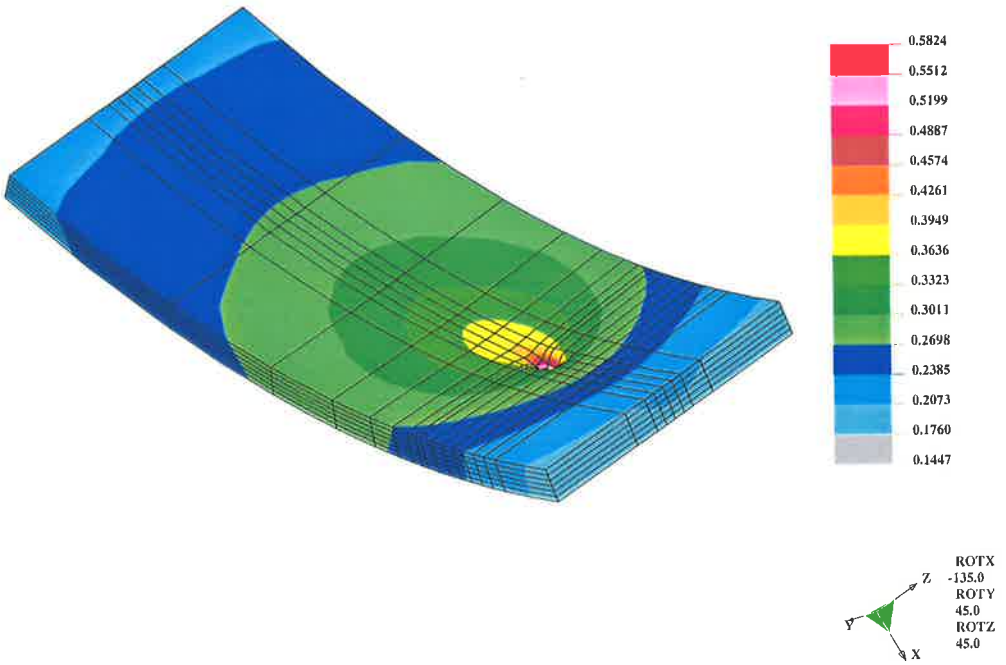


(a) Inside view (10x deflection magnification)

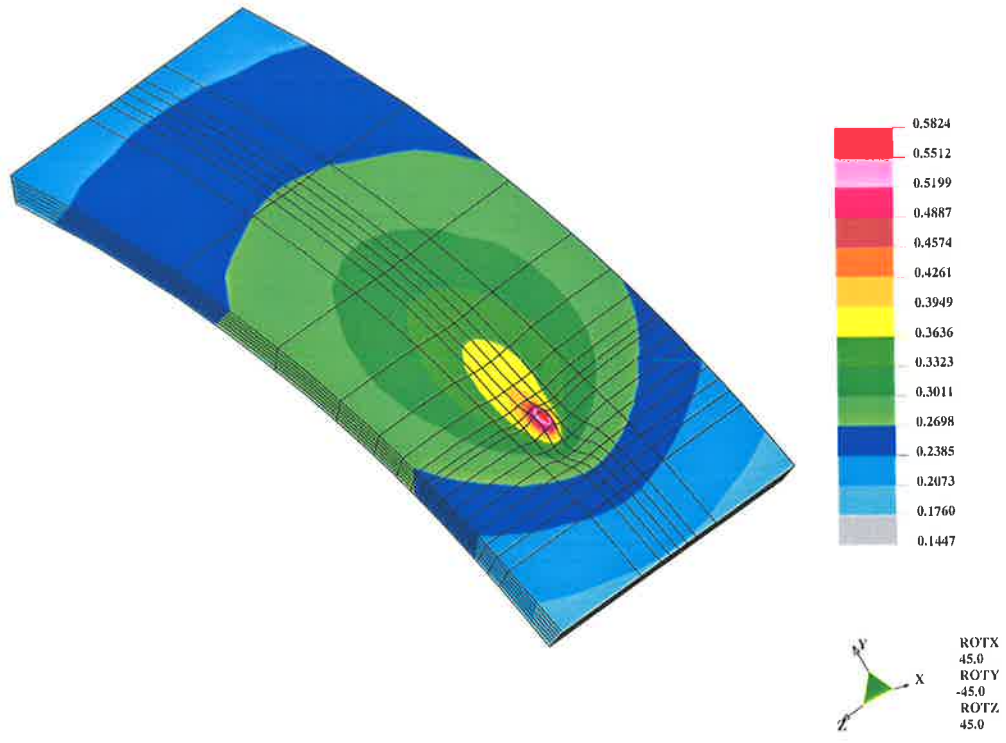


(b) Outside view (10x deflection magnification)

**Figure 6.21:** Example plot of radial deflection from equivalent cavity elastic-plastic FEA models.

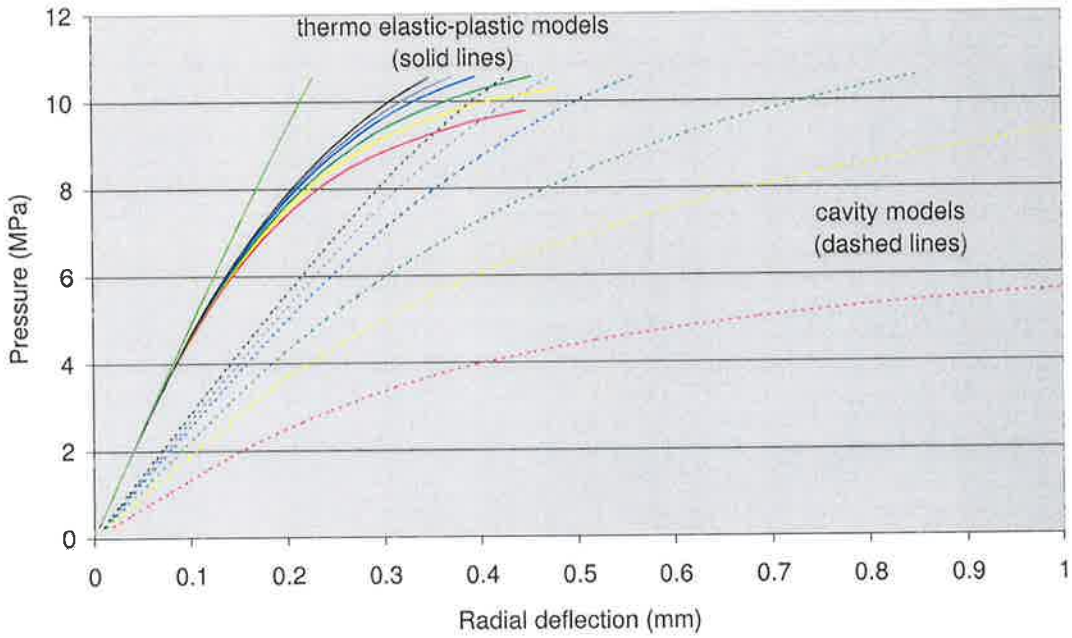


**Figure 6.22:** The variation of maximum radial deflection with pressure for six welds varying in heat input is displayed in the figure. Lines with identical colours represent an identical in-service weld with identical heat input; the dashed line represents equivalent cavity model while the solid line represents the thermal elastic-plastic model. Radial deflection against pressure for a pipe without a cavity at ambient conditions is given in bright green. heat input varies with colour: low(black) to high(red).

of pressure ($4MPa - MAOP$). Clearly, the variation of radial deflection with pressure for different heat inputs is observed to widen for the equivalent cavity models, whereas the trend is not as significant for the thermal elastic-plastic models.

### 6.5.3 Discussion

Clearly, the dimensions of a cavity influence the load carrying capacity of a given pipe. Moreover, the work discussed previously in Section 6.4 involving calculating the gradual deformation of a pipe with a cavity had revealed that cavity dimensions had influenced the nature of pipe deformation. For a given cavity, as the cavity depth is reduced, the maximum radial deflection is also reduced. It is suggested that as the cavity depth is decreased, the variation of maximum radial deflection with pressure begins to shift toward the deflection curve of an ambient pipe without a cavity. Physically, decreasing the depth

of the cavity would eventually lead to a pipe without a cavity. Numerical predictions also reflect this trend as can be seen in Figure 6.23(a). Clearly, as cavity depth is diminished, the plot of maximum radial deflection with pressure tends towards that for a pipe without a cavity.

A similar argument is also proposed for the behaviour of a pipe with varying circumferential cavity length and longitudinal cavity length. The variation of a cavity with decreasing circumferential cavity length can be seen in Figure 6.23(b). Clearly, as the length of a circumferential cavity is reduced, the plot of maximum radial deflection with pressure resembles and tends towards that of a pipe without a cavity. The variation of a cavity with decreasing longitudinal cavity length can also be seen in Figure 6.23(c). As found with cavity depth and circumferential cavity length, as the longitudinal length of a given cavity is reduced, the variation of maximum radial deflection with pressure tends towards that of a pressurised pipe at ambient temperature without a cavity.

The numerical experiments as discussed earlier in Section 6.4.3 and 6.4.4, have revealed that the cavity dimensions significantly influence the shape of the curve representing maximum radial deflection with pressure. In summary, reducing either of the cavity dimensions or a combination of either will cause the plot of maximum radial deflection to shift toward that of an ambient pipe without a cavity. Physically, this is reasonable as decreasing the cavity will result with a pipe with more material and therefore greater stiffness and strength.

The thermal elastic-plastic models had revealed a variation of maximum radial deflection which is similar to that of an ambient pipe without a cavity during the initial loading. The initial portion of the deflection plot is virtually identical to that of an unwelded pipe. The latter portion of the deflection plot for each respective model is obviously due to the different temperature fields and therefore material properties due to different welding heat input. From the argument proposed earlier, the only way an equivalent cavity model will also have this same initial variation of maximum radial deflection with pressure would be if the cavity did not exist. i.e. the thermal elastic-plastic models suggest that the

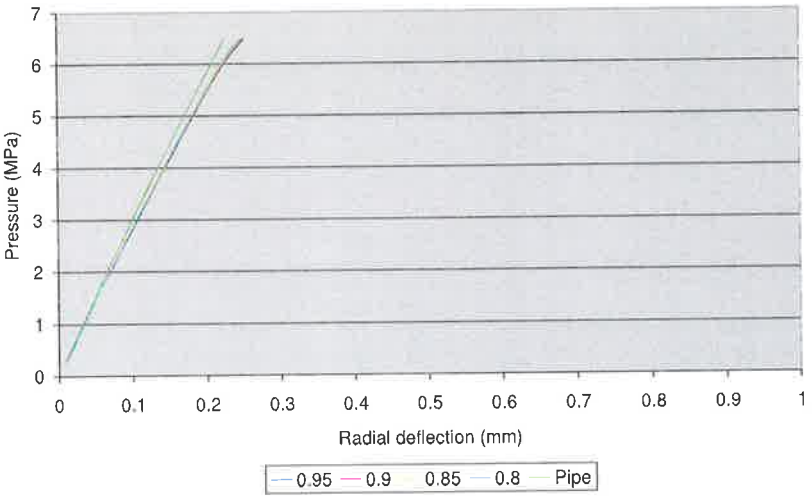


(a) $dc/dn$ (coloured lines)

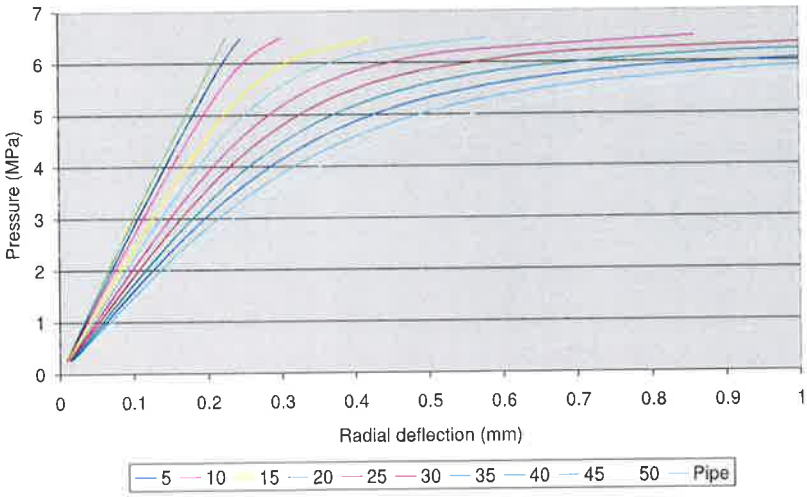


(b) $L_c$ (coloured lines)

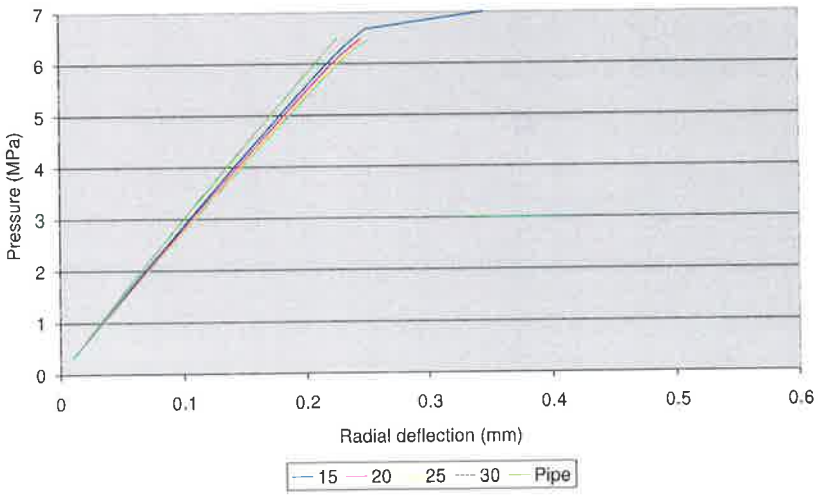


(c) $L_p$ (coloured lines)

**Figure 6.23:** Variation of radial deflection with cavity depth, circumferential length and longitudinal length. Radial deflection against pressure for a pipe without a cavity at ambient conditions is given in bright green.

initial portion of the deflection curve is that of an ambient pipe. Clearly, it is not possible for any cavity geometry to reproduce the same deflection curve of that from a thermal elastic-plastic model. Simply, the size and shape of a cavity influences the slope of the deflection versus pressure curve. The cavity model proposed by Bout & Gretskii [8] is therefore not a valid model as it does not behave in the same manner as a pipe with a temperature field.

### 6.5.4 Conclusions

The simulation of the early stages of pipe wall failure of circumferential fillet welding using a thermal elastic-plastic analysis has been successful and has been demonstrated. However, the cavity model proposed by Bout & Gretskii is considered to not deform in the same manner as a pressurised in-service weld.Predicting the safe pressure at which in-service welding can be applied to a pipeline by approximating the pipe and temperature field as an ambient pipe with a cavity is clearly prone to error.

## 6.6 Conclusions and future work

A complete numerical model to predict the onset of pipe wall failure for circumferential fillet welding and longitudinal welding has been demonstrated. Given enough computing resources, the prediction of the onset of pipe wall failure is readily available using the models and methods proposed within this thesis.

The novel model proposed by Bout & Gretskii [8] led to the discovery of potentially grave inadequacies of the B31G corrosion cavity model. The work within this thesis has clearly outlined the influence of circumferential cavity length in addition to cavity depth and longitudinal cavity length on the safe operating pressure of a given pipeline. The deformation behaviour of the cavity model proposed by Bout & Gretskii [8] was found not be equivalent to a thermal elastic-plastic finite element model. The reduction in wall

thickness due to the equivalent cavity analogy causes the cavity and finite element models to have considerably different predictions. Moreover, it is impossible to make a general statement on the predicted safe operating pressure from the cavity model.

Future work envisaged includes the rigorous testing of the proposed thermal elastic-plastic model with data from experiments.

## PUBLICATIONS ARISING FROM THIS THESIS

Sabapathy, P.N., Painter, M.J., Wahab, M.A. *"Prediction of burn-through during in-service welding of gas pipelines"*, The International Journal of Pressure Vessels and Piping, volume: 77, issue: 11, September 1, 2000, pp. 669-677

Sabapathy, P.N., Painter, M.J., Wahab, M.A. *"Numerical methods to predict failure during the in-service welding of gas pipelines"*, The Journal of Strain Analysis for Engineering Design, 23 November 2001, volume 36, no. 6, pp. 611-619(9)

# References


[1] Adams JR, C. Cooling rates and peak temperatures in fusion welding. *Welding Journal 37*, 5 (May 1958), 210s–215s.

[2] Bailey, N., Coe, F. R., Gooch, T. G., Hart, P. H. M., Jenkins, N., and Pargeter, R. J. *Welding steels without hydrogen cracking*, 2nd ed. Abington Publishing, 1993. ASM International.

[3] Barberis, U., and Rebora, A. Finite element analysis of gma (mig) welded joints. *Welding International 10*, 1 (1996), 44–50.

[4] Barlow, J. One weld or two? the formation of submerged arc weld pool. *Welding Institute Research Bulletin* (June 1982), 177–188.

[5] Barry, J., and Paley, ZVI. Adams JR, C. Heat conduction from moving arcs in welding. *Welding Journal 42*, 3 (March 1963), 97s–104s.

[6] Bathe, K. *Finite Element Procedures*, 1st ed. Prentice Hall, 1996.

[7] Boran, J. The hot tapping of sub-sea pipelines. *Welding Review 6*, 4 (November 1987), 283–284, 286, 288.

[8] Bout, V., and Gretskii, Y. Arc welding application on active pipelines. In *Pipeline Technology. Proceedings, 2nd International Conference, Ostend, Belgium* (September 1995), R. Denys, Ed., vol. 1, pp. 549–558.

[9] Brown, S., and Song, H. Finite element simulation of welding of large structures. *Journal of Engineering for Industry 114* (November 1992), 441–451.

[10] BROWN, S., AND SONG, H. Implications of three-dimensional numerical simulations of welding of large structures. *Welding Journal 71*, 2 (February 1992), 55s–62s.

[11] BROWN, S., AND SONG, H. Rezoning and dynamic substructuring techniques in fem simulations of welding processes. *Journal of Engineering for Industry 115* (November 1993), 415–423.

[12] BRUCE, W. Effect of procedure qualification variables for welding onto in-service pipelines. Tech. rep., Edison Welding Institute, The Welding Institute, July 1994.

[13] BRUCE, W. Welding onto in-service thin-wall pipelines. In *International Conference on Pipeline Repairs* (March 2001), WTIA Technical Panel 7 & Smart Pipelines Group.

[14] BRUCE, W., BUBENIK, T., FISCHER, R., AND KIEFNER, J. Development of simplified weld cooling rate models for in-service gas pipelines. In *Line Pipe Research. Proceedings, 8th Symposium, Houston TX* (September 1993), American Gas Association, pp. 31.1–31.22.

[15] BRUCE, W., HOLDREN, R., AND MOHR, W. Repair of pipelines by weld metal deposition. In *A paper presented at the PRCI 9th Symposium on Pipeline Research, Houston Texas* (1996).

[16] BRUCE, W., AND KIEFNER, J. Repair of pipelines by direct deposition of weld metal. In *Line Pipe Research. Proceedings, 8th Symposium, Houston TX* (September 1993), American Gas Association, pp. 35.1–35.26.

[17] CASSIE, B. The welding of hot tap connections to high pressure gas pipelines. Tech. rep., Pipeline Industries Guild, October 1976.

[18] CASSIE, B. Welding on to live gas pipelines. In *Second international conference on PIPEWELDING* (1980), vol. 1, The Welding Institute, Abington Hall, Abington, Cambridge CB1 6AL, England, pp. 141–148.

[19] CHRISTENSEN, N. DE L. DAVIES, V., AND GJERMUNDSEN, K. Distribution of temperatures in arc welding. *British Welding Journal 12*, 2 (Feb 1965), 54–75.

[20] COLA, M., KIEFNER, J., FISCHER, R., JONES, D., AND BRUCE, W. Development of simplified weld cooling rate models for in-service gas pipelines. Tech. rep., Edison Welding Institute, Kiefner an Associates Incorporated, Battelle Memorial Institute, March 1991.

[21] COLA, M., AND THREADGILL, P. Final report on criteria for hot tap welding to american gas association. Tech. rep., Edison Welding Institute, 1100 Kinnear Road, Columbus, Ohio, 43212, March 1988.

[22] DAVIES, M. *Numerical Modelling of Weld Pool Convection in Gas Metal Arc Welding.* PhD thesis, The University of Adelaide, Adelaide, South Australia, 5005, August 1995.

[23] DE HERTOGH, J., AND ILLEGHEMS, H. Welding natural-gas-filled pipelines. *Metal Construction and British Welding Journal 6*, 7 (1974), 224–227.

[24] EAGER, T., AND TSAI, N. Temperature fields produced by traveling distributed heat sources. *Welding Journal 62*, 12 (1983), 346s–355s.

[25] ENGINEERING MECHANICS RESEARCH CORPORATION. *NISA II User's Manual.* P.O. BOX 696, TROY, MICHIGAN 48099 U.S.A.

[26] FISCHER, R., KIEFNER, J., AND WHITACRE, G. User's manual for model 1 and 2 computer programs for predicting critical cooling rates and temperatures during repair and hot-tap welding on pressurized pipelines. Tech. rep., BATTELE, Columbus Laboratories, 505 King Avenue, Columbus, Ohio 43201, June 1981.

[27] FRIEDMAN, E. Thermomechanical analysis of the welding process using the finite element method. *Journal of Pressure Vessel Technology 97*, 3 (August 1975), 206–213.

[28] FRIEDMAN, E., AND GLICKSTEIN, S. An investigation of the thermal response of stationary gas tungsten arc welds. *Welding Journal 55* (December 1976), 408s–420s.

[29] GERHART, P., GROSS, R., AND HOCHSTEIN, J. *Fundamentals of Fluid Mechanics*, 2nd ed. Addison-Wesley, 1992.

[30] GOLDAK, J. Thermal analysis of welds. In *Modeling in Welding, Hot Powder Forming, and Casting*, L. Karlsson, Ed. ASM International, 1997, ch. 2.

[31] GOLDAK, J., BIBBY, M., MOORE, J., HOUSE, R., AND PATEL, B. Computer modeling of heat flow in welds. *Metallurgical Transactions B 17B* (September 1986), 587–600.

[32] GOLDAK, J., CHAKRAVARTI, A., AND BIBBY, M. A new finite element model for welding heat sources. *Metallurgical Transactions B 15B* (1984), 299–305.

[33] GOLDAK, J., AND GU, M. Computational weld mechanics of the steady state. In *Mathematical Modelling of Weld Phenomena 2* (May 1995), H. Cerjak and H. Bhadeshia, Eds., pp. 208–225.

[34] GOLDAK, J., MCDILL, M., ODDY, A., HOUSE, R., CHI, X., AND BIBBY, M. Computational heat transfer for weld mechanics. In *Advances in Welding Science and Technology TWR'86* (May 1986), S. David, Ed., pp. 15–20.

[35] GOLDAK, J., ODDY, A., AND DORLING, D. Finite element analysis of welding on fluid filled, pressurised pipelines. In *International Trends in Welding Science and Technology* (June 1992), S. David and J. Vitek, Eds., pp. 45–50.

[36] GRAVILLE, B. A., AND READ, J. A. Optimization of fillet weld sizes. *Welding Journal 53*, 4 (April 1974), 161s–169s.

[37] GROSH, R., AND TRABANT, E. Arc welding temperatures. *Welding Journal 35*, 8 (August 1956), 396s–400s.

[38] Gu, M., Goldak, J., and Bibby, M. Computational heat transfer in welds with complex weld pool shapes. *Advanced Manufacturing Engineering 3*, 1 (January 1991), 31–36.

[39] Gu, M., Goldak, J., and Hughes, E. Steady state thermal analysis of welds with filler metal addition. *Canadian Metallurgical Quarterly 32*, 1 (1993), 49–55.

[40] Hibbitt, H., and Marcal, P. A numerical, thermo-mechanical model for the welding and subsequent loading of a fabricated structure. *Computers and Structures 3* (1973), 1145–1174.

[41] Hicks, D. Guidelines for welding on pressurized pipe. *Pipeline and Gas Journal* (March 1983), 17–19.

[42] Holman, J. *Heat Transfer*, 7th ed. McGraw-Hill, 1992.

[43] Hong, K., Weckman, D., Strong, A., and Pardo, E. Prediction of gas metal arc weld bead geometry using a three-dimensional finite element thermal model. In *Transport Phenomena in Processing* (March 1992), pp. 626–6353.

[44] IPSCO. Ipsco hot/wet tapping. Internet, http://www.hottaps.com/tapping.htm.

[45] Jeong, S., and Cho, H. An analytical solution to predict the transient temperature distribution in fillet arc welds. *Welding Journal 76*, 6 (1997), 223s–232s.

[46] Jhaveri, P., Moffatt, W., and Adams JR, C. The effect of plate thickness and radiation on heat flow in welding and cutting. *Welding Journal 41*, 1 (January 1962), 12s–16s.

[47] Kamala, V., and Goldak, J. Error due to two dimensional approximation in heat transfer analysis of welds. *Welding Journal* (September 1993), 440s–446s.

[48] Kasuya, T., and Yurioka, N. Prediction of welding thermal history by a comprehensive solution. *Welding Journal* (March 1993), 107s–115s.

[49] KIEFNER, J., AND FISCHER, R. Models aid pipeline-repair welding procedure. *Oil & Gas Journal 86*, 10 (March 1988), 41–46.

[50] KOU, S., AND LE, Y. Three-dimensional heat flow and solidification during the autogenous gta welding of aluminum plates. *Metallurgical and Materials Transactions A 14A* (1983), 2245–2253.

[51] KOU, S., AND LE, Y. Heat flow during the autogenous gta welding of pipes. *Metallurgical and Materials Transactions A 15A* (June 1984), 1165–1171.

[52] KRUTZ, G., AND SEGERLIND, L. Finite element analysis of welded structures. *Welding Journal 57* (1978), 211s–216s.

[53] KUMAR, B., MOHANTY, O., AND BISWAS, A. Welding of thin steel plates: A new model for thermal analysis. *Journal of Materials Science 27* (1992), 203–209.

[54] LEUNG, C., AND PICK, R. Finite element modelling of multipass welds. *WRC Bulletin*, 356 (August 1990), 11–33.

[55] LEUNG, C., PICK, R., AND MOK, D. Finite element modelling of a single pass weld. *WRC Bulletin*, 356 (August 1990), 1–10.

[56] MAHIN, K., SHAPIRO, A., AND HALLQUIST, J. Assessment of boundary condition limitations on the development of a general computer model for fusion welding. In *Advances in Welding Science and Technology TWR'86* (May 1986), S. David, Ed., pp. 215–223.

[57] MALMUTH, N., HALL, W., DAVIS, B., AND ROSEN, C. Transient thermal phenomena and weld geometry in gtaw. *Welding Journal 53*, 9 (September 1974), 388s–400s.

[58] MOORE, J., BIBBY, M., AND GOLDAK, J. The significance of the point source model assumptions on weld cooling times. Tech. rep., Department of Mechanical and Aeronautical Engineering, Carleton University, Ottawa, January 1985.

[59] MYERS, P., UYEHARA, O., AND BORMAN, G. Fundamentals of heat flow in welding. Tech. Rep. 123, Welding Research Council, 1967. Welding Research Council Bulletin.

[60] NGUYEN, N., OHTA, A., MATSUOKA, K., SUZUKI, N., AND MAEDA, Y. Analytical solutions for transient temperature of semi-infinite body subjected to 3-d moving heat sources. *Welding Journal 78*, 8 (August 1999), 265s–274s.

[61] NUNES J.R., A. An extended rosenthal weld model. *Welding Journal* (June 1983), 165s–170s.

[62] ODDY, A., AND LINDGREN, L. Mechanical modelling and residual stresses, 1997.

[63] ODDY, A., AND MCDILL, J. Burnthrough prediction in pipeline welding. *International Journal of Fracture 97*, 1–4 (1999), 249–261.

[64] PAINTER, M., AND SABAPATHY, P. In-service welding of gas pipelines. Tech. rep., Co-operative Research Centre of Welded Structures Australia, June 2000. Final Project Report.

[65] PALEY, Z., AND HIBBERT, P. Computation of temperatures in actual weld designs. *Welding Journal 54* (November 1975), 385s–392s.

[66] PARDO, E., AND WECKMAN, D. The interaction between process variables and bead shape in gma welding: A finite element analysis. In *Recent Trends in Welding Science and Technology TWR'89* (May 1989), S. David and J. Vitek, Eds., pp. 391–395.

[67] PAVELIC, V., TANBAKUCHI, R., UYEHARA, O., AND MYERS, P. Experimental and computed temperature histories in gas tungsten-arc welding of thin plates. *Welding Journal 48*, 7 (1969), 295s–305s.

[68] PHELPS, B., CASSIE, B., AND EVANS, N. Welding on to live natural gas pipelines. *Metal Construction 8*, 8 (August 1976), 350–354.

[69] Reid, R., Prausnitz, J., and Poling, B. *The Properties of GASES & LIQUIDS*, 4th ed. McGraw-Hill, 1988.

[70] Rietjens, I. Safely weld and repair in-service pipe lines. *Pipe Line Industry 65*, 6 (December 1986), 26–29.

[71] Rosenthal, D. Mathematical theory of heat distribution during welding and cutting. *Welding Journal 20* (May 1941), 220s–234s.

[72] Rykalin, N., and Beketov, A. Calculating the thermal cycle in the heat affected zone from the two dimensional outline of the molten pool. *SVAR. PROIZ 13*, 9 (September 1967), 22–25.

[73] Rykalin, N., and Nikolaev, A. Welding arc heat flow. *Welding In The World 9*, 3/4 (1971), 112–132.

[74] Rykalin, R. Energy sources used for welding. *Welding in the World 12*, 9 (1974), 227–248.

[75] Silva Prasad, N., and Sankara Narayanan, T. Finite element analysis of temperature distribution during arc welding using adaptive grid technique. *Welding Journal* (April 1996), 123s–128s.

[76] Smailes, A. Thermal modelling of gas metal arc welding using finite element analysis. Master's thesis, The University of Adelaide, Adelaide, South Australia, 5005, January 1999.

[77] Tekriwal, P., and Mazumder, J. Finite element modeling of arc welding processes. In *Advances in Welding Science and Technology TWR'86* (May 1986), S. David, Ed., pp. 71–80.

[78] Tekriwal, P., and Mazumder, J. Finite element analysis of three-dimensional transient heat transfer in gma welding. *Welding Journal 67*, 7 (1988), 150s–156s.

[79] Internet, http://www.transcanada.com, 1998. TransCanada Pipelines.

[80] TSAI, C. Finite source theory. In *Modeling of Casting and Welding Processes II* (August 1983), J. Dantzig and J. Berry, Eds., pp. 329–341.

[81] VENTON, P., 1996. Report prepared for pipeline program for Coorperative Research Centre for Materials Welding & Joining.

[82] VIETH, P., AND KIEFNER, J. *RSTRENG2 User's Manual*, March 1993. Final Report on PR-218-9205 to Corrosion Supervisory Committee, Pipeline Research Committee, American Gas Association.

[83] WADE, J. Research report on effect of preheat on hot tapping procedures. Tech. rep., Snowy Mountains Engineering Corporation, September 1978.

[84] WADE, J. Research report on hot tapping of pipelines. Tech. rep., Snowy Mountains Engineering Corporation, September 1978.

[85] WELLS, A. Heat flow in welding. *Welding Journal 31*, 5 (May 1952), 263s–267s.

[86] WILSON, H. On heat convection. *Procedures of Cambridge Philosophical Society 12* (1904), 406–423.